The Development of Luminescence Methods to Measure Thermal Exposure in Lithic and Ceramic Materials

by

Joel Quintus Spencer

Submitted to

University of Glasgow
(Faculty of Science)

for the degree of

Doctor of Philosophy

September, 1996

This research was conducted at the Scottish Universities Research and Reactor Centre, East Kilbride

Abstract

Thermometric analyses provide extremely useful information about heated archaeological materials and fire-damaged modern structures. A number of non-luminescence thermometry methods have been developed for analysing pottery firing temperatures. However, many of these methods are limited in analysis range and accuracy, or are time consuming, expensive and complex. In addition to these techniques there are a number of thermoluminescence (TL) thermometry methods but they are also limited in analysis range and the majority have been developed for specific thermometry problems. The aim of this study was to investigate the use of thermoluminescence (TL) and photostimulated luminescence (PSL) methods to develop rapid, precise, inexpensive thermometry techniques that were applicable to a wide range of thermal events and materials from archaeological and modern contexts.

A basic theoretical treatment of luminescence kinetics in silicate systems was undertaken to develop an understanding of TL glow curve alterations arising from thermal exposure. Kinetic studies showed that a combination of temperature and duration parameters is expected for single trap systems. Kinetic theory was developed to produce a new first order multi-trap system which provides a theoretical means of separating temperature and time components, which may be applicable to synthetic phosphors. Additionally heat transfer solutions were investigated to examine the temperature distribution in heated solids and TL instrumentation.

Isothermal annealing experiments on IAEA F-1 potassium feldspar showed a highly precise progressive thermal exposure monitor, whereby the position of the first rise of an annealed TL glow curve is characterised by a linear increase in temperature and a logarithmic increase in time. First order kinetic simulations and initial rise measurements demonstrated a continuous linear distribution of traps in IAEA F-1 feldspar. Using a high temperature TL system (maximum temperature 700°C) the progressive thermometry method was successfully applied to separated feldspar minerals and polymineral samples from archaeological (ceramics, burnt stones and hearthstones) and modern (fire damaged concrete) materials.

PSL excitation spectroscopy showed potential thermometric behaviour but for some samples the sensitivity of the system was too low. Pulsed infra-red PSL showed there may be a limited trap distribution over which a small range of thermal exposures will operate. Combined TL/PSL measurements showed it may be possible to deconvolute temperature and time parameters.

Acknowledgements

I would like to thank my supervisor Dr. David Sanderson for his continuing help and guidance throughout this project. This thesis has also benefited from stimulating discussions and comments from Prof. Roger Scott.

A big thank you must also go to members of the luminescence and aerial survey group at SURRC (past and present) for their continuing help and good humour, and providing a stimulating working atmosphere:

Peter, Lorna, Christine, Robert, Drew, Simon, Andy, Dave, Keith and Jacqui

I would also like to thank many other members of staff at SURRC for their help and friendship during my research in East Kilbride.

And now on to the people who kept me sane (just) by topping me up with regular pints of beer:

East Kilbride and Glasgow

Kt, Juan, Sarah, Brucey-babes, Ian, Gawen, Jackie, Ellieeeee, Susan, Tony, Jane, Jamie, Dave P., Pauline, Marie...

Aberdeen

Hughsey, Cric & Andy M., Archie, Andy C., Johnny, Stevie, Nick, Helen, Chris, Gill, Cath, Sarah, Stefano, Polly & Neddy, Kathryn & Keith, Lucky Lips, Mengfang...

A special thank you to Shark for all the virtual times...

Finally a big thank you to my ever expanding family for all their love and support:

Eric & Norma

Matthew, Gaye & Louis

Damian & Sarah

Ben Onion

Edney &Vanessa

This research was made possible by receipt of a studentship from the Science Based Archaeology Committee of the Science and Engineering Research Council, and additional support from my parents.

Contents

Chapter 1: Introduction

1.1 Importance of thermal history

Tracing the path of exploitation of fire in antiquity, its use, control and the ability to achieve increasingly higher temperatures provides extremely useful archaeological information. This becomes clear when one examines the number of different materials that have been exposed to heat in the archaeological record. The material foremost in this list are fired ceramics or pottery, which occur on the majority of archaeological sites in domestic, industrial and funerary contexts. Ceramic firing temperatures give further insight to studies of ceramic technology and may also raise interesting questions on broader archaeological issues. These may include such topics as the technological development between contemporary or successive societies; although noticeable distinctions in data sets may have alternative explanations such as variations in fuel availability, due for example to extensification of land use, changes in climate or external aggression.

Other common archaeological materials that have a thermal history linked to human activity include the following; hearthstones; pot boilers; the ceramic and lithic structures associated with pottery kilns, early metal working, and domestic ovens; fire-cracked stone surfaces in early mines; and burnt flints. As with ceramics, analysis of the thermal history of these materials may contribute to a greater understanding of domestic processes and technological developments, and in some instances may imply changes in socio-political structures or environmental factors. Hearthstone studies may suggest, for example, different domestic or industrial processes between houses in a settlement, or as mentioned above may indicate pressure on fuel resources, or merely the type of fuel used. Whereas studies of pot boilers (heated stones perhaps used for heating water, roasting foodstuffs, wool-dying, saunas, etc.) may shed more light on the function of sites known as *burnt stone mounds* (Buckley, 1990). Finally, direct technological information may be gleaned from an analysis of pottery kiln structures, and items such as crucibles and tuyeres from early metal working.

Indicators of thermal history have a role to play in many other disciplines, and perhaps particularly for geological studies. As discussed by McKeever (1985) geological

applications may include studies of meteorites, and the formation of minerals. Using its broadest sense, the scope of thermal history studies may be extended to present day where its uses include the assessment of fire damage to building structures (eg. Placido, 1980).

1.2 Introduction to luminescence

1.2.1 Thermoluminescence (TL) and Photostimulated luminescence (PSL)

TL is light released when insulating crystalline minerals (eg. quartzes and feldspars) are subject to heat. The heating process enables charge carriers, previously held in metastable energy states, to gain enough energy to escape from their trapped state whereupon they may de-excite to recombine at lower energy defects or impurity ions releasing light photons. While the stimulating energy that depopulates the traps in TL is heat, for PSL the stimulating energy is in the form of light.

The initial charge trapping process is a result of the ionisation of parent atoms in the crystal lattice by exposure to natural radiation or artificial radiation sources (in the laboratory). For archaeological materials the radiation mainly comes from a combination of naturally occurring radioactive isotopes of K, Th, and U, with an additional smaller contribution from cosmic radiation and Rb.

1.2.2 Historical perspectives

Details of the historical background to the use of TL are discussed by authors such as Aitken (1985) and McKeever (1985). Some of the key historical markers are as follows; observations by Robert Boyle on the light emission from a diamond (Boyle, 1663) - although Becker (1973) suggests that medieval alchemists were aware that certain minerals glowed faintly when heated in the dark; Wiedemann and Schmidt (1895) induced TL into samples by laboratory irradiation with an electron beam; Trowbridge and Burbank (1898) demonstrate that TL from natural fluorite can be regenerated by exposure to X-rays; recognition by Urbach (1930) of the use of TL to study trap depth distributions; the famous papers of Randall and Wilkins (1945a,b) formalising the theory of TL by considering the

first order mechanism of electron detrapping, followed by Garlick and Gibson (1948) who considered second order TL mechanisms - these papers still form the basis of TL theory today (eg. Chen and Kirsh, 1981; McKeever, 1985; Aitken, 1985), although refinements are still being suggested (eg. Adirovitch, 1956; Halperin and Braner, 1960; Visocekas, 1978); Daniels *et al.* (1953) developed the use of the photomultiplier tube for measuring TL and suggested the use of TL for geological and archaeological age determination; TL of ancient pottery was first detected by Grogler *et al.* (1960) and Kennedy and Knopff (1960); subsequently during the 1960's TL was developed for archaeological dating at Oxford (Aitken, Tite and Reid, 1964; Aitken, Zimmerman and Fleming, 1968b), Kyoto (Ichikawa, 1965), Wisconsin (Mazess and Zimmerman, 1966), Philadelphia (Ralph and Han, 1966), and Denmark (Mejdahl, 1969); extension from pottery dating to burnt flint (Göksu *et al.*, 1974), burnt stones (Mejdahl, 1983) vitrified stones (Sanderson *et al*, 1988), and volcanic lava (Wintle, 1973; Guérin and Valladas, 1980); extension to various types of sediment began with work in the then U.S.S.R. (eg. Morozov, 1968); resetting of the TL clock by sunlight bleaching was recognised, windblown and waterlain sediments dated, and a residual luminescence component which could not be readily bleached was identified which lead to the partial bleach method (Wintle and Huntley, 1979, 1980, 1982).

In 1985 the demonstration by Huntley *et al*, (1985) of a much lower residual luminescence signal from sediment samples analysed by PSL, opened up an exciting new field of study with the prospect of much more reliable dating for samples that had been optically bleached. The various advances in photostimulated dating have been recently reviewed by Aitken (1992, 1994) and Wintle (1993).

1.3 Thermoluminescence thermometry

Although TL is most familiar in the context of dating and radiation dosimetry studies (eg. Aitken, 1985; McKeever, 1985; Horowitz, 1984; Fleming, 1979; McKeever, 1984; Mahesh, Weng and Furetta, 1989; McKeever, Moscovitch and Townsend, 1995; Horowitz and Yossain, 1995), the underlying phenomena are also sensitive to thermal history. Thermometry methods exploiting TL may be broadly grouped into 4 main areas; those methods exploiting an equilibrium condition between trap filling and eviction at a constant

temperature; those based on the absolute reduction of TL intensity due to heat treatment; methods measuring the shift of the TL glow curve due to heat treatment; and those exploiting the property of thermal sensitisation of TL before accumulating dose (commonly referred to as pre-dose sensitisation).

The methods summarised in Table 1.1 are thus based on TL equilibrium (EQUIL), intensity (INT), glow curve shift (SHIFT) and pre-dose sensitisation (PDS). The subscripts denote whether the methods are based on measurements from a single *peak*, a number of *peaks*, (for convenience a specific region of the glow curve is also termed a "peak"), or the entire *TL glow* curve. An exception to these general subscripts is the suggestion of a palaeothermometry method put forward by Levy (1979) based on the SHIFT of the TL *emission* spectrum peak energy observed in albite ($NaAlSi_3O_8$) samples annealed at 1050°C for various times prior to irradiation.

The temperatures sensed by those methods which have developed to a stage of either laboratory testing and/or sample application varies from environmental (terrestrial) to high temperature pottery firing. However, the limits of temperature ranges are often not reported although this may be because the investigations are mainly for a specific thermal event(s). In the majority of cases no details of precision are reported, and as listed the "analysis type" has been divided into Comparative, Temperature, Temperature/time and Exposure categories. *Comparative* are those methods where the results of luminescence measurements are compared to simply ascertain whether samples have been heated or not heated, or whether there are temperature variations between a group of samples (eg. Dort *et al.*, 1965). *Temperature* are those methods where a value for duration of the thermal event has to be assumed. *Temperature/time* are those methods where a temperature value has been estimated (although this value may be a maximum temperature of a dynamic thermal exposure, an average temperature, or an average-maximum temperature from a cyclical event), and in some studies an estimate of duration is also made. *Exposure* are those methods where a quantity which involves both temperature and time variables is measured.

As shown a wide range of minerals have been previously studied ($CaMg(CO_3)_2$, $CaCO_3$, $CaSO_4$:Mn, $NaAlSi_3O_8$, "SiO_2", chert (flint), LiF, polymineral samples) from a number of geological, archaeological, archaic-lunar, extra-terrestrial and modern thermal events.

Table 1.1 Summary of thermoluminescence thermometry methods

Author (s)	Method[a]	Temperature range	Analysis type[b]	Precision	Mineral	Material / Investigation[c]
Lovering (1958)	INT_{peaks}	Over natural TL	Comparative	no data	Dolomite & limestone	Temp. of hydrothermal dolomitization
Ronca (1964)	$EQUIL_{peak}$	Environmental	Temp./time	no data	230°C peak in calcite	Min. time of frigid conditions in Antarctica
Dort *et al.* (1965)	$EQUIL_{peak}$	Environmental	Comparative	no data	230°C peak in calcite	Temp. differences in archaeological cave site
Johnson (1966)	$EQUIL_{peak}$	~950°C	Temp./time	no data	230°C peak in calcite	Temp. of magma inferred from contact zone
Zeller (1968)	$EQUIL_{peak}$	Environmental	Comparative	no data	230°C peak in calcite	Influence of microclimate on TL
Aitken & Thompson (1968)	$SHIFT_{peak}$	Over natural TL	Temperature	no data	No details	Temp. of enamelling oven (~500 AD)
Christodoulides *et al.* (1971)	$EQUIL_{peaks}$	Environmental	Temp./time	no data	n/a	Paper discusses a possible method
Romberg & Prepejchal (1977)	INT_{peak}	Environment (5-30°C)	Temperature	no data	~100°C peak in $CaSO_4$:Mn	Water temp. & thermal exposure of fish
Durrani *et al.* (1977)	$EQUIL_{peak}$	Lunar environment	Temp./time	no data	45-106 μm soil samples	Temp. and duration of shaded lunar soil
Levy (1979)	$SHIFT_{Emission}$	1050°C	Temperature	no data	Albite	Effect of annealing on TL emission spectra
Placido (1980)	$SHIFT_{peak}$	~300-500°C (nat. TL)	Exposure	no data	Quartz-sand from concrete	Fire damage in modern concrete structures
Valladas (1980)	INT_{peak}	Over natural TL	Temperature	~ 20°C	Quartz from sandstones	Temp. of prehistoric fireplaces
Sheppard *et al.* (1982)	INT_{TLglow}	n/a	Comparative	no data	Flint samples	Heat treatment of Epipalaeolithic flints
Sunta & David (1982)	PDS_{peak}	~700-900°C	Temperature	no data	110°C peak in quartz	Firing temperature of pottery
Vaz (1983)	$EQUIL_{peak}$	Environment (43°C)	Temp./time	no data	220°C peak in calcite	Insolation of limestone gargoyle (~1550 AD)
Göksu *et al.* (1989)	PDS_{peak}	~300-600°C	Temperature	no data	110°C peak in flint	Heat treatment of ancient flint
Kitis *et al.* (1989)	PDS_{peaks}	Expts at 900°C	Temperature	no data	Quartz, LiF & fine grains	Firing temp. of ancient and "test" ceramics

Notes: [a,b] see section 1.3; [c] Temp. = temperature

1.4 Non-luminescence archaeothermometry

A number of analytical methods have been developed to estimate the temperature of pottery firing. The methods include observations of physical and chemical properties, but most procedures address the mineralogical characteristics of pottery. A comparison of archaeothermometric techniques is shown in Table 1.2. Rice (1987) has reviewed the various methods and the following points summarise her findings:

a) Many methods depend upon prior knowledge of the clay mineral constituents, although many sherds are comprised of several clays (with a variety of mineral inclusions). The results from XRF and thermal methods may therefore be difficult to interpret, and, in addition, many of these mineral-based methods are not useful for firing temperatures above 500-700°C.
b) It is difficult to find methods that are reliable in the 600-900°C range.
c) Accuracy usually has an uncertainty between 30-100°C (Tite *et al.*, 1982).
d) In addition to firing temperature, several methods (eg. SEM and porosity) show the extent of vitrification. These methods measure not only a technical property but also cultural and functional characteristics. However, vitrification may occur over a temperature range of 200°C (Tite and Maniatis, 1975).
e) Characteristics of fired wares, especially vitrification, are a function of the firing temperature, duration of firing and atmosphere (Tite and Maniatis, 1975).
f) Due to possible rapid cooling, sintering may have taken place at a lower temperature than the firing maximum. Additionally temperatures are apt to fluctuate widely in both bonfire and kiln firings.
g) Post-depositional processes - leaching, mineral recrystallisation, rehydration - may affect the properties measured to estimate the firing temperature of the clay vessels. Thus the current properties may not be equivalent to the ancient properties.

Table 1.2 Comparison of Archaeothermometric Techniques

Technique or Property	Advantages	Disadvantages	Range (°C)
Colour (refiring expts)	Simple. Requires no prior knowledge of clay mineral constituents. Minimal equipment - kiln and colour charts	Sensitive to variations in time and atmosphere. Organic material may confuse interpretations. Damage/destruction of sample. Low accuracy.	500
Porosity	Requires no prior knowledge of clay mineral composition. Indication of temperature as a function of vitrification.	Damage/destruction of sample. Results are a function of granulometry. Results affected by leaching, mineralisation, or recrystallisation.	900
Mössbauer spectroscopy	Relatively non-destructive. Based on Fe; relatively common constituent. Fine temperature discriminations	Time consuming. Requires comparison with clays. Less useful or not applicable with nonferruginous (< 5% Fe) clays.	750-1100
ESR	Useful for low temperatures (< 600°C).	Requires comparison with clays and expensive equipment	< 600
Quartz inversion	_	Must have quartz inclusions. Unreliable - may not have visible manifestations in pottery. Destructive - requires thin sectioning.	~573
Anisotropy of matrix	Measured in parallel with general petrographic study.	Requires thin sectioning and petrographic microscope	<850
Calcite decomposition	Can be observed without a petrographic microscope	Calcite must be present. Range of decompostion is wide	700-900
SEM	Info. on degree of vitrication and firing temperature.	Expensive equipment. Destruction of sample (for re-firing)	800
X-ray diffraction	Low and high temperature firing estimates. Especially useful on illites (500-950°C) and calcareous clays.	Must know clay mineral constituent(s). Not good on kaolinites (600-1000°C). No information on virtrification. Complex equipment.	Best <500 or >900
Differential thermal analysis (DTA)	Useful for low to midrange firing temperatures	Must know clay mineral constituents. Estimates complicated when other mineral constituents (temper) react thermally.	250-900
Thermal gravimetric analysis (TGA)	_	Must know clay mineral constituents. No information on vitrification. Elaborate equipment. Narrow temperature range	500-700
Thermal expansion analysis	Accurate to ± 30°C. Good for high temperature. Detects vitrification in addition to temperature.	Problems with "bloating". Requires correction for deviation of rate of heating. Very complex process of refiring. Problems if calcite present.	800

Notes: Table adapted from Rice (1987). ESR = electron spin resonance. SEM = scanning electron microscope

1.5 Thesis aims and content

The aim of this thesis was to investigate the use of luminescence methods to study the control and use of fire in past and modern day contexts, and in so doing develop a thermometry technique that was rapid, precise, in-expensive, and applicable to a wide range of materials. The thesis is structured in the usual manner with theory, instrumentation, experimentation, application and discussion chapters.

Chapter 2 (Theory) deals with two theoretical areas of relevance to luminescence studies of thermal exposure. The first of these is a basic treatment of luminescence kinetics enabling the development of understanding of TL glow curve alterations in insulating materials arising from thermal exposure. The second area examined is that of heat transfer which is important because of the variation in temperature distribution both in solids exposed to heat due to thermal gradients, and also between the heater plate and sample in TL experiments. Chapter 3 (Instrumentation and measurement methods) deals firstly with TL measurement and discusses the TL equipment, instrumental developments and temperature calibration of glow curves. The equipment used to perform PSL experiments is then described with details of a scanning excitation spectrometer and pulsed infrared diode array. Chapter 4 (Thermoluminescence experiments) initially discusses annealing experiments on a standard potassium feldspar, and then these results are compared with kinetic simulations. Finally an extension of the empirical observations is made to the TL characteristics of material from an experimental hearth. Chapter 5 (Thermoluminescence applications) discusses the results of TL measurements on archaeological ceramics, burnt stone mounds and hearthstones, and a modern day fire damaged concrete tunnel. Chapter 6 (Photostimulated luminescence) describes measurements made using an excitation spectrometer and pulsed diode array on the same material used in Chapter 4 to investigate whether PSL has potential as an indicator of thermal exposure, and includes discussion of the complimentary information revealed by TL and PSL analyses. Finally Chapter 7 (Discussion) has 3 sections; summary and discussion, suggestions for future work and the conclusions of the project.

Chapter 2: Theory

2.1 Introduction

This chapter deals with two theoretical areas of relevance to luminescence studies of thermal exposure. The first of these is a basic treatment of thermoluminescence (TL) kinetics enabling the development of understanding of TL glow curve alterations arising from thermal exposure. Sections introduce the concept of the energy band model of solids, then set out the equations governing first order kinetic behaviour, discuss kinetic studies made of the effect of thermal exposure on hypothetical systems containing well defined components, and finally summarise a treatment of the kinetics associated with the optical eviction of charge carriers via photostimulated luminescence (PSL).

The second area examined is that of heat transfer which is important because of the variation in temperature distribution both in solids exposed to heat due to thermal gradients, and also in TL experiments between the heater plate and sample. Accordingly sections firstly deal with macroscopic solutions of heat transfer in solid shapes, and secondly discuss heat transfer models that have been formulated to estimate the temperature distribution and thermal lags associated with TL measurements.

2.2 Analytical models of the TL process

The following sections discussing kinetic models of the luminescence process (2.2.2, 2.2.3, 2.2.4 and 2.2.8) are based on the pioneering work of Randall and Wilkins (1945a,b) and Garlick and Gibson (1948). Although refinements have subsequently been suggested (eg. Adirovitch, 1956; Halperin and Braner, 1960; Visocekas, 1978), these papers from the 1940's still form the basis of TL theory discussed in kinetic (eg. Chen and Kirsh, 1981; Braünlich, 1979) and more general application (eg. Aitken, 1985; McKeever, 1985) textbooks.

2.2.1 Energy band model

According to quantum theory orbiting electrons of a single atom can only occupy discrete energies. The atom has a number of associated energy levels and the electrons occupy the lower levels and obey the Pauli exclusion principle. In a solid, as the atoms become closer together the narrow energy levels become wider bands of allowed energies, each band consisting of a large number of closely spaced energy levels individually capable of containing two electrons. The bands of permissible energy are called the allowed bands. These may either be filled or empty depending on whether they correspond to filled or empty levels in the system. The energy regions between these are called the forbidden bands. The band of energies of the valence electrons in a solid is called the valence band.

The theory of these energy bands in solids depends on quantum mechanics. In general, the Schrödinger equation is solved for an electron moving in a varying electric potential the periodicity of which is created by the spacing of the ions in the crystal lattice. The allowed solutions give the allowed bands of energy and the energies for which there are no solutions are the forbidden bands. Within any allowed energy bands the number of constituent discrete energy levels varies with the energy. A curve showing this variation is called a density of states curve.

Figure 2.1 is a representation of the energy bands in metals, semiconductors and insulators at absolute zero. In metals the valence band is partially filled, whereas in semiconductors and insulators the valence band is completely filled with a forbidden band or band gap between it and the next highest empty band, termed the conduction band. The Fermi level, E_f, is a level below which the energy levels are completely full and above which completely empty. Thus at absolute zero the Fermi level in semiconductors and insulators lies above the upper most valence energy and it is not possible to obtain a net transport of charge in the valence band in the direction of an applied electric field. The forbidden band in semiconductors is small and at temperatures above absolute zero some electrons gain enough thermal energy to escape into the conduction band, making conduction possible with conductivity rising with temperature.

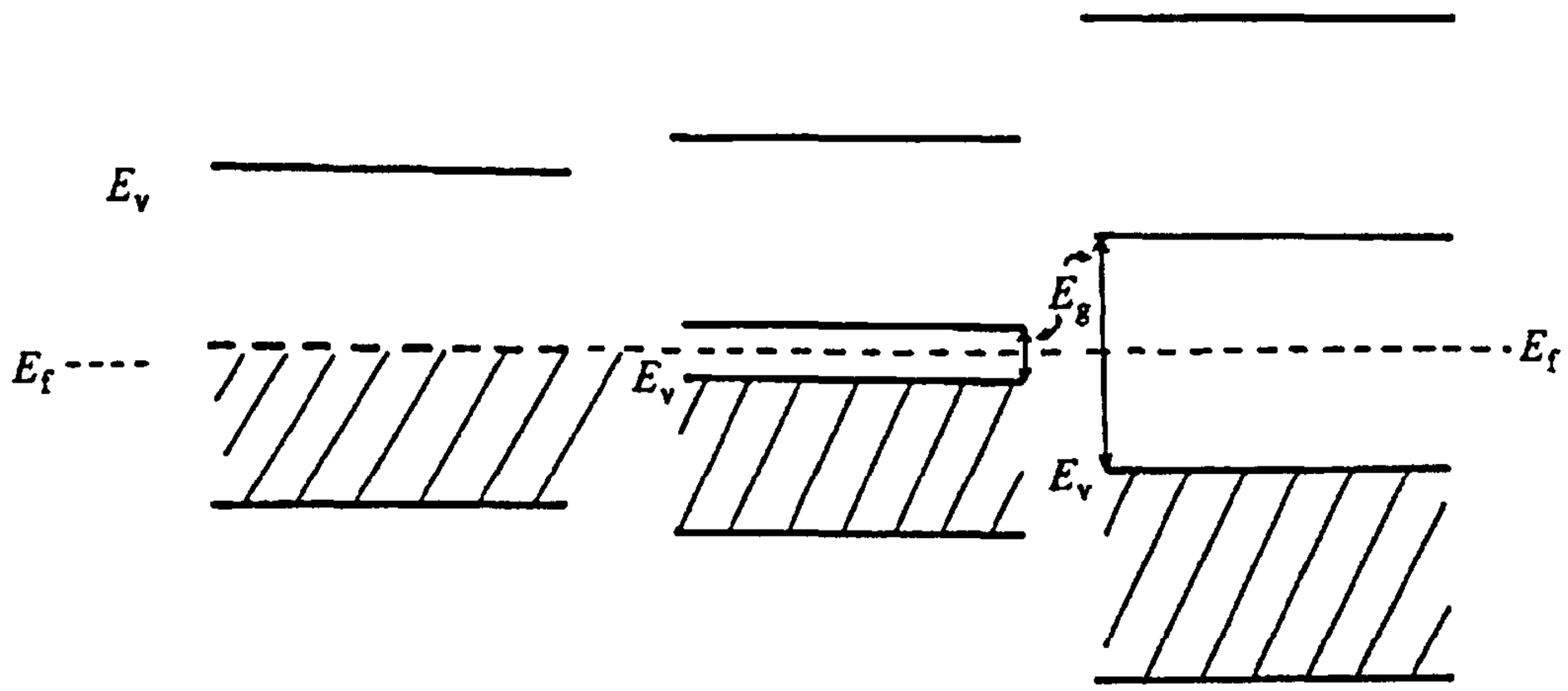

Figure 2.1 (a) The partially filled valence band for a metal at absolute zero. The shaded area represents the fully occupied states. This is compared with the completely filled valence bands for (b) a semiconductor and (c) an insulator. Here the filled bands are separated from the next highest empty band by a so-called 'forbidden' gap E_g. E_f is the position of the Fermi level and E_v is the top of the valence band (from McKeever, 1985).

The presence of either structural defects or impurity ions within the lattice causes a breakdown in the periodicity of the crystalline structure and it becomes possible for electrons to possess energies which are forbidden in the perfect crystal. Lattice imperfections are many and varied and are strongly determined by the natural crystal formation processes. They are classed into two types; point defects and line defects. Important point defects are Frenkel defects (interstitial molecules, atoms or ions and corresponding vacancies) and Schottky defects (lattice vacancies caused by diffusion of host ions to the crystal surface). Line and planar defects such as dislocations and grain boundaries may also give rise to allowed energy levels within the forbidden band. The valence and conduction bands extend throughout the crystal whereas the defect states are centred upon the defects themselves and are thus termed localised energy levels.

The localised energy levels may be discrete, or they may be distributed, depending upon the exact nature of the defect and of the host lattice. McKeever (1985) uses the example of an alkali halide crystal of the type M^+X^- to explain, in general terms, how impurities and structural defects give rise to localised energy levels. An electron freed from the valence band and moving through the crystal may become attracted by the coulombic field of a vacant anion site (ie. a missing X^-

ion) and become *trapped* (no longer able to take part in conduction). The energy required to release the electron from the trap is less than that required to free a valence electron from an X^- ion and thus the anion vacancy has associated with it an energy level which lies somewhere between the valence and the conduction bands. A similar situation arises with cation vacancies where the missing M^+ ion results in a deficiency of positive charge which in turn results in a decrease in the energy required to free an electron from a neighbouring X^- ion. Once again a localised energy level within the forbidden gap is associated with this vacancy. The position of the localised level within the gap is determined by the decrease in the energy required to free the electron. Thus for cation vacancies the energy level turns out to be below the equilibrium Fermi level and the centres are full of electrons and are thus potential hole traps. The anion vacancies, however, have an energy level above the Fermi energy meaning that the level is empty of electrons and that the defects are potential electron traps. Similar arguments apply to the incorporation of impurity ions (cation or anion) within the crystal lattice, either in substitutional or interstitial positions.

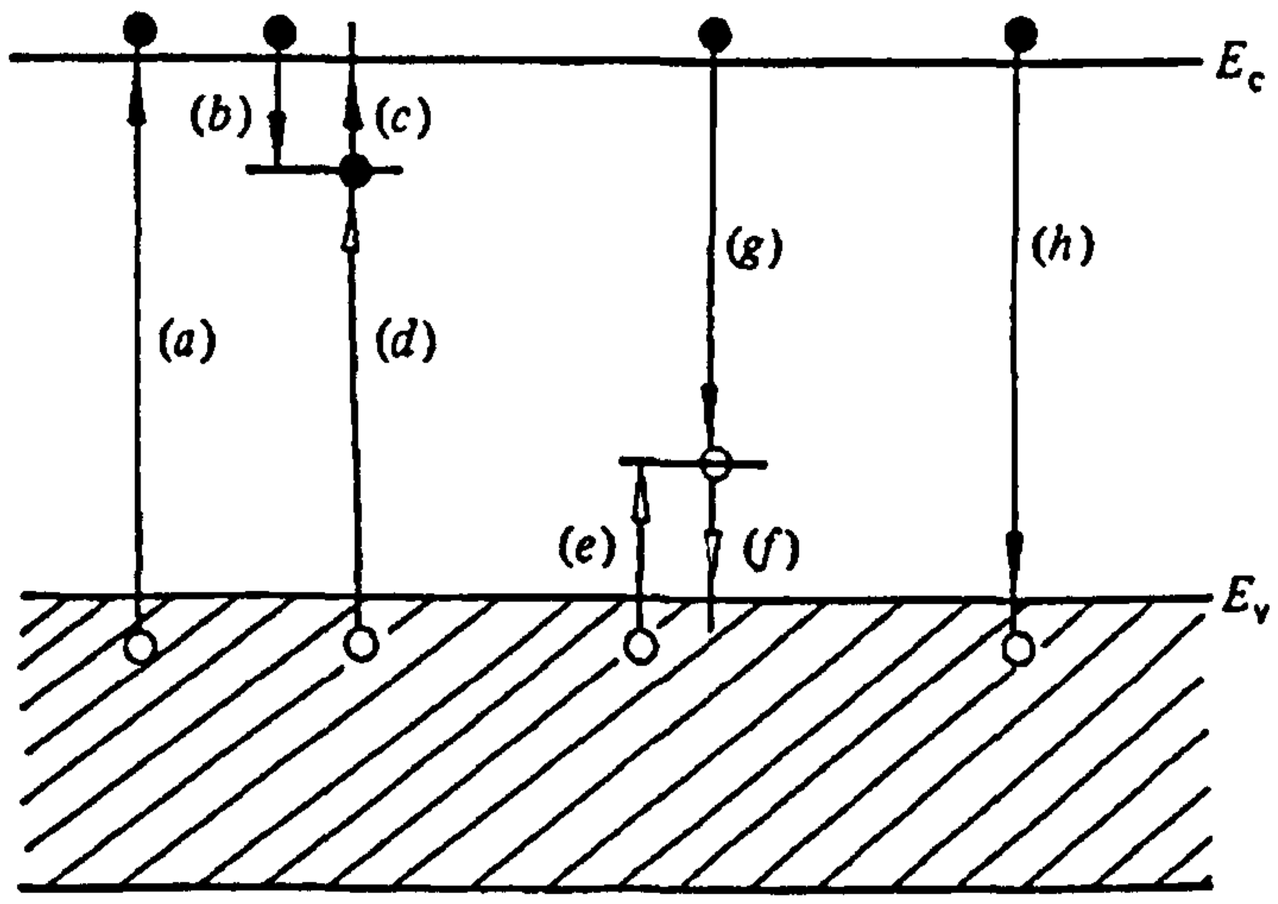

Figure 2.2 Common electronic transitions in (crystalline) semiconductors and insulators: (a) ionisation; (b) and (e) electron and hole trapping respectively; (c) and (f) electron and hole release; (d) and (g) indirect recombination; (h) direct recombination. Electrons, solid circles; electron transitions, solid arrows; holes, open circles; hole transitions, open arrows (from McKeever, 1985).

Luminescence processes are governed by changes in the occupancy of the various localised energy states, by electronic transitions from one state to another. There are several permissible transitions for both holes and electrons, some of which are shown in Figure 2.2. Localised energy levels can act either as traps or recombination centres and they are distinguished by their relative probabilities of recombination and thermal eviction.

From thermodynamic considerations the probability of escape per second is governed by the following exponential expression

$$p = s\,e^{-\frac{E}{kT}} \qquad (2.1)$$

where E is the trap depth or activation energy measured in electron volts (eV), k is Boltzmann's constant which relates the average energy provided by the lattice vibrations to the absolute temperature T, and s is a frequency factor. The frequency factor may be crudely thought of as the number of attempts to escape per second. The trap depth is the energy difference between the trap and the edge of the corresponding delocalised band.

Transitions may also occur that do not involve the delocalised bands for both electrons and holes. The transitions may occur as a result of either energy levels (representing traps and centres) within the same atom or if the defects responsible for the levels are situated close to each other in the host lattice; in this case the transition occurs by a process known as tunnelling (Garlick and Robinson, 1972; Visocekas, 1979; Visocekas *et al.*, 1976). An alternative possibility is that the charge carrier has to be elevated to a higher energy level before recombination can take place. Additionally for indirect transitions (ie. either band-to-centre or centre-to-centre transitions) the energy dissipated is much less than in direct transitions (ie. band-to-band transitions) and may thus be dissipated either radiatively (via photons) or non-radiatively (via phonons). Whether or not a material will exhibit luminescence following irradiation and the absorption of energy, depends upon the relative probabilities of the radiative and non-radiative transitions and is called the luminescence efficiency of a phosphor. The luminescence efficiency has been shown to be strongly temperature dependent in a variety of materials. The occurrence of the reduction of the luminescence efficiency as a function of temperature (for eg. 325°C peak in quartz samples; Wintle, 1975) is commonly referred to as thermal quenching.

2.2.2 Assumptions of first order kinetics

The simplest theoretical treatment of luminescence based on the energy band model is first order kinetics which was developed by Randall and Wilkins (1945a,b) to describe phosphorescence and TL observed in experiments on alkaline earth and zinc sulphides. This model considers the thermal eviction of a charge carrier from a single trap and subsequent recombination at a single centre (thereby assuming there are no adjacent traps where interaction may occur). Radiative recombination is assumed to be the dominant process having a higher probability than either retrapping or a non-radiative transition.

2.2.3 Solution for peak shape: TL

The kinetics governing eviction are those of thermal emission from the trap. Thus the intensity of TL at a particular temperature and time is equal to the product of a recombination probability constant C and the rate of change of the trap population dn/dt, thus

$$I(T,t) = -C\frac{dn}{dt} \tag{2.2}$$

The rate of release of charge carriers is the product of the trap population n and the probability function expressed in Equation 2.1. Therefore, combining Equations 2.1 and 2.2 gives the first order kinetic equation

$$I(T,t) = Csn\, e^{-\frac{E}{kT}} \tag{2.3}$$

For a linear TL ramp a uniform heating rate of β Ks^{-1} is employed, where

$$\beta = \frac{dT}{dt}$$

and

$$dt = \frac{dT}{\beta} \tag{2.4}$$

Combining Equations 2.2 and 2.3 and substituting an expression to include heating rate from Equation 2.4 gives

$$\frac{dn}{dT} = -\frac{s}{\beta} n e^{-\frac{E}{kT}} \tag{2.5}$$

which by separation of variables gives the integral expression

$$\int \frac{1}{n} dn = -\frac{s}{\beta} \int e^{-\frac{E}{kT}} dT \tag{2.6}$$

which may be solved for boundary conditions of temperature T and charge population n for time $t = t$, and initial conditions of T, n_o and $t = 0$ to give a solution for $n(T)$, thus

$$n(T) = n_o e^{-\frac{s}{\beta}\int_{T_o}^{T} e^{-\frac{E}{kT}} dT} \tag{2.7}$$

This expression can be substituted back into Equation 2.3 to give the peak shape expression for first order kinetics

$$I(T) = Csn_o e^{-\frac{E}{kT} + \frac{s}{\beta}\int_{T_o}^{T} e^{-\frac{E}{kT}} dT} \tag{2.8}$$

A simulated first order TL peak shape is shown in Figure 2.3. The peak is asymmetrical with the majority of the signal being emitted on the low temperature side of the peak maximum. The peak position depends on the variation of activation energy E and frequency factor s of the trap, and the heating rate of analysis β. The height of the peak depends on the charge population n. The kinetic simulation code is introduced in Chapter 3 (Section 3.1.2) and further details are described in Chapter 4 (Section 4.1.4). In real samples TL measurement produces a *glow curve* which comprises of a number of peaks which may be clearly defined, or be clustered together forming composite broad features or continua.

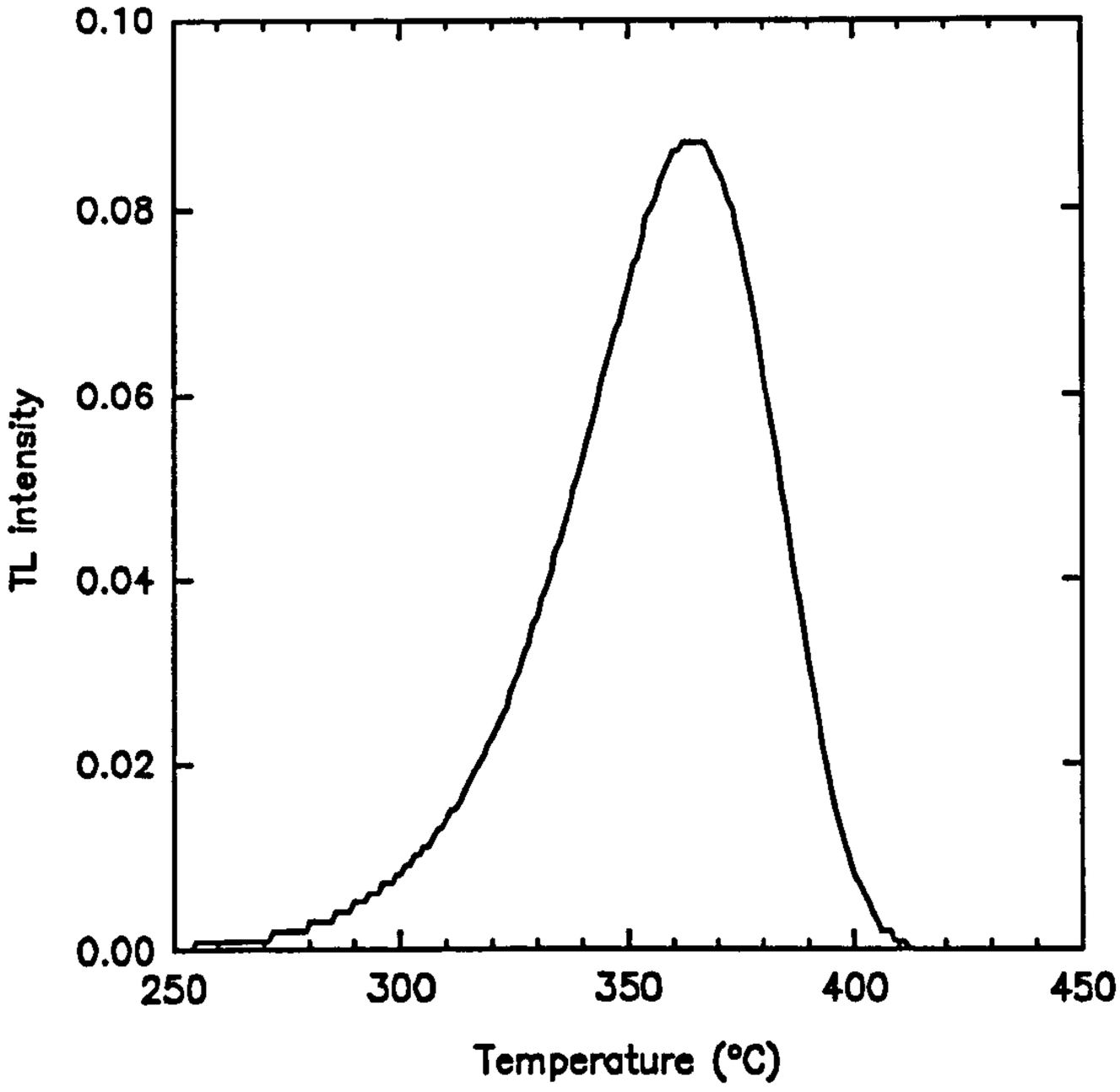

Figure 2.3 Simulation of a first order TL peak. E = 1.6 eV, s = 1.2 x $10^{12}s^{-1}$, b = 1.

2.2.4 Isothermal decay: Phosphorescence

The lifetime or meanlife of trapped charge carriers τ may be defined as

$$\tau = s^{-1}e^{\frac{E}{kT}} \tag{2.9}$$

and combining Equations 2.2 and 2.3 the rate of change of the trap population may be expressed as

$$\frac{dn}{dt} = -sn\,e^{-\frac{E}{kT}} \tag{2.10}$$

Therefore, from Equations 2.9 and 2.10 we have

$$\frac{dn}{dt} = -\frac{n}{\tau} \tag{2.11}$$

Separating variables and integrating with boundary conditions of n, n_o, t, t_o gives

$$\ln\left(\frac{n}{n_o}\right) = -\frac{t}{\tau} \tag{2.12}$$

Since I is proportional to n from Equation 2.3 it therefore follows that

$$I = I_o e^{-\frac{t}{\tau}} \tag{2.13}$$

This result is the first order expression for isothermal decay or phosphorescence. Figure 2.4 shows the increased rate of exponential decay of a single first order trap with increased isothermal temperature.

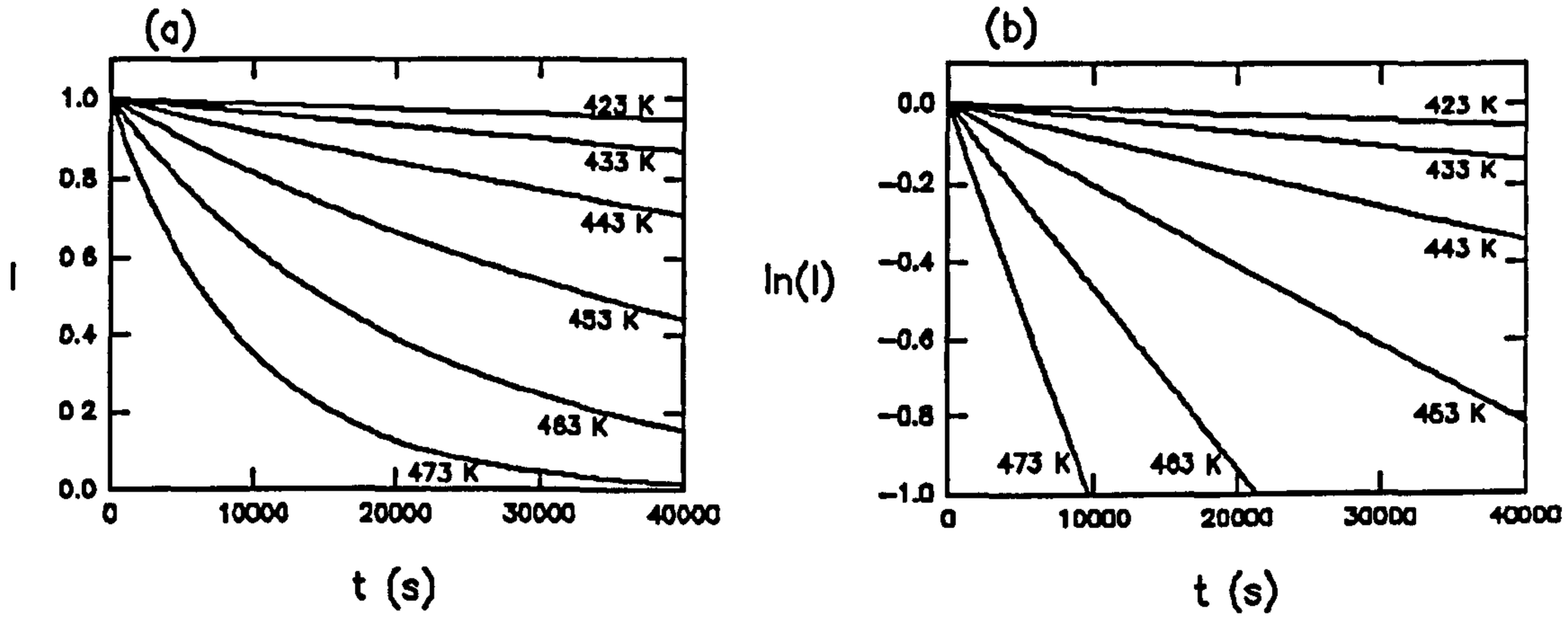

Figure 2.4 Simulated phosphorescence from a first order trap at different temperatures with parameters of $E = 1.5$ eV, $s = 10^{12}$ s^{-1} and $I = I_o = 1$ when $t = 0$. (a) Exponential decay, and (b) linear relationship with logarithmic intensity.

Equation 2.9 shows that the meanlife depends on the activation energy E, the frequency factor s, and the storage temperature T. Thus the survival of the TL signal depends on these 3 parameters. Additionally, the expression for isothermal decay (Equation 2.13) involves both storage temperature and time parameters. This equation implies the possibility of using TL as a monitor of thermal exposure and also shows the complementary relationship of temperature and time variables.

2.2.5 Relative retention for a three trap system

For a first order system containing two non-interacting TL peaks, the first one stable (τ_1, E_1, s_1) and the other metastable (τ_2, E_2, s_2), exposed to a temperature T, the fraction of the signal

remaining after a certain time t has elapsed, assuming no anomalous or athermal fading, can be expressed from Equation 2.13 for the stable peak as

$$\left(\frac{I}{I_o}\right)_1 = 1 \tag{2.14}$$

when $t << \tau_1$, and for the metastable peak as

$$\left(\frac{I}{I_o}\right)_2 = e^{-\frac{t}{\tau_2}} \tag{2.15}$$

Values for I_1, ($=I_{o1}$) and I_2 can be estimated from the natural TL signals and the ratio of I_{o2} to I_{o1} can be estimated from the second glow after reirradiation. It therefore follows that

$$\left(\frac{I}{I_o}\right)_2 = \frac{(I)_2}{(I)_1} \cdot \frac{(I_o)_1}{(I_o)_2} \tag{2.16}$$

If a second metastable peak is considered (t_3, E_3, s_3) the fraction of the signal remaining can be estimated in the same manner:

$$\left(\frac{I}{I_o}\right)_3 = \frac{(I)_3}{(I)_1} \cdot \frac{(I_o)_1}{(I_o)_3} \tag{2.17}$$

From the definition of the lifetime τ (Equation 2.9) it therefore follows that

$$\left(\frac{I}{I_o}\right)_2 = e^{-ts_2 e^{-\frac{E_2}{kT}}} \tag{2.18}$$

and

$$\left(\frac{I}{I_o}\right)_3 = e^{-ts_3 e^{-\frac{E_3}{kT}}} \tag{2.19}$$

The above two equations may be combined in the following manner with the time variable t cancelling out:

$$\ln\left(\frac{I}{I_o}\right)_3 - \ln\left(\frac{I}{I_o}\right)_2 = \frac{s_3}{s_2} e^{\frac{(E_2 - E_3)}{kT}} \tag{2.20}$$

Rearranging further gives the following solution for the temperature T, thus

$$T = \frac{E_2 - E_3}{k \ln\left\{\frac{s_2}{s_3}\left(\ln\left(\frac{I}{I_o}\right)_3 - \ln\left(\frac{I}{I_o}\right)_2\right)\right\}} \qquad (2.21)$$

Equation 2.18 (or Equation 2.19) gives the following solution for time t

$$t = -\ln\left(\frac{I}{I_o}\right)_2 s_2^{-1} e^{\frac{E_2}{kT}} \qquad (2.22)$$

The multipeak system described above is a new model that demonstrates it may be possible to obtain by experiment the temperature and time parameters of thermal exposure for a material that approximates the behaviour of first order kinetics. The system must contain a minimum of three traps (one stable and two metastable) giving three independent TL peaks from which glow curve measurements may be made of natural and artificial peak intensities, and E and s parameters. This model assumes that the eviction of charge carriers from the traps is the dominant process taking place during thermal exposure. The thermal event must therefore be necessarily short compared to the time associated with capture of charge by electron-hole pair production. Additionally the temperature range is limited - the higher the thermal event the less chance of a 3 peak system remaining.

This model may possibly be utilised for short thermal exposure monitoring using synthetic phosphors (eg. LiF, CaF_2), and might be useful for modern technological applications. Although there may possibly be scope for utilising peaks or integrated regions (cf. Durrani *et al.*, 1977) from natural phosphors such as quartz and feldspar, the main thrust of this thesis was the development of archaeological thermometry tools to measure relatively high temperature thermal events.

2.2.6 Trap filling

The first order model of Randall and Wilkins (1945a,b) only considers eviction and recombination of charge carriers. A treatment of charge capture or filling of traps is necessary

where competing processes of capture and eviction are taking place, in particular when capture becomes a significant factor with the rate of change of charge population not only dependent on the probability of eviction. This situation may occur, for example, where a body is heated for a long time at a low temperature.

From Equations 2.1 and 2.10 the rate of change of the trapped charge population for eviction is given by

$$\frac{dn}{dt} = -np \tag{2.23}$$

where the lifetime τ is the reciprocal of the escape probability p. The rate of trapping should be proportional to the concentration of free electrons in the conduction band n_c and to the concentration of unoccupied traps N - n where N is the concentration of traps and n is the concentration of the instantaneous trapped electrons. Thus for trapping,

$$\frac{dn}{dt} = n_c(N-n)A_n \tag{2.24}$$

where A_n is a proportionality factor and is referred to as either the (re)trapping probability (Chen and Kirsh, 1981) or the transition coefficient (McKeever, 1985). Adirovitch (1956) equates A_n as the product of the thermal velocity v of *free* carriers in the conduction band with the capture cross section σ of the trap, with units of m^3s^{-1}. Combining Equations 2.23 and 2.24 thus gives an expression for the rate of change of trapped charge concentration in terms of capture and eviction:

$$\frac{dn}{dt} = n_c(N-n)A_n - np \tag{2.25}$$

This is the same form as the second of three differential rate equations that Adirovitch (1956) used to explain the observed decays of phosphorescence in the general case. Separation of variables gives the following integral expression

$$\int \frac{dn}{A_n n_c N - (A_n n_c + p)n} = \int dt \tag{2.26}$$

and for initial conditions of $t = 0$ and $n = 0$ the solution for n (with the exponential relationship for the escape probability p: Equation 2.1) is given by

$$n = \frac{A_n n_c N\left(1 - e^{-t\left(A_n n_c + s e^{-\frac{E}{kT}}\right)}\right)}{A_n n_c + s e^{-\frac{E}{kT}}} \qquad (2.27)$$

Similarly a relationship involving n and n_o terms may be solved, and since I is proportional to n (from Equation 2.3) a mathematical treatment considering a 3 trap system may be pursued similar to section 2.2.5. However, a possible problem with models of this type is that it is difficult to determine the necessary parameters by independent physical means.

2.2.7 Continuous distributions of traps

The preceding sections have thus far dealt with hypothetical systems where there are a small number of discrete traps, giving rise to non-interacting luminescence peaks (cf. interactive kinetic solutions, for eg. Levy, 1985), which may or may not vary in activation energy. In many materials the picture is likely to be far more complex with individual traps themselves being distributed in energy. From phosphorescence measurements Randall and Wilkins (1945a,b) suggested uniform trap distributions in alkaline earth phosphors and exponential trap distributions in zinc sulphide phosphors. Results of experiments on amorphous Selenium have been interpreted as uniform and Gaussian distributions (Grenet *et al*, 1973); an exponential distribution is used by Owen and Charlesby (1974) to explain results from a wide variety of insulating solids; both discrete (Garofano *et al*, 1977) and distributed (Helfrich *et al*, 1964) traps have been proposed for anthracene. The feldspar materials analysed in this thesis (Chapters 3, 4, 5) display TL glow curves that suggest silicate systems with trap distributions. In Chapter 4 (Section 4.1.4) a non-interactive simulation of a system with continuous uniform first order components is utilised to account for the results of annealing experiments on a pure standard potassium feldspar.

2.2.8 Second and general order kinetics

Further complexity is introduced when it is found that the decay of phosphorescence is non-exponential. One reason for this may be a number of first order processes overlapping, so that at any one temperature several traps each with different activation energies are being sampled. An

alternative explanation, dealt with by Randall and Wilkins (1945b) concerns the possibility that there is equal probability of an evicted charge carrier either re-trapping or recombining. The following solutions for *second order kinetics* were formalised by Garlick and Gibson (1948) which correspond to the first order solutions of Equation 2.3

$$I(T,t) = Csn^2 e^{-\frac{E}{kT}} \tag{2.28}$$

and Equation 2.8

$$I(T) = Csn_o^2 e^{-\frac{E}{kT}}\left[1 + n_o \frac{S}{\beta}\int_{T_o}^{T} e^{-\frac{E}{kT}} dT\right]^{-2} \tag{2.29}$$

respectively.

Fuelled by observations on glow peak shapes not conforming to either first or second order kinetics, May and Partridge (1964) formulated similar expressions for *general order kinetics* where b (the kinetic order) is neither 1 nor 2:

$$I(T,t) = Csn^b e^{-\frac{E}{kT}} \tag{2.30}$$

$$I(T) = Csn_o^b e^{-\frac{E}{kT}}\left[1+(b-1)n_o^{b-1}\frac{S}{\beta}\int_{T_o}^{T} e^{-\frac{E}{kT}} dT\right]^{-\frac{b}{b-1}} \tag{2.31}$$

Although higher order kinetic solutions are not made further use of in this thesis, they are included here both for completeness of analytical solutions, and also to emphasise the increasing complexity that may be encountered in certain samples.

2.2.9 Summary

New multipeak models (Sections 2.2.5 and 2.2.6) developed from basic luminescence kinetics (2.2.1 - 2.2.4) have considered an idealised system in which there are three non-interacting and resolvable first order peaks which may be able to resolve temperature and time components. The

first of these (Section 2.2.5) considers the case where eviction of charge carriers from traps is the dominant process taking place during thermal exposure. The thermal event is therefore short compared to the time associated with capture of charge as a result of electron-hole pair production. Any dose accumulation or fading after the thermal event must not effect relative intensity of measured peaks (although fading corrections may be implemented). The second model (Section 2.2.6) considers the case where the thermal event is long enough and at a low enough temperature for the capture of charge to become significant.

Examples of materials where these models may be applicable are synthetic phosphors (LiF, CaF_2). However the temperature range is limited - the higher the temperature of the thermal event the less chance of a three peak system remaining. Additionally, in materials where the glow curve comprises of broad features or a continuum (eg. feldspars) as opposed to a number of distinct peaks, individual broad features or integrated regions may perhaps be treated in the same way as individual peaks.

The above models are based on the assumptions of first order kinetics. The actual behaviour in many systems may well be more complicated. Some of the complicating factors include transitions not involving delocalised bands, non-radiative transitions, proximity effects, continuous distributions of traps, and variation in retrapping and recombination probabilities. However, in many instances first order (or second order) kinetics provide good theoretical approximations to empirical data.

TL kinetics provides a general basis for interpreting results from silicate systems, and Chapter 4 will utilise these concepts to explain the nature of thermal exposure observed from feldspars. A combination of temperature and time parameters is expected from single systems on kinetic grounds, and the new multi trap system discussed above provides a theoretical means of separating both components.

2.3 Photostimulated luminescence (PSL)

In this stimulation process the energy required to evict charge carriers trapped at impurity and defect sites is provided by the absorption of light photons, and the corresponding luminescence signal is the emission of photons due to charge carrier recombination at luminescence centres.

A similar approach to TL kinetics can be considered for PSL, whereby the luminescence emitted is related to the eviction rate by optical processes. One such treatment proposed by Clark (1992) is summarised below:

The PSL analogy to the probability expression for thermal escape (Equation 2.1) is defined as

$$P(\lambda) = \Phi(\lambda)\sigma(T,\lambda) \qquad \textbf{(2.32)}$$

where $P(\lambda)$ is the probability of charge carrier eviction when stimulated by light of a wavelength $\lambda \pm \delta\lambda$ per unit time (s^{-1}), $\Phi(\lambda)$ the total incident photon flux at wavelength $\lambda \pm \delta\lambda$ per unit area per unit time ($m^{-2}s^{-1}$), and $\sigma(T, \lambda)$ the photon eviction cross section at wavelength $\lambda \pm \delta\lambda$ and temperature T (m^2). This expression thus proposed that the probability of photo-eviction of a charge carrier from a single trapping site was proportional both to the total photon flux incident upon it and also to the photo-eviction cross section.

Hence, as with thermal eviction, the total photo-eviction (analogous to Equation 2.23) is given by

$$Eviction\ Rate = n\,P(\lambda) \qquad \textbf{(2.33)}$$

Thus there are two eviction mechanisms for trapped charge carriers; thermal and photo-eviction. If photo-excitation is taking place at low temperatures with respect to the trap depth, eviction by optical processes will dominate; at higher temperatures with respect to the trap depth thermal eviction mechanisms dominate. As with thermal stimulation alone, equations describing combined optical and thermal eviction only hold true for a single trap and centre model and for no interaction between thermal and optical eviction.

Clark (1992) proceeded further to produce an expression for the detected intensity I due to photo-eviction alone:

$$I(\lambda) = \frac{Q(\lambda)A\Phi(\lambda)}{\mu(\lambda)}\left[1 - e^{-\mu(\lambda)x}\right]p_r n\sigma(T,\lambda) \qquad \textbf{(2.34)}$$

with the following definitions:

$Q(\lambda)$	=	detector quantum efficiency at wavelength λ
A	=	sample area (m^2)
$\mu(\lambda)$	=	photo absorption coefficient at wavelength $\lambda \pm \delta\lambda$
x	=	trapped charge carrier depth beneath the illuminated surface (m)
p_r	=	assumed fixed radiative recombination probability.

However, he noted that this expression did not take into account of the attenuation of emitted photons through the sample, and also the correction from 4π solid angle emission to 2π detection.

2.4 Heat transfer and thermal gradients

External heating or cooling of the surface of solids produces thermal gradients where temperature differences exist either between surfaces, or between a surface and the solid body. Energy is transferred between regions of different temperature in the form of heat. Conduction (by direct molecular communication without appreciable displacement of molecules) is the only mechanism by which heat can flow within opaque solids. Heating events involving archaeological structures or artefacts will produce gradient effects. It is therefore important to consider macroscopic solutions of heat conduction in a variety of solid shapes to give estimates of temperature distribution in both transient (unsteady - with variation of temperature with time) and equilibrium (steady) conditions, to provide a connection between thermal gradients and luminescence measurements.

2.4.1 General heat transfer equations

The conduction of heat in solids is dealt with comprehensively by Carslaw and Jaeger (1959) although in parts it is more accessible to the non-specialist by consulting authors such as Kreith (1965), White (1984), Ingersoll *et al.* (1954) and Incropera and De Witt (1990). The differential equation of conduction of heat in an isotropic solid whose thermal conductivity is independent of temperature is given by

$$\frac{\delta^2 T}{\delta x^2} + \frac{\delta^2 T}{\delta y^2} + \frac{\delta^2 T}{\delta z^2} - \frac{1}{\alpha}\frac{\delta T}{\delta t} = 0 \qquad \textbf{(2.35)}$$

which describes the variation in temperature T at any point $P\ (x,y,z)$ with time t, where α is the thermal diffusivity, given by

$$\alpha = \frac{K}{\rho c} \qquad \textbf{(2.36)}$$

with K the thermal conductivity, ρ the density and c the specific heat (at temperature T) of the solid. Another important concept is that of the flux of heat across a surface, which is the rate at which heat is transferred across any surface with cross-sectional area S at a point P per unit area per unit time. In an isotropic solid in the direction of increasing x normal to the surface the flux f_x may be expressed as

$$f_x = -K\frac{dT}{dx} \tag{2.37}$$

2.4.2 One dimensional steady state solution for a solid bounded by two parallel planes

This solid shape may also be considered as an isotropic slab or wall. If the flow of heat is perpendicular or normal to the parallel planes in the direction of x, with one plane at $x = 0$ and temperature T_1, and the other at $x = l$ and temperature T_2, then Equation 2.35 reduces to

$$\frac{d^2T}{dx^2} = 0$$

where the rate of change of temperature $dT/dt = 0$, and

$$\frac{dT}{dx} = constant = \frac{T_2 - T_1}{l}$$

From Equation 2.37 the flux at any point is given by

$$f = -\frac{K(T_2 - T_1)}{l} \tag{2.38}$$

and it therefore follows that the rate of heat transfer, dQ/dt, is given by

$$\frac{dQ}{dt} = \frac{KS(T_1 - T_2)}{l} \tag{2.39}$$

To apply this solution it must be assumed that the two planes are of such an extent that, so far as points well in the centre are concerned, the two surfaces may be supposed infinite. The temperature gradient and the heat flow do not vary with time and the cross sectional area over the heat flow path is uniform.

This may possibly be used to describe the heat transfer in some archaeological heating events but appropriate caution must be taken when assessing the ability of this solution to approximate real situations. For example, if a free-standing (ie. finite wall thickness) oven or pottery kiln (constructed, perhaps, from either stone or clay) is considered any periodicity or variation in internal firing temperature, external environmental temperature, or periods of non-use must be

assumed to be insignificant. Similarly this solution may approximate one dimensional heat conduction in a domestic hearthstone. Again temperature periodicity and periods of non-use must be assumed insignificant. For this case T_1 is the surface temperature, T_2 the temperature at a semi-infinite position, and the temperature is also T_2 when $x > l$.

2.4.3 One dimensional transient solution for a semi-infinite slab

As in the above discussion the term semi-infinite is used since a surface effect is being modelled with the temperature of the interior of the solid unaffected. From Equation 2.35 the linear flow of heat for transient conditions in the x direction is given by

$$\frac{\delta^2 T}{\delta x^2} - \frac{1}{\alpha}\frac{\delta T}{\delta t} = 0$$

Carslaw and Jaeger (1959) give the following solution to this equation with boundary conditions of constant (or surface) temperature T_1 at $x = 0$ and initial temperature T_o of zero. The temperature T_2 at a depth x from the surface at time t, is given by

$$T_2 = T_1\left\{1 - \frac{2}{\sqrt{\pi}}\int_o^{\eta} e^{-z^2} dz\right\} = T_1\, erfc(\eta) \qquad (2.40)$$

where

$$\eta = \frac{x}{2\sqrt{\alpha t}} \qquad (2.41)$$

and *erfc*(η) is the *complementary error function*. When $T_o \neq 0$ the following solution applies

$$\frac{T_2 - T_o}{T_1 - T_o} = 1 - \frac{2}{\sqrt{\pi}}\int_o^{\eta} e^{-z^2} dz = erfc(\eta) \qquad (2.42)$$

Coupled with estimates of temperature gradients (from observation of the extent of vitrification using SEM analyses which are calibrated with refiring experiments) this heat conduction solution has been used to estimate the maximum surface temperatures and duration of heating for fragments of furnace linings, tuyeres and crucibles used in early copper smelting (eg. Kingery and Gourdin, 1976; Tite *et al.* 1982, 1990). Again the usefulness of this solution must be viewed

with appropriate caution especially where the solid concerned is not a semi-infinite body. However, potentially there are many archaeological situations where this solution may be applied including the fire-cracked ore seams of early mines, the vitrified remains of hillforts, the stone troughs of burnt stone mounds, the walls of pottery kilns and furnaces (as above), and the stone hearths in houses.

2.4.4 Thermal properties

Table 2.1 lists examples of density, ρ, specific heat, *c*, diffusivity, α, at temperature *T*, and

Table 2.1 Thermal properties for different materials[a]

Material	**T**	**ρ**	**c**	**α**	**K ($Wm^{-1}K^{-1}$) at various temperatures (K)**					
	(°C)	**(kgm^{-3})**	**($Jkg^{-1}K^{-1}$)**	**($m^2s^{-1}x10^{-6}$)**	**273**	**400**	**523**	**600**	**773**	**800**
Rocks										
Granite	20	2640	800	1.4	3.0		1.5-2.0		1.0-1.5	
Sandstone	20	2200	740	1.7	2.8		1.5-2.5		1.0-2.0	
Quartzite	27	2640	1105	1.85	5.4		3.0-3.5		2.5-2.75	
Limestone	20	2400	860	1.0	2.0					
Marble	20	2650	1000	1.0	2.7					
Minerals										
Feldspars	100	2600	600	0.63						2.5±1.5
Quartz	20	2300	780	0.79		4.5-7.5		3.5-5.0		3.0-4.3
Earths										
Clay	20	1450	880	1.0	1.4					
Sand	20	1500	880	0.25	0.3					
Concrete	20	2300	880	0.49	1.0					
Bricks										
Common	20	1600	840	0.52	0.7					
Fireclay	20	2000	960	0.52	1.0					
Masonry	20	1700	837	0.46	0.7					

[a]Data: Touloukian *et al.* (1981), White (1984), Grigull and Sandner (1984), and Incropera and De Witt (1990).

thermal conductivity, K, for a variety of temperatures for a range of materials. The data emphasise the dependence on temperature of thermal conductivity and the difference in values between separated minerals and composite matrices.

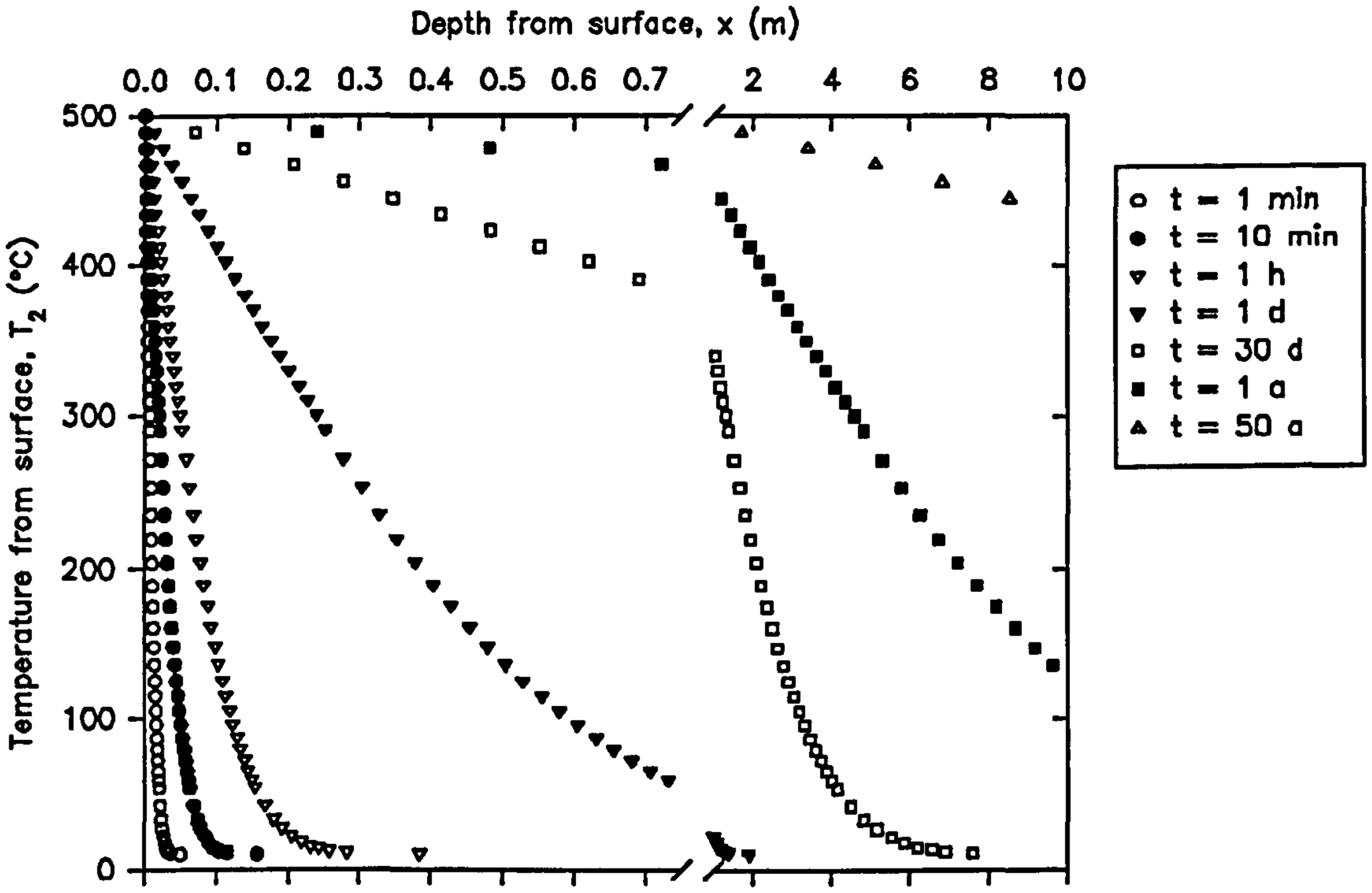

Figure 2.5 Simulation of the temperature distribution in an archaeological hearthstone.

2.4.5 Thermal gradients in archaeological structures and artefacts.

Using Equation 2.42 it is possible to simulate the temperature distribution heat transfer theory predicts in a solid body with a similar shape to an archaeological hearthstone. The assumptions made are that the heat conduction is one dimensional, the body is a semi-infinite medium, and the body has constant thermal properties. Figure 2.5 is a simulation of the distribution of temperature T_2 within a semi-infinite body at initial temperature T_o of 10°C with a temperature T_1 of 500°C heating the surface after time t. The value for α was taken as 1.15×10^{-6} m^2s^{-1} which mirrors the thermal properties of both sandstones and granites between about 250 to 500°C.

This figure demonstrates the rapid drop in temperature in the first few cm for short periods, and the progressive reduction in thermal gradient over longer periods. After 50 years of constant heating the temperature at 1.7 m is about 489°C, and the original temperature of the solid (10°C) is only maintained below about 255 m.

Similarly there are so called 'lumped capacitance' or convection solutions for spherical shapes which may be used to model the heat transfer in, for example, archaeological burnt stones which approximate spherical shapes.

The implications of heat transfer solutions for luminescence thermometry analyses will be discussed in Chapters 5, 6 and 7.

2.5 Heat transfer in TL experiments

Another area where a consideration of heat transfer is important is in the assessment of the temperature distribution between heater plate and sample in TL experiments. Accurate sample temperatures are a requirement in, for example, kinetic studies and inter-laboratory comparisons and not surprisingly this topic has created a fair amount of interest. Bonfiglioli, *et al.* (1959) used an empirical method of estimating sample temperature by constructing a calibration curve of thermocouple temperature (sensed at the heater strip) with the temperature of the emitting surface, as detected by the moment of melting of tiny pellets of pure metals (Bi, Pb, Zn) lying on the specimen itself. Investigations have also included heat transfer solutions to model temperature distribution (eg. Bonfiglioli, 1968; Gotlib *et al.*, 1984; Betts and Townsend, 1993; Piters, 1993). The following sections (2.5.1 and 2.5.2) mainly concentrate on those heat transfer solutions that have most recently been formulated (ie. Betts and Townsend (1993) and Piters (1993)) and they are used to provide estimates of the temperature distribution in the TL experiments conducted in this project.

2.5.1 Static temperature distribution in the heater strip

Modelling the temperature distribution in the heater strip allows an assessment of both the uniformity of the temperature in the area of the strip beneath the sample and also the difference

in average temperature moving away from the centre of the strip (where the heater strip temperature is sensed by a thermocouple) with an allowance for possible sample displacement. From Carslaw and Jaeger (1959) the equation of linear conduction in a thin wire of cross-section ω, perimeter p, with a coefficient of surface heat transfer h ($Wm^{-2}K^{-1}$), heated by an electric current of constant strength is given by

$$\frac{\delta T}{\delta t} = \alpha \frac{\delta^2 T}{\delta x^2} - \frac{hp(T_x - T_o)}{\rho c \omega} + \frac{jI^2}{\rho c \omega^2 \sigma} \qquad (2.43)$$

The first two terms on the left describe the linear flow of heat for transient conditions from the general equation of conduction of heat (Equation 2.35). The next term describes linear heat transfer at the surface (or the "radiation" boundary condition) with T_x and T_o (at position x) the temperature of the wire and medium respectively. The final term is the rate of generation of heat in the wire where I is the current in amperes, j is the number of calories in a joule ($j = 0.239$), and σ is the electrical conductivity of the wire.

The heat transfer in a heater strip may be considered as one of linear or one-dimensional conduction of heat since the strip is usually thin and therefore the temperature at all points of the section may be taken to be the same. Additionally the heat loss from the ends of the strip is minimised by using brass terminals which thermally anchor the end temperatures close to T_o. For steady state conditions (ie. $dT/dt = 0$) in a strip of length l, width b and thickness s, the solution given by Carslaw and Jaeger (1959) for the above equation is

$$T_x - T_o = \frac{w}{\mu^2 K}\left(1 - \frac{\cosh(\mu x)}{\cosh(\mu l/2)}\right) \qquad (2.44)$$

where w is a steady heating rate per unit volume delivered uniformly over the bulk of the strip given by

$$w = \frac{jI^2}{(bs)^2 \sigma} \qquad (2.45)$$

and

$$\mu^2 = \frac{2h(b+s)}{bsK} \qquad (2.46)$$

This is the form (Equation 2.44) of the solution given in Betts and Townsend (1993) which allows one to estimate the temperature difference (T_x-T_o) of a point in the strip distant x from the centre of the strip at time t.

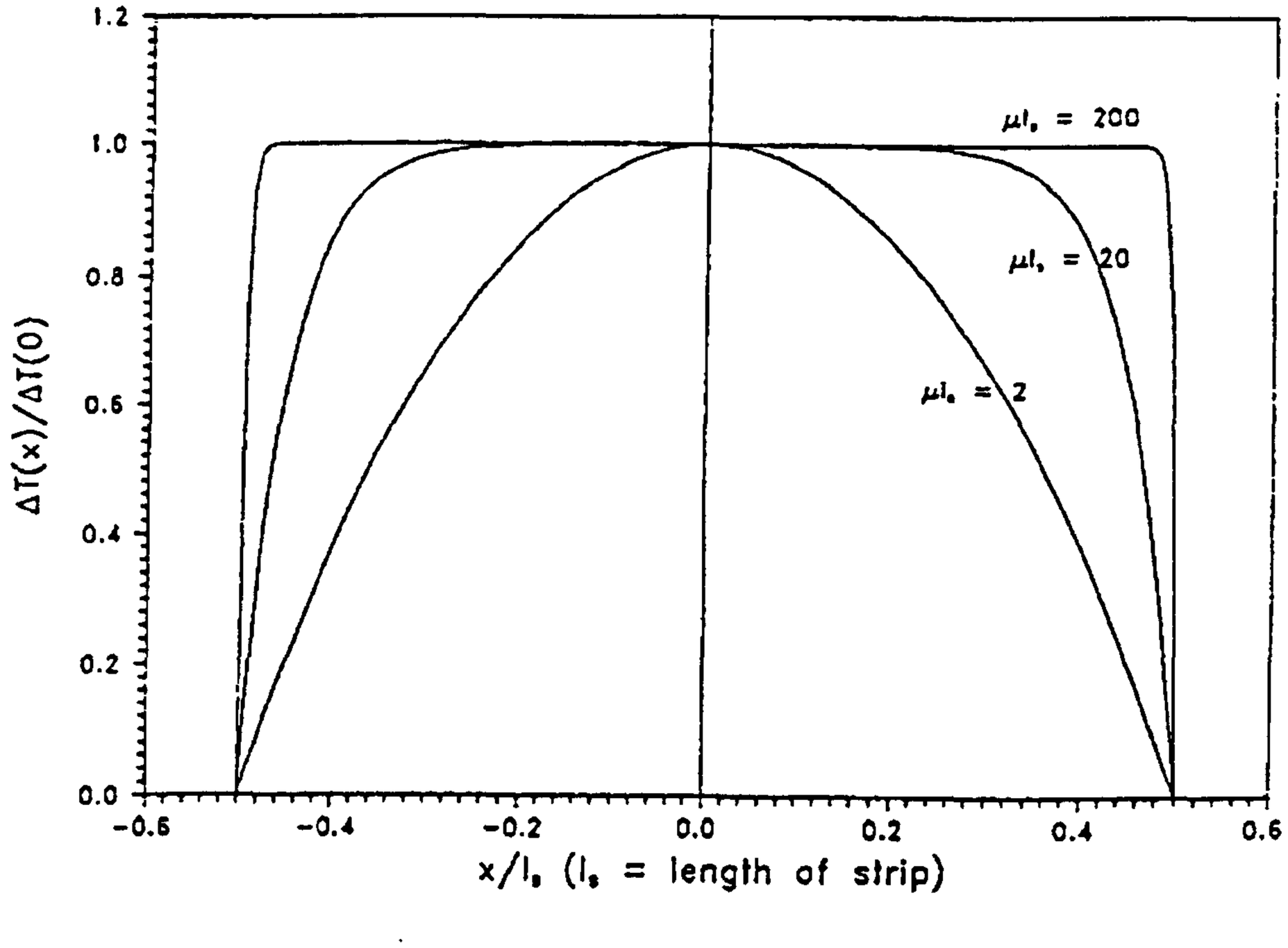

Figure 2.6 Distribution of temperature along a strip of length l_s, whose ends are held at a fixed temperature T_o while heat is supplied uniformly. $\Delta T(x)/\Delta T(0)$ is the ratio of static temperature difference between the point x and T_o and that between the centre and T_o. x is measured from the centre of the strip. μ is defined in Equation 2.46 and is a measure of the relative importance of the two routes of escape of heat (by conduction along the strip and by heat loss through the surrounding gas) $\mu = 0$ corresponds to no heat losses through the surrounding gas; $\mu = \infty$ corresponds to no conduction through the strip (from Betts and Townsend, 1993).

A graphical representation of how this solution operates is shown in Figure 2.6. $\Delta T(x) / \Delta T(0)$ is equivalent to T_x / T_o from Equation 2.44. Using the value for the coefficient of surface heat transfer h from Piters (1993) of 38 ± 20 $Wm^{-2}K^{-1}$, the error range of which encompasses estimates from Gotlib *et al.* (1984) (42 $Wm^{-2}K^{-1}$) and Betts and Townsend (1993) (25 $Wm^{-2}K^{-1}$), the value of μl_s for the system used in this thesis (b = 0.01 m, s = 0.002 m, l_s = 0.06 m, K (Inconel 600) = 14.8 $Wm^{-1}K^{-1}$) is about 3.3 ± 1.0 which agrees reasonably well with Betts and Townsend's estimate for their apparatus ($\mu l_s = 4$). For a 1 cm diameter disc positioned at the

centre of the heater strip 6 cm in length, Figure 2.6 suggests there is likely to be significant temperature gradients between the centre and edge of the sample disc.

Betts and Townsend also give the following solution which allows estimates to be made of how the average temperature (T_x-T_o) differs from the temperature at the centre of the strip (T_c-T_o) where the thermocouple is attached:

$$(T_c - T_o) - (T_x - T_o) = (T_c - T_o)\frac{\left(\frac{\sinh(\mu\delta/2)}{\mu\delta/2}\cosh(\mu\xi) - 1\right)}{\cosh(\mu l/2) - 1} \qquad (2.47)$$

which corresponds to a section of width δ whose centre is displaced from the centre of the strip by ξ. This equation can only provide a rough estimate when the temperature distribution is transient which will be the case when ramping. Static temperature distribution is discussed further in Chapter 3 (Section 3.3.3.1).

2.5.2 Heat transfer between strip-sample and sample-gas interfaces

The transmission of heat from the heater strip to the sample and surrounding gas takes place by conduction through metallic contact points (between heater strip and sample disc) and the exchange gas, and by radiation and convection. As well as the cooling effect of the gas it is very probable that temperature gradients exist across the sample, particularly when considering mineral inclusions (as opposed to fine grain powders) and TLD chips. Mathematical models to assess thermal lag between the heater strip and the top of the sample only consider transmission of heat by conduction and have all been formulated by considering the thermal boundary resistances and associated energy transfer at the top and bottom of the sample. The models of Betts and Townsend (1993) and Gotlib *et al.* (1984) consider thermal gradients through the sample with no lateral loss of heat. Whereas in Piters' (1993) model the sample is assumed to have a homogeneous temperature distribution but a simplified allowance is made (in terms of the total surface area of the sample) for the contribution of the sides of the sample to the heat transfer surface of the sample-gas interface.

Piters' model considers a finite sample (TLD-100) in imperfect contact with the heating element with a constant temperature T_g for the surrounding gas. The heat capacities of the contact layer (heating element-sample) and sample-gas interface are assumed to be zero, and the heat capacity C_s of the sample and the thermal conductance of the contact layer and sample gas interface (H_c and H_d respectively in WK^{-1}) are assumed temperature independent. The difference or lag in temperature ΔT between the heater strip (T_1) and the sample (T_2) with a steady heating rate β is estimated by the following equation

$$\Delta T = T_1 - T_2 = \frac{H_c C_s}{(H_c + H_d)^2}\beta + \frac{H_d(T_1 - T_g)}{(H_c + H_d)} \qquad \textbf{(2.48)}$$

The unknown parameters in this equation are C_s, H_c, H_d and T_g. The value of C_s can be calculated from the sample dimensions and data from the literature:

$$C_s = c_s \rho_s A_s l_s \qquad \textbf{(2.49)}$$

where A_s is the area of the top surface of the sample and l_s is the sample thickness. Piters estimates values for H_c, H_d and T_g empirically by observing the change in position of the glow peak maximum for LiF:Mg,Ti(TLD-100) peaks 2, 3, 4 and 5 (in terms of the heater strip temperature T_1) with variation in sample thickness and heating rate, and fitting the data to the following relationship

$$T_1 = T_2 + \frac{H_d(T_2 - T_g)}{H_c} + \frac{\beta C_s}{H_c + H_d} \qquad \textbf{(2.50)}$$

where

$$H_d = h_d(A_s + p_s l_s) \qquad \textbf{(2.51)}$$

with h_d the heat transfer coefficient ($Wm^{-2}K^{-1}$) of the sample-gas interface and p_s the perimeter of the sample.

Betts and Townsend's model considers the relative importance of the thermal boundary resistances at the top and bottom of a homogeneous infinite slab of material of finite thickness in terms of the heat transfer coefficients h_t (subscript t for top) and h_b (subscript b for bottom). The model is similar to that of Bonfiglioli (1968) in as much as it considers an infinite slab (no lateral heat loss). The heat conduction equation is solved to give the following solution

$$\Delta T(z,t)\Big/\beta\gamma_b = t\left\{\frac{(1+\gamma_t)-\gamma_t(z/l)}{(\gamma_b+\gamma_t+\gamma_b\gamma_t)}\right\} - \frac{l^2}{3\alpha}\left(3+3\gamma_t+\gamma_t^2\right)\left\{\frac{1+\gamma_b(z/l)}{(\gamma_b+\gamma_t+\gamma_b\gamma_t)^2}\right\} + \frac{l^2}{6\alpha}\left\{\frac{3(1+\gamma_t)(z/l)^2-\gamma_t(z/l)^3}{(\gamma_b+\gamma_t+\gamma_b\gamma_t)}\right\} \quad \textbf{(2.52)}$$

This equation allows one to estimate the temperature difference above ambient at a vertical point z in the sample after a time t ($\Delta T(z,t)$) subjected to a steady heating rate β Ks^{-1}. The sample has thickness l, diffusivity α, thermal conductivity K, and $\gamma_t = h_t l / K$ and $\gamma_b = h_b l / K$ are dimensionless parameters. A zero value of γ_t or γ_b indicates perfect insulation (no heat transfer) while an infinite value indicates perfect thermal contact.

Betts and Townsend give solutions of the above equation when $z = l$ (ie. ΔT at the top of the sample) and $z = 0$ (ΔT at the bottom) and make an important observation that for transparent samples luminescence will be emitted from all temperature regions varying with position z having the effect of broadening the observed glow peaks.

By making the assumption that the heat transmission is by gas conduction alone, the sample is perfectly insulated from its surroundings (ie. $\gamma_t = 0$; poor thermal conductivity of the thick gas medium), and additionally that there is imperfect contact between the strip and sample, Betts and Townsend's model simplifies to the following form (which they suggest is a reasonable description of what happens) for the temperature above ambient at the top of the sample:

$$\Delta T(l,t) = \beta t - \frac{\beta l^2}{2\alpha}\frac{(2+\gamma_b)}{\gamma_b} \quad \textbf{(2.53)}$$

The only unknown parameter here is γ_b and in a similar manner to Piters, Betts and Townsend suggest an empirical method to measure this by recording the variation in heater strip temperature at which a particular sample peak occurs at different heating rates and sample temperatures.

As shown by Betts and Townsend it follows from Equation 2.53 that the thermal lag between the strip and the top of the sample (T_l) is given by

$$\Delta T_{lag} = T_{strip} - T_l = \frac{\beta l^2}{2\alpha} \frac{(2+\gamma_b)}{\gamma_b} \qquad (2.54)$$

For perfect contact (ie. $\gamma_b = \infty$) there is still a lag of $bl^2 / 2\alpha$ which is half of the value approximated by Bonfiglioli (1968) (ie. bl^2 / α).

Table 2.2 lists various known parameters for a typical sample disc used in the laboratories at SURRC. The samples (in this example quartz: SiO_2) are dispensed on to stainless steel discs (AISI 316) which have been sprayed with a layer of silicon grease.

Table 2.2 Physical quantities for 100 µm quartz grains on a stainless steel disc

Parameter	Value	Units	Comment	Ref. / notes
A_{disc}	7.85×10^{-5}	m^2	Area of disc	
l_{disc}	2.5×10^{-4}	m	Thickness of disc	
p_{disc}	3.14×10^{-2}	m	Perimeter of disc	
ρ_{disc}	7.96×10^{3}	kgm^{-3}	Density of disc	(a)
c_{disc}	6.11×10^{2} (773 K)	$Jkg^{-1}K^{-1}$	Specific heat of disc	(a)
C_{disc}	0.095	JK^{-1}	Heat capacity of disc	
K_{disc}	21.5 (773 K)	$Wm^{-1}K^{-1}$	Thermal conductivity	(a)
α_{disc}	4.42×10^{-6}	m^2s^{-1}	Diffusivity of disc	
l_{quartz}	1×10^{-4}	m	Thickness of quartz grains	
ρ_{quartz}	2.65×10^{3}	kgm^{-3}	Density of SiO_2	(a)
c_{quartz}	1.2×10^{3} (773 K)	$Jkg^{-1}K^{-1}$	Specific heat of SiO_2	(a)
C_{quartz}	2.50×10^{-2}	JK^{-1}	Heat capacity of SiO_2	(b)
K_{quartz}	5 (773 K)	$Wm^{-1}K^{-1}$	Thermal conductivity	(a)
α_{quartz}	1.57×10^{-6}	m^2s^{-1}	Diffusivity of SiO_2	
l_{grease}	1×10^{-6}	m	Thickness of grease layer	(c)
ρ_{grease}	9.8×10^{3}	kgm^{-3}	Density of grease	(d)
c_{grease}	1.606×10^{3} (773 K)	$Jkg^{-1}K^{-1}$	Specific heat of grease	(d), (e)
C_{grease}	1.24×10^{-3}	JK^{-1}	Heat capacity of grease	
K_{grease}	0.16 (50 K)	$Wm^{-1}K^{-1}$	Thermal conductivity	(d)
α_{grease}	1.02×10^{-8}	m^2s^{-1}	Diffusivity of grease	

(a) Kaye and Laby (1986); (b) Assumes quartz grain layer behaves as a cylindrical slab the size of disc; (c) Estimated value; (d) Electrolube technical data sheet for aerosol silicon grease compound (SCO200H); (e) Linear extrapolation of specific heat capacity data.

Using the appropriate parameters from Table 2.2 for a blank stainless steel disc heated at 5 Ks^{-1} in a nitrogen atmosphere values for ΔT have been estimated using Betts and Townsend's simplified model (Equation 2.54). Assuming that the heat transfer mechanism at the bottom of the disc is by gas conduction alone, the gap between heater plate and sample is about 0.05 mm, and the temperature of the gas is 373 K, gives a value $h_b = K_{Nitrogen} / gap = 3.09 \times 10^{-2} / 5 \times 10^{-5}$ = 618 $Wm^{-2}K^{-1}$. With the further assumption that the density of the disc is independent of temperature over the analysis range, Table 2.3 lists values for ΔT allowing for variation in disc properties (K, c, α) with increase in temperature of the top of the disc (T_l). A simple approximation is also made of the effect of introducing heater plate to disc contact. This is achieved by treating the metal as a fraction of the gas layer which has a much higher thermal conductivity over the same gap. Accordingly values for the heat transfer coefficient h_b increase dramatically, with a corresponding decrease in ΔT. In comparison the value for h_b empirically derived by Betts and Townsend (h_b = 10 $kWm^{-2}K^{-1}$) gives a value of ΔT for the disc of 0.64 K when T_l is 773 K.

Table 2.3 Estimated values for ΔT using Betts and Townsend's model, with additional allowance for variation in sample contact.

T_l	K_{disc} [a]	c_{disc} [b]	α_{disc}	γ_b	ΔT	ΔT for increasing disc contact (K)		
(K)	($Wm^{-1}K^{-1}$)	($Jkg^{-1}K^{-1}$)	($10^{-6}m^2s^{-1}$)		(K)	1%	10%	100%
373	15	519	3.63	0.010	8.4	1.5	0.21	0.13
573	18.5	555	4.19	0.008	9.0	1.3	0.18	0.11
773	21.5	611	4.42	0.007	9.9	1.3	0.17	0.11
973	24	657[c]	4.59	0.006	10.6	1.2	0.17	0.10
1273	28.5	726[c]	4.93	0.005	11.7	1.2	0.16	0.10

[a] Thermal conductivity values for AISI 316 from Kaye and Laby (1986)
[b] Specific heat capacity values for 18 Cr / 8 Ni stainless steel from Kaye and Laby (1986)
[c] Linear extrapolation of specific heat capacity values

In a similar manner thermal lags across a sample disc have been estimated using Piters model (Equation 2.48). Table 2.4 shows the variation in ΔT for different heater plate temperatures (T_l) using both Piters estimates of the heat transfer coefficients [$h_d = 38 \pm 20$ $Wm^{-2}K^{-1}$ and $h_c = (2.3 \pm 0.2) \times 10^3$ $Wm^{-2}K^{-1}$ corresponding to thermal conductance values for a sample disc of $H_d = (3.28 \pm 1.73) \times 10^{-3}$ WK^{-1} (from Equation 2.51) and $H_c = (18.1 \pm 1.6) \times 10^{-2}$ WK^{-1} (assuming $H_c = h_c \times A_{disc}$) respectively], and also using a different value of the heat transfer coefficient for the

strip-sample interface (while keeping the same value for h_d) by assuming as before that the heat transfer mechanism at the bottom of the disc is by gas conduction alone (h_c taken as 618 $Wm^{-2}K^{-1}$ as in Table 2.3 above). Again a simple approximation has been made of the effect of introducing heater plate to disc contact, as well as an allowance for variation in the thermal conductivity of the disc material with variation in temperature. C_s is taken as 0.095 JK^{-1} (Table 2.2), and the temperature of the gas in the oven (T_g) as 373 K.

The values for ΔT estimated for a gas conduction mechanism with increasing disc contact for a heater strip temperature of 373 K are almost identical to the corresponding values estimated by the Betts and Townsend model (Table 2.3). For these values the heater strip and exchange gas are at the same temperature and therefore the contribution to the thermal lag due to heat loss to the surroundings (which corresponds to the second term on the right hand side of Equation 2.45: $H_d(T_1-T_g)/(H_c+H_d)$) is zero. The magnitude of the thermal lags estimated by Piters expression are mainly dependent on the difference between the temperature of the heater strip and exchange gas, and it would therefore be reasonable to suggest that having a constant surrounding temperature doesn't work for this model, particularly at higher heater strip temperatures. Additionally it is not unreasonable to envisage elevated exchange gas temperatures over the sample-gas interface compared with the temperature of the gas in the main body of the oven.

Table 2.4 Thermal lags estimated using Piters model, with additional allowance for variation in sample contact.

T_1 (K)	ΔT (Piters) (K)	ΔT (gas conduction) with increasing contact (K)			
		None	1%	10%	100%
373	2.5	8.6	1.7	0.20	0.10
573	6.1	21.3	3.3	0.38	0.19
773	9.7	33.9	4.6	0.52	0.26
973	13.2	46.6	5.7	0.64	0.32
1273	18.6	65.6	6.9	0.76	0.38

A TL sample resting directly on the heater plate can be treated in the same way as a disc if it is assumed to be either an infinite slab (eg. applicable to Betts-Townsend) or a finite squat cylinder (eg. applicable to Piters) of material. Taking values for a quartz sample from Table 2.2 above, the values used by Betts and Townsend for feldspar ($\alpha = 1 \times 10^{-6}$ m^2s^{-1}, $K = 2.5$ $Wm^{-1}K^{-1}$), and

the values for h_b and β used in Table 2.3, Betts and Townsends model estimates the ΔT values for varying sample thickness (with $T_l = 773$ K and $T_{gas} = 373$ K) listed in Table 2.5.

Table 2.5 ΔT values for varying thicknesses of quartz and feldspar samples from Betts and Townsends model, with additional allowance for variation in sample contact

l	ΔT for quartz varying sample contact (K)				ΔT for feldspar varying sample contact (K)			
(μm)	None	1%	10%	100%	None	1%	10%	100%
1	0.03	0.01	0.002	4.8×10^{-6}	0.02	0.01	0.002	7.5×10^{-6}
10	0.26	0.10	0.015	4.8×10^{-4}	0.20	0.11	0.02	7.5×10^{-4}
100	2.59	1.00	0.167	0.048	2.05	1.15	0.25	0.075
1000	27.4	11.5	3.10	4.8	22.7	13.7	4.75	7.5

Table 2.6 gives the corresponding values according to Piters model ($T_l = 773$ K, $T_g = 373$ K).

Table 2.6 ΔT values for varying thicknesses of quartz and feldspar samples from Piters model, with additional allowance for variation in sample contact (for feldspar ρ = 2600 kgm^{-3}, $c = 800$ $Jkg^{-1}K^{-1}$)

l	ΔT for quartz varying sample contact (K)				ΔT for feldspar varying sample contact (K)			
(μm)	None	1%	10%	100%	None	1%	10%	100%
1	23.2	9.2	1.4	0.003	23.2	13.2	2.7	0.006
10	23.5	9.3	1.5	0.03	23.4	13.4	2.7	0.06
100	26.3	10.5	1.6	0.35	25.5	14.6	3.0	0.67
1000	53.5	22.0	3.5	7.3	46.0	26.8	5.6	12.3

As with the calculations for sample discs Piters model has estimated far higher values for quartz and feldspar samples than the Betts-Townsend model. Even when Piters own estimates for h_c and h_d are used his model still estimates thermal lags for quartz and feldspar of 6.5-7.5 K for 1-100 μm thickness and 13-16 K for 1000 μm thickness ($T_l = 773$ K, $T_g = 373$ K). The estimates from Betts and Townsends model confirm Betts *et al.* (1993) assumption that temperature gradients across fine grain powders (1-10 μm) are negligible, but for thick TL samples (eg. 100 μm) temperature gradients become significant unless one allows some partial solid contact. In comparison with Piters model Betts and Townsends value for h_b estimates ΔT values for both quartz and feldspar around the 10% sample contact region.

In general both models give higher values for feldspar than quartz in the approximate calculations for increasing sample to disc contact. This is principally due to the lower value for thermal conductivity used for feldspar. However, this is mainly a means to highlight the fact that there may be slight variations depending on sample properties (eg. Touloukian *et al.* (1981) give the following thermal conductivity values at 800 K in $Wm^{-1}K^{-1}$: Feldspar group 2.5 ± 1.5; Pure quartz 3 - 4.5; Quartzite 2 - 3; Granite 1.5; Sandstone 1.5 - 2; also see Table 2.1).

If we consider a single grain of feldspar or quartz as a cube with one of its surfaces resting on the heater plate, Betts and Townsends model would predict exactly the same ΔT values for the same sample thicknesses. However, since Piters model takes into account the heat loss to the sides of the sample the values for ΔT are higher due to the ratio of the top surface to the sides decreasing. Accordingly for a 1 μm grain the value for feldspar or quartz would increase from about 6.5 to 30.5 K using Piters estimates of the heat transfer coefficients as above.

2.5.3 Summary and discussion.

Heat transfer solutions can allow estimates to be made of the temperature distribution in solids which approximate the shape of many archaeological and modern artefacts and structures that have been exposed to heat. Measurements of firing conditions within the body of a structure, along a temperature gradient, may thus be corrected to estimate surface conditions. The implications of thermal gradients within fired structures will be discussed further in Chapters 5, 6 and 7.

Heat transfer solutions may also be applied to estimate temperature distribution in the heater strip, and between the heater strip and sample in TL experiments. In kinetic analyses and laboratory intercomparisons accurate sample temperature determination is a requirement. This is also important in TL thermometry analyses, although this may be avoided by calibrating a thermometry system to an external furnace. The estimates of thermal lags from heat transfer models will be compared to the results of an empirical assessment of the thermal lag between the heater plate and sample for a typical measurement geometry in Chapter 3 (Section 3.3.3).

Chapter 3: Instrumentation and measurement methods

This chapter describes the instrumentation used in the project to measure TL and PSL. Sections include details of the TL measurement and recording system, instrumental developments to enable measurement of TL above 500°C, an investigation into the accuracy of absolute TL temperature measurement, and details of a PSL excitation spectrometer and pulsed IR diode array.

3.1 TL measurement

TL signals recorded during this project were made on instrumentation designed and constructed at the Scottish Universities Research and Reactor Centre (SURRC). The instrumentation was similar to earlier apparatus (for eg. those developed at the Oxford laboratories: Aitken, 1974, 1985; Fleming, 1979) but as with modern equipment signal detection had a digital basis, with computerisation developed from previous systems (Sanderson, 1982, 1983). In the first few months of the project initial annealing experiments to investigate the behaviour of a pure feldspar under controlled conditions (discussed in Chapter 4, Section 4.1) were carried out using TL apparatus or a *TL reader* interfaced to an Apple IIe computer. For the remaining experimental period results were obtained using a similarly constructed TL reader linked to a PC. A schematic diagram of the latter TL system and computer interface is shown in Figure 3.1. The basic elements shown here are a TL oven to provide linear heating of samples, a sensitive photomultiplier tube (PMT) to detect light emission, an equipment housing for power supplies and temperature feedback system, and a PC with dedicated software linked to Analogue to Digital Converter (ADC) and Multi-Channel Scalar (MCS) cards for heating system control and signal recording respectively.

3.1.1 TL oven and heating system

The TL oven consisted of an aluminium chamber containing a sample heater plate. The plate was heated resistively in a linear fashion with the temperature measured by a Chromel-Alumel (Type K) thermocouple spot welded to the underside. Interference with the thermocouple

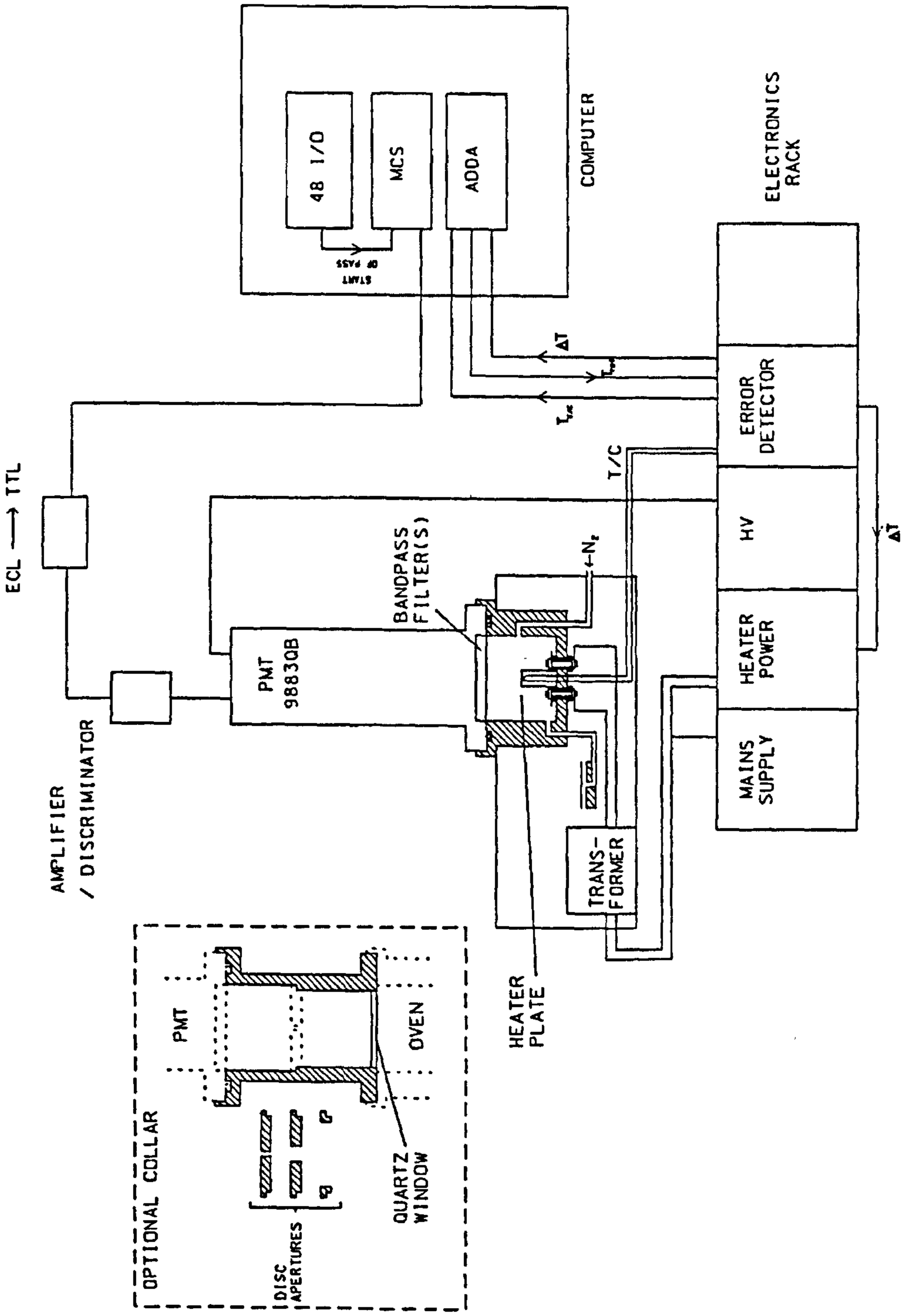

Figure 3.1 Diagram (semi-schematic) of TL apparatus

signal may be produced if a voltage drop is created across the wires at the hot junction as a result of the current passing through the heater plate. This effect was minimised with the use of a fine grade of wire (∅ 0.125 mm) and by bringing the hot junction and the plate together at a single spot weld. Additionally thin thermocouple wires were used to conduct less heat away from the plate to enable greater accuracy in temperature sensing. The thermocouple signal was amplified by a cold junction compensating thermocouple amplifier (Analog Devices AD595AQ, ± 3°C calibration accuracy). The amplifier is a linear device and therefore the non-linearity of the output arising from the thermocouple response must be corrected for accurate heater plate temperature measurements (see section 3.3.1). The heater plate was made into a strip (10 x 70 mm) from a 0.2 mm foil of heat resisting nichrome alloy (Goodfellow metals, Inconel 600 - Ni72/Cr16/Fe8).

The plate was shaped so that thin (0.25 mm) stainless steel sample discs (∅ 10 mm) rested horizontally on the middle cm^2 (with the thermocouple welded centrally beneath); to either side the strip was vertical and secured at the base of the oven at brass terminals. The n-shape was similar to the heater plate design employed in other readers (Bøtter-Jensen and Bungaard, 1978; Bøtter-Jensen, 1988; Galloway, 1990, 1991). This was preferable to a flat horizontal plate or strip used in earlier (eg. Tite and Waine, 1962; Aitken, 1974, 1985; Fleming 1979) and later (eg. Bailiff and Younger, 1988; Vana *et al.*, 1988) systems as the area of heater plate material within the light path was smaller, hence the background signal due to incandescence (black body) was reduced. Additionally this design enabled accurate positioning (within about 0.5 mm) of sample discs on the plate (so that the centre of the disc was directly above the thermocouple) improving disc-to-disc reproducibility in terms of the variations in thermal lag between the temperature of the heater plate and sample (cf. sample overhang and off-centre problems discussed by Betts *et al.*, 1993; Betts and Townsend, 1993; and sections 2.51 in Chapter 2 and 3.3.3.1 in this Chapter). Problems associated with variable disc position may also be minimised with the use of computerised multi-sample automatic TL systems (eg. Bøtter-Jensen and Bungaard, 1978; Bøtter-Jensen, 1988; Bailiff and Younger, 1988; Galloway, 1991; Henzinger *et al.*, 1994) allowing complex procedures of preheating, dosing and read-out without removing any of the sample discs. A further advantage of the n-shape geometry employed in this system was that it compensated for much of the thermal expansion and contraction, thereby reducing buckling or warping (as noted by McKeever (1985) and Betts and Townsend (1993)) without the need for

flexible clamps, ridged sides and central clamps (made from thermal insulating material) employed to combat this problem. These advantages far outweighed the difficulty of achieving a perfectly flat cm^2 surface for sample discs.

A linear heating-ramp was generated using a temperature feedback system or servo system similar in operation to the heating circuits described, for example, by Tite (1966) used in much of the early equipment in the TL laboratories in Oxford, and in many TL reader systems today. The SURRC PC system was controlled by a program which according to the desired heating or ramp rate addressed the ADC card (FPC-011A, PC ADDA-14) to send out a linearly increasing voltage, referred to as the reference voltage (or reference temperature). The error detector module compares the reference voltage with the output from the thermocouple amplifier. The difference or error (also referred to as the servo-lag or ΔT_{servo}) between the reference and thermocouple voltages was amplified and fed to a phase angle trigger unit, which in turn controlled the fraction of the cycle for which a thyristor module conducted mains current to the heater plate. The heating system was designed to enable fine adjustments to be made to the comparator circuitry in the error detector (while simulating thermocouple input from an external mV source (Time Electronics Ltd)) and the gain of the phase control and error signal. An accurate heating ramp was obtained with correctly balanced thermocouple and reference voltages, whereas linearity and smoothness of heating were obtained by matching the power requirements of the heater to the power supplied in response to a given temperature error. A slight disadvantage of this system (although for the majority of applications not a significant problem) was that the heating circuit had a tendency to surge for low values of ΔT_{servo} due to a slight over compensation in power delivery, a problem which could perhaps be overcome with the use of a non-switching continuous full sine wave heat generator (eg. Bøtter-Jensen and Bungaard, 1978; Bøtter-Jensen, 1988; Galloway, 1990, 1991).

The temperature of the heater plate could also be raised manually by switching the reference to an internal voltage supply which was varied using a 10-turn potentiometer set with a front panel mounted dial on the error detector module. The oven was operated in a oxygen-free nitrogen atmosphere (OFN) to suppress spurious luminescence (eg. triboluminescence, chemiluminescence, etc.) which has been attributed or indirectly linked to the presence of oxygen and / or water vapour (eg. Schulman *et al.*, 1960; Nash *et al.*, 1965; Aitken *et al.*,

1968a; Sutton and Zimmerman, 1977; Fleming, 1979; Aitken, 1985) in the oven chamber and / or adsorbed on the surface of sample grains. Argon has also been favoured as a suitable oven atmosphere and Betts *et al.* (1993) have suggested the use of helium in favour of other exchange gases due to its relatively high thermal conductivity. However, Spanne (1984) has suggested that the tube vacuum can be spoiled by helium penetration if the PMT housing is not adequately sealed. The flow of nitrogen into the oven passed directly over the heater plate and sample disc. A heater plate made from a thin foil of material cooled fairly rapidly in a steady nitrogen flow, although an increase in flow rate was extremely effective for fast cooling.

3.1.2 Detection and recording of TL

The photomultiplier tube (PMT) used was a Thorn EMI 9883QB fast single photon counting detector with a bialkali photocathode and a quartz (fused silica) end window, enabling unfiltered optical detection from about 200 nm to around 600 nm (although observations at SURRC suggest the detection at the long wavelength end continue at a very low level out to about 830 nm), with a peak quantum efficiency (the fraction of photoelectrons emitted per incident photon at a given wavelength) of 27% at about 350 nm and a nominal gain of 6.7×10^7 at 2150 V. The dark count is reported as being typically 200 cps at this EHT rating although occasionally tubes are produced which have a much lower dark emission; the dark counts from a variety of tubes at the SURRC have ranged from as low as about 15-20 cps up to 150-200 cps. The dark counts occur from the combined effects of single Photoelectron equivalent pulses (thermal electrons) and multi-Photoelectron equivalent pulses (Cosmic radiation, natural radioactivity in the window, and afterpulses). The thermal electrons contribute the majority of the dark counts and for low level applications significant reduction can be achieved by cooling the photocathode (data from THORN EMI, 1986). The PMT was operated in pulsed or photon counting mode with the EHT supplied by a Brandenburg negative high voltage unit (2479N) located in the electronics rack. To find the optimum PMT operating voltage the signal or light count from a low level light source (^{14}C doped plastic scintillator; NE102 with peak emission at 423 nm) and dark count are recorded over a range of EHT settings. The optimum voltage maximises the signal to noise ratio while minimising the dark count and preferably lies on the counting *plateau* to give values independent of small changes in applied voltage or PM gain. An example of the

plateau region for the 9883QB PMT is shown in Figure 3.2. The tube was operated at 1830 V with a corresponding dark count of about 30 cps.

A variety of glass filters (supplied by Schott, Kopp Corning, etc.) could be placed in a filter cup in the base of the tube in front of the PMT window to alter the detection band, and / or to reduce the light intensity. Rather than using neutral density filters, a preferable method of attenuating a signal was achieved with the introduction of an aluminium collar between the sample oven and tube (see Figure 3.1), into which could be inserted a variety of spacer discs with different circular apertures (Table 3.1). The use of a collar was advantageous because the integrity of the transmitted spectrum was retained which is not the case with neutral density filters particularly in the short wavelength region (< 400 nm). Also glass filters could be temporarily inserted into the collar to investigate their performance which negated the need to dismantle the PMT. A Thorn EMI amplifier discriminator unit (C604-A) was used to convert voltage pulses from the PMT to fast ECL logic pulses (-0.7 to +1.7 V) and the upper and lower thresholds on the discriminator were set to remove large electronic spikes and smaller noise pulses respectively. An ECL to TTL translator chip (MC10H125, Motorola) converted the

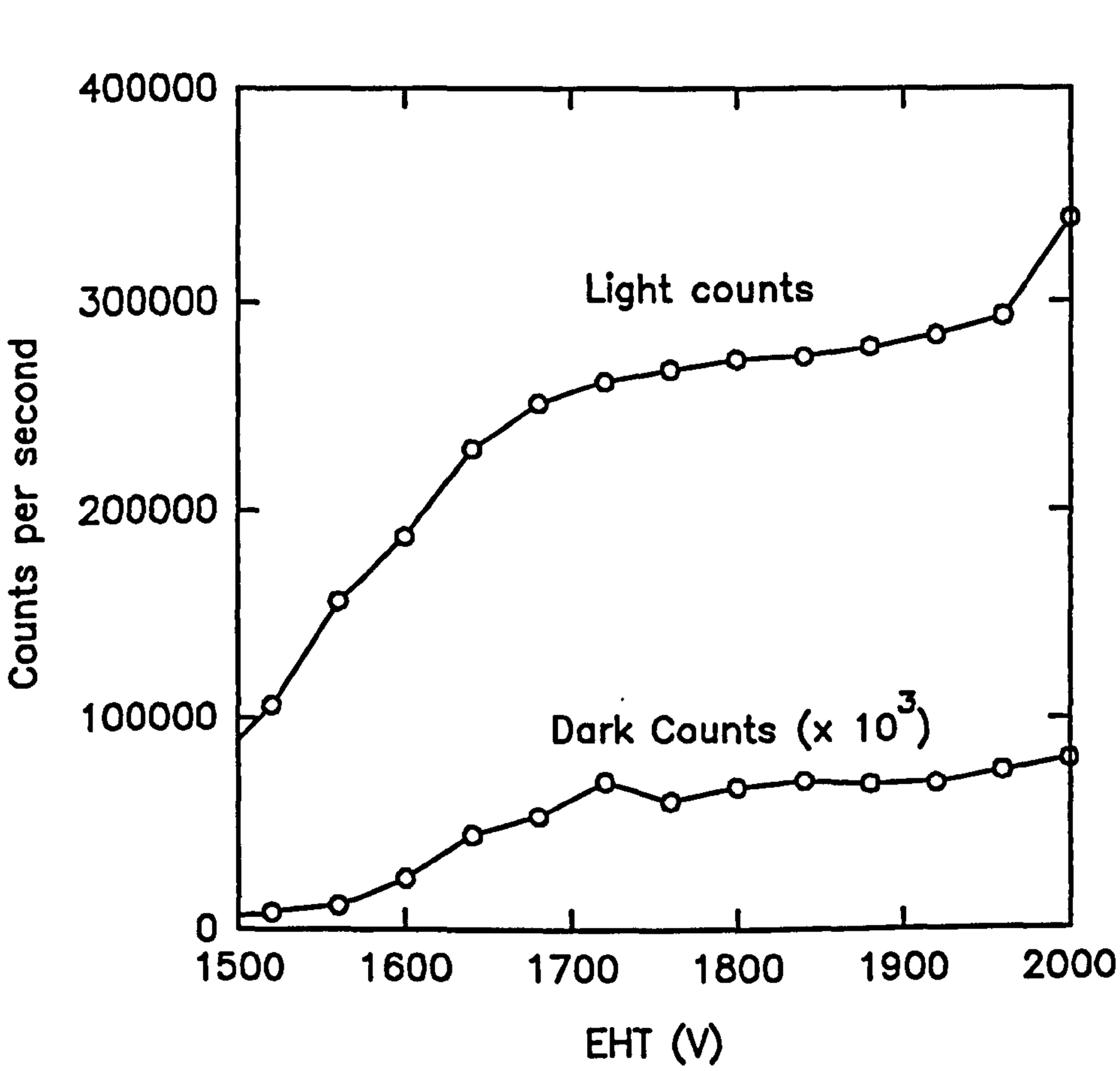

Figure 3.2 Light and dark counts for 9883QB with a 2 mm BG39 filter

signal to TTL logic pulses (0 to +5 V) which were in turn recorded on a MCS card (EG&G ORTEC ACE MCS).

The TL software was run from within the MCS emulation software. Read-out was initiated by running a DOS batch file which set the following on the MCS card; multi pass mode with successive passes overwriting the previous pass, start of pass trigger to external, channel dwell time according to the desired heating rate, number of passes (pass count), number of channels per pass (pass length). The batch file then activated the card and ran the TL program. Alternatively the MCS card was manually set up and the TL program entered. At this stage although activated the MCS card did not begin a scan or sweep until it had received a start of pass trigger (a rising TTL edge supplied by the I/O card). This was controlled by the program and synchronised with the start of the temperature ramp software loop (supplying reference voltages to the temperature controller via the ADDA card). During a scan the contents of each channel were read after the next channel commenced.

Table 3.1 Attenuation factors for various spacer collar apertures

Aperture diameter (mm)	**Light count (n = 30) Mean ± 1σ (cps)**	**Attenuation factor**
- (no collar)	174588 ± 432	1.0
50 (no spacer disc)	73266 ± 334	2.4
8	6024 ± 268	29.0
4	1460 ± 41	119.5
2	348 ± 19	501.5

The PC system TL software was based on the software developed by David Sanderson for the Apple IIe system, and it was developed from software (written by a former PhD student (Clark, 1992)) for system control of the SURRC excitation spectrometer. The software was written in Borland Turbo basic and was designed as an integrated package with the aim of combining data acquisition and manipulation / analysis without having to leave the program environment. Data was stored in an ASCII format with a header for sample and instrumental details. The software performed the following functions; data input / output to disk, data calculations - arithmetic combination and manipulation of data (including integration, differentiation and smoothing), acquisition (TL ramp, ramp and hold, ramp and reheat, change ramp delay to alter heating rate),

plot (on screen with cursor control and HPGL output to file or plotter), isothermal decay analysis, arrhenius transform, linear regression analysis, statistical analysis, data conversion for 3D plotting by UNIRAS, simulation (TL peak shapes and kinetic parameter calculations), and DOS commands (type, print, rename, delete, directory, dosshell).

3.1.3 Specifications and performance

The following table summarises the instrumental specifications and performance.

Table 3.2 Specifications and performance

Specification	Value	Comment
Heating rates	3 - 20°Cs^{-1}	This range of heating rates is possible with the same ramp delay setting (changing the dwell time on the MCS for each heating rate). Lower heating rates are possible by altering the ramp delay.
Linearity of PMT	1.6 x 10^7 cps	Upper limit of PMT linearity
Stability of PMT	206978 ± 736 (1σ) cps	9883QB with 7-59 & KG1 filters. Mean of 15 light count readings taken between 12.03.91 and 19.02.92.
Stability of heater	16.0 ± 0.8 (1σ)°C	Mean of 270 servo-lag or ΔT_{servo} readings at a reference temperature of 700°C taken from 03.09.92 to 04.02.94.[a]

[a] Refers to measurements made subsequent to instrumental developments detailed in section 3.2.2.

3.2 Measurement of TL signals above 500°C

The involvement of the TL dating laboratory in November 1991 in a project carried out by Glasgow University Archaeological Research Division (GUARD), who were investigating two burnt stone mound sites at Crawford, provided the opportunity to undertake some exploratory thermometry work on burnt stone mound material (for further details of the TL thermometry analyses on this material see Chapter 5, Section 5.2). TL measurements up to glow temperatures of 500°C on alkali feldspar mineral separates showed no detectable remnant geological signals from comparison of first and second glow curves from additive dose runs. Analysis of the glow curves from the 150 archaeological samples previously submitted to the TL dating laboratory confirmed this observation for a range of thermally exposed materials (including prehistoric ceramics, burnt stones, burnt clay and daub, and hearthstone fragments),

the vast majority of which showed no evidence of geological TL. Therefore it was necessary to develop the instrumentation to enable the extension of TL measurement above 500°C. This is complicated for two reasons. Firstly because many TL readers, either commercial or in-house systems, are either not designed or simply not able to heat to temperatures much exceeding 500-600°C as this is not a requirement for conventional dating / dosimetry systems. Secondly, and the main reason that TL above 500°C is not often attempted, there is the advent of intense black body radiation or incandescence from the heater plate material at higher temperatures swamping the luminescence signal. Thus to enable measurement of TL above 500°C it was necessary to develop oven and detection capabilities. The following sections (3.2.1, 3.2.2, 3.2.3) discuss possible methods to achieve this and the developments which were followed through in this research.

3.2.1 Discussion of possible methods for > 500°C TL

3.2.1.1 Restricting PMT detection to ultraviolet wavelengths

It is possible with the use of suitable filters to restrict the wavelengths reaching the PMT to the ultraviolet thereby reducing the effect of the greatly enhanced infra-red to red emission at high temperature. This was carried out successfully by Valladas and Valladas (1978) with the use of a 10 mm thick Schott VG11 filter (Specivex type 325; Aitken, 1985), which has a maximum transmission of 50% at 325 nm (with a cut off at about 400 nm), and the transmission at 700 nm is reduced from 15% at a thickness of 2 mm to less than 10^{-4}. Using the oven designed by Georges Valladas (Brou and Valladas, 1975), they reported it was possible to measure TL to 650°C without significant black body emission.

This set up was principally investigated to address the problem of anomalous or athermal fading (Wintle, 1973, 1977), and as with phototransfer methods (eg. Bailiff, 1976; Bowman, 1979) Aitken (1985) suggests this is a plausible avenue to explore since theoretically the probability of fading occurring by a mechanism such as tunnelling (Garlick and Robinson, 1972; Visocekas, 1979; Visocekas *et al.*, 1976) should be lower for deep traps because the energy barrier to be penetrated is higher. Valladas and co-workers (Valladas *et al.*, 1979; Guérin and Valladas, 1980) successfully dated plagioclase feldspars (labradorite) extracted from lava samples from

the Chaîne des Puys in the Massif Central of France, similar to the material from which Wintle (1973) first observed anomalous fading resulting in dates too low by an order of magnitude.

Ultraviolet filters have also been used by research groups in India to detect high temperature TL from both natural and synthetic calcium fluoride (fluorite). Sunta (1979) used a Chance Pilkington OX1 and HA3 combination (with an asbestos thermal radiation mask; see section 3.2.1.2 below) and recorded TL up to 650°C with a slow heating rate of 25°Cmin^{-1}. El-Kolaly *et al.* (1980) also used an OX1 filter but with a higher heating rate of 17°Cs^{-1} recorded TL up to 750°C. With a similar experimental arrangement to Sunta (1979), Ganguly and Kaul (1984) have increased the measurement temperature to 900°C with a heating rate of 15°Cs^{-1} detecting peaks at 720, 790 and 845°C.

3.2.1.2 Masking and restricting the light path

The intensity of the black body emission may be reduced by placing a mask in the form of a disc with a small circular aperture between sample and photomultiplier. A thermal radiation mask was used by Sutton and Zimmerman (1976) for exactly this purpose when recording TL from individual zircon grains. Their mask was a brass disc with a 2 mm aperture which effectively shielded the photomultiplier from all hot parts except the zircon grain and the 200 µm aluminium stub disc on which it sat. This enabled measurement of glow curves up to 475°C using a PMT with a bialkali photocathode (EMI 9635QA) without the need for the usual filters to reduce the black body component. A similar thermal radiation mask made from asbestos was used by Sunta (1979) to assist the measurement of high temperature peaks in natural calcium fluoride.

Additionally there are a number of ways of restricting the light path thereby assisting in the elimination of large signals due to black body radiation. McKeever (1985) lists a number of examples including reflecting cones, lenses (eg. Templer and Smith, 1988), fibre optics and light guides (eg. Aitken, 1985).

3.2.1.3 Emissivity of heater plate material

The spectral emissivity ε_λ of a body for a given wavelength is given by Kirchhoff as being equal to its spectral absorption factor a_λ for the same wavelength. This law stems from a definition of spectral emissivity given by

$$\varepsilon_\lambda = \frac{a_\lambda E_\lambda \delta\lambda_{specimen}}{E_\lambda \delta\lambda_{black\ body}} \qquad (3.1)$$

where $E_\lambda\delta\lambda$ is the energy radiated per m^2 per second in a narrow band of wavelengths between λ and $\lambda + \delta\lambda$, E_λ is the emissive power in the region of λ, and both the specimen (or body) and the black body are in equilibrium with an enclosure at temperature T. The spectral absorption factor a_λ is the fraction of radiation that the specimen absorbs in the region of λ which is analogous to the total absorption factor a (ie. for all wavelengths) in the following expression for the total emissivity;

$$\varepsilon = \frac{a E_{specimen}}{E_{black\ body}} \qquad (3.2)$$

which is a ratio of the total power radiated per m^2 by a given specimen compared to that emitted by a black body at the same temperature.

As well as being a function of temperature and wavelength, the emissivity of a material is also dependent on surface shape and texture. Examples of spectral emissivity values, together with data on electrical resistivity and thermal conductivity, for a variety of metals and metallic alloys are shown in Table 3.3. The majority of the materials are used for various components of luminescence ovens (heater plates, sample discs, etc.) described in the literature. The emissivity figures were selected from data compiled by Touloukian and De Witt (1970) and are only shown as a guide to values that may be encountered in practice. The general trends in emissivity values are large variations between polished and oxidised surfaces, and a greater dependence on emission wavelength than enclosure temperature. In a constant small wavelength band the emissivity for many materials does not vary considerably over a wide range of temperatures, whereas at constant temperature and variable wavelength there is an apparent trend towards higher values of emissivity at shorter wavelengths.

For luminescence detection systems incorporating bialkali photocathodes high black body emission is the indirect result of measurement temperature increase. As shown by Burch (1967) the simulated spectral emission from a black body increases dramatically towards shorter wavelengths with increased temperature. Although the heater plates in TL readers are by no

Table 3.3 Properties of various metals and metallic alloys

Material	T (K)	Emissivity at 665 nm[a]	Surface remarks	Electrical resistivity @ 20°C (μΩcm)	Thermal conductivity 0-100°C ($Wm^{-1}K^{-1}$)
Al	600	0.1 (2000)	Polished	2.67	237
Al_2O_3	1200	0.3	-		
	1800	0.6	-		
Ag	1213	0.044 (650)	-	1.63	429
Au	300	0.17	Very pure	2.20	318
	1050	0.18	Very pure		
Cu	1262	0.116 (650)	Polished	1.69	401
Mo	1100	0.39	Polished	5.7	138
Pt	1125	0.335	All surface types	10.58	71.6
Re	298	0.425 (655)	Polished	18.7	48.0
	1156	0.448 (655)	Polished		
Rh	1100	0.25	All surface types	4.7	150
	1400	0.2	All surface types		
	1800	0.17	All surface types		
Ta	1100	0.45	Polished	13.5	57.5
	1500	0.42	Polished		
	1100	0.79	Oxidised		
	1500	0.77	Oxidised		
Ti	1000	0.6 (650)	Polished	54	21.9
W	1200	0.48 (650)	Polished	5.4	173
Inconel	922	0.3 (2000)	Electropolished	103	14.8 (RTP)
	922	0.58 (1500)	Moderate oxidation		
	1050	0.88 (1500)	Heavy oxidation		
Kanthal	1339	0.89 (650)	Oxidised		
AISI 316	1100	0.4	Polished	70 - 78	16.3 (RTP)
	1100	» 0.7	Oxidised		

[a] All emissivity values are measured at 665 nm except those with figures in brackets.

means perfect black bodies, it would seem reasonable to assume that as higher temperatures are reached and the material is actually glowing red that the emission is increasing from the infrared through into the visible region. Indeed, according to Aitken (1985), there is a significant green component by the time the temperature reaches 500°C. Careful choice of materials as composite elements or coatings for heater plates and sample discs can reduce the intensity of black body emission at high temperatures. The use of rhodium (and silver undercoat) as a coating on copper sample discs and sample plates has been used effectively by Templer (Templer, 1986; Templer and Smith; 1988) to reduce black body emission for auto-regenerative dating of zircons. Similarly, thin coatings of, for example, gold, silver or rhodium on heater plates may also significantly reduce black body emission.

3.2.1.4 Variation in heating rate

The glow temperature at a peak maximum, the peak width, and hence the peak position are related to a small degree on the rate at which the temperature is raised. This can be demonstrated from a consideration of the kinetics governing the system by simulating the shape of glow peaks with the same trapping parameters (activation energy and frequency factor) but varying the heating rate. Figure 3.3 illustrates a first order simulation at 3 different heating rates. By slowing the heating rate the time is increased for the same number of electrons to escape and thus the

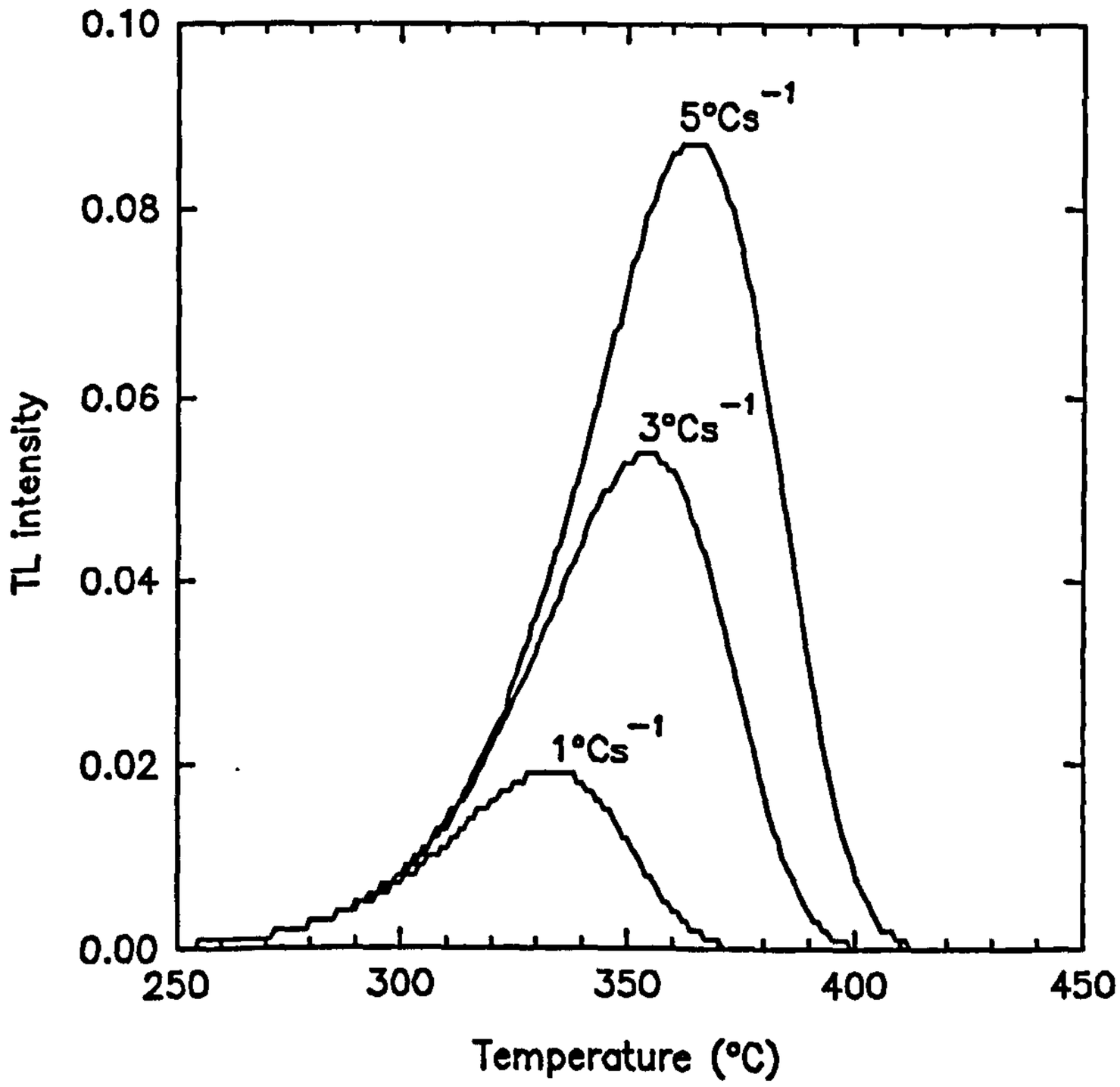

Figure 3.3 First order kinetic simulation of the effect on a single glow peak (E = 1.6 eV, s = $1x10^{12}s^{-1}$, b = 1) of varying heating rate

signal intensity decreases. At a given temperature the fraction remaining trapped is lower for the slower rate because there has been more time for emptying; hence the peak maximum temperature is lower, in this case by about 32°C from 5 to 1°Cs^{-1}.

Potentially, therefore, the need to alter the heating system to reach higher temperatures is removed since lowering the heating rate moves the glow curve to the left revealing further details of the TL signal. However, as shown above, decreasing the heating rate from 5 to 1°Cs^{-1} has only a small effect compared with the increased analysis time by a factor of 5. Decreasing the heating rate further from 5 to 0.2°Cs^{-1} lowers T_{max} by about 61°C with the analysis time increased by a factor of 10. Thus reducing the heating rate would make the measurement of a large number of samples impractical, and rates of 1°Cs^{-1} and below is likely to make the heater circuit surge. Additionally, as shown in the figure, the peak height is reduced by about 4½ times; hence a signal recovery problem may be created with samples of low intensity.

3.2.2 Oven and detection developments

Prior to alterations of the heater circuit the maximum temperature that the TL oven could ramp to was approximately 600°C. As the temperature approached 600°C the ΔT_{servo} value increased rapidly indicating the limit of the available power was being reached. To enable an increase in the maximum temperature the secondary windings of the transformer were increased to increase power to the heater plate. With this complete instrument tests revealed a sudden loss of power after 740-750°C. This was an indication of the maximum voltage from the DAC channel (ie. 7.5 V) corresponding to the reference signal from the computer. A later development to increase temperature further was made with the addition of a non-inverting op-amp (operational amplifier) circuit (Horowitz and Hill, 1990) to provide an optional x2 gain on the reference voltage (ie. approx. 15 V max.). With this in place the oven could readily ramp to 800°C; the maximum temperature of the oven was now limited by the maximum available heating current, by the melting points of the metallic alloys (brass terminals, Inconel heater strip, stainless steel sample discs) and by possible thermal damage to the glass filters and PMT photocathode.

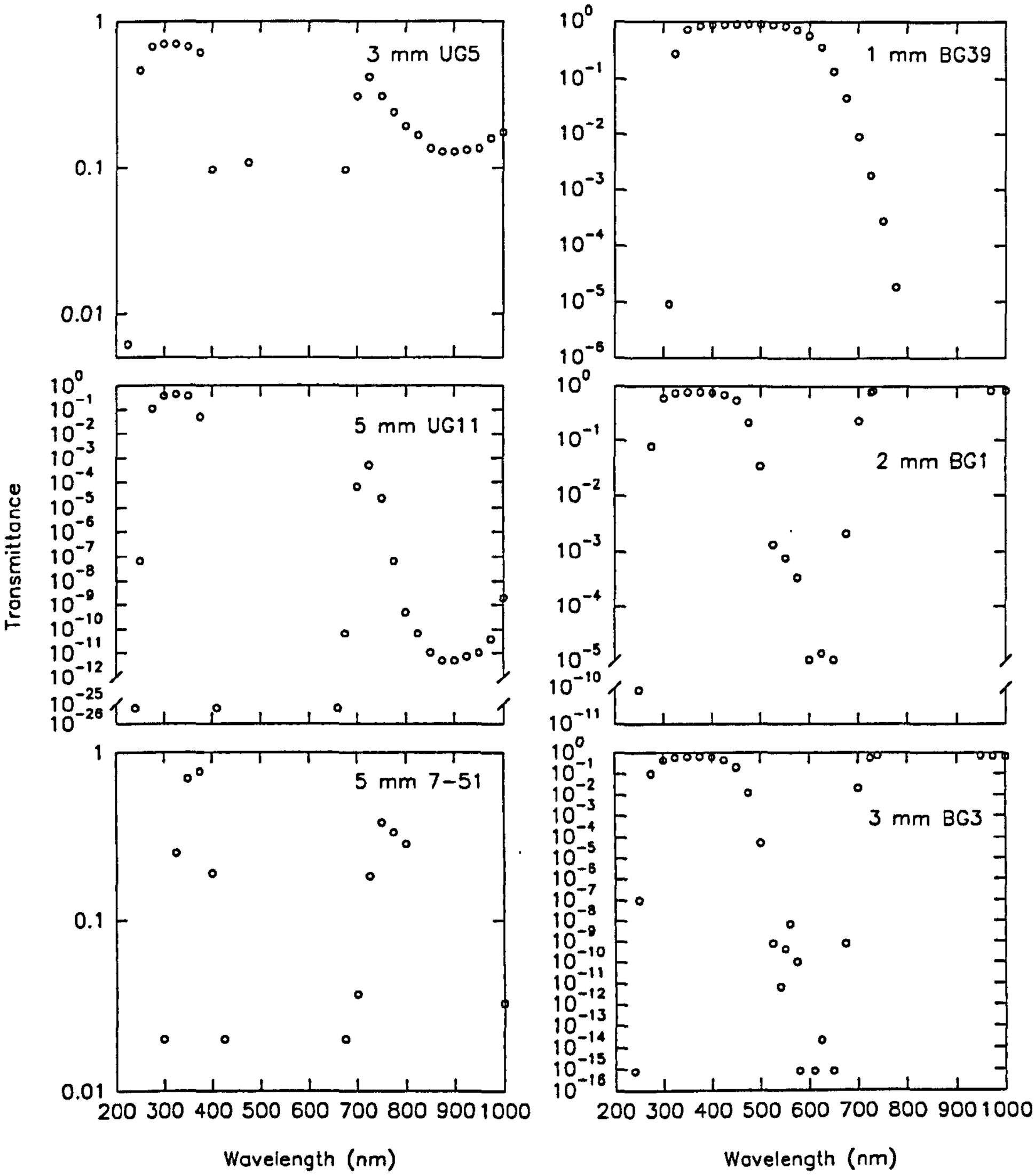

Figure 3.4 Transmission data for various glass filters

In a similar manner to the methods discussed in section 3.2.1.1 the method chosen to reduce black body emission at high temperature was to restrict the wavelength of light reaching the PMT to the ultraviolet. The purpose of the exercise was to reduce the black body emission as much as possible, with a minimum requirement of linear PMT response at the highest black body levels, while maintaining an adequate luminescence signal. Transmission spectra from the main filters investigated are shown in Figure 3.4. As shown there are three filters, Schott UG5, Schott UG11 and Corning 7-51, which have a sharp transmission in the ultraviolet with peaks at 315, 325 and 380 nm respectively and a lower transmission beginning in the red with a sharp

rise to a peak (about 20% lower than the UV peak for UG5; almost an order of magnitude lower for UG11; about 50% lower for 7-51) and continuing into the infrared. The Schott BG39 has a far broader transmission rising sharply in the ultraviolet, peaking in the green at about 480 nm, with a long tail through the yellow / orange and diminishing in the red / beginning of the infrared. Thus in terms of red / infrared the transmission of the BG39 is in contrast to the UG5, UG11 and 7-51. The final filters shown are the Schott BG1 and BG3, with main transmission bands in the ultraviolet-blue and the infrared. The advantage of both these filters, when combined with a BG39, is the very low transmission in the green-orange region, in particular the BG3 which for 1 mm thick is $\leq 10^{-3}$ between about 525-650 nm.

These filters and various others were investigated singularly and in combination using a variety of thicknesses in an attempt to reduce the black body signal at high temperature while maintaining optimum detection in the ultraviolet. Measurements were made both with an empty oven and also beta dosed (^{90}Sr) F-1 IAEA standard potassium feldspar discs to monitor the black body level (with and without sample discs) and the signal level. All measurements were made with a heating rate of $5°Cs^{-1}$. Initial measurements were made before the instrumentation was modified to ramp to higher temperatures. Figure 3.5 shows the variation in luminescence and black body intensity with different filter arrangements for a 1 Gy dosed F-1 disc. The following general points may be made on these glow curves. Firstly they all have the same general shape although the higher signal levels (ie. d & e) have a relatively higher first peak and slightly better defined structure. Conversely these glow curves have a higher than desirable black body signal (especially in d) and the evidence of higher temperature TL is absent, only being present in those glow curves measured using UV filters (ie. a, b & possibly in c). At the limit of the available power of the heating circuit the reproducibility of the heating ramp between signal and black body measurements decreases. Thus for higher black body signals, when the signal to background level is relatively small, the effect of small temperature fluctuations in the heating ramp on the net signal will be much greater. This is a plausible explanation for the absence of high temperature TL in d & e, where the black body signal at high temperature rises above the luminescence signal.

The variation of black body intensity with different filter arrangements for both the sample runs (Figure 3.5) and the empty oven chamber runs are listed in Table 3.4. Values of light intensity

(a) Signal and black body

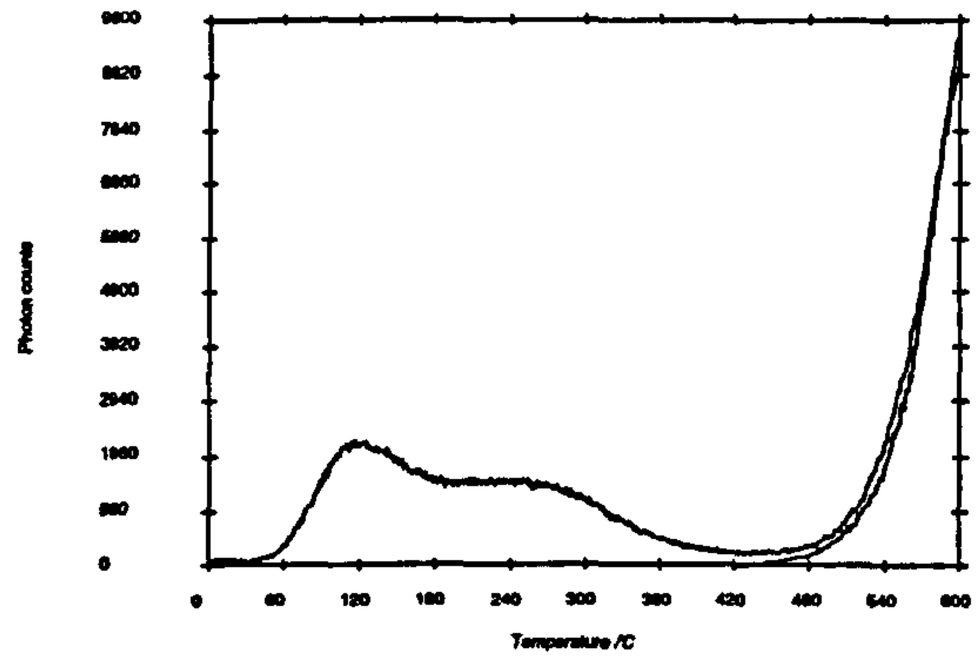

Net signal

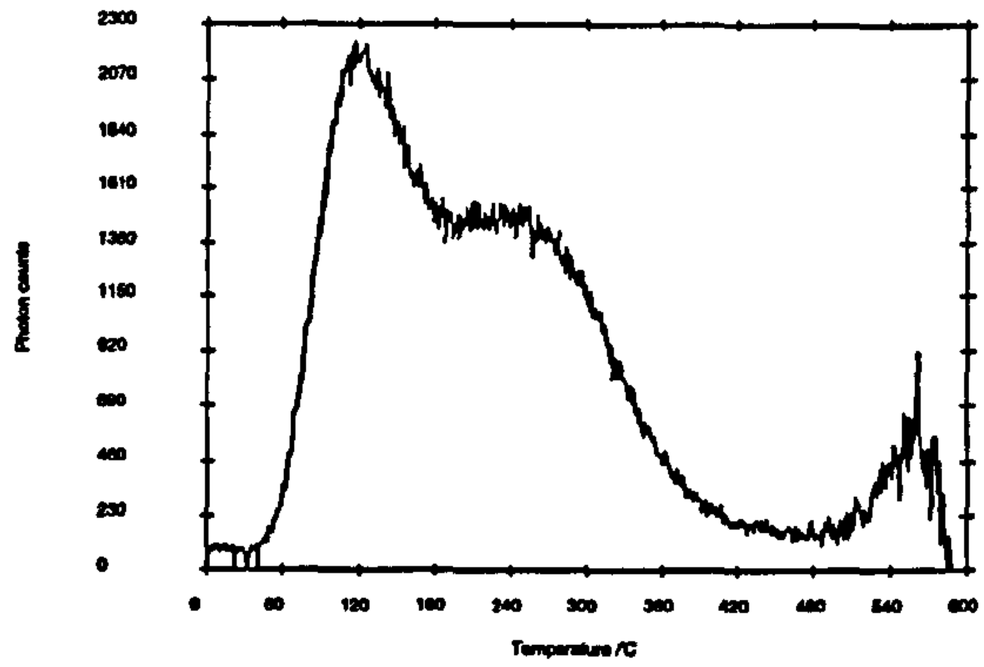

(b) Signal and black body

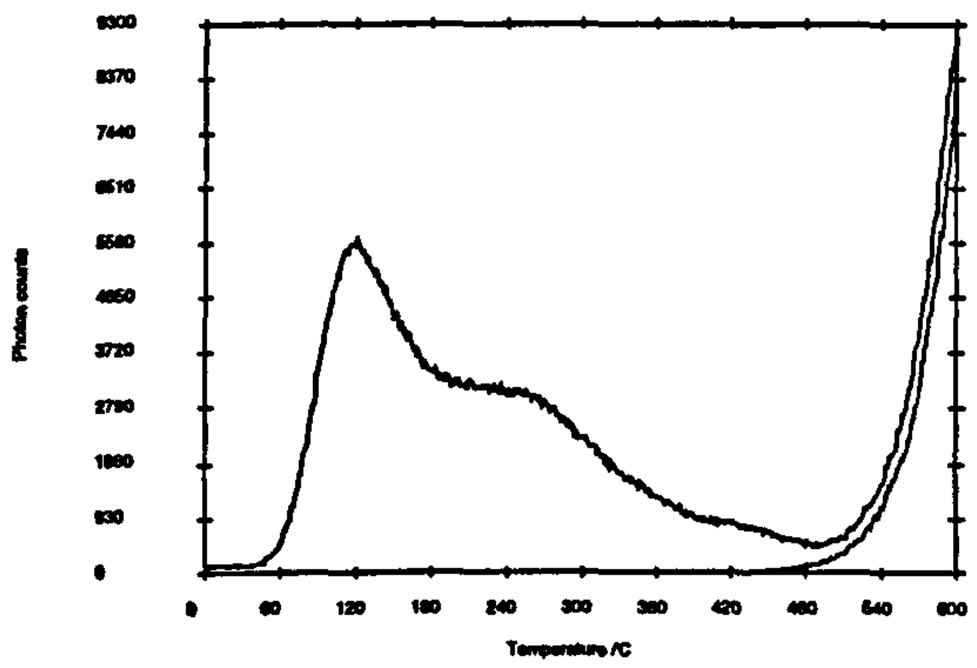

Net signal

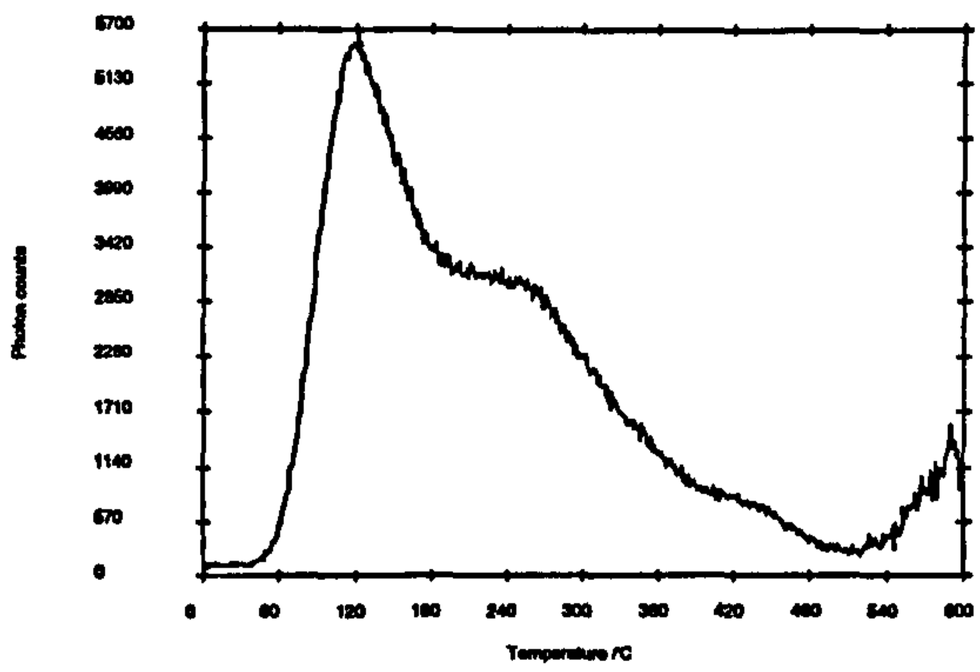

(c) Signal and black body

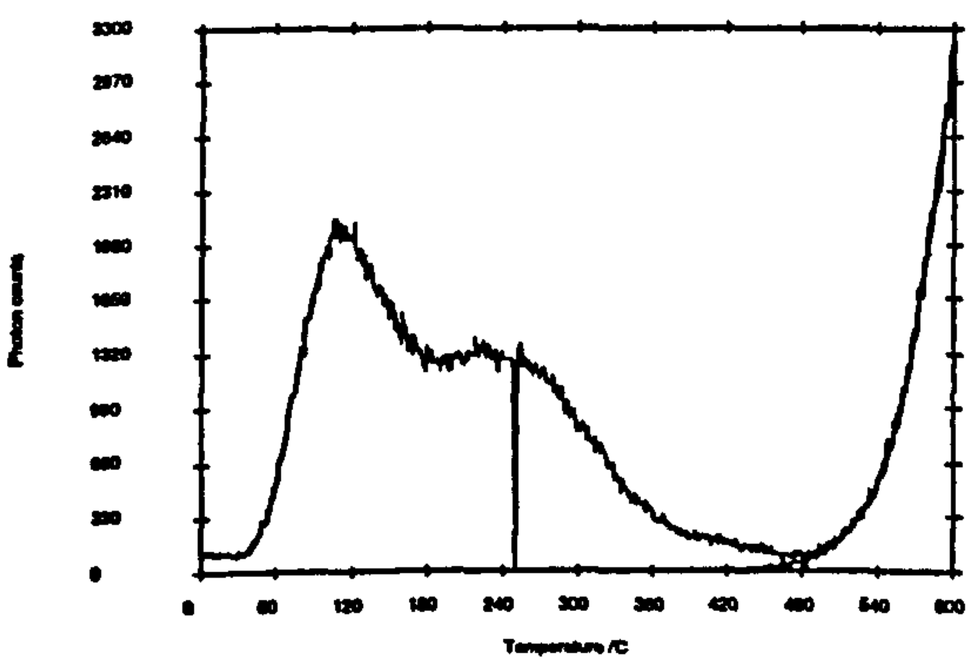

Net signal

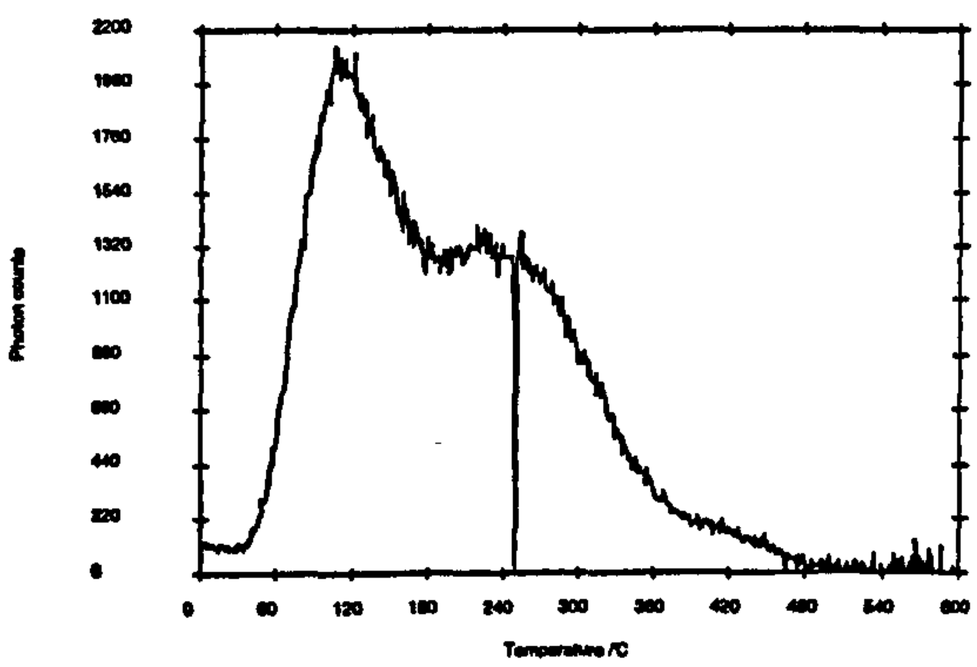

Figure 3.5 Variation in luminescence and black body intensity with different filter arrangements. Integral counts for black body intensity are listed in Table 3.4 under sample columns. All glow curves were measured using the same disc; 1 Gy beta dosed F-1 K-feldspar. The filters were housed in a spacer collar and are additional to a 2 mm BG39 in the PMT housing. (a) 3 mm UG11; (b) 3 mm UG5; (c) 3 mm UG5 + 3 mm UG11.

(d) Signal and black body

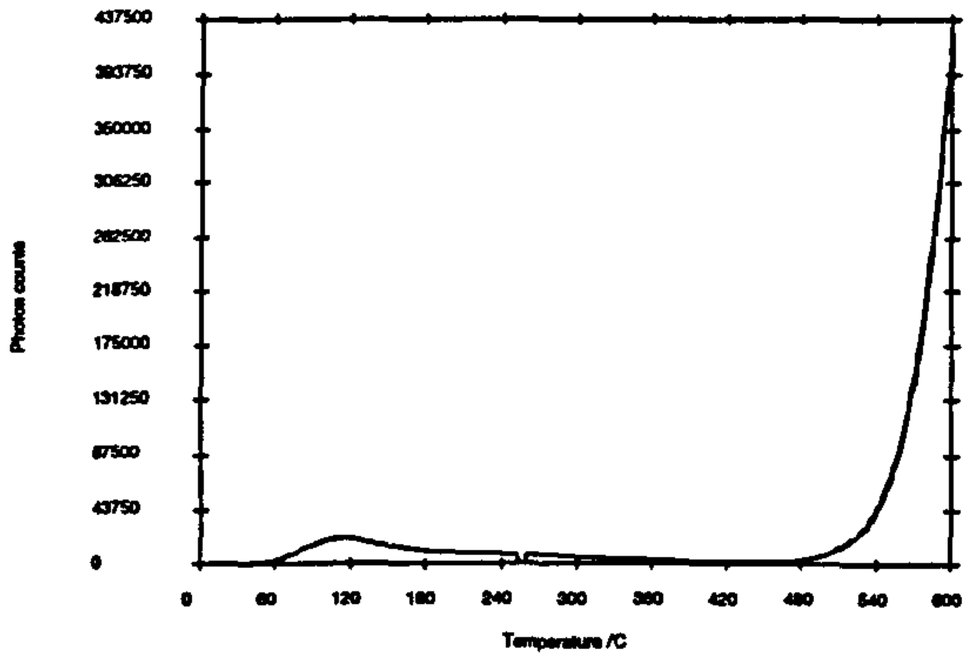

Net signal

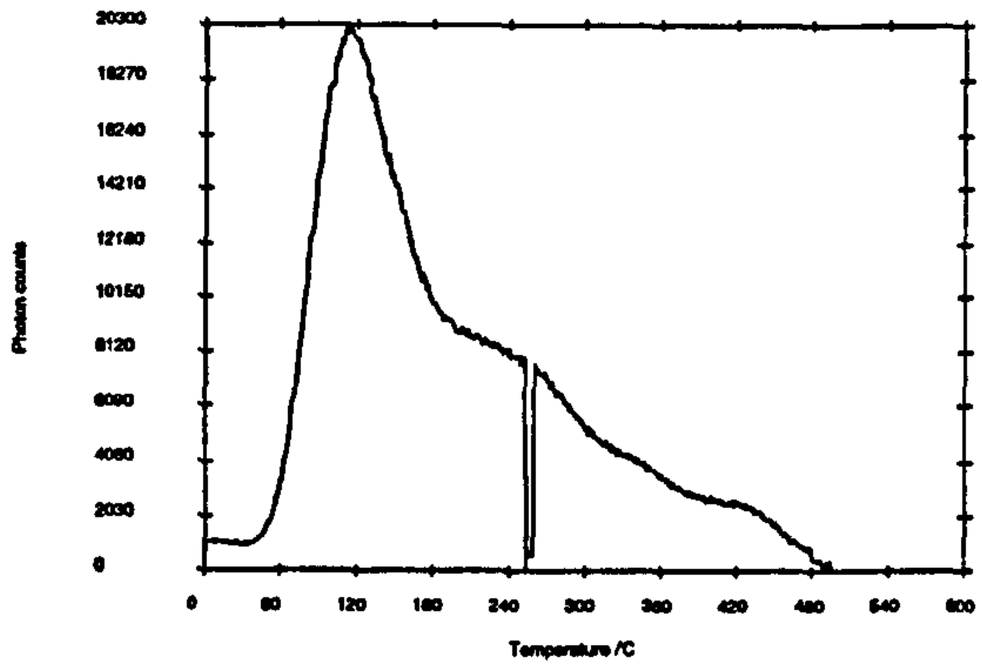

(e) Signal and black body

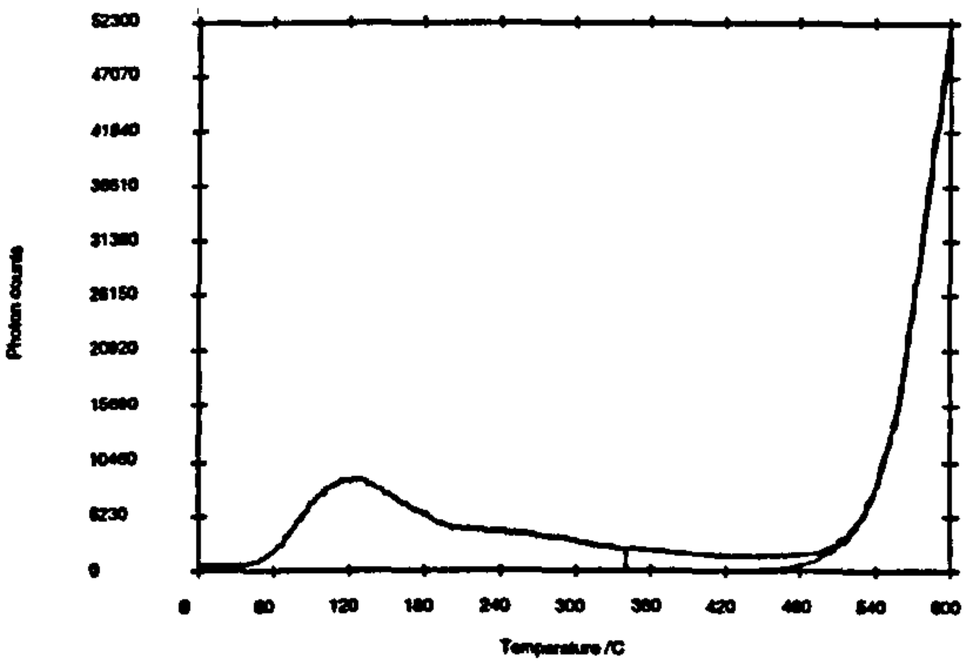

Net signal

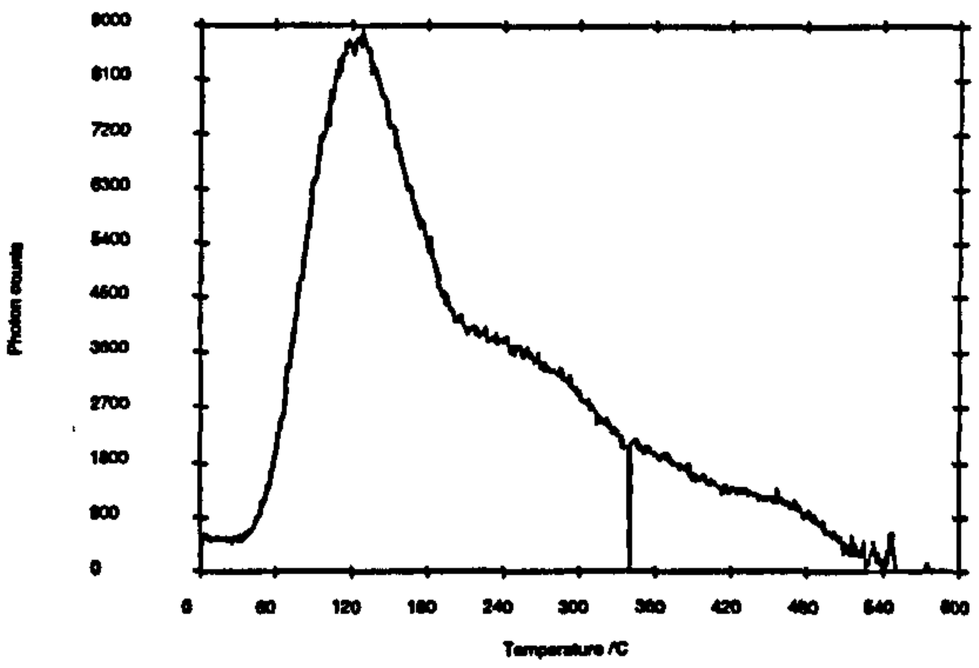

Figure 3.5 continued... (d) 2 mm BG1; (e) 3 mm BG3 + 3 mm BG39

from two 10°C temperature integrals (490-500°C and 590-600°C) are tabulated. The data show the following general points. Firstly an increase in black body intensity by a factor of about 2 between empty chamber and sample runs for both temperature integrals. This is due to the additional black body signal from the sample disc and sample (whereas the higher ΔT_{servo} values, as shown in Figure 3.8, due to a slightly lower effective heater plate resistance or higher thermal mass, will have the effect of a slight reduction in black body in terms of the reference signal). Secondly the marked increase in black body intensity between temperature integrals for both empty chamber and sample runs ranging from a factor of about 25 to 75 depending on filter arrangement. Thirdly the effect on the intensity of the black body signal from an empty chamber in the 490-500°C temperature band by increasing the thickness of the BG39 filter; an increase in thickness of 2.5 (2 mm to 5 mm) has a corresponding reduction in intensity by a factor of about 2, whereas an increase of 3.5 (2 mm to 7 mm) is equivalent to a reduction of about 2.5. The

next general point to make is the large reduction in intensity by addition of filters to restrict transmission principally to the ultraviolet (UG5, UG11) and the ultraviolet-blue (BG1, BG3) regions, with reduction of intensity for an empty chamber (490-500°C) of the order of three and two orders of magnitude respectively. Also important to note here is the very much lower intensity at 590-600°C (empty chamber) for the UG11 + BG39 than the BG1 + BG39 or BG3 + BG39, and the relatively small effect from the addition of 600 nm and 450 nm short wave pass filters. From consideration of their transmission curves (Figure 3.4) and experimental performance the most useful filters appear to be the UG5, UG11, BG39 and BG3.

Table 3.4 Variation in black body intensity with different filter arrangements. All filters listed are additional to a 2 mm BG39 in the PMT housing.

Filters in spacer collar (2 mm BG39 in PMT)	**Temperature[a] integral (photon counts)**			
	490-500°C		**590-600°C**	
	Empty	**Sample**	**Empty**	**Sample**
none	3019376	-	-	-
3 mm BG39	1573782	-	-	-
5 mm BG39	1142646	-	-	-
3 mm UG5	1563	3599	-	90890
3 mm UG11	857	2026	38287	72672
3 mm UG5 + 3 mm UG11	505	1030	19539	29791
2 mm BG1	27975	63973	2078594	3788552
2 mm BG1 + 600 nm swp[b]	24970	-	1812797	-
3 mm BG3	7470	-	524733	-
3 mm BG3 + 600 nm swp[b]	6938	-	449658	-
3 mm BG3 + 450 nm swp[c]	4009	-	252792	-
3 mm BG3 + 3 mm BG39	5468	12026	376609	482851

[a] Reference temperature
[b] 2 mm 600 nm short wave pass filter
[c] 4 mm 450 nm short wave pass filter

The black body intensity values in Table 3.5 were measured after the modification of the reader to enable 700°C TL with the oven chamber empty. As before various combinations of filters were investigated in addition to a 3 mm BG39 and 3 mm BG3 in the PMT. As shown there are 3 filters which reduce the black body intensity to a satisfactory level in the 690-700°C temperature band, namely the 400 nm band pass, the Corning 7-51 and the Schott UG11. An

assessment of the relative signal transmission of these 3 filters (in combination with the BG39 and BG3) was made by measuring the light from a "stabilised" phosphorescence signal (ie. when the rate of decay had slowed considerably) from a sample of F-1 potassium feldspar. As shown in Table 3.6 the Corning 7-51 combination allows the most light through.

Table 3.5 Variation in black body intensity with different filter arrangements. All filters listed are additional to a 3 mm BG39 and a 3 mm BG3 in the PMT housing.

Filters in spacer collar	**Temperature[a] integral (photon counts)**		
(BG39 + BG3 in PMT housing)	**490-500°C**	**590-600°C**	**690-700°C**
none	10967	841693	17129282
6 mm BG39	6414	500913	12484747
8 mm BG39	4503	354190	9277645
8 mm BG39 + 450 nm swp[b]	1689	135349	4480270
8 mm BG39 + 2 x 450 nm swp[b]	872	75384	2591874
2 x 450 nm swp[b]	1649	142841	5213238
2 x 450 nm swp[b] + 2 mm BG1	1238	109247	3838299
2 x 450 nm swp[b] + 400 nm bp[c]	136	5721	258623
2 x 450 nm swp[b] + 2 x 400 nm bp[c]	102	3299	154877
2 x 400 nm bp[c]	92	1558	85519
5 mm 7-51	153	6082	338779
5 mm UG11	101	1084	43720

[a] Reference temperature
[b] 4 mm 450 nm short wave pass filter
[c] 2 mm 400 nm band pass filter

Table 3.6 Transmission of "stabilised" phosphorescence from a K-feldspar (F-1) through different filters. Filters investigated are in addition to a 3 mm BG39 and a 3 mm BG3 combination in the PMT housing.

Filter (in collar)	**Total photon counts in MCS channels[a]**			**Relative transmission (%)**
	No filter (2 chn's)	**Filter (4 chn's)**	**No filter (2 chn's)**	
5 mm UG11	47511	6876	35578	8.3
2 x 400 nm bp[b]	32573	6000	26172	10.2
5 mm 7-51	25572	13728	21333	29.3

[a] The photon counts were recorded from left to right (ie. no filter, filter, then no filter) firstly with the UG11, then the 400 nm band pass and finally the 7-51. Thus the progressive reduction in channel contents is due to continuing phosphorescence decay. Dwell time = 1s.
[b] 2 mm 400 nm band pass filter.

In addition a similar assessment was made of the reduction in signal transmission (if any) incurred by using the BG3 filter in light of its useful transmission characteristics (ultraviolet-blue peak but sharp cut off in the green-orange; see Figure 3.4), and the effective black body reduction (Table 3.4). The results showed the addition of the BG3 to a BG39 and 7-51 combination reduced the transmission by about 13%.

3.2.3 700°C TL

Using a selection of the most promising optical configurations TL glow curves up to 700°C (reference temperature) at a heating rate of 5°Cs^{-1} were measured on material from the Crawford burnt stone mounds to investigate whether remnant geological signals could be detected from archaeological samples. Glow curves were measured both from whole sample sections and alkali feldspar separates. The whole sample sections were produced by removing eight thin slices from a uniform cuboid core (0.65 x 0.8 x 1.45 cm) with a water-cooled diamond rock saw. Using a scalpel an approximate quarter of each section (approx. 4 x 3.25 mm) was removed for TL measurement. The sections were placed on stainless steel sample discs in the usual manner. The alkali feldspar separates were obtained using a feldspar inclusion method. Eight stones (30-40 g; sub-sampled with cold chisel / rock saw if too large) were crushed in an agate pestle and mortar, sieved to produce a 90-125 μm grain size fraction, acid washed (HCl, HF), and density separated using sodium polytungstate heavy liquid with a centrifuge. Approximately 5 mg of material was dispensed onto disc.

A number of examples are shown in Figure 3.6. The results clearly show that it is possible to measure TL up to 700°C using a variety of filter combinations. The high temperature peak present in all these examples is interpreted as the remnant geological TL signal. This is made evident by the low sensitivity of this region to subsequent artificial dose compared to the lower temperature "archaeological" continuum implying the natural dose responsible for the higher temperature peak is very much larger (see Section 5.2 of Chapter 5 for further details).

Table 3.7 shows the variation in black body intensity for the different filter arrangements for all the samples that were measured. The black body signal is not very highly reproducible which

may be a reflection of changes in sample mass and distribution on the discs (causing variations in emissivity), or differences in disc to disc or sample to sample emissivity. Other possible (although perhaps less likely) reasons are variations in disc positioning and heater plate contact. The best filter combination in terms of reduction in the black body signal level is a BG39, 7-51 and BG3. The introduction of the BG3 reduces the level by over a factor of 2 which easily compensates the slight loss of transmitted light (13%). Even though the reproducibility is not particularly high, the results reinforce the general observations seen in the earlier filter work described above.

(a) Signal and black body

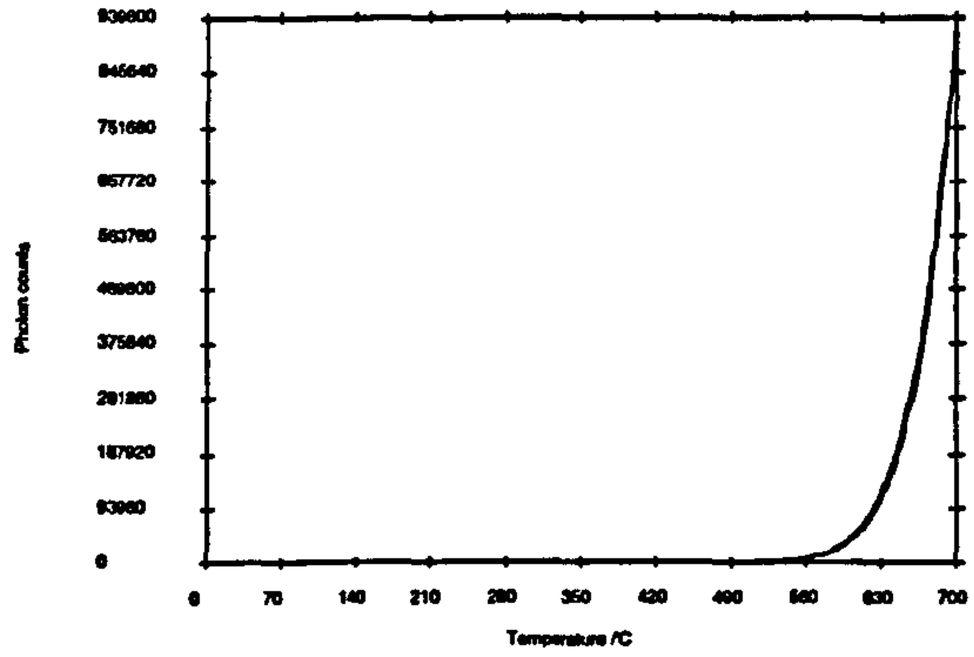

Net signal

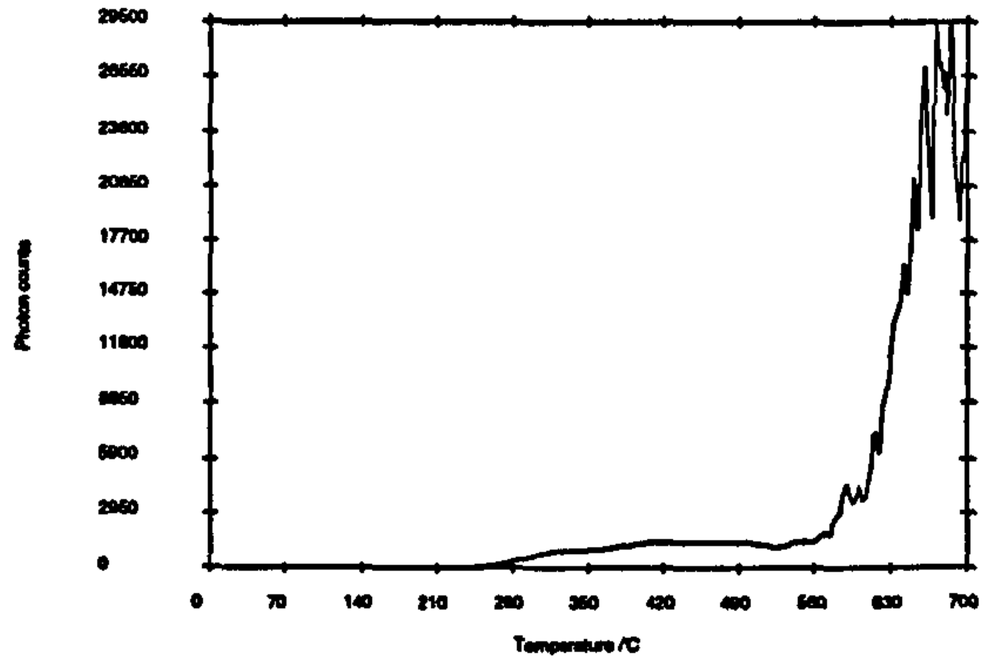

(b) Signal and black body

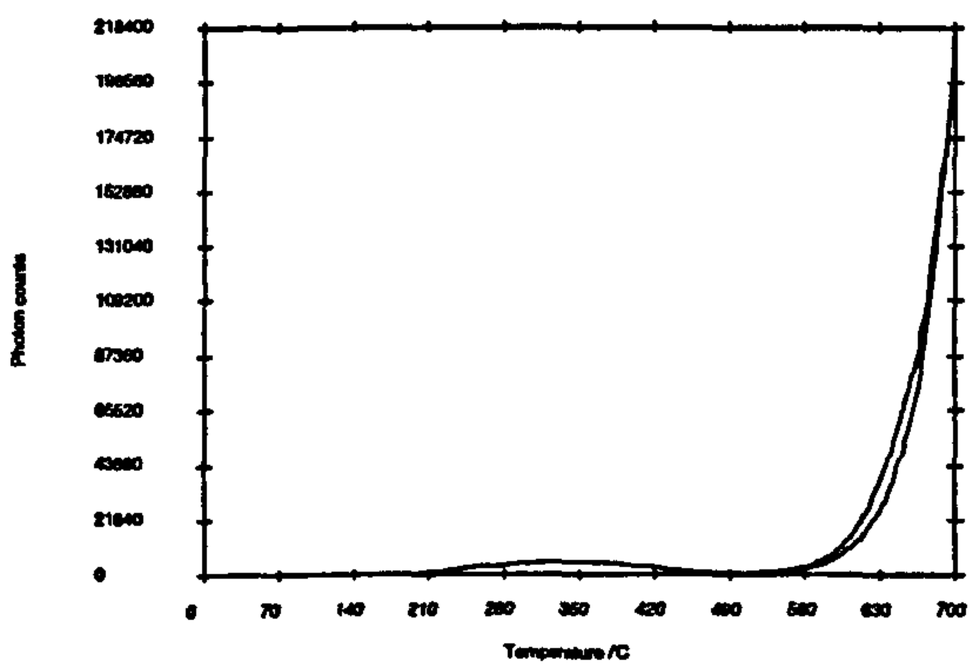

Net signal

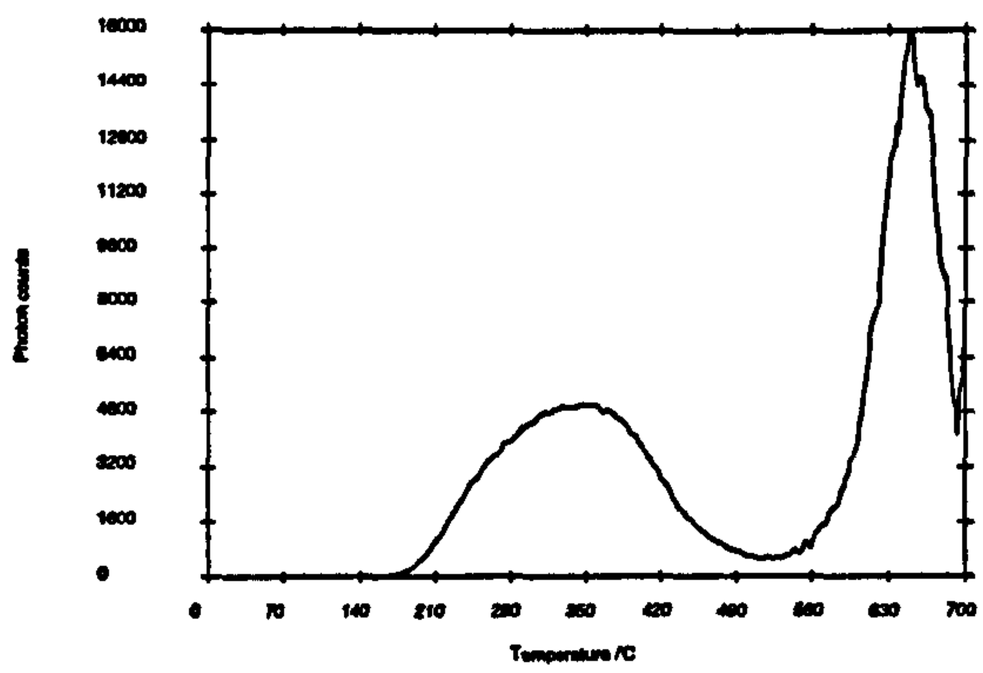

(c) Signal and black body

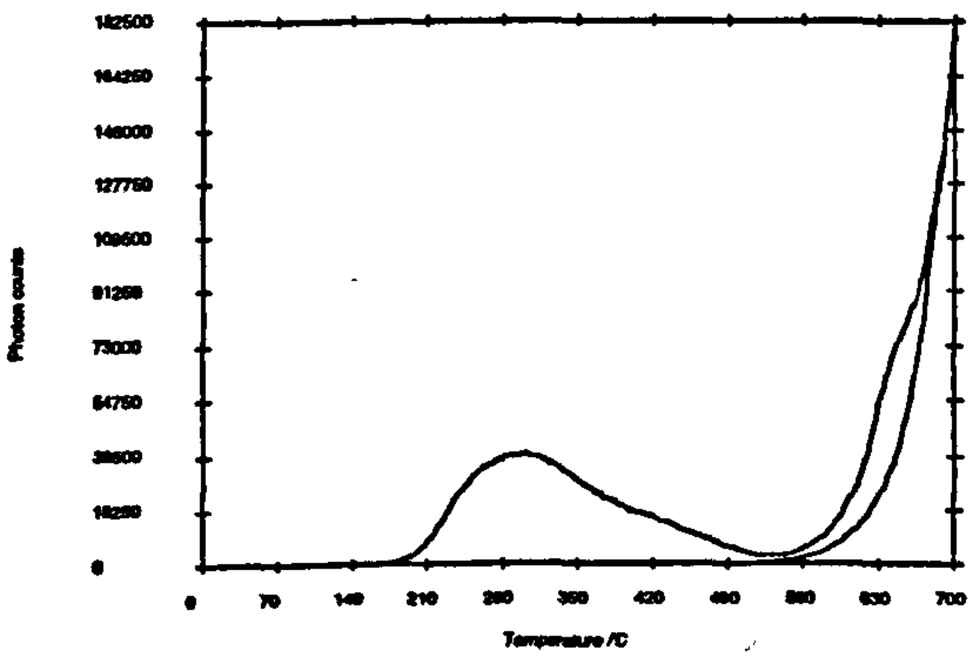

Net signal

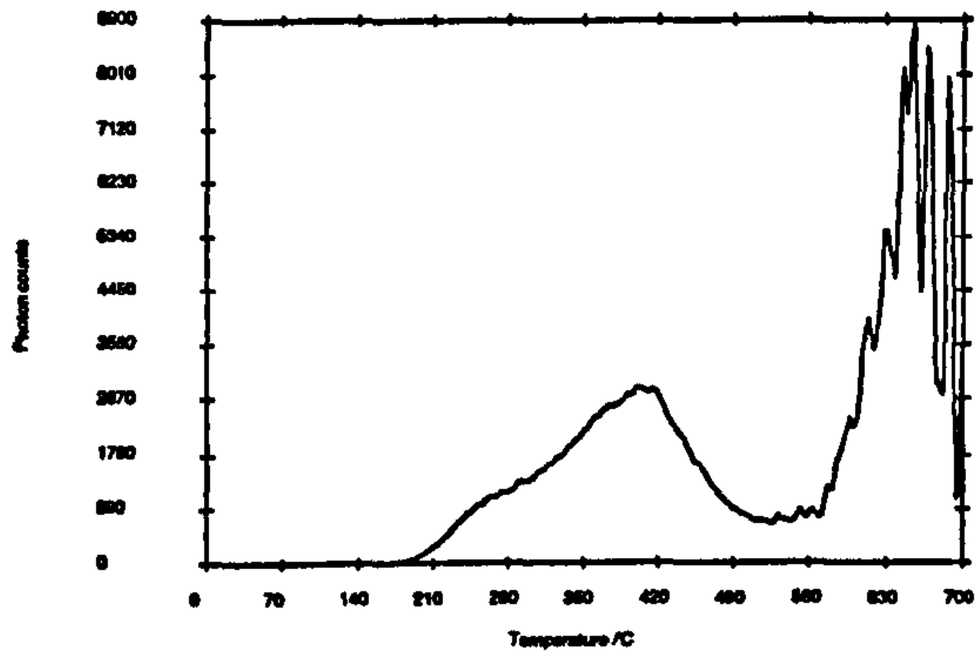

Figure 3.6 Examples of 700°C TL from Crawford burnt mound samples using different sample types ((a) whole sample section; (b) & (c) Na-feldspar; (d)-(h) K-feldspar) and different filter arrangements. (a) TL219: 3 mm BG39 + 3 mm UG5; (b) TL188: 3 mm BG39 + 5 mm 7-51; (c) TL219: 3 mm BG39 + 5 mm 7-51.

(d) Signal and black body

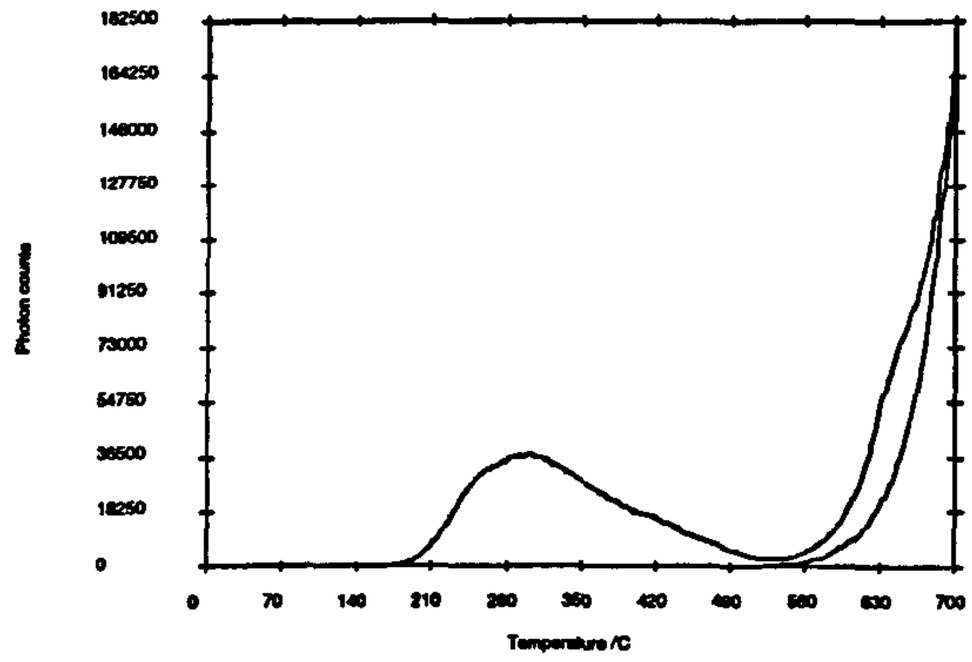

Net signal

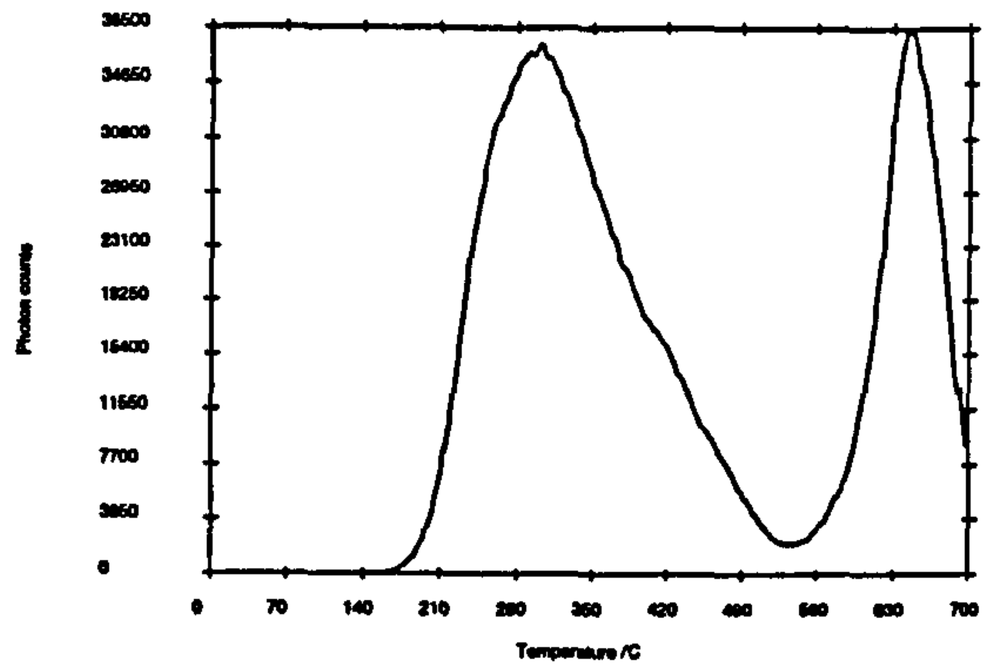

(e) Signal and black body

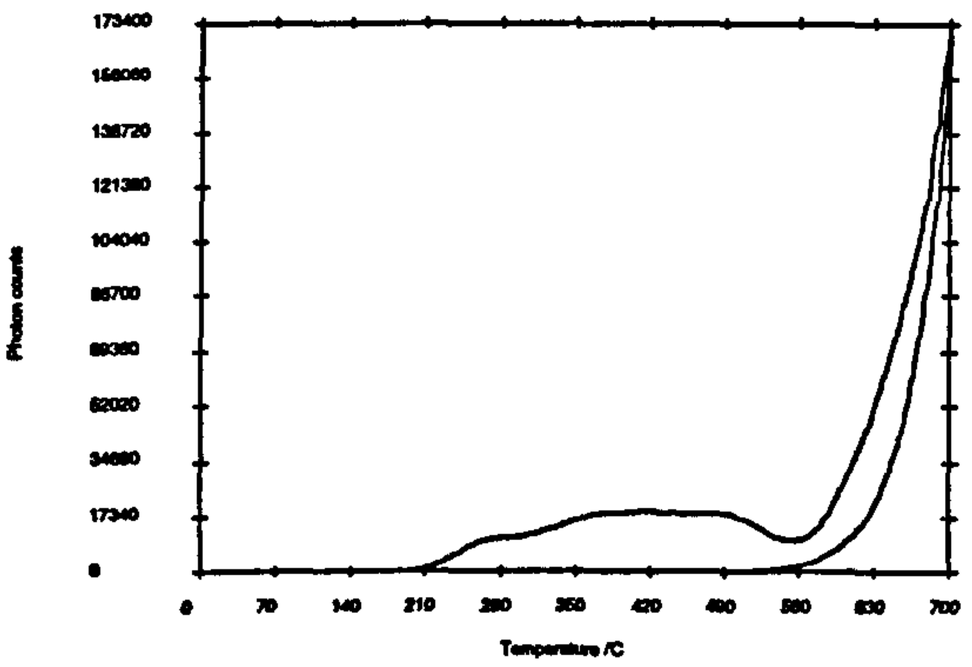

Net signal

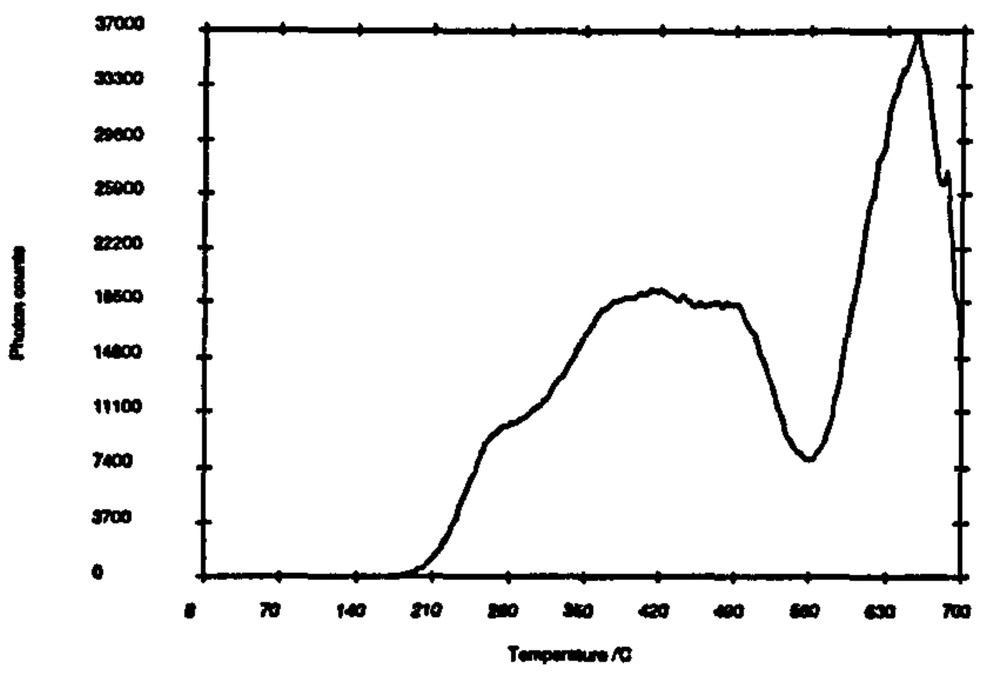

(f) Signal and black body

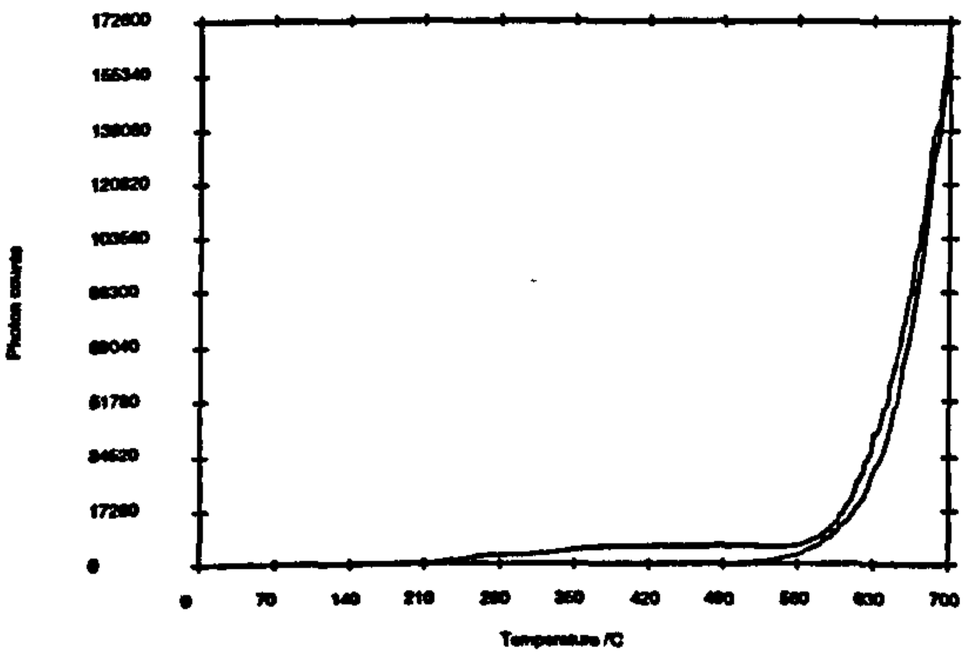

Net signal

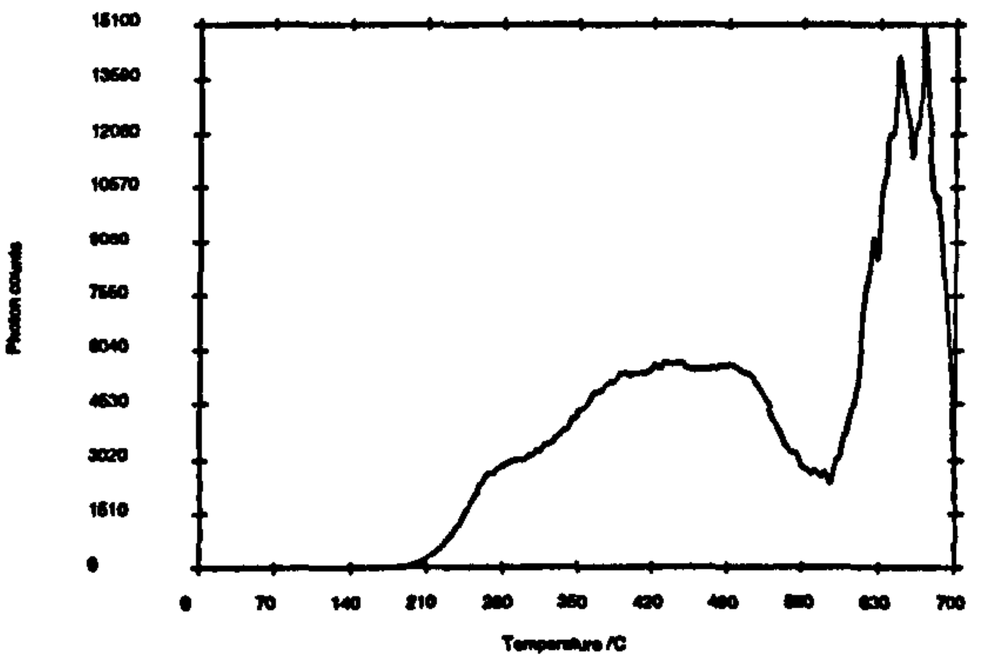

Figure 3.6 cont... (d) TL222: 3 mm BG39 + 5 mm 7-51; (e) TL225: 3 mm BG39 + 5 mm 7-51; (f) TL225: 3 mm BG39 + 3 mm UG11.

(g) Signal and black body

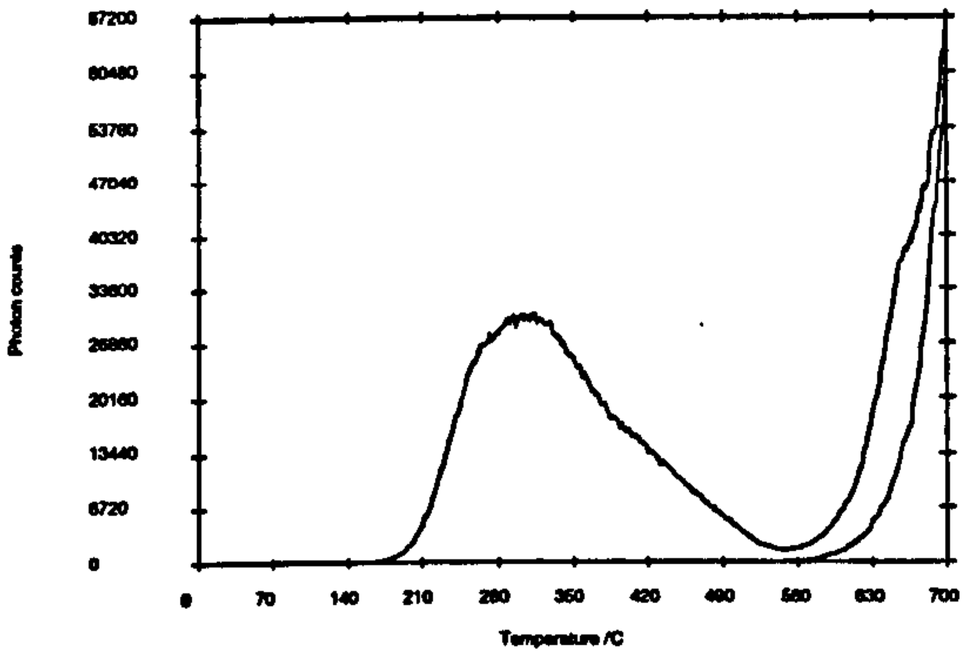

Net signal

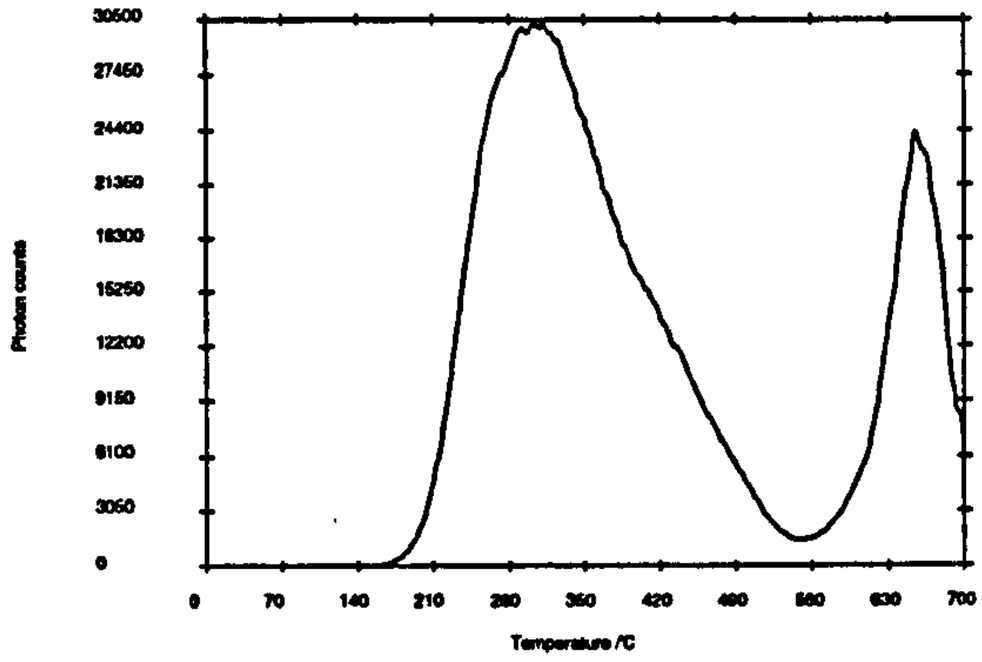

(h) Signal and black body

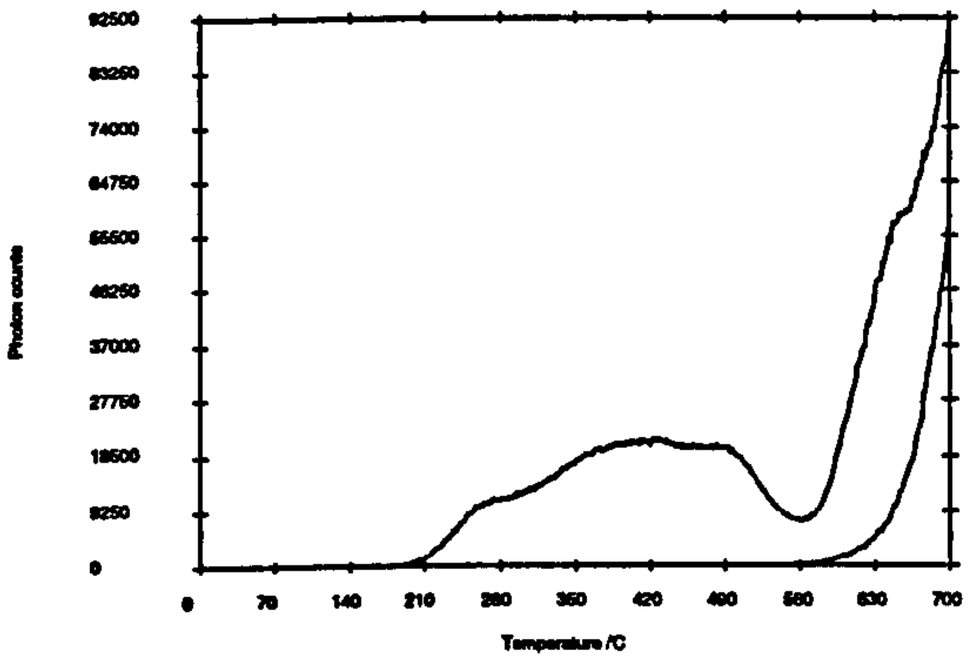

Net signal

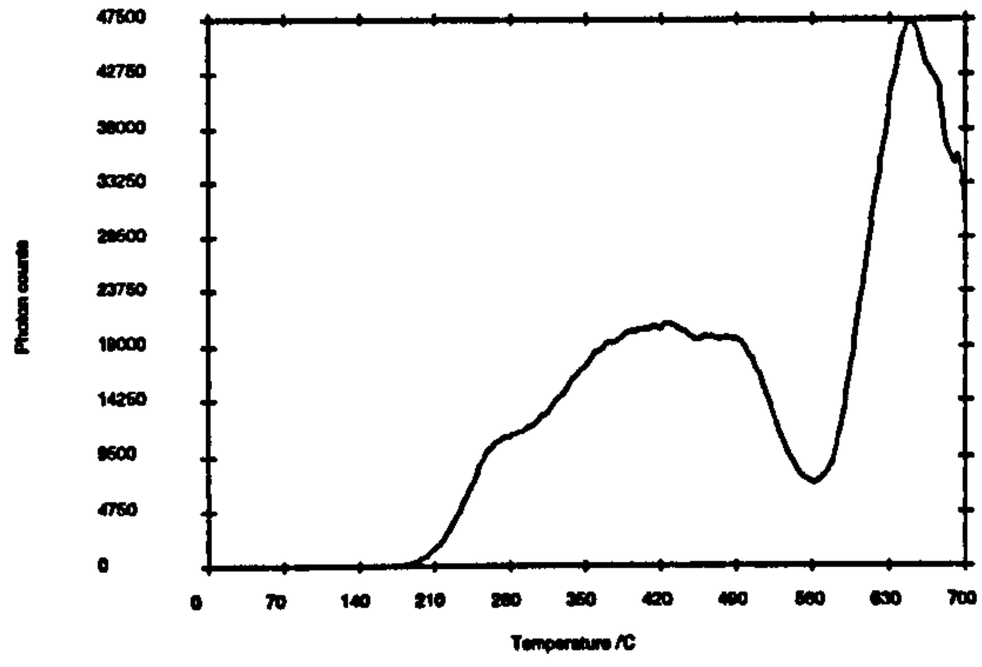

Figure 3.6 cont... (g) TL222: 3mm BG39 + 5 mm 7-51 + 3 mm BG3; (h) TL225: 3 mm BG39 + 5 mm 7-51 + 3 mm BG3.

Table 3.7 Variation in black body intensity with different filter arrangements for 700°C TL on Crawford burnt mound samples.

Sample type	Filters[b]	Glow[c]	No. of obs.	Temperature[d] integral (mean photon counts ± $1\sigma_{n-1}$)		
				490-500°C	590-600°C	690-700°C
Whole sample	BG39 + UG5	1st + 2nd	16	5669 ± 782 (14%)	308140 ± 40638 (13%)	7755776 ± 903850 (12%)
sections[a]	(filters in tube;	1st	8	6284 ± 365 (6%)	339879 ± 22920 (7%)	8478218 ± 358318 (4%)
	collar also used)	2nd	8	5055 ± 561 (11%)	276400 ± 26661 (10%)	7033334 ± 655163 (9%)
Alkali feldspar	BG39 + 7-51	1st + 2nd	16	2260 ± 501 (22%)	76121 ± 12766 (17%)	1573395 ± 212575 (14%)
separates	(7-51 in collar)	1st	8	2496 ± 602 (24%)	82189 ± 13548 (16%)	1595651 ± 187751 (12%)
		2nd	8	2023 ± 216 (11%)	70052 ± 9029 (12%)	1551138 ± 245864 (16%)
	BG39 + UG11	1st + 2nd	16	4840 ± 1067 (22%)	148815 ± 36898 (25%)	2249126 ± 630964 (28%)
	(UG11 in collar)	1st	8	3978 ± 398 (10%)	119657 ± 11391 (10%)	1741256 ± 208656 (12%)
		2nd	8	5702 ± 764 (13%)	177973 ± 29059 (16%)	2756995 ± 469052 (17%)
	BG39 + 7-51 + BG3	1st + 2nd	16	375 ± 155 (41%)	16231 ± 3139 (19%)	668941 ± 112984 (17%)
	(filters in tube;	1st	8	393 ± 194 (49%)	14784 ± 2602 (18%)	644455 ± 102340 (16%)
	collar also used)	2nd	8	356 ± 115 (32%)	17677 ± 3093 (17%)	693427 ± 124541 (18%)

[a] Eight thin sections (1.01 ± 0.11 (std. error) mm) cut from a cuboid core (0.65 x 0.8 x 1.45 cm) from sample SUTL219. Average mass = 23.55 ± 3.42 (std. error) mg.
[b] 3 mm BG39; 3 mm UG5; 5 mm 7-51; 3 mm UG11; 3 mm BG3.
[c] 1st glow is the black body of the natural TL. 2nd glow is the black body of a normalisation dose; whole sample = 5 Gy ß, feldspars = 100 Gy γ.
[d] Reference temperature.

3.3 Temperature calibration of glow curves

3.3.1 Thermocouple signal

The output from the thermocouple that senses the temperature of the TL oven heater plate is slightly non-linear. Figure 3.7a illustrates the response of the thermocouple amplifier (with the cold junction and package at 25°C), which is a linear device, as a function of the temperature at the thermocouple hot junction. This shows that for accurate heater plate temperature measurements (assuming the hot junction of the thermocouple and the underside of the heater plate are welded at a single point, ensuring the thermocouple is sensing the temperature of the heater plate and not at a point beneath the surface) the non-linearity must be corrected for.

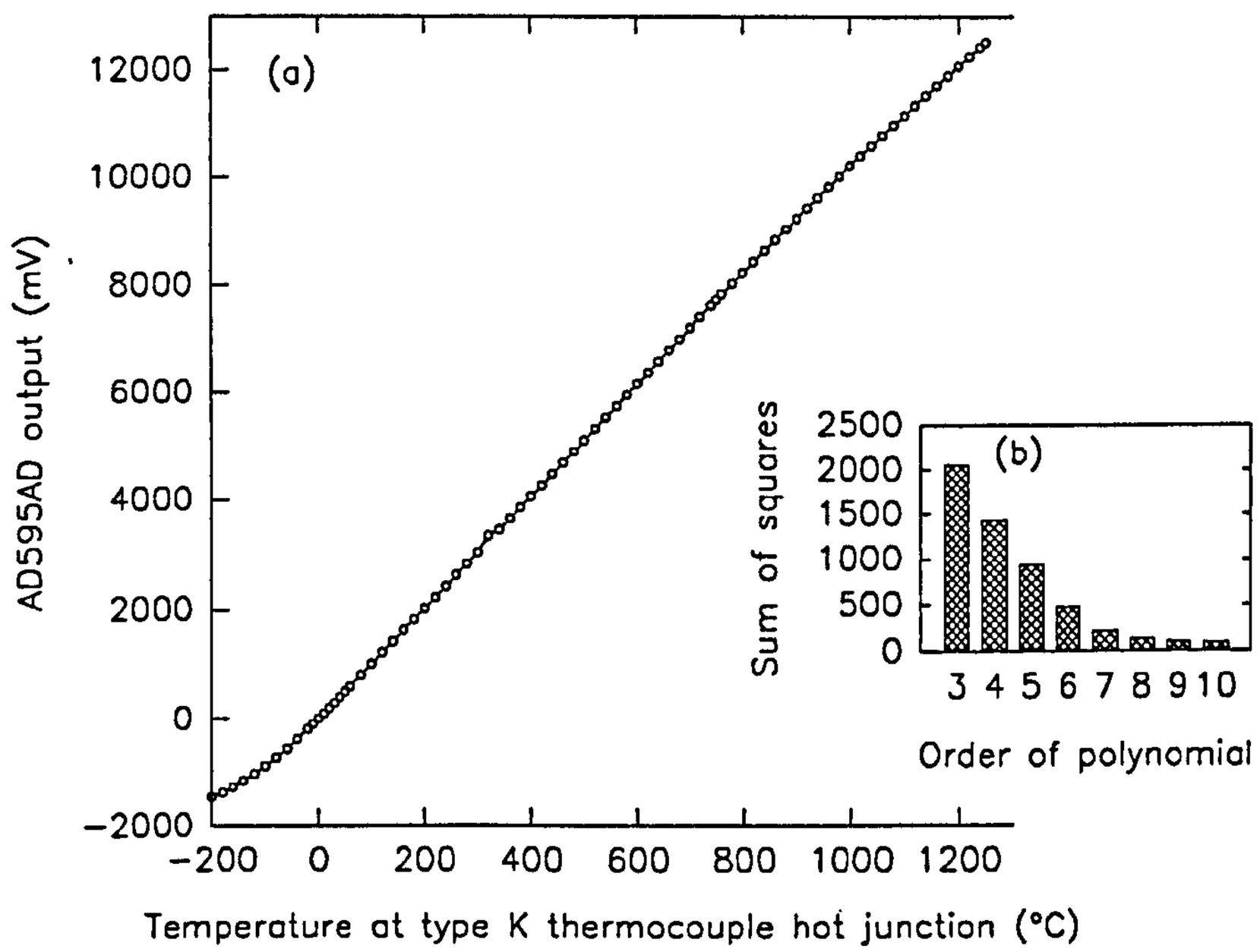

Figure 3.7 Relationship between the temperature at the hot junction of a type K thermocouple and the output of an AD595AD (Analogue Devices) thermocouple amplifier; cold junction and amplifier package at 25°C. Data [open circles] from RS data sheet 6957, November 1986.

Inverse functions were fitted to the amplifier data over the whole working range using both polynomial and combined exponential-linear expressions. The results from summing the squares of the residuals showed that polynomial expressions fitted the data best. Figure 3.7b demonstrates that further increase in polynomial order after eight terms has a progressively

smaller effect. However, for the temperature range used in TL measurements in this thesis (ie. about 50-800°C) a 3rd order polynomial relationship (Equation 3.3) enables suitable corrections to be made, although for accurate cryogenic work a higher order polynomial correction must be incorporated.

$$T = -8.15 + 1.09\text{x}10^{-1} V - 2.67\text{x}10^{-6} V^2 + 1.59\text{x}10^{-10} V^3 \qquad \textbf{(3.3)}$$

For example, using the above expression, an amplifier output V of 7000 mV corresponds to a hot junction temperature T of 680.51°C.

3.3.2 Servo-lag (ΔT_{servo})

This is the difference or error between the reference voltage (or reference temperature) from the computer compared with the output from the thermocouple amplifier (as described in section 3.1.1 above). As a temperature ramp proceeds the increase in the rate of heat loss from the heater plate to the exchange gas causes an increase in the power requirements of the heater. The servo-lag increases as the power requirements of the heater increase above the power supplied in response to a given temperature error. The magnitude of the servo-lag varies depending on the temperature at which the thermocouple and reference voltages are balanced, the matching of power requirements, the rate of gas flow, and whether sample discs and/or samples have a

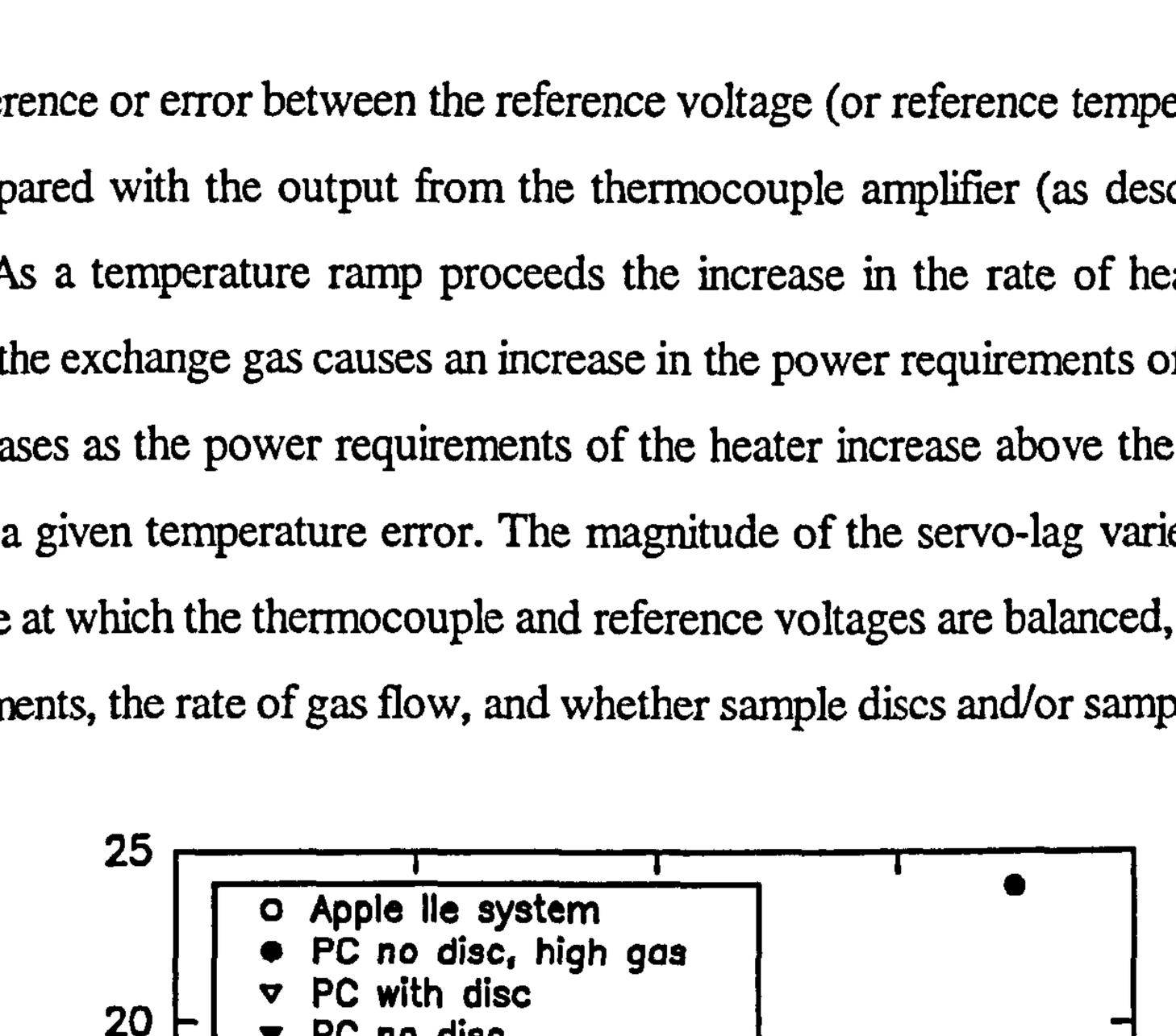

Figure 3.8 Variation in servo-lag with reference temperature

significant thermal mass. This variation is shown in Figure 3.8 and is approximately linear.

3.3.3 Thermal contact

Two experiments were devised to investigate the thermal contact between the heater plate, disc and sample, to enable the thermal lags involved to be estimated. The first of these looked at the effect of stainless steel discs, and the second at variations in grain size and heating rate.

3.3.3.1 Effect of stainless steel discs

The standard potassium feldspar used elsewhere in this project (IAEA F-1) was prepared for this experiment. Two portions (A & B, approx. 300 mg each) of 90-125 μm grain size were placed in small silica glass vessels and annealed in a muffle furnace at approximately 500°C for 10 minutes to remove any geological TL in the desired measurement region. The portions were given a 1 minute irradiation in the ^{60}Co facility (approx. 13.5 Gy) and then annealed once again in the muffle furnace on a copper plate which was temperature sensed by a number of type K thermocouples bolted to it. Portion A was annealed for 1 hour at 110.6 ± 0.6 (1σ)°C, and portion B for 1 hour at 298.3 ± 1.2 (1σ)°C (the temperatures recorded were the mean for the central T/C on the copper plate). The two annealing temperatures were designed to remove the TL signal to two distinct positions in terms of analysis temperature. The annealing conditions were derived from the results of controlled experiments discussed in Section 4.1 of Chapter 4.

From each portion of feldspar TL was measured from 8 aliquots on stainless steel (AISI 316) discs and 8 aliquots directly on the heater plate. Silicon grease spray was used to adhere grains both to the discs and the heater plate. Care was taken when dispensing grains in an attempt to keep the area and volume of the sample constant to allow the experiment to show solely the effect of the sample disc. To keep the sample area constant grains were dispensed over the whole sample disc area and the same area of grains were dispensed onto the heater plate (the silicon grease was sprayed onto the heater plate through a circular sticky paper template). The volume was controlled by attempting to achieve a mono-layer of grains. This was done by tapping off any loose grains from the sample discs (a method routinely employed in sample

dispensing) and tapping and air-dusting the grains on the heater plate. The TL measurement was performed with a heating rate of $5°Cs^{-1}$ with a Corning 7-59 and Schott KG1 filtered PMT. An estimate of the thermal lag from the top of the heater plate to the top of the sample disc was made by measuring the difference in the position to which the TL signals had been removed for each portion of feldspar in terms of analysis (reference) temperature. The reference temperature was measured at the maximum (T_{max}) of the first peak in the annealed glow curves, and also at a position on the rising edge of the first peak measured from half the peak maximum (this parameter [$T_{1/2}$] is introduced and discussed in Section 4.1.2 of Chapter 4). The results are shown in Table 3.8.

Table 3.8 Effect of stainless steel sample discs on glow curve position (I)

Anneal	Surface	Mean $T_{max} \pm 1\sigma$ (°C)[a]	Mean $T_{1/2} \pm 1\sigma$ (°C)[b]
A	Sample disc	251.4 ± 3.5	202.0 ± 2.6
	Heater plate	215.9 ± 2.9	172.3 ± 0.7
	S.D.- H.P.	35.5 ± 4.6	29.7 ± 2.6
B	Sample disc	441.8 ± 5.1	403.0 ± 3.8
	Heater plate	388.9 ± 4.2	351.5 ± 1.6
	S.D.- H.P.	52.9 ± 6.6	51.8 ± 4.1

[a] Reference temperature at the maximum of the first peak in the annealed glow curve.
[b] Reference temperature at a position on the rising edge of the first peak measured from half the peak maximum (this parameter [$T_{1/2}$] is introduced and discussed in Section 4.1.2 of Chapter 4).

Subsequent to this experiment it was discovered that the gas flow was higher than the usual setting which would probably result in the temperature measurements being erroneously high due to the greater than usual cooling effect of the gas. However the results in themselves are still valid and some interesting observations can be made. Firstly the effect of the stainless steel disc is quite striking, introducing a lag of about 30°C at the lower temperature and about 50°C at the higher temperature. Secondly, as might be expected, the standard deviation on measurements made at a position where the rate of light emission is at a maximum (ie. $T_{1/2}$) is consistently lower than the standard deviation at the peak maximum position. Thirdly the standard deviations for the higher temperature position are greater than the lower temperature position, which may be due to greater variation in power delivery as the temperature gradient between the heater plate and exchange gas increases. Finally the spread of values for sample discs are consistently higher than the spread of values for the heater plate. This is the most important observation here

as it may suggest that the heater plate has a non-uniform surface and / or temperature distribution, which has perhaps been revealed by slight variations in disc-to-disc positioning on the heater plate.

To ascertain whether the final observation was correct a rapid exploratory experiment was carried out to estimate the magnitude of any temperature variations over both the surface of the heater plate and the sample disc. The same annealed feldspar was used as above, although the gas flow was reduced to the usual level. The sample size was reduced to a 2 mm diameter circle by dispensing the grains onto an area of silicon grease produced using sticky paper templates as before. The results are summarised in Table 3.9.

Table 3.9 $T_{1/2}$ values across the heater plate and sample disc

Anneal	Surface	Lateral position[a]		Central	Longitudinal position[b]		Mean ±1σ
		Left (°C)	Right (°C)	(°C)	Top (°C)	Bott. (°C)	(°C)
A	Disc	184	187	190	190	177	186 ± 5
	Heater	167	183	172	166	166	171 ± 7
	D - H	17	4	18	24	11	15 ± 9
B	Disc	373	384	373	385	377	378 ± 6
	Heater	347	380	359	347	342	355 ± 15
	D - H	26	4	14	38	35	23 ± 16

[a]Perpendicular to direction of current flow (ie. across width of heater strip)
[b]In direction of current flow (ie. along length of strip)

Bearing in mind the values are all from single measurements, the following general points may be made:

(i) The results show significant lateral variations in temperature distribution across the heater plate for both A & B and across the sample disc for B, with the right side at a lower temperature than the left side. The magnitude for the variation is higher for B than A.

(ii) Again significant variation longitudinally, although interestingly for both A and B the central point of the heater plate appears to be cooler than the top or bottom.

(iii) The figures for the difference in $T_{1/2}$ values between the sample disc and heater plate for both A and B suggest the surface of the heater plate is non-uniform, with the best contact on the right side (lowest difference) and the worst contact at the top (highest difference).

(iv) The mean data suggest there is less variation across the disc compared with the heater plate possibly indicating a smoothing effect perhaps dominated by the temperature of the area of best contact. The $T_{1/2}$ values from two additional full area discs run during the same experiment (A = 188°C; B = 386°C) may give some credence to this suggestion.

These results suggest that the heater plate has both a non-uniform surface and temperature distribution. The variation in temperature distribution is in agreement with the findings of Betts and Townsend (1993) (Equation 2.44 and Figure 2.6 from Chapter 2) although the results here emphasise that the distribution in real set-ups may well be more complex with significant lateral variations (assumed negligible by Betts and Townsend's model) and non-uniform distribution. Since the majority of routine samples are dispensed in the central region of the stainless steel discs, the results from the central position were replicated (6 fold) to allow an estimate of the effect of the sample discs. The results are shown in Table 3.10.

Table 3.10 Effect of stainless steel sample discs on glow curve position (II)

Anneal	Surface	Mean $T_{max} \pm 1\sigma$ (°C)[a]	Mean $T_{1/2} \pm 1\sigma$ (°C)[b]
A	Sample disc	225.2 ± 3.7	186.8 ± 2.1
	Heater plate	209.0 ± 1.8	170.7 ± 0.8
	S.D.- H.P.	16.2 ± 4.1	15.7 ± 2.3
B	Sample disc	413.3 ± 4.5	377.0 ± 3.7
	Heater plate	391.8 ± 2.1	356.3 ± 1.6
	S.D.- H.P.	21.5 ± 5.0	20.7 ± 4.0

[a] Reference temperature at the maximum of the first peak in the annealed glow curve.
[b] Reference temperature at a position on the rising edge of the first peak measured from half the peak maximum (this parameter [$T_{1/2}$] is introduced and discussed in section 4.1.2 of chapter 4).

These results suggest that for a heating rate of $5°Cs^{-1}$ the stainless steel sample discs are introducing a thermal lag of about 16°C for glow curve temperatures around 200°C, and about 21°C for glow curve temperatures around 400°C. For the same analysis temperatures Betts and

Townsends modified model predicts thermal lags of about 8.5 and 10°C (based on gas conduction; Equation 2.54 and Table 2.3, Chapter 2), and Piters model predicts thermal lags of about 4 and 8°C (Equation 2.48 and Table 2.4, Chapter 2). Both models underestimate the values measured in the experiment here, although equivalent ΔT values are estimated by modifying Piters' model so that the heat transfer mechanism at the bottom of the disc is by gas conduction alone (Table 2.4, Chapter 2).

3.3.3.2 Variation in grain size and heating rate

The standard potassium feldspar was only available in a ready crushed form with the majority of grains about 100 μm in size with very few larger grains. Therefore a microcline feldspar (Syenite-S374) was selected from the Geology rock store at SURRC which had previously been crushed and sieved to give a mixture of grain sizes from 215 μm up to about 1 mm. Amphibole impurity was removed from the sample using a magnetic separator. Very few grains sank in a 2.61 gcm^{-3} sodium polytungstate solution and therefore the sample was deemed to have satisfactory purity. The material was sieved and crushed to produce a number of grain sizes. Feasibility tests showed the sample to have low sensitivity, therefore a ^{60}Co dose of approximately 200 Gy was administered. Each grain size was split into 2 to form 2 sets (A and B) of different grain sizes and the same annealing procedure as above was carried out. Set A was annealed for 1 hour at 109.6 ± 2.7 (1σ)°C and B for 1 hour at 293.0 ± 5.3 (1σ)°C. Feasibility tests on the annealed material showed the TL signal from all grain sizes from set B to have poor, barely measurable signals. Set A showed TL signals dominated by an initial annealed peak (about 220°C at $5°Cs^{-1}$), a secondary high temperature peak (about 365°C at $5°Cs^{-1}$; not present in grain sizes less than 60 μm), and in many glow curves possible evidence of a larger peak still rising past 500°C. Therefore only material from set A was run, with glow curve measurements recorded from the first and second peaks. The material was dispensed to give roughly a 5 mm circle in the centre of sample discs, with six fold replication. Samples were measured with the same conditions as the above experiments but with 2 additional heating rates. The results are shown in Table 3.11 and 3.12.

Table 3.11 Effect of varying grain size and heating rate: Initial annealed peak

Grain size	Heating rate of 3°Cs^{-1}		Heating rate of 5°Cs^{-1}		Heating rate of 10°Cs^{-1}	
(μm)	$T_{1/2}$ (°C)	T_{max} (°C)	$T_{1/2}$ (°C)	T_{max} (°C)	$T_{1/2}$ (°C)	T_{max} (°C)
< 30	176.3 ± 1.4	205.8 ± 4.5	187.8 ± 1.2	220.0 ± 3.9	205.0 ± 1.6	236.8 ± 1.6
30-60	176.5 ± 1.1	208.5 ± 5.1	190.5 ± 1.2	224.5 ± 3.3	207.8 ± 2.5	238.5 ± 2.7
90-125	177.7 ± 2.3	210.2 ± 3.7	190.8 ± 1.6	223.7 ± 3.4	209.0 ± 4.4	241.3 ± 6.1
180-250	179.2 ± 1.8	214.0 ± 5.2	191.2 ± 1.2	222.2 ± 2.6	212.3 ± 2.2	246.7 ± 3.8
500-710	182.2 ± 1.5	213.3 ± 3.6	195.0 ± 1.5	228.3 ± 3.9	215.6 ± 2.4	247.8 ± 2.7

Table 3.12 Effect of varying grain size and heating rate: Secondary peak

Grain size	Heating rate of 3°Cs^{-1}		Heating rate of 5°Cs^{-1}		Heating rate of 10°Cs^{-1}	
(μm)	$T_{1/2}$ (°C)	T_{max} (°C)	$T_{1/2}$ (°C)	T_{max} (°C)	$T_{1/2}$ (°C)	T_{max} (°C)
90-125	296.0 ± 2.4	342.8 ± 9.3	**302.0 ± 2.0**	361.8 ± 4.1	**322.0 ± 4.0**	380.2 ± 5.2
180-250	304.3 ± 3.0	352.5 ± 4.8	**311.5 ± 2.5**	363.3 ± 2.3	335.8 ± 2.1	389.7 ± 2.5
500-710	**304.0 ± 4.0**	357.2 ± 4.1	-	371.3 ± 4.1	**347.5 ± 2.5**	393.8 ± 3.6

Figures in bold are the mean of less than six observations and the corresponding error estimates are half the difference between highest and lowest values. Blanks (-) are where no values could be measured.

If it may be assumed that the contribution to the thermal lag from grains of < 30 μm is almost negligible then the $T_{1/2}$ data from Table 3.11 gives a value of the lag for 100 μm grains of about 3 ± 2°C for a heater strip temperature (corrected for ΔT_{servo}) of about 188°C and heating rate of 5°Cs^{-1}. The corresponding heater strip temperatures and thermal lags at 3 and 10°Cs^{-1} are 175°C and 1.4 ± 2.7°C, and 206°C and 4 ± 5°C respectively. Further if one assumes that a curve of peak shift with reduction in grain size for the secondary peak has a similar form to the first (albeit with a greater rate of decay), an estimate of the thermal lag due to 100 μm grains may be obtained. By simple ratios this gives a value at 5°Cs^{-1} of about 7 ± 3°C at an approximate $T_{1/2}$ (corrected for ΔT_{servo}) of about 306°C. In comparison Betts and Townsends model estimates a thermal lag of about 2°C (2.6°C for a "quartz" sample) for a 100 μm feldspar sample at 500°C (Table 2.5, Chapter 2), whereas for the same parameters Piters' model estimates thermal lags for quartz and feldspar of about 7.5°C. Both models thus underestimate the thermal lag measured in this experiment, although, as with thermal lags associated with sample discs, equivalent ΔT values may be estimated utilising Piters model by allowing a variation in sample contact.

3.3.3.3 Combined effect of disc and sample

The results from measurements in sections 3.3.3.1 and 3.3.3.2 thus suggest the thermal lag associated with 100 μm grains on a stainless steel sample disc ramped at $5°Cs^{-1}$ is about 19°C at a heater plate temperature of 200°C, and about 30-40°C at a heater plate temperature of 400°C.

Treating the thickness of the sample as the sum of the disc plus the grain the ΔT_{servo}-corrected heater strip temperatures for both T_{max} and $T_{1/2}$ can be fitted to a second order polynomial (Equation 2.54) as Betts and Townsend (1993) suggest (Figure 3.9a). However, the curves all underestimate the additional thermal lag due to the sample disc and the form of the curve is incorrect in all cases since Betts and Townsend (1993) have positive first (a_1) and second (a_2) polynomial coefficients. This outlines that their model either does not fit cases of composite samples or it suggests that the disc to sample contact is far better than the heater plate to disc.

A linear fit to the data as suggested by Piters (1993) (Equation 2.50) is shown in Figure 3.9b. The linear regression coefficients and correlation coefficients (r) are shown in Table 3.13.

Table 3.13 Coefficients from Figure 3.9b

Coefficient	Heating rate of $3°Cs^{-1}$		Heating rate of $5°Cs^{-1}$		Heating rate of $10°Cs^{-1}$	
	$T_{1/2}$ (°C)	T_{max} (°C)	$T_{1/2}$ (°C)	T_{max} (°C)	$T_{1/2}$ (°C)	T_{max} (°C)
a_0 (y-intercept)	169.6	200.8	182.0	213.8	197.8	228.7
a_1 (slope)	9.80×10^{-3}	1.01×10^{-2}	9.76×10^{-3}	1.01×10^{-2}	1.55×10^{-2}	1.68×10^{-2}
r (correlation)	0.985	0.732	0.933	0.813	0.927	0.851

For a heating rate of $5°Cs^{-1}$ for a 100 μm disc this would yield a thermal lag of 3.6°C ($T_{1/2}$ data). This is clearly an underestimate compared with the empirical results and suggests, as with Betts and Townsends result, that the model is not applicable in the case of composite samples.

(a)

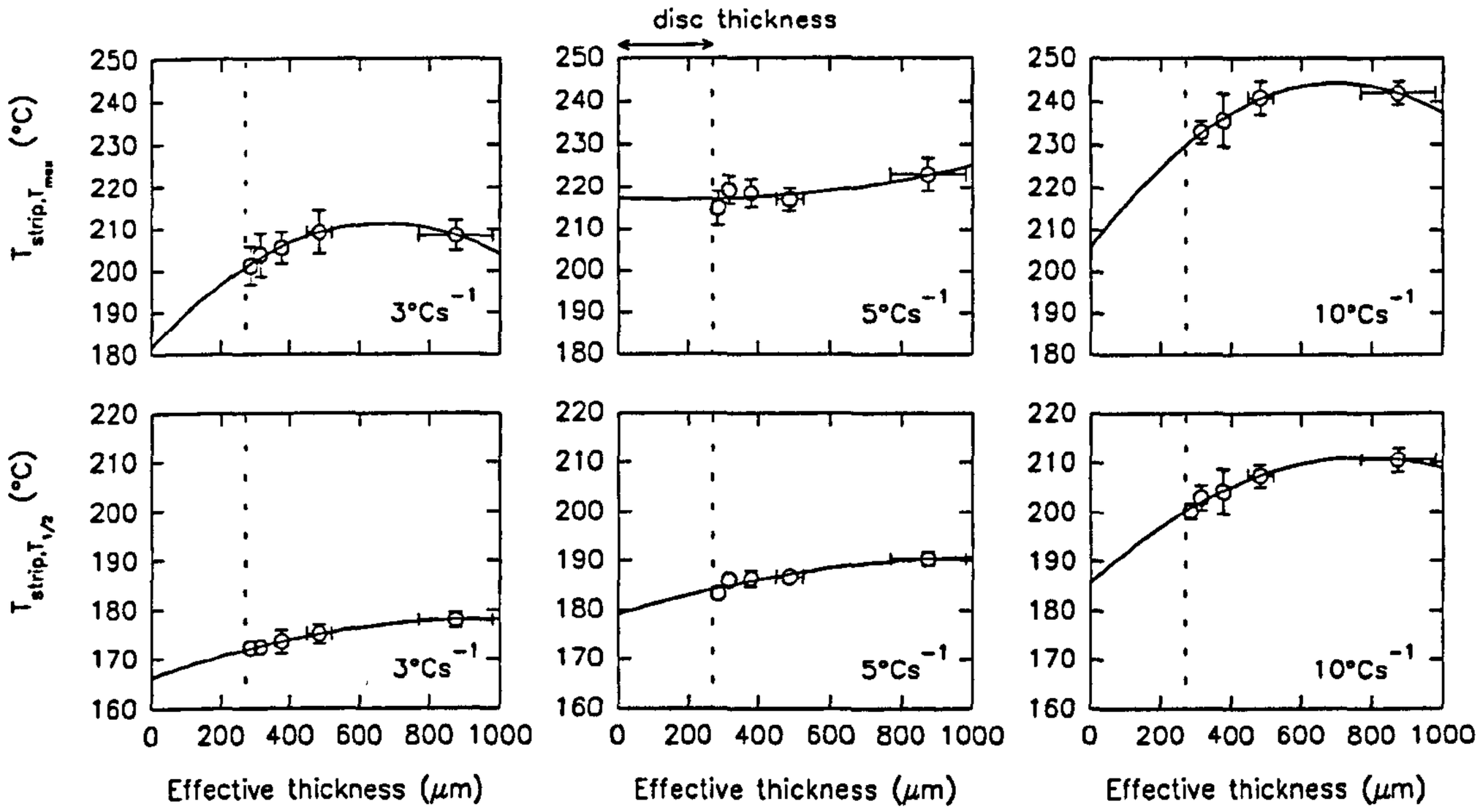

(b)

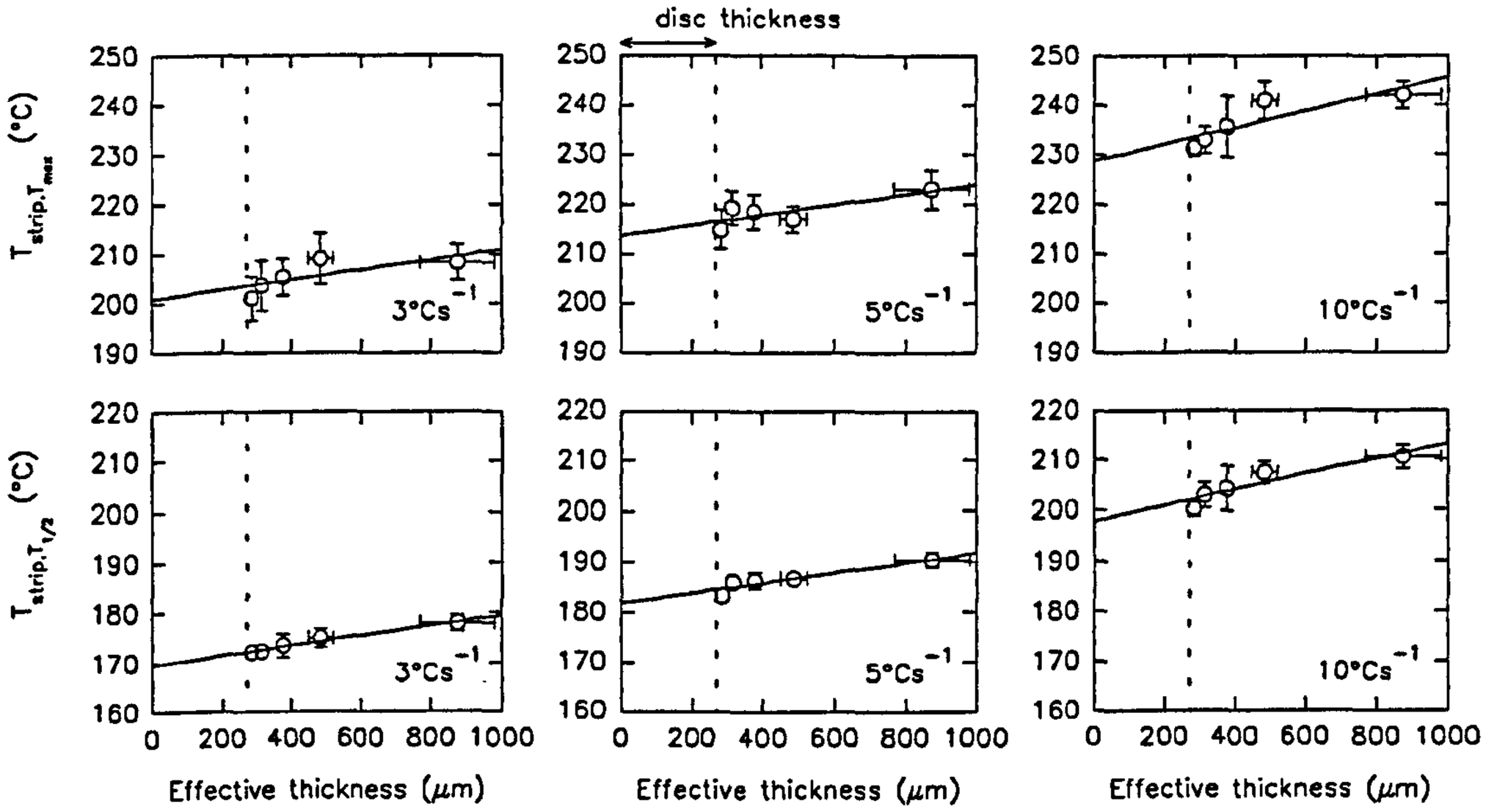

Figure 3.9 This illustrates the reference temperature data from Table 3.11 corrected for the servo-lag and non-linearity of the thermocouple response. The data was firstly corrected for the servo lag using a linear interpolation from the *PC with disc* data from Figure 3.8 ($\Delta T_{servo} = 1.3 \times 10^{-2} T_{ref} + 0.36$), and then these values were corrected for the non-linearity of the thermocouple response using the 10th order polynomial expression in Equation 3.3. The abscissa values are termed the *effective thickness* because the grain thickness is taken as the sum of the grain and the disc. In (a) a second-order polynomial has been fitted to the data in line with Equation 2.53 from Betts and Townsend (1993), and in (b) a linear relationship according to Piters (1993); Equation 2.50. Discussion of these relationships is in the accompanying text.

3.3.4 Overall glow curve accuracy

Many analyses of TL glow curves from spectral features such as shape and position require an accurate assessment of sample temperature. This is essential in kinetic studies if accurate parameters are required. Additionally accurate glow curve temperature (or precise relative behaviour) is a requirement in interlaboratory comparison studies. A number of problems present themselves in this respect for many TL systems. For this study these have been identified as the correction for the non-linearity of thermocouple response, the servo-lag between computer reference and heater plate (thermocouple) voltages and the thermal lag between the heater plate (or thermocouple) and the emitting surface of the sample. Sections 3.3.1 and 3.3.2 show that thermocouple non-linearity and servo-lag corrections are relatively straight forward. However, thermal lag corrections between heater plate and sample (3.3.3) are complex and either involve complicated heat transfer solutions (which at best only provide rough estimates and do not consider composite samples which are the most common geometry) or detailed characterisation experiments for particular minerals.

An alternative and simpler approach for the characterisation of TL apparatus for thermometry studies is proposed here which involves characterisation of minerals to an external isothermal anneal from a precise furnace, and the use of finely characterised TL apparatus giving high reproducibility on servo-lag. These procedures have been implemented in experiments in Chapter 4 and thermometry studies in Chapter 5. The IAEA F-1 potassium feldspar thermometry analyses described in Chapter 4 have subsequently been adopted by SURRC as the basis of international intercomparison studies of temperature calibration of luminescence readers from food irradiation testing laboratories (Sanderson *et al.*, 1996a). Although the empirical results for $5°Cs^{-1}$ TL (Section 3.3.3) give estimates of thermal lags of about 20°C at a glow curve temperature of about 200°C and 30-40°C at 400°C, the results for the SURRC instrumentation from intercomparison studies are very close to the average from all the laboratories tested. In general for the majority of laboratories tested the temperature calibration of luminescence apparatus was shown to be fairly poor.

3.4 Photostimulated luminescence excitation spectrometer: Instrumental details

The SURRC photostimulated luminescence excitation spectrometer has been described elsewhere (eg. Sanderson, 1990, 1991; Clark, 1992; Clark and Sanderson, 1994) and is illustrated in Figure 3.10. The spectrometer comprised a 300W Cermax Xe lamp which was coupled to a stepping motor driven f 3.4 monochromator and beam producing optics to illuminate samples with tuneable photon beams. The sample chamber contained a heater plate similar to the TL system described above, but the plate was mounted at a 45° angle to the incoming illumination beam and had a temperature range from -140°C to 500°C. To achieve the cryogenic range gaseous nitrogen was passed through a copper coil immersed in a liquid nitrogen dewar and from there passed through a capillary coil silver soldered to the base of the heater plate. Stimulated luminescence detection was via a Thorn EMI 9883 QB PMT in single photon counting mode (similar to the TL system described above) coupled through to a PC based MCS system, with control and analysis software (again the software was similar to the TL system described above, although additional routines in the acquisition code control the stepping motor and data acquisition from a pyroelectric radiometer). Optical filters were used to define both the detection window of the PMT, and for order sorting through the monochromator.

The diffraction grating used for experiments had a 1000 nm blaze with 600 lines mm^{-1} and a working range of 660-1500 nm; beyond these limits there was a decrease in efficiency. Adjustable slits at the entrance and exit to the monochromator governed the spectral bandpass.

Clark (1992) investigated characterisation of the light source in terms of the power spectrum and stability. Power spectrum measurements were obtained with a pyroelectric radiometer and showed, in particular, the spectral lines from the Xe lamp above 750 nm, and the necessary correction needed to enable analysis of excitation spectra without superimposition of the lamp power spectrum. Characterisation also showed the increased resolution of spectral lines from the Xe lamp with decreasing slit width at the expense of overall spectrum intensity. Warm up characteristics measured using a photodiode showed the most rapid change to occur over the first 20 minutes, and therefore a standard warm up time of 30 minutes was implemented. The power stability of the lamp was monitored with the pyroelectric radiometer by measuring the peak position and peak height of the two principal infra red peaks at 840 and 900 nm. For both

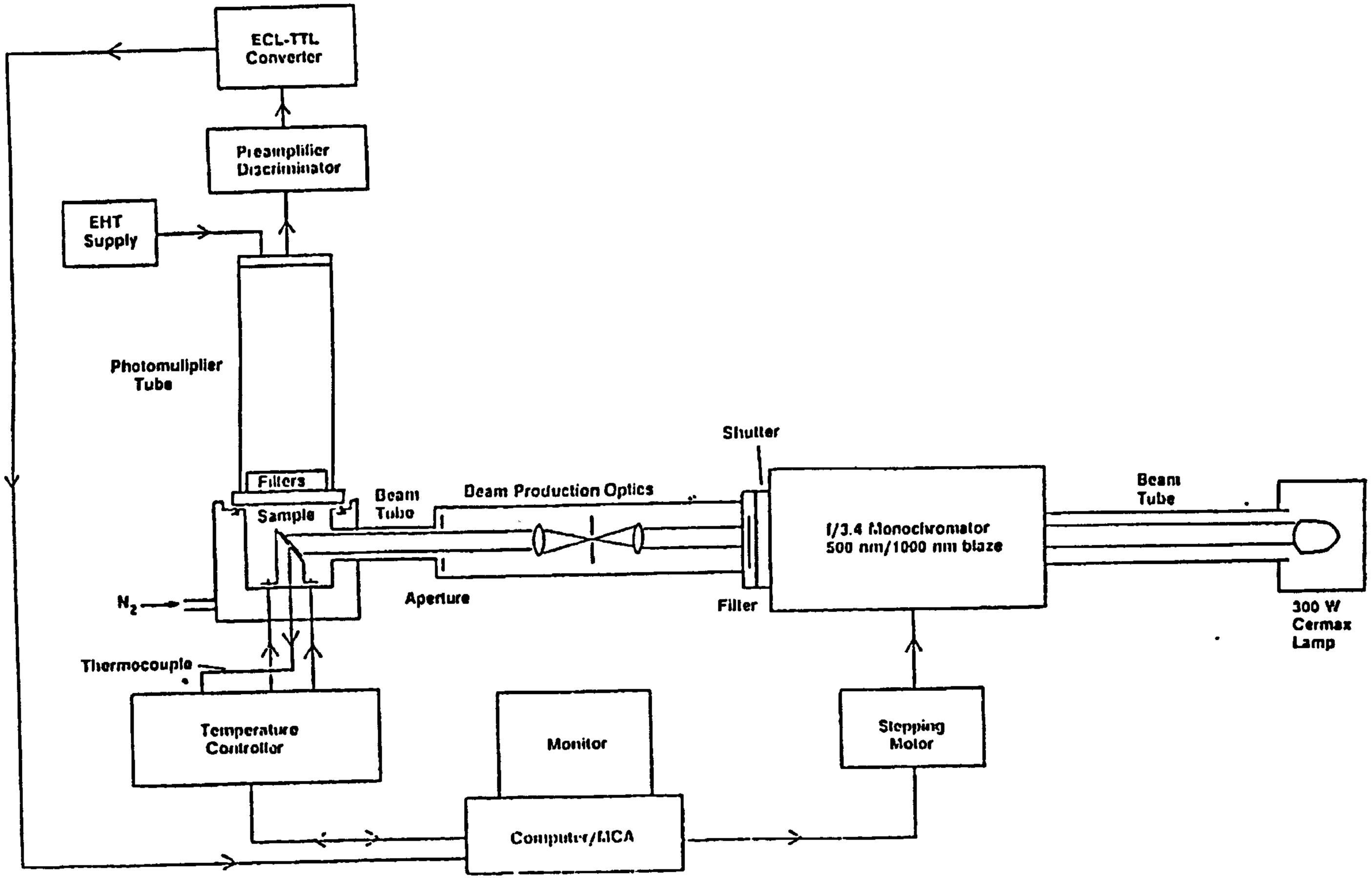

Figure 3.10 The SURRC excitation spectrometer (from Sanderson, 1990)

peaks monitored the peak height was shown to reduce in the same manner as the warm up characteristics, and the peak position remained stable within run-to-run scatter.

For scanning PSL excitation experiments (discussed in Chapter 6) the spectrometer was configured with a standard filter set up (eg. Sanderson, 1990, 1991; Clark, 1992; Clark and Sanderson, 1994) with detection of emitted luminescence defined by 3 mm of Schott UG11 and 2 mm of Schott BG39 (300-400 nm) and a 3 mm Schott GG475 to block second order effects through the monochromator, enabling excitation from 450-950 nm.

3.5 Pulsed infra red diodes: instrumental details

Research at SURRC into stimulating luminescence using pulsed infra red diodes has been in progress for a number of years, in connection with the detection of irradiated foods (Sanderson *et al.*, 1996b) and evaluation for archaeological dating (Clark, 1992). In 1991 a prototype pulsed system was constructed to improve signal detection from unseparated materials of intermediate or low sensitivity foods. Further developments produced a high power, long-pass filtered, pulsed IR system, utilising digital lock-in photon counting. The pulsed IR system used for experiments in this thesis (Chapter 6) was similar in design to a commercial instrument developed at SURRC for screening irradiated foodstuffs.

The IR light emitting diode (LED) array consisted of 3 clusters of 3 diodes arranged in a circular collar with 120° between each cluster. The collar was designed to slot into position between the oven and PMT on the TL system described above. Each cluster of diodes was angled to illuminate a sample positioned on the heater plate in the TL oven. The diodes were high power GaAlAs IR LED's (RS components Ltd.) with peak emission of 880 Δ 80 nm with a power of 20 mW at 100 mA.

The detection of signals was characterised with a 4 mm Schott BG39 band pass filter, and stimulation restricted by 3 mm Schott RG780 long pass filters. The digital lock-in counting system operated by accumulating sample counts and background counts (principally PMT dark counts) while the LED's were on, and subtracting the background count from the accumulated counts while the LED's were off. The LED's were pulsed on and off for equal periods of 15 µs.

A control unit contained a pulsed current source for the IR LED's, and photon counting electronics. Additionally a data port connected the control unit to the PC attached to the TL system. Software, written in Quick Basic, had control, run and filing menus. The control menu enabled the user to test the photon counters (clear, count down, hold, up/down count), establish dark count, turn a line printer off or on, and set the temperature of the heater plate. The run menu enabled the user to enter filename, cycle time (ie. length of time the LED's pulse on and off), and the number of cycles for measurement and automatic data recording.

The pulsed PSL system achieved both high sensitivity and high signal to background ratio. The IR source was relatively high power compared to other systems (180 mW cf. typically 60 mW) which lead to high sensitivity. The combination of the long-pass filtering of the IR source and the band-pass filtering of the PMT minimised cross-talk while allowing a high proportion of the luminescence signal through. The pulsed mode of the IR source allowed phase-sensitive detection which minimised the effect of the system background signal. It was estimated that these elements combined together improved the signal to background ratio of this PSL system by about 1-2 orders of magnitude compared to most IR systems.

3.6 Summary

This chapter initially discusses details of the TL instrumentation used in this project with comparisons to other systems. The development of TL oven and detection capabilities to record TL to 700°C to enable measurement of remnant geological signals in archaeological materials is described, with details of later developments for an 800°C TL system. Signal detection to 700°C was particularly difficult due to the advent of intense black body radiation. This was achieved using various optical configurations, with the best results from a Corning 7-51, Schott BG39 and Schott BG3 filter combination. The high temperature system was shown to be extremely stable with a mean servo-lag of 16.0 ± 0.8°C (1σ; n = 270 readings). Application of the high temperature set up to many archaeological samples is discussed in Chapter 5.

The problems associated with the temperature calibration of glow curves were then discussed with sections dealing with the non-linear correction of the thermocouple response, the servo lag

correction between the computer reference and heater plate temperature, and the thermal lag between the heater plate and the emitting surface of the sample. Empirical results were related to current heat transfer models for TL measurement previously discussed in Chapter 2. A further section assessing the overall glow curve accuracy emphasised the complexity of heat transfer models and detailed characterisation experiments for particular minerals, and suggested an alternative external characterisation approach which is developed in experiments in Chapter 4 and used in thermometry studies in Chapter 5.

Finally the instruments used to investigate the potential of PSL thermometry (discussed in Chapter 6) were described.

Chapter 4: Thermoluminescence experiments[†]

4.1 Controlled annealing experiments of feldspar

This experiment was set up to explore the effects of varying the temperature and time of annealing conditions in the laboratory on the TL properties (eg. remnant glow curve position, modification in glow curve shape, sensitivity changes, etc.) of a standard potassium feldspar.

4.1.1 Experiment design and methodology

The experimental procedure comprised comparison between glow curves from aliquots which were beta irradiated, stored, thermally annealed and measured, and control measurements (made on the same aliquots) identical with the exception of the annealing step. TL measurements were made on several sequential annealing cycles from each of the samples, interleaved with further control measurements of the pure β response. Annealing results were normalised to the mean of the control measurements bracketing each observation. In this way the effects of thermal treatments could be observed independently of confounding factors such as TL sensitivity changes and post-irradiation fading.

The standard material used was a 90-125 μm sieve fraction of an IAEA potassium feldspar (F-1). Stainless steel discs (10 mm diameter; 0.25 mm thick) were cleaned in acetone, dried in tissue and sprayed with silicon grease. Approximately 2 mg aliquots of the feldspar sample was dispensed onto each of five discs. Preparation included heating each sample for 30 s at 600°C in the Apple IIe TL system oven by raising the temperature of the heater plate manually (ie. using the internal reference voltage). This was done to remove the remnant geological TL from the feldspar. The standard irradiation step was a 2 Gy dose from a 1.48 GBq (40mCi) ^{90}Sr β source (dose rate approximately 30 $mGys^{-1}$). An estimate for the largest systematic error in timing irradiations is ± 2 s equivalent to ± 0.06 Gy (66 s ≡ 2 Gy). The source was housed in a lead castle with a drawer facility for single disc irradiations. The drawer was air dusted before sample irradiation. Seven annealing temperatures were investigated: 50, 100, 150, 200, 250, 300, 350°C. The experiment was split into 3 stages:

[†] The majority of this chapter is summarised in a published article, a copy of which is in Appendix A.

(1) At each temperature samples were annealed for 20 to 100 s in steps of 20 s. Samples were annealed using the Apple IIe TL system oven. The temperature of the heater plate was raised manually and all samples were annealed in the usual oven atmosphere of nitrogen (OFN).

(2) 100 to 2100 s in steps of 500 s. Samples were annealed in the TL oven as in (1).

(3) 2100 s to 22100 s in steps of 5000 s. Samples were annealed in a muffle furnace in a nitrogen atmosphere. The discs were placed in the furnace inside small aluminium foil trays. The temperature of the furnace was measured with a chromel-alumel thermocouple spot welded at the hot junction to a sample disc. A thermocouple thermometer (Digi-Sense 8528-20) was used to measure the temperature of the thermocouple. Temperature gradients of the order of 5-10°C were measured across the furnace cavity, hence at the position of required temperature samples were placed as close to the hot junction as possible to minimise annealing error. Annealed samples were removed from the furnace and allowed to cool in air. Samples were only annealed to 300°C as this proved to be the limit of the experiment.

Table 4.1 shows the annealing regime for 20 and 100 s at annealing temperature *T*. The annealing regimes for discs 2, 3 and 4 were 40 s then 80 s, 60 s then 60 s, and 80 s then 40 s respectively. Upon completion each temperature / time combination had been run twice and the glow curves corresponding to these pairs could be compared. Also each disc had been subjected to a total annealing time of 120 s with normalising glows before and after each annealing run. As shown there was an elapsed time between irradiation and read-out of 180 s for each run. Thus the normalising / annealing sequence was directly comparable. From analysis of TL sensitivity change within the 35 five measurement sequences of stage 1, it was decided that 2 normalising or control runs bracketing an annealing cycle were adequate, thus the middle control run was removed in stages 2 and 3. Additionally due to the longer annealing times involved the delay between irradiation and read-out was 2200 and 22300 s respectively.

Table 4.1 Annealing regime for 20 and 100 s at T, where T = 50-350°C in steps of 50°C

Disc	Run	Annealing regime		
1	1	Dose	180 s delay	Measure
1	2	Dose	30 s delay + 20 s at T°C + 130 s	Measure
1	3	Dose	180 s delay	Measure
1	4	Dose	30 s delay + 100 s at T°C + 50 s	Measure
1	5	Dose	180 s delay	Measure
5	1	Dose	180 s delay	Measure
5	2	Dose	30 s delay + 100 s at T°C + 50 s	Measure
5	3	Dose	180 s delay	Measure
5	4	Dose	30 s delay + 20 s at T°C + 130 s	Measure
5	5	Dose	180 s delay	Measure

The resulting glow curve from each temperature / time combination was recorded from ambient temperature to 450°C with the Apple IIe based system. Photon detection comprised a THORN EMI 9883QB PMT (bialkali photocathode) with a blue-ultraviolet Corning 7-59 filter and a Schott KG1. This was the same set up used for routine dating work in the laboratory. The Schott filter had a similar function to the Chance Pilkington HA3, and this detection set up was therefore in line with well established TL dating configurations (Fleming, 1979; Aitken, 1985). The system automatically carried out a second temperature ramp to record and subsequently subtract the black body component from each glow curve. The heating rate used was 6.2°Cs^{-1}. All measurement (read-out) of discs was carried out in an N_2 atmosphere. All experiments were carried out under safe light conditions.

The glow curve data was smoothed and integrated into 10°C temperature bands. The annealed glow curves were normalised to the control runs to produce a representation of the thermal treatment, whereby the effect of annealing was characterised by a rising edge in the data and thereafter a plateau, analagous to the plateau test used in luminescence dating. The plateau response P of each disc i at a particular annealing temperature T can be expressed by

$$P(i, T_{glow}) = \frac{I_A(i, T_{glow})}{\overline{I_C}(i, T_{glow})} \qquad (4.1)$$

where I_A and T_{glow} are the TL intensity of the annealed glow curve and the temperature integral, respectively. $\overline{I_C}$ is the mean intensity of the control runs performed on the same disc before and after the thermal treatments.

The modification thermal treatment has on glow curve position and shape may be expressed by calculating the product of the plateau response and the mean intensity of all controls (or alternatively a typical control glow curve) for each temperature integral to give the annealed response A, thus

$$A(i, T_{glow}) = P(i, T_{glow})\, \overline{I_C(T_{glow})}. \qquad (4.2)$$

This enables the direct comparison of the effect of any number of individual thermal exposures on an un-annealed (control) glow curve.

4.1.2 Glow curve analysis: $T_{1/2}$ parameter

Part of the research in the luminescence group at SURRC has been involved in developing methods for the detection of irradiated foodstuffs (eg. Sanderson *et al.*, 1989, 1994; Sanderson, 1990). An important aspect in the development of detection methods was knowledge of signal stability over fridge / shelf storage periods. An unpublished pilot study was undertaken to investigate the thermal stability or thermal fading of the TL of a 1 kGy ^{60}Co dosed standard microcline feldspar. Sufficient feldspar discs were irradiated to enable duplicate TL signals to be measured promptly after irradiation, and then after 1, 3.5, 7,

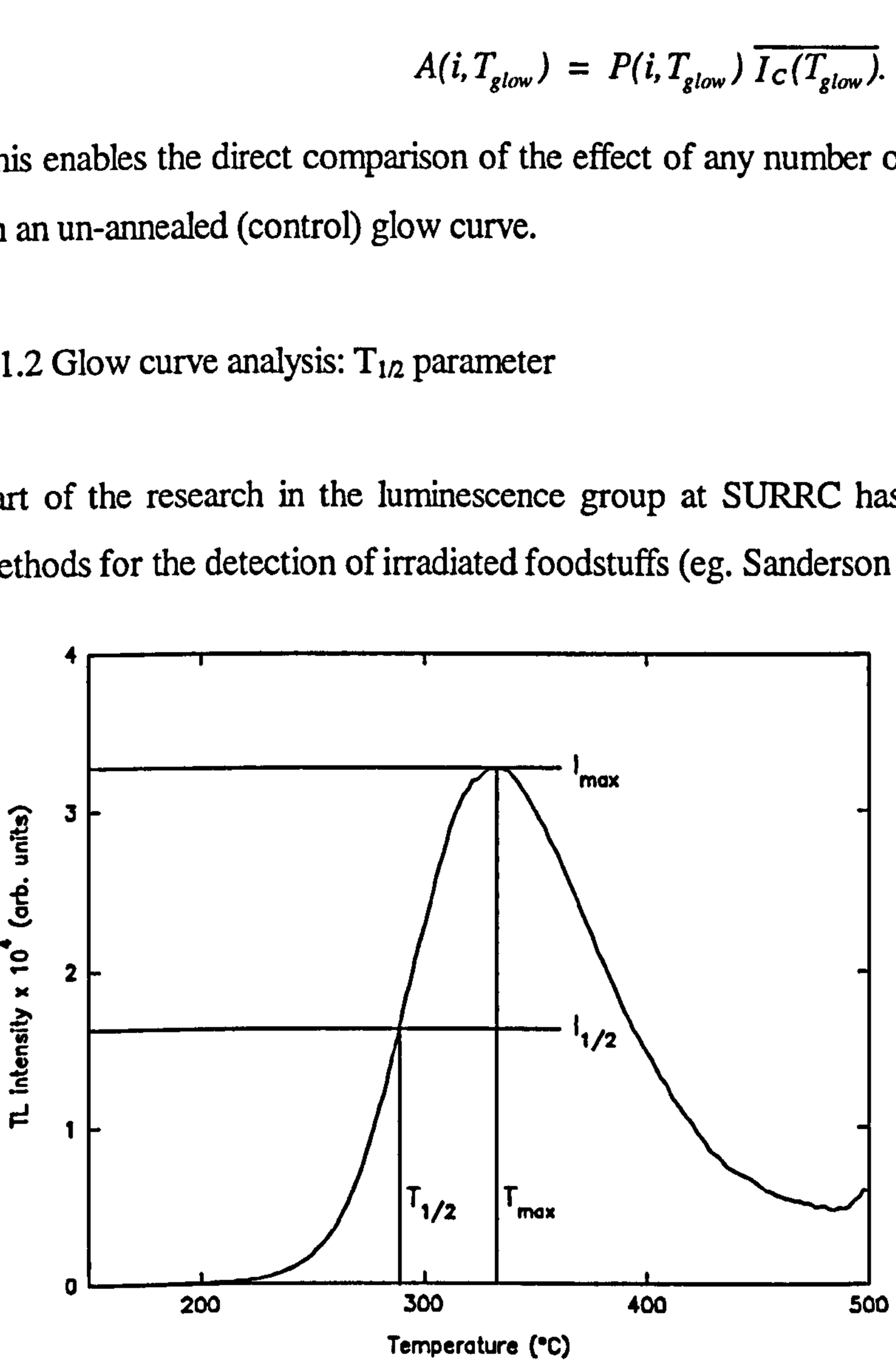

Figure 4.1 Derivation of $T_{1/2}$ parameter

14 and 28 days dark storage at temperatures of 5, 30 and 55°C. The temperature of the rise of the glow curves were recorded at 10, 50 and 90% of the height of the associated peak maximum. The results demonstrated that the curves with time were equally spaced over the narrow range of storage temperatures.

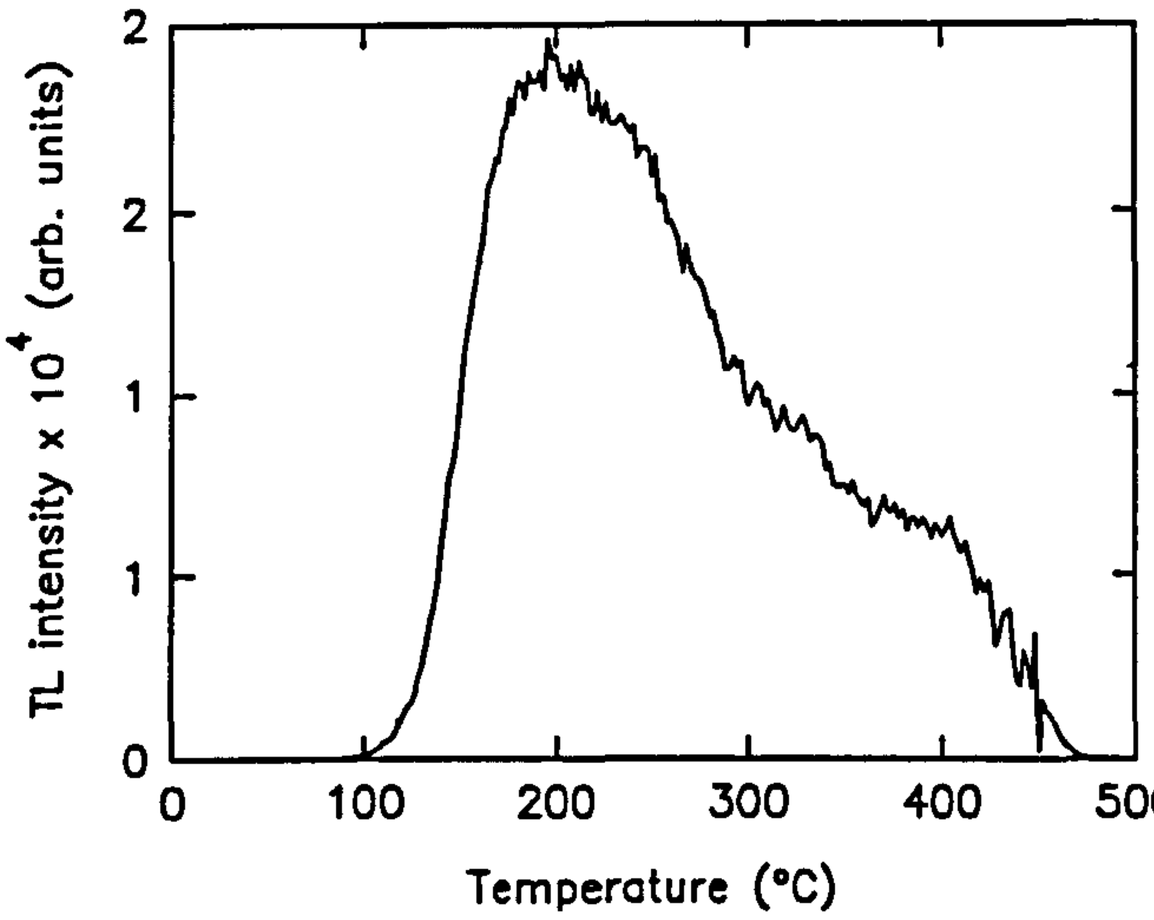

Figure 4.2 Net TL glow curve from F-1 disc annealed for 80 s at 100°C before read-out.

Measuring temperatures from positions on the first rise of the glow curve was preferable to the peak maximum position because the peak was often ambiguous due to system noise (even after smoothing operations), or there was a broad multiple component feature which did not relate exclusively to the first rise of the glow curve, or the maximum was obscured by further combinations of peaks in the glow curve continuum. The temperature at 50% or $T_{1/2}$ was the best parameter to measure (Figure 4.1) as it behaved in a similar manner to a mathematical inflection and the count rate was at a maximum, and therefore the effect of undesirable noise (due to for eg. a surging heater circuit, low signal level with respect to background or spurious luminescence) had on the glow curve was far less as demonstrated by the relative smoothness of the first rise of a typical glow curve in Figure 4.2. It followed, therefore, that the position of $T_{1/2}$ was at a maximum in the first numerical derivative of a glow curve, and zero in the second (Figure 4.3). This was a further advantage as a value for $T_{1/2}$ could still be determined in

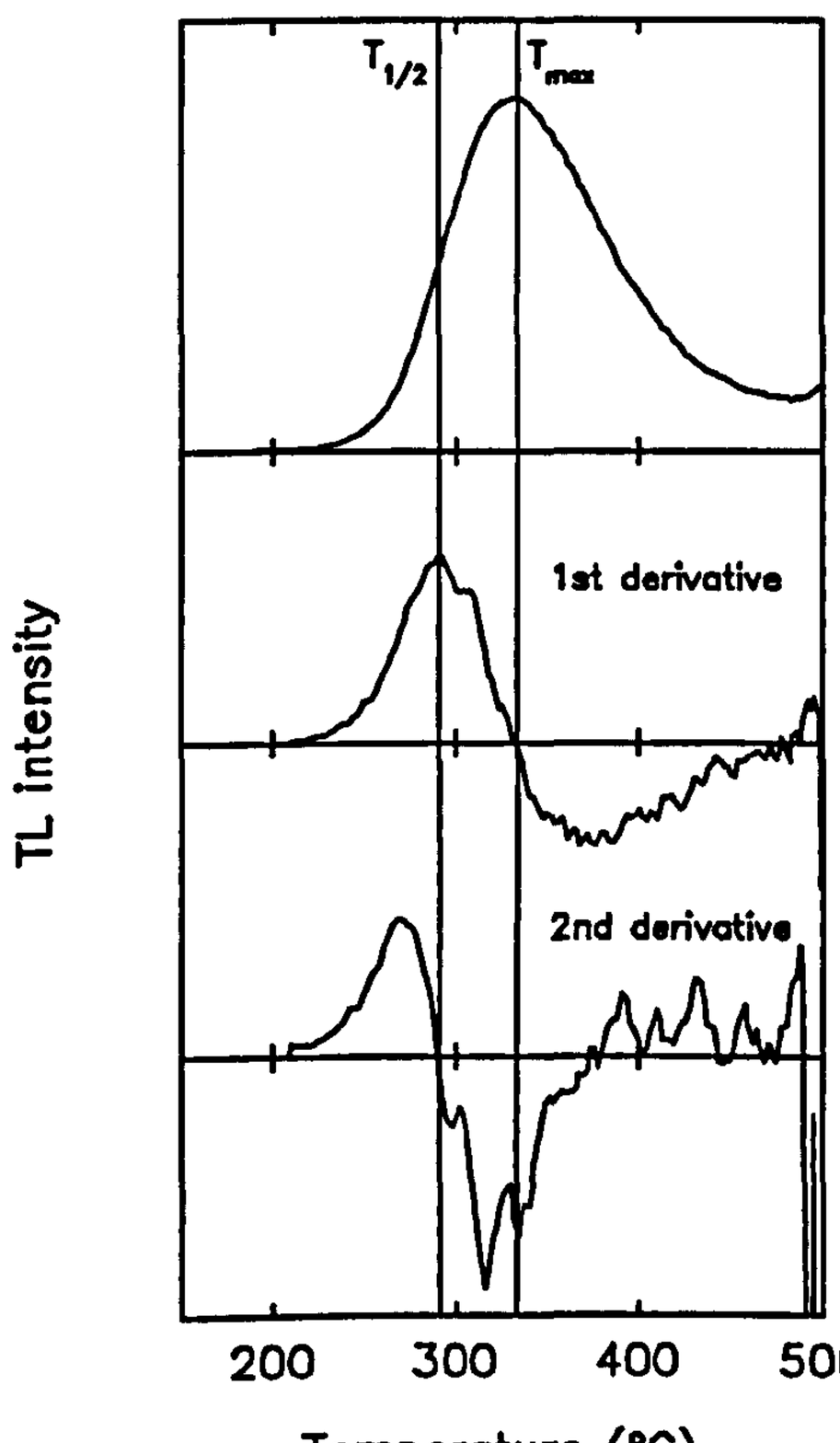

Figure 4.3 $T_{1/2}$ position for 1st and 2nd derivatives

instances where the maximum was uncertain (eg. masked by close proximity higher intensity single peaks or multiple component interactions, low intensity noisy signals (low S/B ratio), or at the extremes of $T_{1/2}$ detection).

4.1.3 Results

4.1.3.1 Removal of TL signal

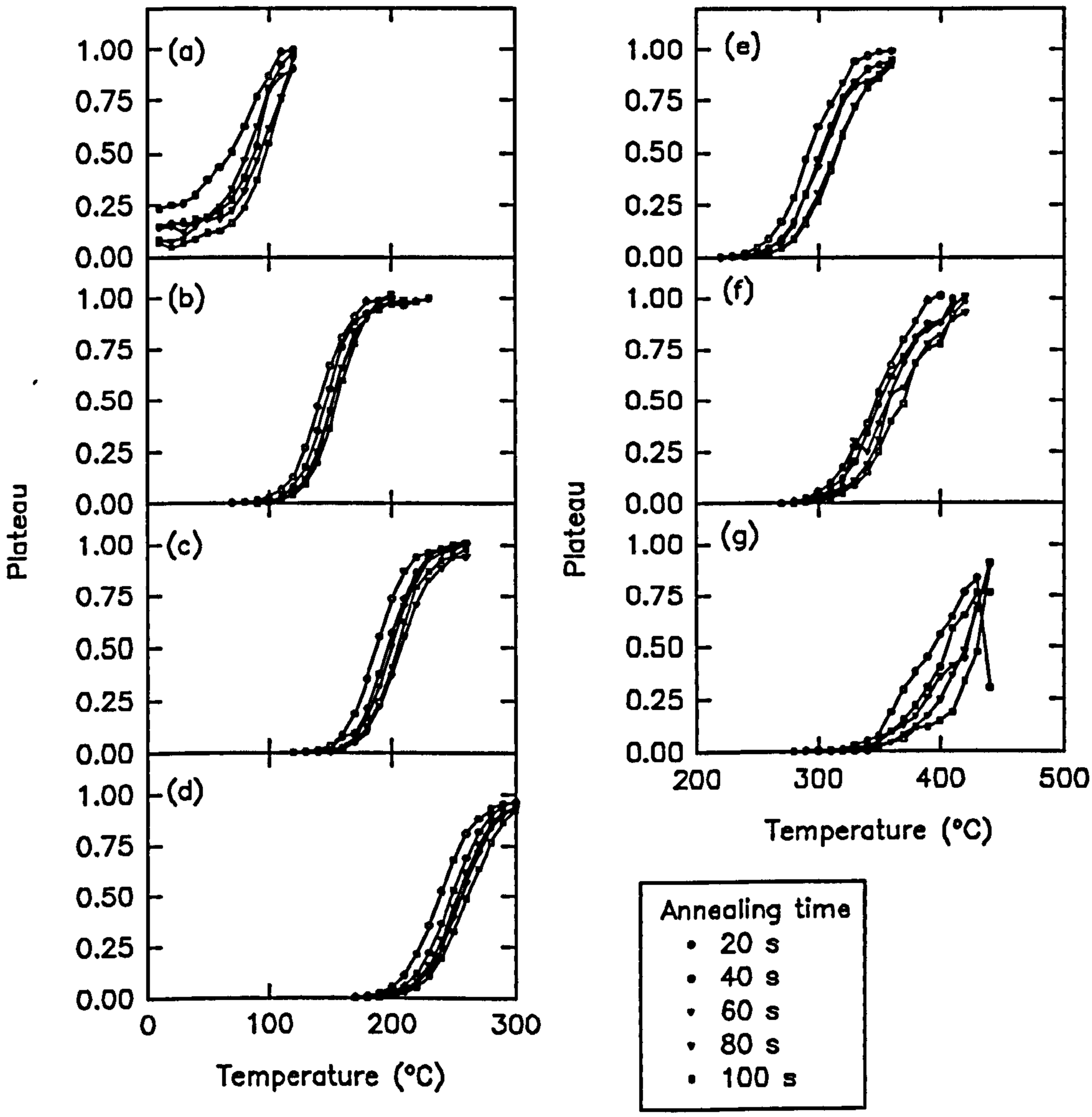

Figure 4.4 Stage 1 results of controlled annealing of F-1 expressed as the mean plateau response. (a) 50°C; (b) 100°C; (c) 150°C; (d) 200°C; (e) 250°C; (f) 300°C; (g) 350°C.

The results of the 3 stages of the controlled annealing experiments expressed as the mean plateau response (ie. mean of 2 cycles) are illustrated in Figures 4.4, 4.5 and 4.6. A linear interpolation has been used to improve the clarity of contrasting sets of data points, and in all cases only the data occurring before a plateau is reached (ie. before unity) is represented.

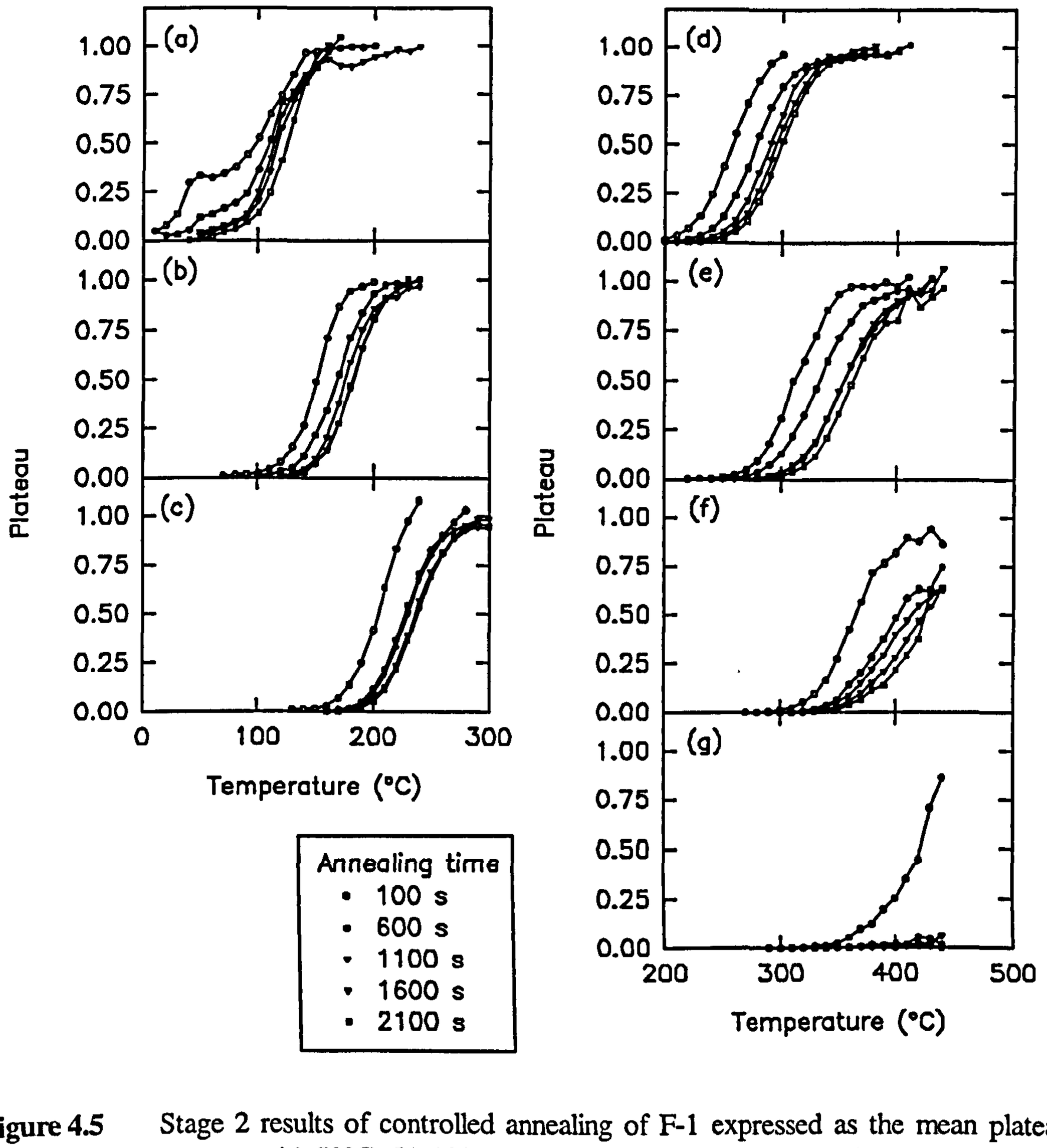

Figure 4.5 Stage 2 results of controlled annealing of F-1 expressed as the mean plateau response. (a) 50°C; (b) 100°C; (c) 150°C; (d) 200°C; (e) 250°C; (f) 300°C; (g) 350°C.

The results show the expected behaviour of decreasing remnant TL signal as the lower temperature components are progressively removed with increased thermal exposure. The feldspar shows clear thermometric behaviour, the mechanism which determines the position

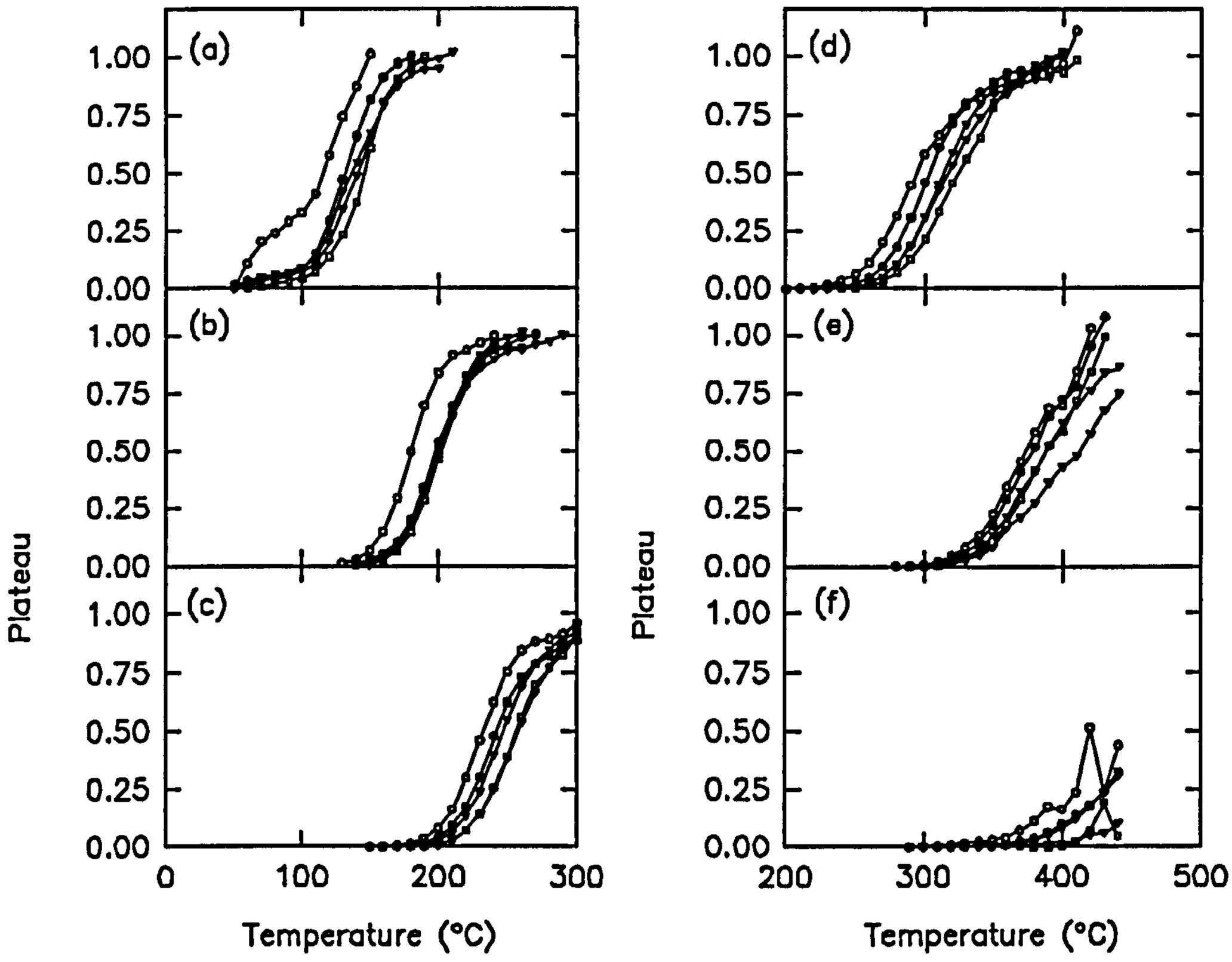

Figure 4.6 Stage 3 results of controlled annealing of F-1 expressed as the mean plateau response. (a) 50°C; (b) 100°C; (c) 150°C; (d) 200°C; (e) 250°C; (f) 300°C.

of the remnant glow curve relating to both temperature and duration. In all the results the same general pattern is repeated as the data rises smoothly through an inflection to a plateau. Deviations from this pattern in Figures 4.4a, 4.5a and 4.6a are due to the presence of phosphorescence and / or spurious luminescence, and the scatter in Figures 4.4g, 4.5g and 4.6f is due to the signal to noise ratio increasing as the black body component becomes more prominent at high temperature, implying the limit of detectable plateau for the standard dose employed and the instrumental conditions (eg. see Section 3.2.1, Chapter 3). Clearly varying the

temperature of thermal treatment dominates the remnant glow curve position, whereas increase in duration generally has a progressively smaller effect.

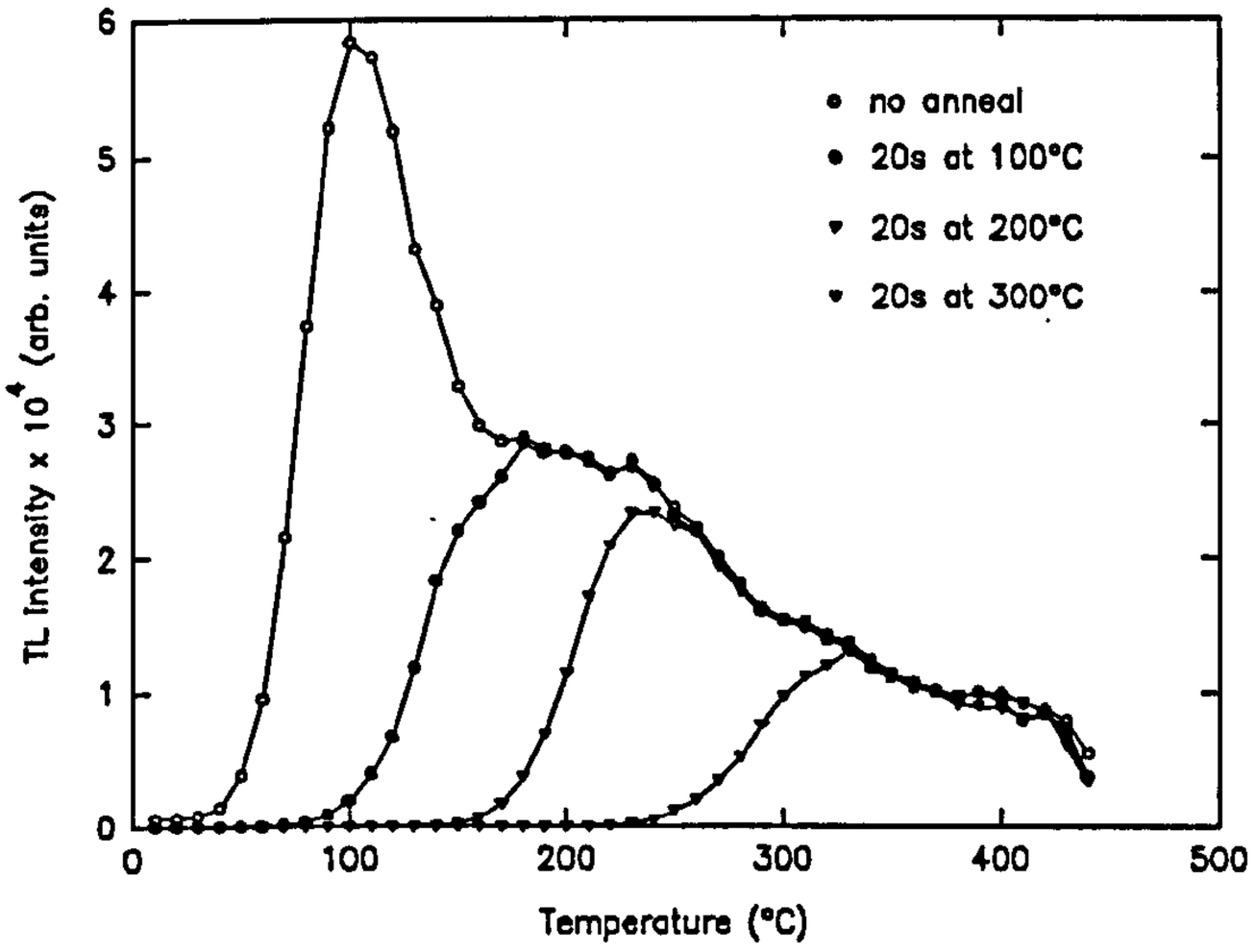

Figure 4.7 Results of controlled annealing of F-1 expressed as the annealed response of the TL glow curve. 20 s annealing for 100, 200 and 300°C.

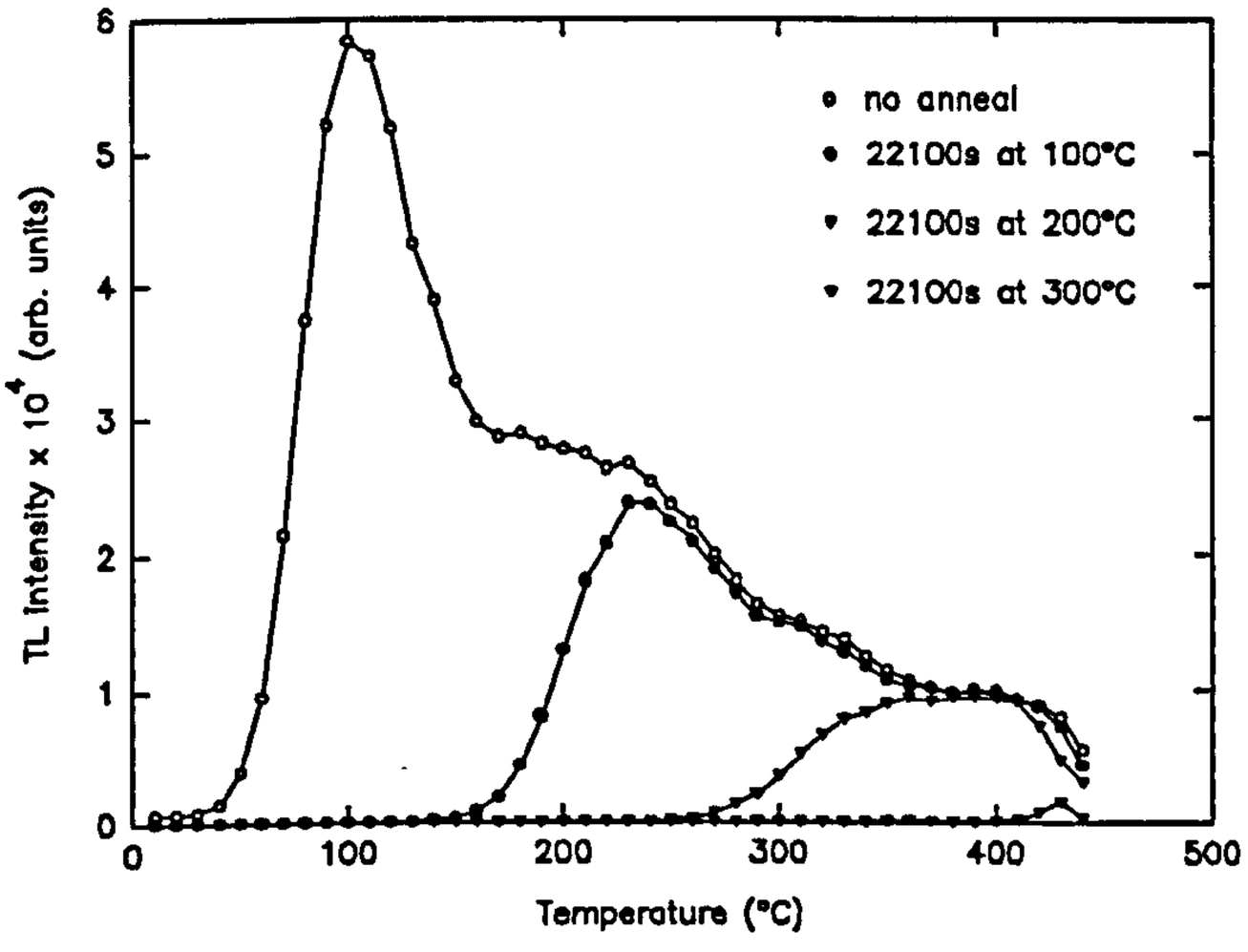

Figure 4.8 Results of controlled annealing of F-1 expressed as the annealed response of the TL glow curve. 22100 s annealing for 100, 200 and 300°C.

The progressive modification resulting from annealing at temperatures of 100, 200 and 300°C is expressed in glow curve form at the two extremes of annealing duration (20 s and 22100 s) in Figures 4.7 and 4.8 respectively. The annealed glow curves represent the effective modification thermal treatment has on a typical control glow curve by calculating the annealed response (Equation 4.2). As with the plateaux data, the data symbols represent photon counts in a 10°C temperature integral. As before a linear interpolation has been used between data points. The unannealed glow curve has a typical feldspar shape with a number of common features including a large low temperature peak and general broad overlapping features. The progressive modification of the glow curves, expressed as the annealed response, may be represented for all 13 annealing durations for a particular isothermal with the use of a three dimensional plot. Figure 4.9 shows the data for an annealing temperature of 200°C. A log time scale has been used here to show more details of the glow curve modification. The log time

scale clearly shows the progressively smaller effect of the annealing time, with the main modification occurring in the first 20 s.

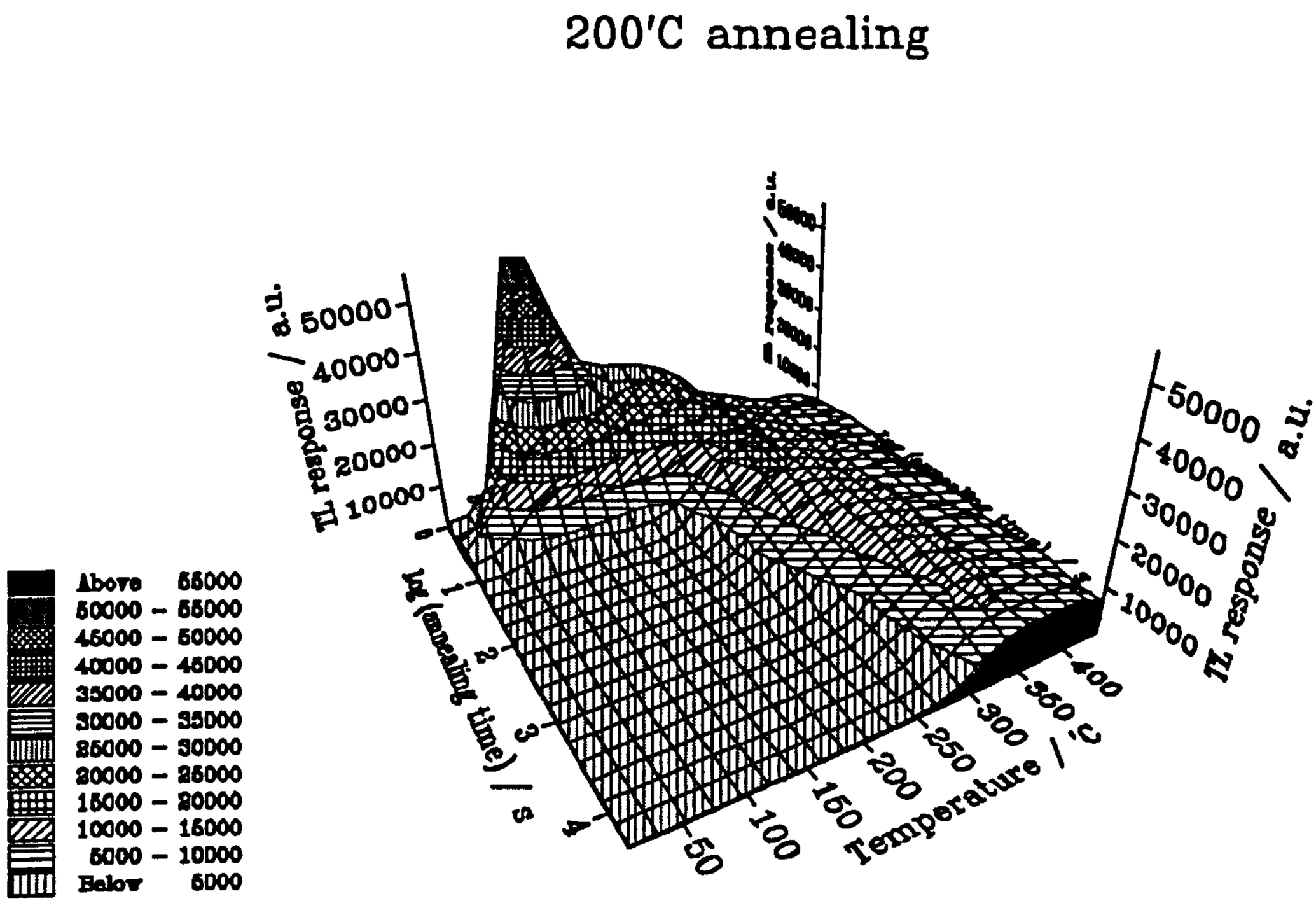

Figure 4.9 Progressive glow curve modification at an annealing temperature of 200°C

4.1.3.2 $T_{1/2}$ values

$T_{1/2}$ values for all 100 duplicated glow curves were measured and are shown plotted against the annealing time in Figure 4.10. These data reinforce the observations made above of the dominant effect of temperature compared with the progressively smaller effect of time, and go. further to suggest that the effect on $T_{1/2}$ by an increase in temperature appears to be linear whereas the effect of time is non-linear, with $T_{1/2}$ stabilising rapidly for each isothermal. Indeed, when a logarithmic representation is examined (Figure 4.11) the progressive log(t) dependence, which appears to characterise this process, is revealed. The dashed lines on the figure are the results from a constrained linear regression analysis performed on the $T_{1/2}$ data which statistically confirms the hypothesis that a linear-log temperature-time dependence provides a reasonable description of the behaviour. This supports the concept of a simple complementary relationship, whereby the thermal exposure for any combination of thermal events may be evaluated by integrating the product of temperature and log(time), thus:

$$Thermal\ exposure \propto \int_0^t T(t).\log(t)dt \qquad (4.3)$$

where T is the annealing temperature and t the annealing time. In this way, non-isothermal heating cycles may also potentially be represented by a similar thermal exposure index, which in principle correlate with the measured $T_{1/2}$ parameters from subsequent TL measurement.

The error associated with each pair of measurements was taken as half their difference and as Figure 4.12 illustrates the majority of $T_{1/2}$ values are reproducible to 1 or 2°C, with a mean error for all the observations of 3.3 ± 3.7 (1σ) °C. High errors occur principally for four reasons;

i) comparison of $T_{1/2}$ at the end of stage 1 with the beginning of stage 2, or the end of stage 2 with the beginning of stage 3;

ii) at the extremes of signal detection when the signal to noise ratio is low and a plateau is not achieved creating problems in determining $T_{1/2}$ values;

iii) when the duration of annealing is short compared with the time taken to heat / cool the sample;

iv) timing of short annealing.

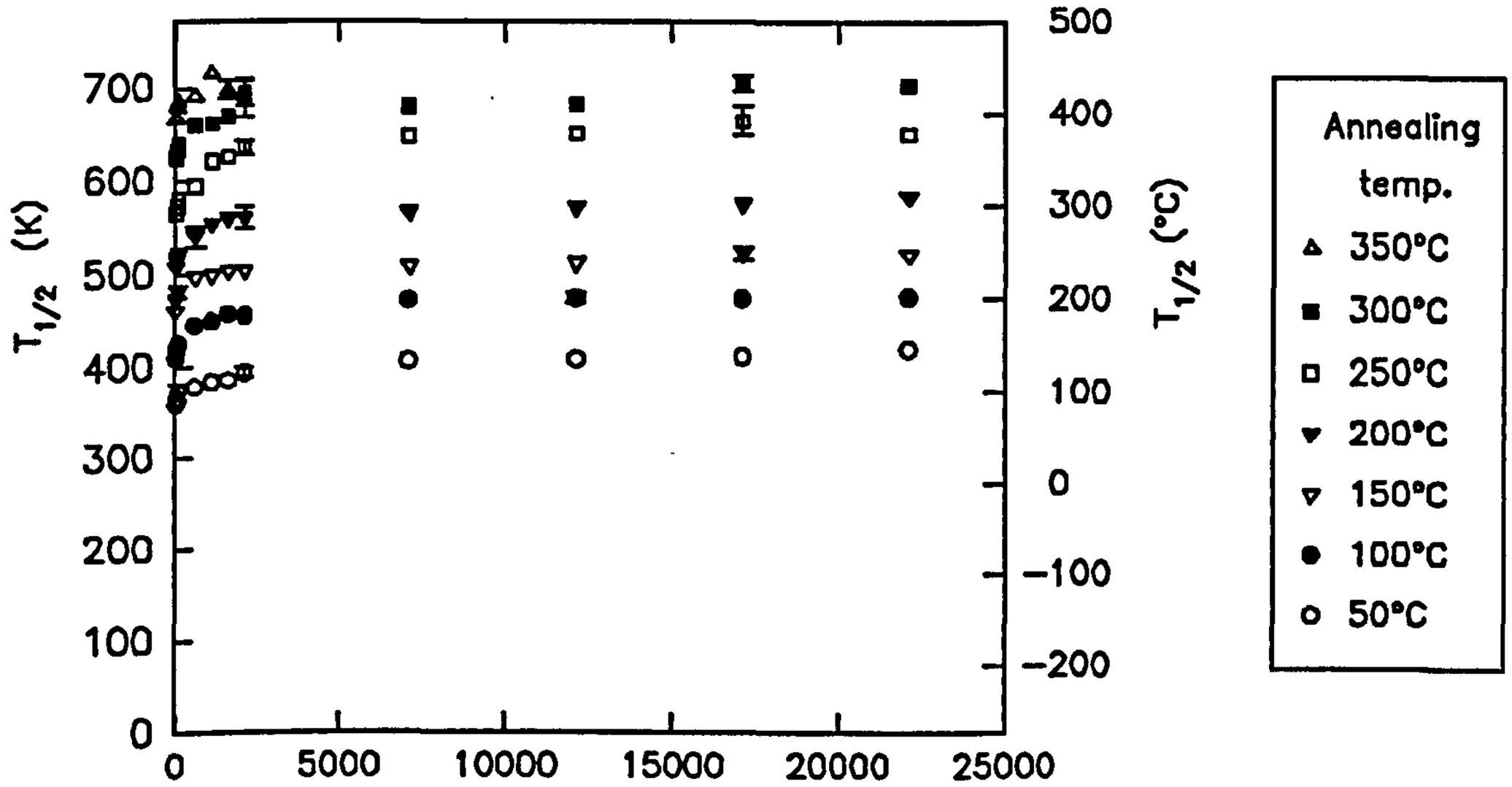

Figure 4.10 Variation in $T_{1/2}$ with annealing time for different annealing temperatures

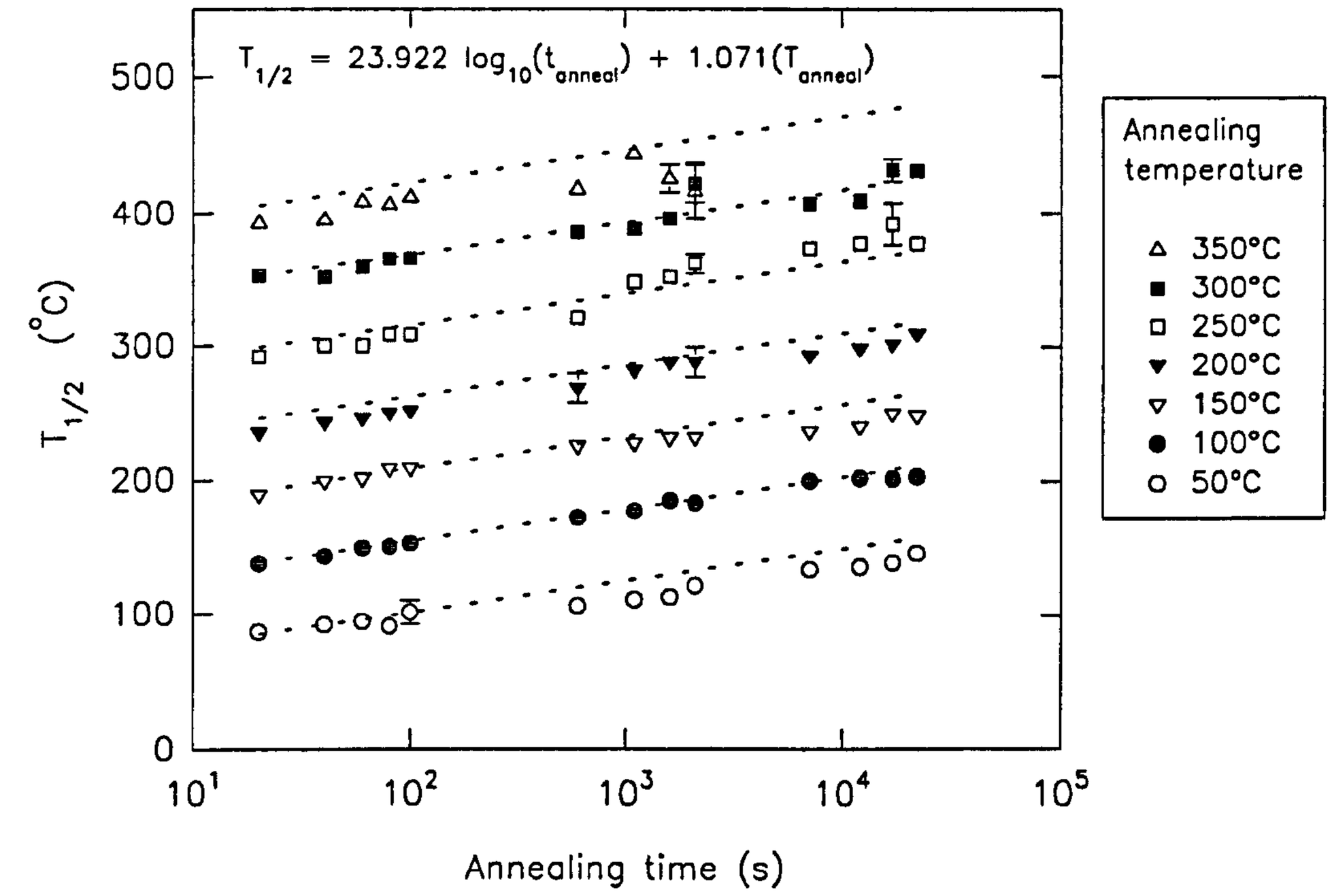

Figure 4.11 Relationship between $T_{1/2}$ and the temperatures and durations of isothermal annealing for samples of IAEA F-1 potassium feldspar (--- = constrained linear regression analysis).

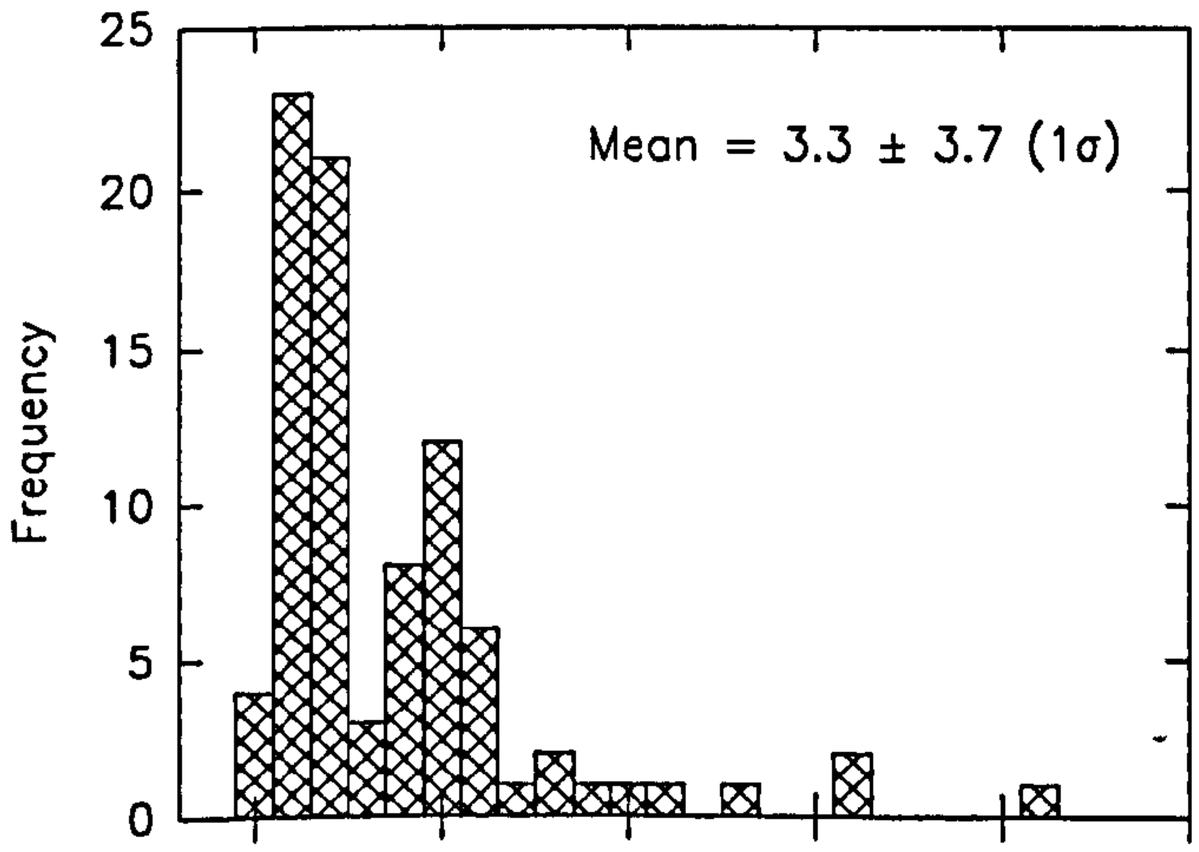

Figure 4.12 Histogram illustrating the reproducibility of the $T_{1/2}$ parameter

Similar to the 3d figure above (Figure 4.9) by interpolating between the $T_{1/2}$ values a surface may be created mapping temperature, time and $T_{1/2}$ variables as shown in Figure 4.13. Thus, for the feldspar system described, when $T_{1/2}$ is known a range of permissible values for annealing temperature and time may be estimated.

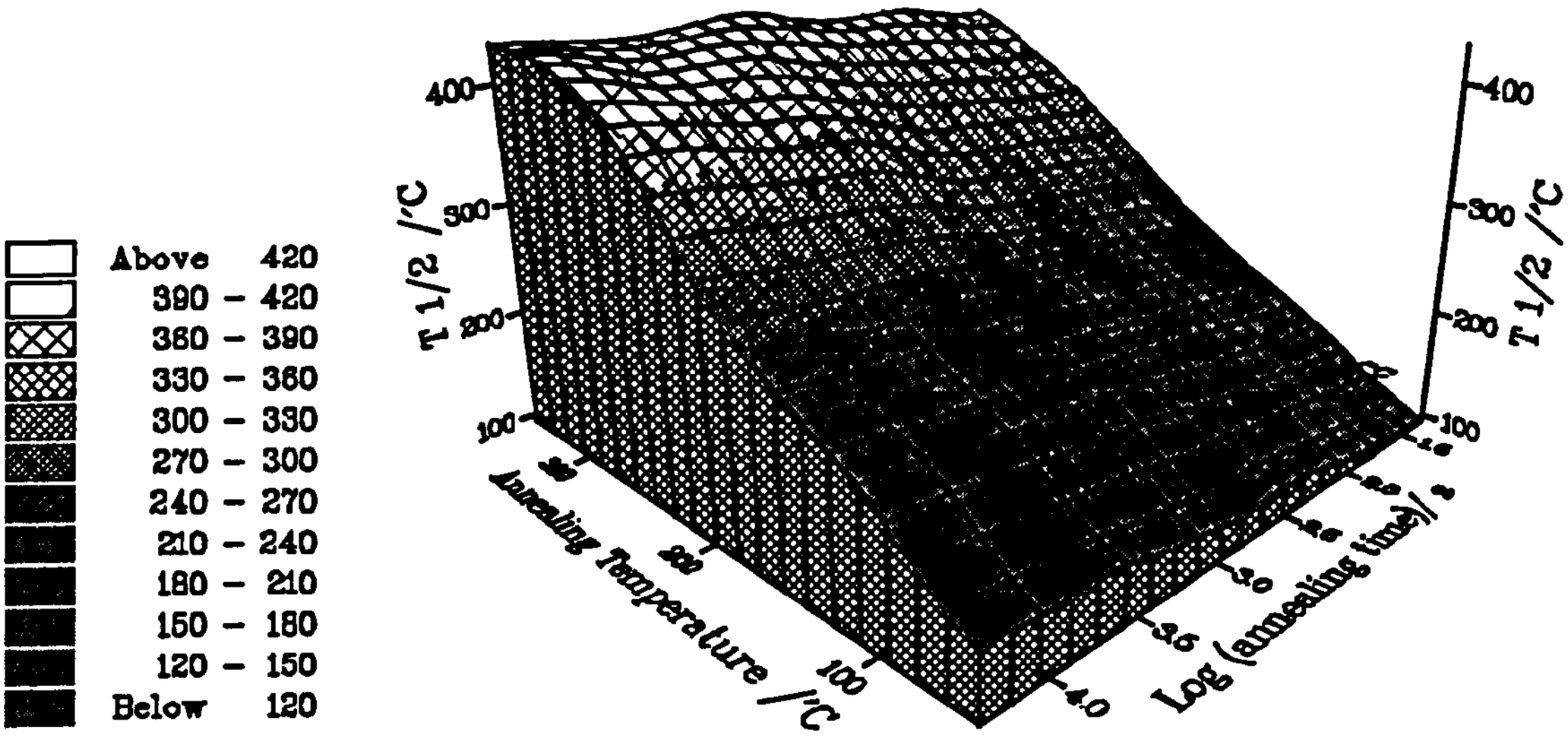

Figure 4.13 3d surface incorporating temperature, time and $T_{1/2}$ variables.

4.1.4 Simulations using first order kinetics

Kinetic simulations were undertaken to investigate whether theory predicts the same behaviour shown by the potassium feldspar experiment. A pseudo glow curve was created by summing a suite of individual peaks formed with a range of trapping parameters, and then introducing storage temperature and simulating the decay. Individual peak shapes were created using the simulation menu in the TL software. The routines follow the same steps as those in the peak simulation code written by Sanderson (1982).

The peak shape expression for first order kinetics (Equation 2.8) is given by

$$I(T) = Csn_o e^{-\frac{E}{kT} + \frac{s}{\beta}\int_{T_o}^{T} e^{-\frac{E}{kT}dT}} \qquad (4.4)$$

The peak shape integral

$$\int_{T_o}^{T} e^{-\frac{E}{kT}dT} \qquad (4.5)$$

is evaluated numerically in increments of 1 K for all the points in the curve. The simulated curve is then calculated point by point using Equation 4.4 with values for C and n_o set to unity, and is

stored in an identical array to measured glow curves to enable all the usual plotting, filing and data manipulation procedures to be carried out. Simulated peaks were transformed into a UNIRAS (x, y, z) format and transferred into the SigmaPlot® graphics package. Here the peaks were renormalised to unit area to represent the joint probability distribution for the emission of a single photon at any given temperature. They were then summed together to produce a pseudo glow curve.

A section of code was included to allow one to estimate various parameters for simulated glow peaks including values for the fraction of remnant signal after a particular thermal exposure. These values are calculated from Equation 2.13, where the fraction of the signal remaining after time t_s is given by

$$\frac{I}{I_o} = e^{-\frac{t_s}{\tau}} \tag{4.6}$$

and τ is the electron lifetime (Equation 2.9) given by

$$\tau = s^{-1} e^{\frac{E}{kT_s}} \tag{4.7}$$

and T_s is the storage temperature. Values were calculated to weight the simulated glow peaks thereby creating a dynamic system effected by temperature and time variations.

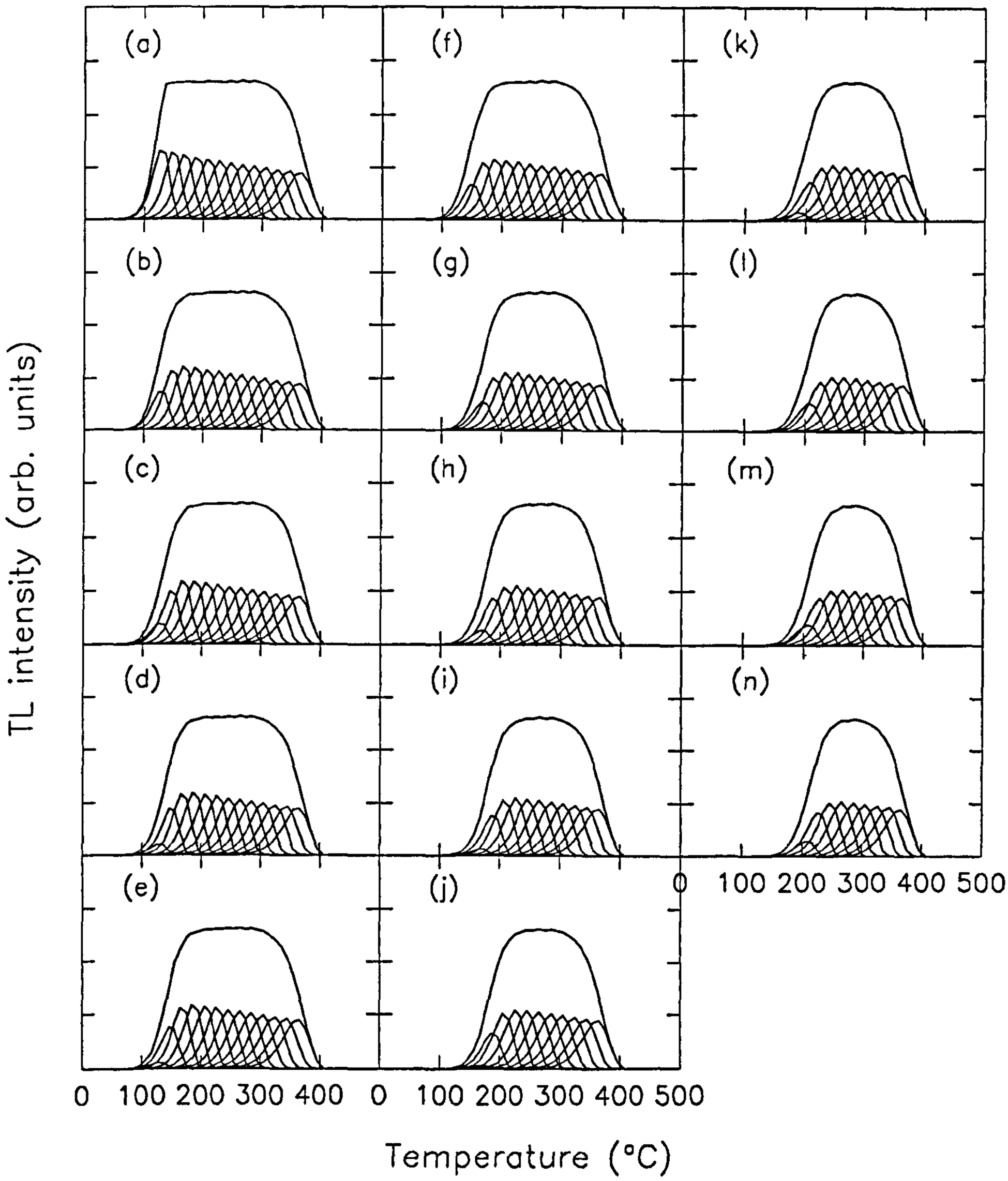

Figure 4.14 Simulation using first order kinetics of annealing at 100°C. Annealing times are as follows: (a) unannealed; (b) 20s; (c) 40s; (d) 60s; (e) 80s; (f) 100s; (g) 600s; (h) 1100s; (i) 1600s; (j) 2100s; (k) 7100s; (l) 12100s; (m) 17100s; (n) 22100s.

The first simulation assumed a uniform or linear distribution of traps with a constant frequency factor of $10^{12}s^{-1}$ and a heating rate of $5°Cs^{-1}$. Peaks were simulated with activation energies from 1 to 1.6 eV in steps of 0.05 eV. It was also assumed there was no peak to peak interaction. This simulation is shown in Figure 4.14 for an annealing temperature of 100°C. The same distribution was considered for 200°C. Simulations were also investigated with a constant activation energy

(1 eV) and a uniform variation in frequency factor (10^6 to 10^{14} s^{-1} in steps of 10^1 s^{-1}) for 100 and 200°C annealing. $T_{1/2}$ values for the simulated peaks are shown in Figure 4.15. Varying the activation energy with constant frequency factor gives a linear relationship between $T_{1/2}$ and the log of the annealing time, whereas varying the frequency factor gives a stepped result.

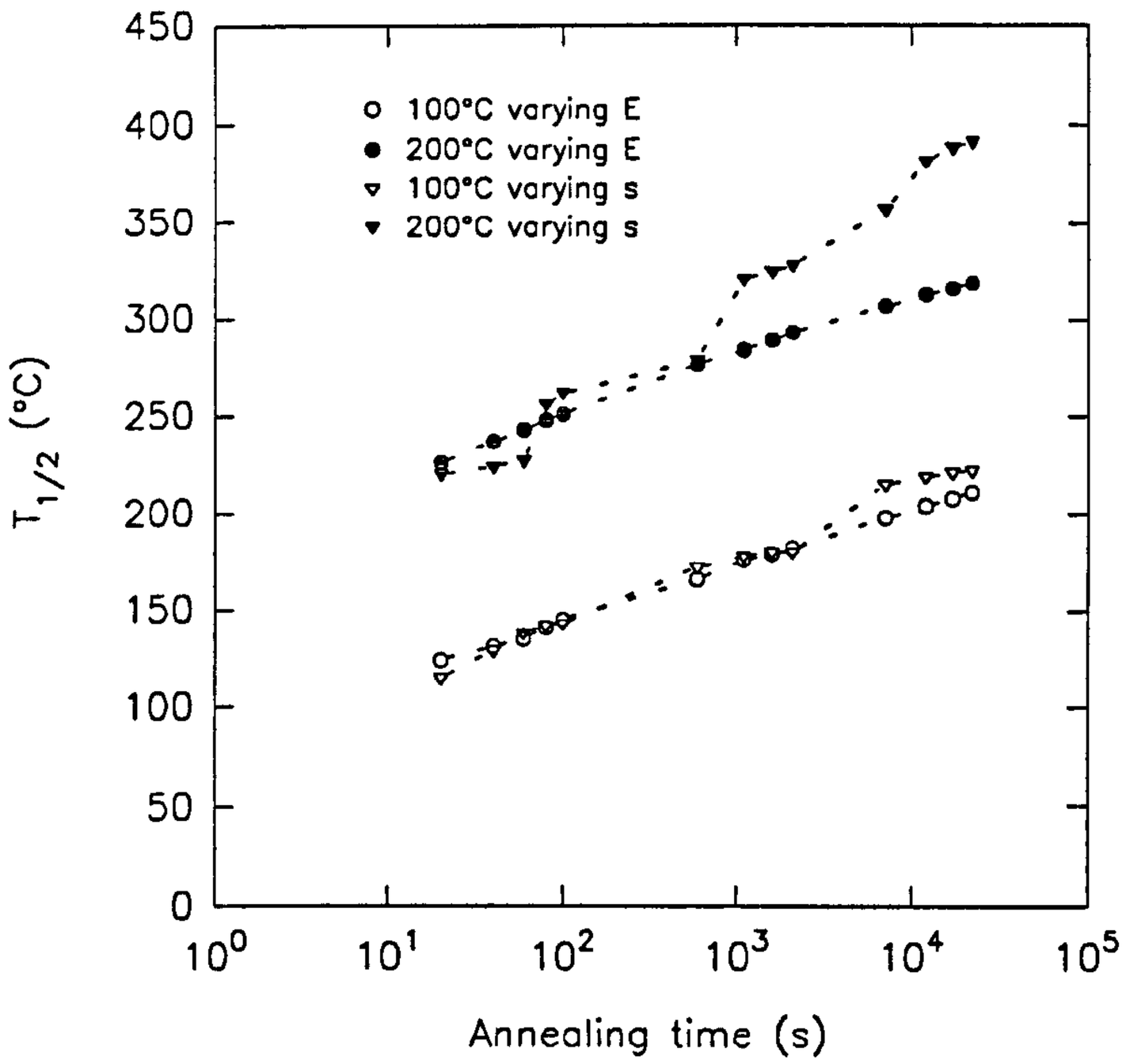

Figure 4.15 Relationship between $T_{1/2}$ values and time for simulated annealing at 100 and 200°C.

When varying the activation energy the $T_{1/2}$ values are slightly less linear with respect to annealing time at 200°C than 100°C; correlation coefficients for linear regressions are 0.9994 at 100°C and 0.9981 at 200°C, with a closer fit to the 200°C data obtained with a 2nd order regression. In comparison the stepped pattern is more pronounced at 200°C than 100°C when s is varied at constant E. Results from linear regression through the data varying E give equations ($T_{1/2,100°C} = 29.1 \times \log(t_{anneal}) + 85.5$; $T_{1/2,200°C} = 30.4 \times \log(t_{anneal}) + 189.5$) which produce values agreeing closely with the general equation for the parallel line model tested on the empirical results (Figure 4.11: $T_{1/2} = 23.922 \times \log(t_{anneal}) + T_{anneal} \times 1.071$). These results therefore suggest that there is a quasi-continuous or continuous distribution of charge traps in the feldspar sample and the distribution is linear.

4.1.5 Initial rise

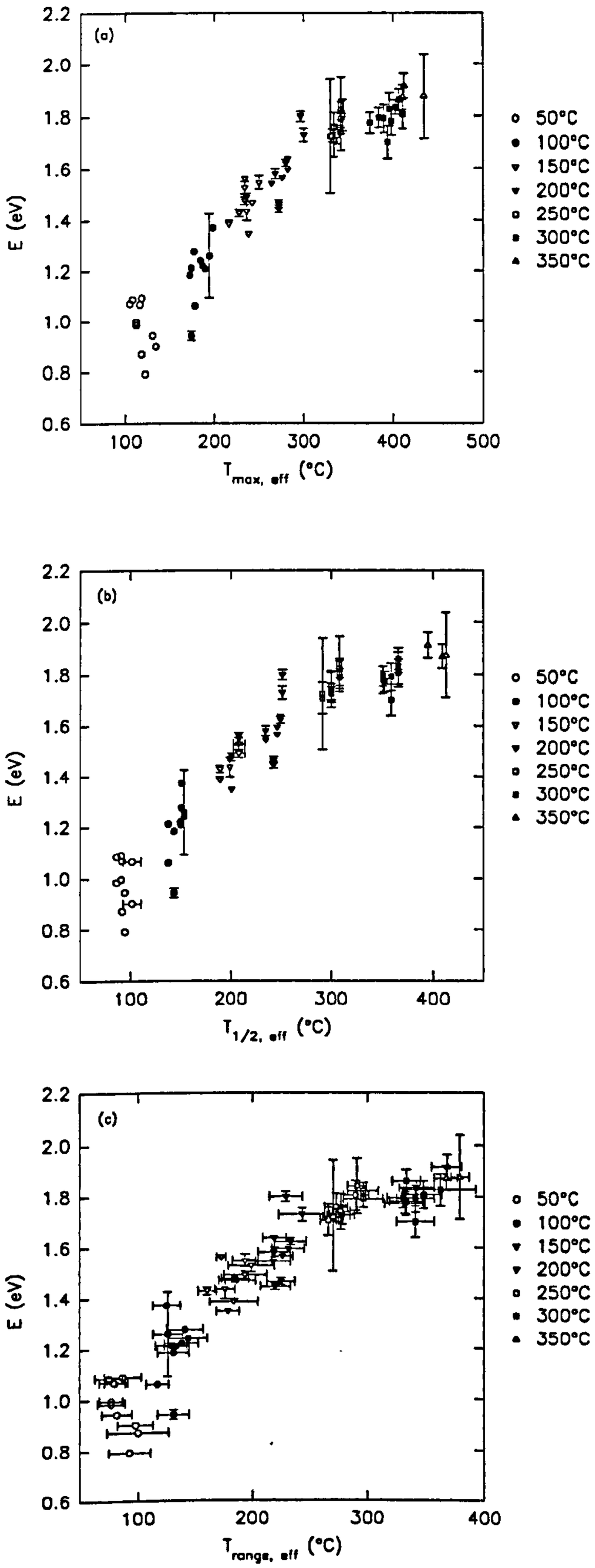

Figure 4.16 Activation energies plotted against (a) peak maximum, (b) $T_{1/2}$ and (c) temperature range for calculation of E.

To further test the assumptions in 4.1.5 values for E were estimated from the annealed glow curves of the F-1 data using the initial rise or Arrhenius plot method (Garlick and Gibson, 1948) to investigate the distribution of activation energies. The data was restricted to annealing times from 20-100 s, but over the full range of annealing temperatures (50-350°C). The temperature range over which the analysis was carried out was restricted so that the TL intensity reached did not exceed a tenth of the peak maximum intensity; for some of the Arrhenius plots the minimum intensity was extended to 15% to improve the linear regression analysis. The results are shown in Figure 4.16.

As shown the activation energies are plotted against the reference temperature values of the peak maximum ($T_{max,ref}$), $T_{1/2}$ ($T_{1/2,ref}$) and the range ($T_{range,ref}$) over which the linear regression analysis was applied; the most precise variable is $T_{1/2}$. These results suggest not only a distribution of charge traps but also a distribution of energy levels within the traps themselves. The gaps in the

data set (most pronounced in Figure 4.16b) are an artefact of the data chosen for analysis; further analysis of the remaining data set (annealing times of 600-22100 s) would give a fuller curve of the activation energy distribution. The distribution of charge traps shows similarities to those shown by Strickertsson (1985), from fractional glow analysis of microcline samples, who reports a continuous distribution (slope) up to about 250°C (T_{range}) and thereafter a single valued charge trap (plateau) with scattered values above 400°C. Correction of the reference temperature to sample temperature before initial rise analysis was not attempted because the result would be likely to be no more accurate due to the scatter in the data. Corrected data would be shifted down to lower temperatures and lower activation energies.

4.2 Investigation of a model hearth

Sections 4.2.1 and 4.2.2 summarise details of an earlier experimental investigation (Spencer, 1989) carried out to accurately map the progression of heat from experimental fires through a simulated archaeological hearth. This work was carried out in response to observations of anomalous peaks in some of the natural TL glow curves from alkali feldspar extracts from ancient hearthstones, which were interpreted as partially reset TL. As a first order approach temperatures above 300°C for short periods were taken as the criteria to constitute the zeroing event.

Sections 4.2.3, 4.2.4 and 4.2.5 describe the sampling and TL measurements carried out on the fired model hearthstone material during the course of PhD study.

4.2.1 Experiment design and set up

The experiment was set up by embedding a 3-dimensional matrix of 64 thermocouples (4 x 4 x 4) in a uniform cuboid stone and logging the temperature-time characteristics of two fires and associated cooling curves by computer.

4.2.1.1 64-way thermocouple amplifier-multiplexer

To log the temperatures sensed by the thermocouple matrix a 64 way thermocouple amplifier-multiplexer was designed, built and tested. The basic function of the interface was the amplification and then selection, in turn, of each thermocouple input. Each thermocouple was amplified using an AD595AQ thermocouple amplifier as described in Chapter 3. The amplified thermocouple signals were selected in turn by four 16 channel multiplexers. Four line binary decoding was used so that the 16 channels could be controlled by 4 address inputs; additionally a fifth input was provided to be used as a system enable. The multiplexers were addressed using an I/O card, and the multiplexer output was read using an ADDA card.

The control program was designed to allow the user to vary the interval between successive readings of the 64 thermocouple array. The subroutine to read the array addressed the 4 multiplexers simultaneously, read the 4 respective ADC inputs and converted the e.m.f into degrees centigrade. This process was repeated 16 times to read all 64 thermocouple inputs. The data snapshot was updated on screen and filed.

4.2.1.2 Preparation of stone

An unfired sandstone flag was transported from mainland Orkney to the SURRC. The original dimensions of the stone were 60 x 44 x 12 cm. The stone was cut using industrial water-cooled rock saws to a uniform cuboid with dimensions of 41 x 41 x 7 cm. Holes for thermocouple insertion were drilled using a milling machine with 4 mm masonry drill bits cooled with a mixture of water and maxicool. Sixteen sets of 4 holes were drilled into the stone in a 4 x 4 grid. The depths of the 4 holes within each set were 15, 30, 45 and 60 mm producing 4 distinct layers with which to sense temperatures within the stone. Sixty four thermocouples were threaded with alumina-porcelain ceramic sheathing, spot welded and then cemented into the holes using Polycell tile cement.

4.2.1.3 Mounting of hearth in use

The stone was inverted for firing experiments and therefore the 4 layers of 16 thermocouples were 10, 25, 40 and 55 mm from the upper surface respectively. The hearth was surrounded by a wall of concrete blocks to shelter the fires from the wind. The blocks also protected the

interface instrument and the thermocouple wires behind the hearth. A cylindrical wire mesh (approximate dimensions: diameter 25 cm, height 25 cm) was placed on the surface of the stone to contain the fire in the same area throughout the experiment.

4.2.2 The fires and thermocouple results

The full data sets of two fires are appended in Spencer (1989). Figure 4.17 shows thermocouple data for the experimental fires ((a): peat; (b): wood) from two distinct areas of the stone; one

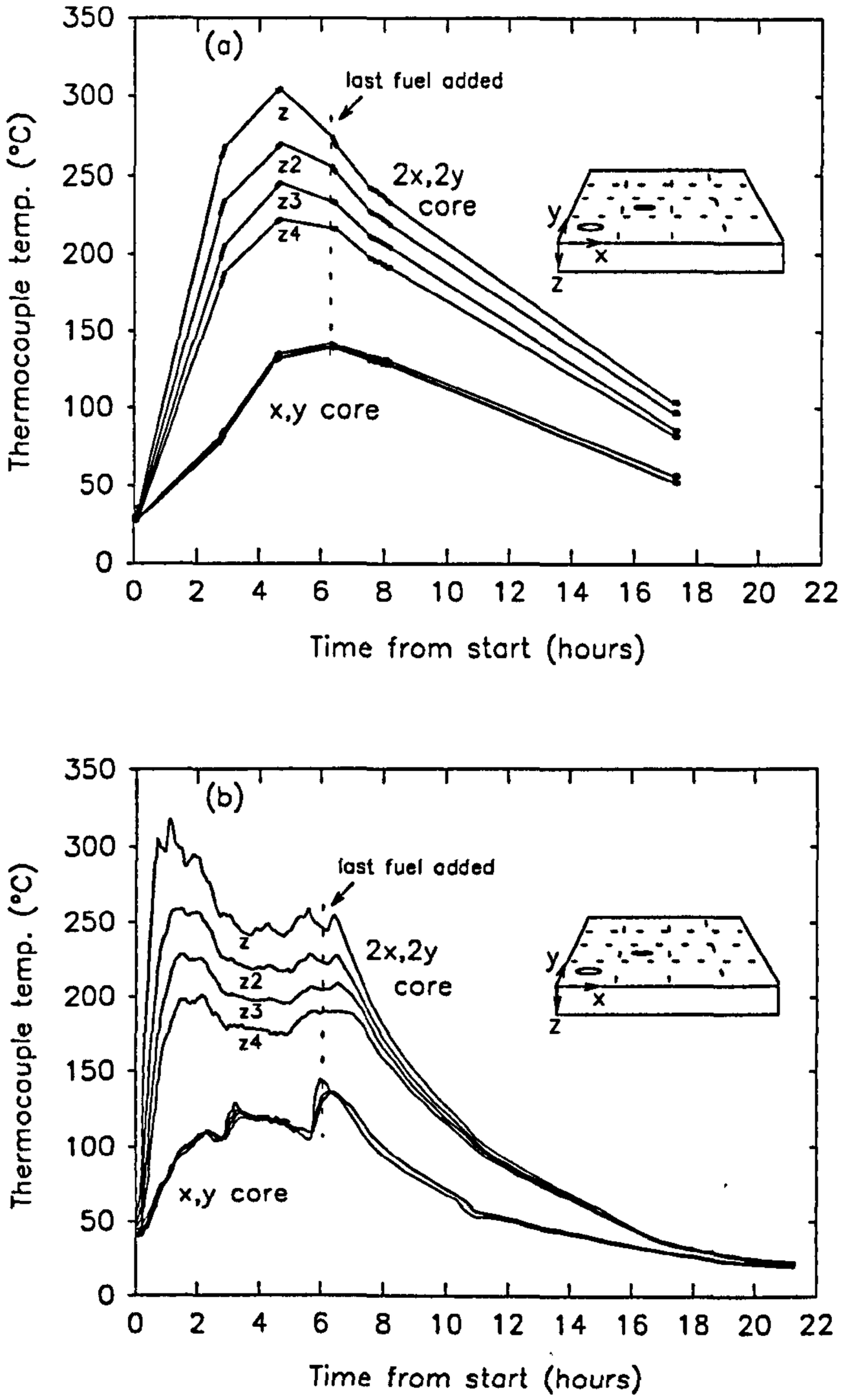

Figure 4.17 Examples of thermocouple data for the experimental fires: (a) peat and (b) wood; z = 10 mm, $z2$ = 25 mm, $z3$ = 40 mm, $z4$ = 55 mm.

centrally located (2x,2y) and beneath the main heat of the fires, the other at a corner (x,y). The data from both fires clearly demonstrate a temperature gradient in the centre compared with equilibrium conditions at the edge, and a large temperature gradient in the x-y plane. The thermal gradients observed in the stone are higher than a simulation closer to a real archaeological hearth due to a higher flow from beneath and at the sides of the stone. A linear interpolation has been used to approximate the temperature distribution between points in Figure 4.17a, where data was lost.

4.2.3 Preparation of model hearth material: Coring, sectioning, mineral preparation and SEM analyses

Cores were removed from the stone using an 11 mm internal diameter water-cooled diamond tipped coring drill. Eighteen cores were removed in total; 16 from the 4 x 4 grid positions in the x-y plane sampled between the four thermocouples at each position, and at a further two locations to interpolate the radial temperature distribution. Each core was cut into 14 approximately 5 mm long sections using a water-cooled diamond impregnated rock saw. Sections corresponding to the thermocouple positions were selected, providing a representative set of samples which had been exposed to different maximum temperatures and a dynamic thermal exposure.

Initially minerals were prepared from core 2x,3y to investigate both coarse grain polymineral and separated alkali feldspar mineral preparation techniques. For the coarse grain polymineral method the following steps were carried out:

(i) the core sections were washed in demineralised water to remove any cross-contamination as a result of the sawing process;

(ii) oven dried at 50°C for 10 minutes;

(iii) scraped with a scalpel to remove any excess tile cement or possible bleached surfaces (ie. due to any light exposure to the surfaces of the stone);

(iv) length, diameter (using a micrometer) and mass recorded;

(v) crushed using a mortar and pestle;

(vi) sieved using disposable nylon sieves to produce grains of < 150 μm;

(vii) given a 30 min 10% HCl wash, 3 H_2O washes, 2 acetone washes and oven dried at 50°C for 30 minutes;

(viii) grains dispensed onto discs in the usual manner.

For preparation of alkali feldspar mineral separates the following steps were carried out:

(i) steps (i) to (v) above;

(ii) sieved to produce a 90-125 μm grain size fraction;

(iii) given a 30 min 10% HCl wash, 30 min 10% HF, neutralised with ammonia solution, 30 min 10% HCl, then given H_2O and acetone washes and oven dried as above;

(iv) grains separated into the following density fractions using sodium polytungstate heavy liquids and a centrifuge:

(a) < 2.51 g cm^{-3};

(b) 2.51 - 2.58 g cm^{-3} (potassium feldspar);

(c) 2.58 - 2.62 g cm^{-3} (sodium feldspar);

(d) 2.62 - 2.74 g cm^{-3} (plagioclase feldspar (& quartz));

(e) > 2.74 g cm^{-3};

(vii) grains washed in H_2O and acetone and oven dried at 50°C for 30 min;

(viii) dispensed onto discs in the usual manner.

Some exploratory SEM analyses were carried out on the alkali feldspars to establish the purity of the separates thereby indicating the success of the heavy liquid separation technique. Due to the low yield of the potassium feldspar density fraction (2.51-2.58 gcm^{-3}) only a few grains were available for SEM analysis. Microprobe analysis gave strong iron and sulphur signals but little in the way of potassium. In the sodium feldspar fraction (2.58-2.62 gcm^{-3}) visually there appeared to be mainly quartz grains in the sample (which one would expect to be predominantly in the next denser fraction (2.62-2.74 gcm^{-3})). A grey scales composition analysis confirmed this observation. Further analysis of individual crystals revealed inclusive material high in potassium content. In terms of feldspar content the analyses indicated the sample was higher in potassium than sodium. For the plagioclase / quartz fraction (2.62-2.74 gcm^{-3}) the grains were identified as either quartz or potassium feldspar with little indication of plagioclase feldspars.

Assuming the separation technique successfully concentrated grains into the correct density fractions, the SEM analyses suggest the density of individual grains is strongly governed by impurities, fused conglomerates, inclusive material (for eg. K-feldspar within quartz grains) or air bubbles. Despite these observations the TL signals (results presented below) from the potassium, sodium and plagioclase fractions could all be distinguished by their glow curve shapes.

4.2.4 TL measurements

Initial TL measurements were made on core 2x,3y to compare the results from the coarse grain polymineral and the separated alkali feldspar preparation methods. The instrument was set up to record TL from room temperature to 700°C at 5°Cs^{-1} using the UV filtered PMT arrangement (Corning 7-51 and Schott BG39) established in Chapter 3. $T_{1/2}$ values for both polymineral and separated alkali feldspar methods with increase in depth z (Figure 4.18) show some variation, although there is no observable trend for a particular sample type and the scatter in the data appears to be random. Therefore the coarse grain polymineral preparation method was adopted for the remaining 17 cores.

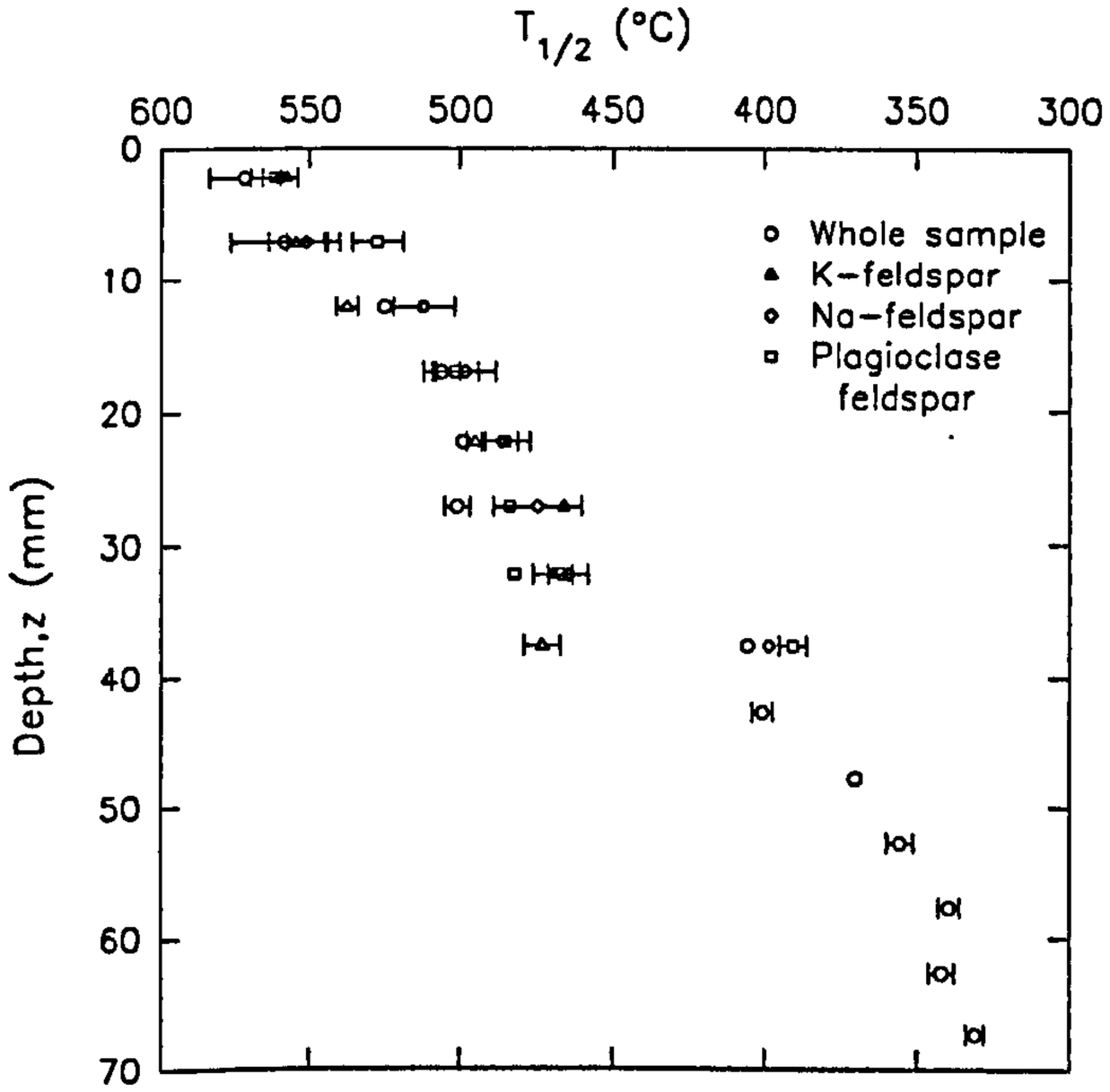

Figure 4.18 Variation in $T_{1/2}$ with depth; polymineral and separated feldspars from core 2x,3y from the model hearthstone.

After the natural TL signals were read-out the samples were given a normalisation dose of 200 Gy in the ^{60}Co source, and annealed in a muffle furnace (set to 200°C) on a copper plate before

performing normalisation TL measurements. The annealing temperature was monitored by five Cr-Al thermocouples bolted to the plate. The plate reached a maximum temperature of 195°C in 29 min and was then removed from the furnace.

4.2.5 TL results

As before the TL glow curves were measured in terms of the position of the residual geological signal $T_{1/2}$. The $T_{1/2}$ values for the 72 samples measured range from 247 to 577°C. For the normalisation runs, the mean $T_{1/2}$ value was 304.06 ± 9.67°C (1σ). Examples of the natural residual geological signals observed down a core from the central region of the stone are shown in Figure 4.19. As sampling depth is increased (from z to z4) away from the surface of the stone (and the source of heat), there is clearly a dramatic increase in the signal remaining due to the thermal gradient. Problems encountered in the determination of $T_{1/2}$, for example the unclear peak maximum in curve z and the two components in curve z3, were resolved by calculating the maximum of the first derivative.

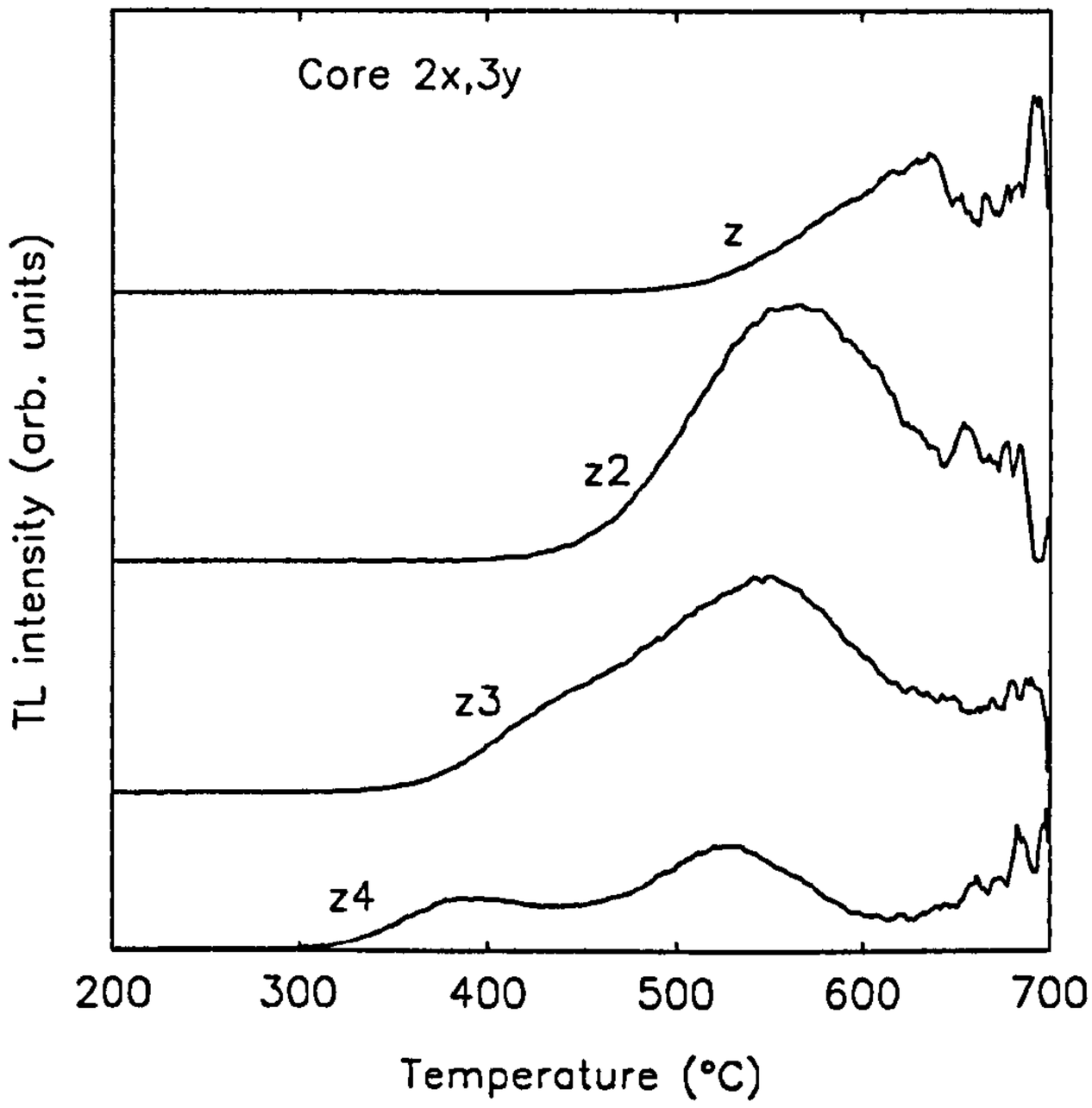

Figure 4.19 Examples of residual geological TL signals observed down a core removed from the central region of the stone.

4.2.6 Extension of F-1 model to hearthstone simulation results

The demonstration of a linear correlation between TL parameters and the thermocouple integrated *T(t)log(t)* function for the sum of the two fires is shown in Figure 4.20. The integration was calculated from a start time of 10 s for both fires. Additive and multiplicative corrections were made to the $T_{1/2}$ values using the normalisation results. In both instances, the correlation coefficient (*r*) gave lower values of 0.95 and 0.94, respectively.

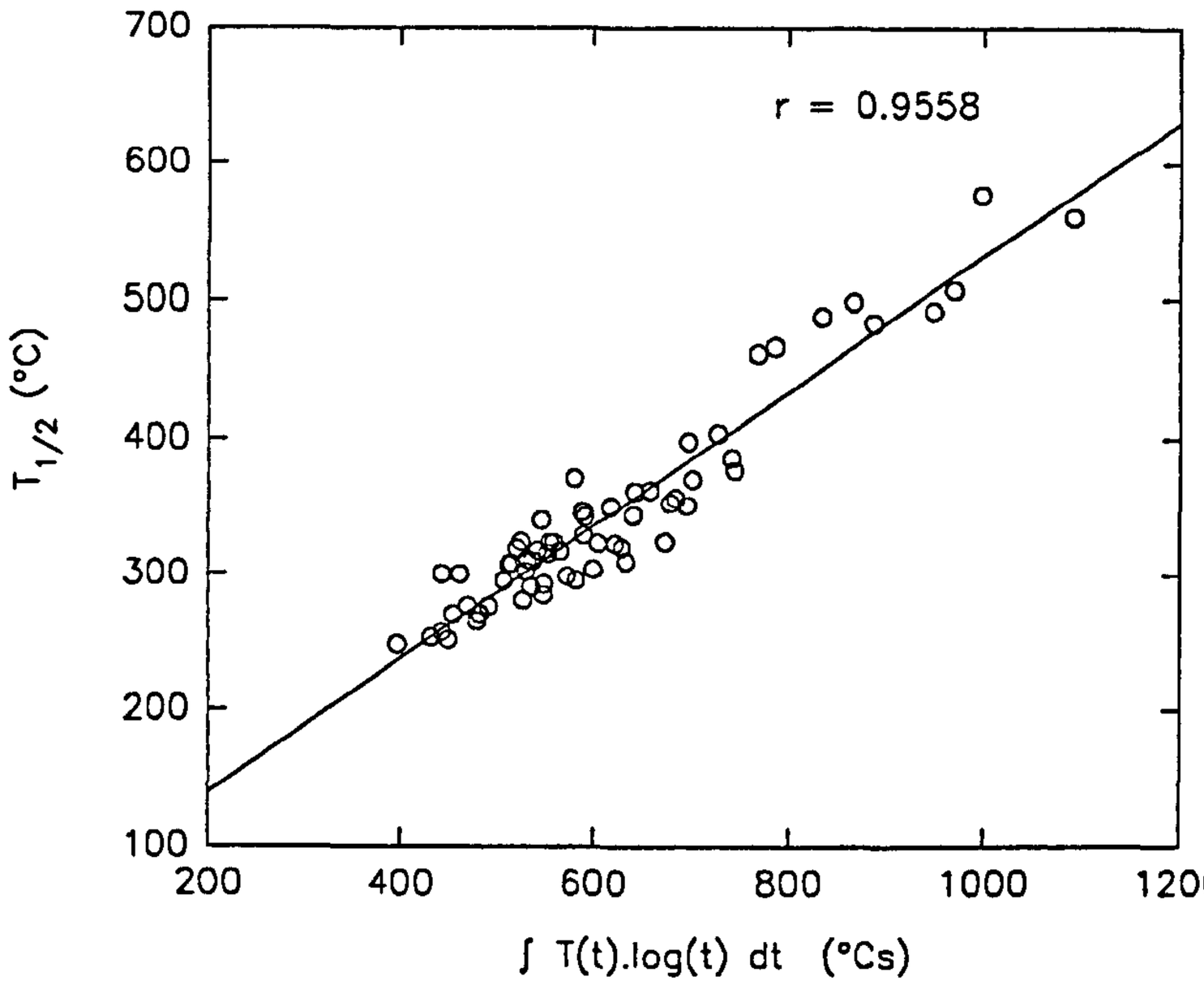

Figure 4.20 Correlation between $T_{1/2}$ results and thermal exposure index values ($\int T(t).\log(t)\,dt$) for samples from a simulated hearth.

As described above, cores were removed in the central square centimetre region between each set of four thermocouple holes. Therefore, the temperatures sensed at the thermocouples and the temperatures responsible for the position of measured geological TL may be to some extent spatially separated, and due to observed thermal gradients, varying to some degree, either higher or lower, depending on relative position. This is perhaps the most likely reason for any scatter in the correlation, although stone inhomogeneities and the conductive influence of alumina-porcelain ceramic sheathes (used for thermocouples) may be contributing factors. Additional scatter in $T_{1/2}$ values may be due to variations in mineral composition, although this is not implied from the general trend in the normalisation results.

The resultant linear correlation between the $T_{1/2}$ results and the thermocouple data expressed as an integrated T(t)log(t) function, allows acceptance of the complementary behaviour of temperature and duration variables and provides a means of quantifying thermal exposure unambiguously for specimens of unknown temperature and time profile. It also confirms that this relationship can be extended to the non-isothermal behaviour in a real hearthstone and that the form of the relationship can be cautiously extended to other silicate matrices.

4.3 Summary

The first section (4.1) of this chapter has explored the effects of varying the temperature and time of annealing conditions on the TL glow curve position of an IAEA standard potassium feldspar (F-1). The relationship of glow curve position, annealing temperature and annealing time has been investigated and kinetic studies have been undertaken to model the empirical results and explore the distribution of trapped charge. The main results are summarised as follows:

(i) The feldspar shows clear thermometric behaviour; the mechanism which determines the position of the remnant glow curve relating to both temperature and duration. Varying the temperature of thermal treatment dominates the remnant glow curve position, whereas increase in duration has a progressively smaller effect.

(ii) The annealed glow curve position measured from the $T_{1/2}$ position is characterised by a linear increase in temperature and a logarithmic increase in time. A constrained linear regression analysis confirms the hypothesis that a linear-log temperature-time dependence provides a reasonable description of the behaviour. The general equation from the regression results is $T_{1/2} = 23.922 \times \log_{10}(t_{anneal}) + T_{anneal} \times 1.071$

(iii) Kinetic simulations have shown that a continuous linear distribution of first order traps give a reasonable fit to the general equation derived from the regression analysis on the empirical results.

(iv) Values for the activation energies estimated from the glow curves show not only a distribution of charge traps but also possible evidence of a distribution of energy levels within the traps themselves.

The thermocouple data from the experimental hearth (Section 4.2) has emphasised the variable temperatures in real fires, showing that a estimate of maximum or average temperature for a thermal event is a poor measurement for real situations. The $T_{1/2}$ results from TL respond to the temperature gradients involved in the experiment. The linear correlation between $T_{1/2}$ and the thermocouple integrated function allows acceptance of the complimentary behaviour of temperature and duration variables and provides a means of quantifying thermal exposure unambiguously for specimens of unknown temperature and time profile.

The progressive thermometry system shown here by F-1 feldspar and polymineral whole-sample specimens is applied to archaeological and modern materials in Chapter 5. The empirical relationship formulated from the F-1 experiment is cautiously extended to certain examples in Chapter 5 and utilised in thermometry investigations in Chapter 6.

Chapter 5: Thermoluminescence Thermometry Applications

This chapter discusses TL thermometry analyses of heated materials from archaeological and modern contexts. The archaeological studies include ceramics from Early and Late Neolithic contexts from Pool on Sanday, Orkney, burnt stones from two burnt stone mounds at Crawford in Clydesdale, and hearthstones from two further sites; examples from three contemporary house structures from the Iron Age Hillfort at Dunion Hill in the Borders, and hearths associated with different construction phases of a Late Bronze Age round house at Tofts Ness, Sanday, Orkney (see Figure 5.1 for a map of archaeological sampling sites). The modern study was an investigation of fire damaged concrete from the lining of a rock bored tunnel beneath the Store Bælt channel in Denmark (Figure 5.2).

5.1 Neolithic ceramics from Pool, Sanday

5.1.1 Site/material description

The multi-period coastal settlement at Pool, Sanday, Orkney was investigated seasonally between 1982 and 1988 (Hunter *et al.* forthcoming). Two main periods of occupation were identified, the earlier being the Neolithic (c. 4000-2000 BC) and the later being the Iron Age (c. 400-1200 AD). The Neolithic deposits form a large mound covering an area of about 75 m in diameter with a maximum depth of about 1.5 m. The mound was created by the gradual deposition of hearth debris and associated midden, pottery and faunal/floral material, producing a number of tipping layers reddish-brown or darker in colour. Fourteen Neolithic buildings were identified in the excavation area positioned throughout the depositional sequence; above, surrounded by and below the tip-like deposits. Figure 5.3 shows examples of sections of the Neolithic deposits on the site.

The ceramic phasing of the site is based on the formation of these tips (Hunter and MacSween, 1991) although it does not necessarily coincide with changes in settlement (MacSween, 1992). Seven major stratigraphic events were identified each representing changes within the depositional character of the mound:

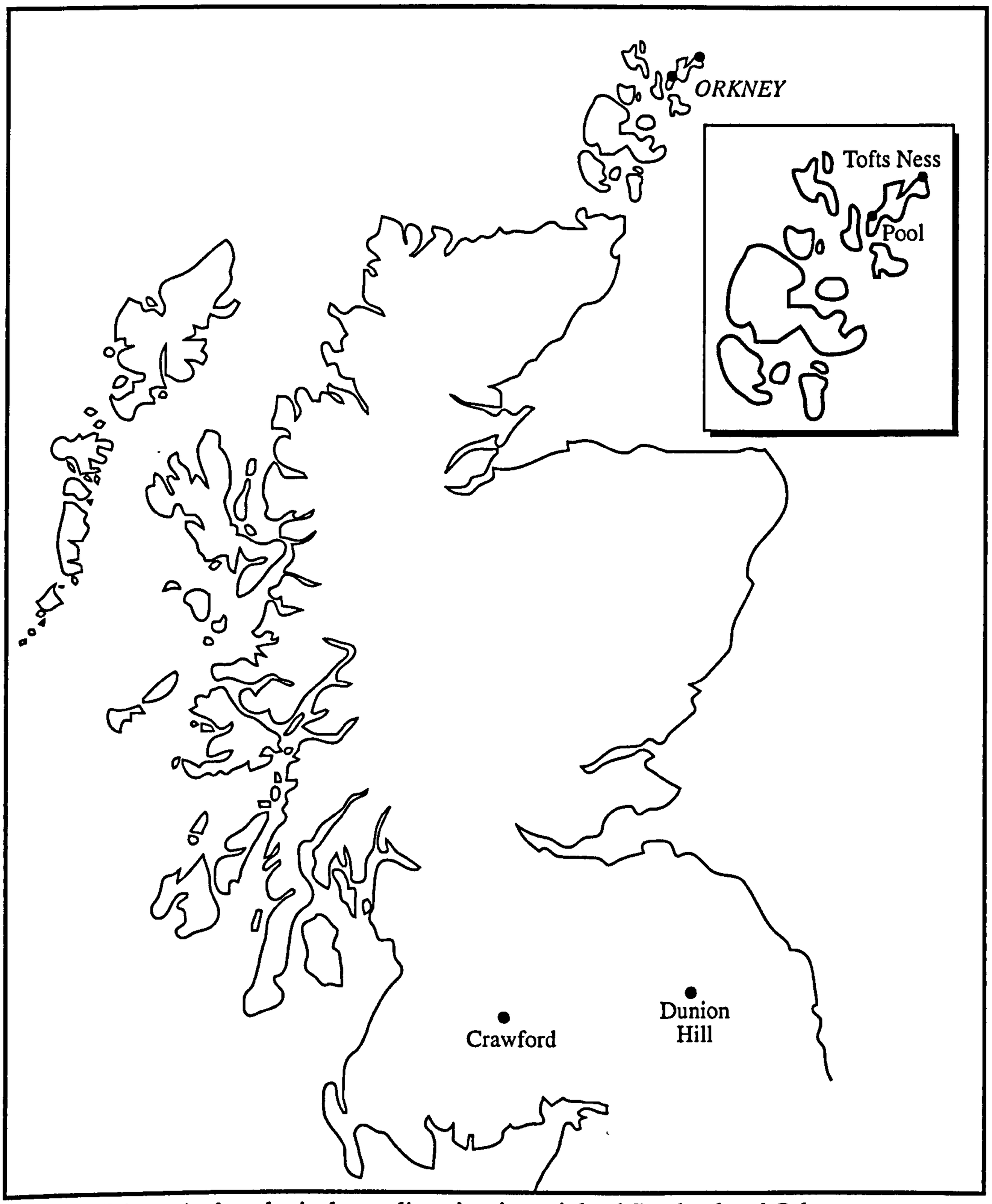

Figure 5.1 Archaeological sampling sites in mainland Scotland and Orkney

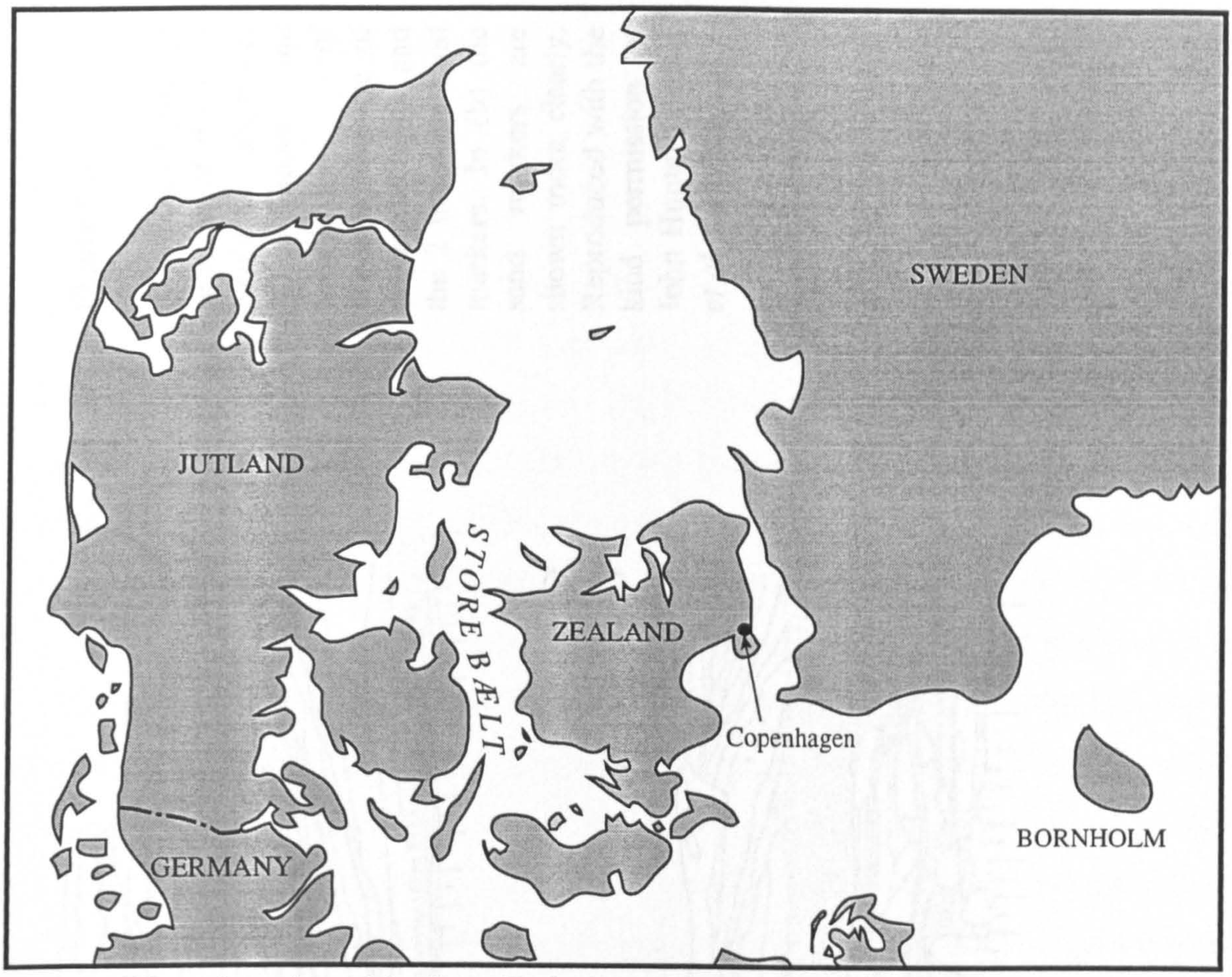

Figure 5.2 Location of the Store Bælt channel in Denmark

Phase 3.2 Structures (latest)

Phase 3.1 Dark tips and structures

Phase 2.3 Reddish brown tips and structures

Sand marker

Phase 2.2 Reddish brown tips

Sand marker

Phase 2.1 Reddish brown tips

Phase 1.2 Structures

Phase 1.1 Dark tips (earliest)

Natural

The two sand markers are aeolian deposits which, as far as could be ascertained, cover the entire site on two occasions in the course of the Neolithic occupation. Neither showed evidence of intrusion providing useful trans-site stratigraphic markers and, particularly for

(a)

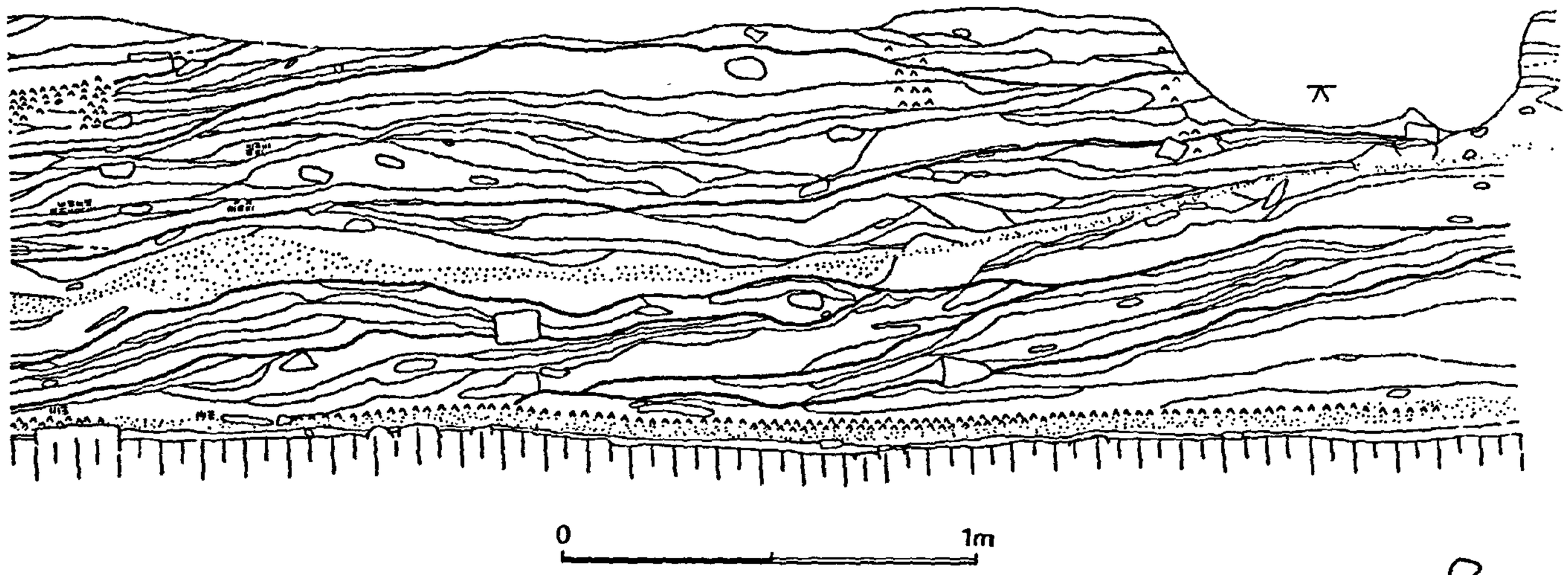

(b)

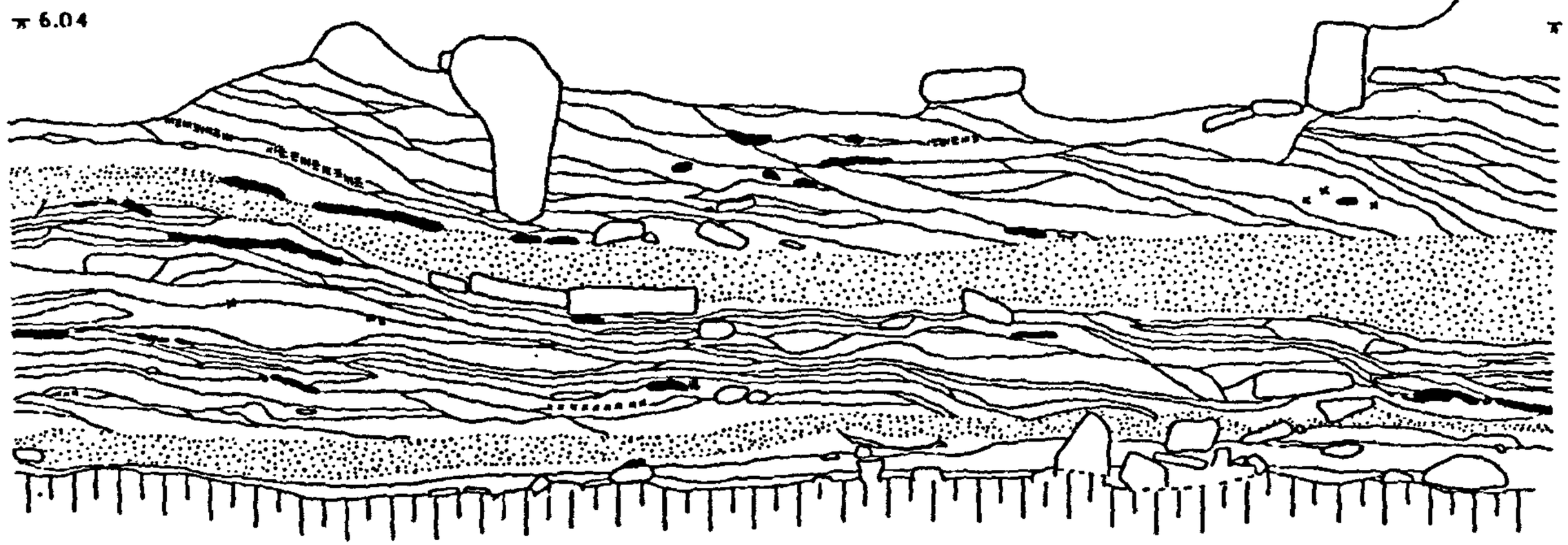

Figure 5.3

Examples of parts of sections of the Pool Neolithic sequence. (a) Shows the complexity of deposits, the use of contoured spits and the 2 trans-site sand markers. In (b) the sand markers are shown more clearly. Reproduced with the kind permission of John Hunter (Hunter *et al.* forthcoming)

those phases immediately above and below, gave a reassuring stratigraphic integrity indicating there was no major re-depositional activity during the occupation.

The ceramic assemblages in each of the Neolithic phases were described by MacSween (Hunter and MacSween, 1991; MacSween, 1992). Phase 1 is characterised by pottery from the round-based tradition, including possible Unstan bowls. The vast majority is undecorated, although an increase in the variety of rim types in the later part of the phase is noted. Petrological analysis of local clays (MacSween, 1990) indicates that both primary clays, from the degrading cliff section adjacent to the site, and boulder clays were used. 20% of the material is shell tempered, 35% is tempered with small amounts of gravel and the remainder is untempered. In phase 2 the vessels are predominantly made from finer primary clay and the majority is shell-tempered. Decoration is by incision, the majority of the decorated vessels coming from sub-phases 2.2 (parallel lines) and 2.3 (dots and chevrons). 'Baggy' vessels (with angled sides narrowing into a tiny base) are common in both these two sub-phases, but the phase 2.2 assemblage is dominated by flat-based, angle-sided vessels. In phase 3 there is a complete change in pottery style, fabric and decoration. There is a decrease in the use of primary clays with a corresponding increase in the use of secondary, probably boulder, clays; the assemblage is dominated by pottery heavily tempered with crushed sedimentary rock fragments. Only a small proportion of the wares is shell tempered. The rock-tempered pottery is generally thinner-walled, the commonest vessel type being bucket-shaped with straight or slightly angled walls, and the exterior surfaces are often slipped. The 'baggy' vessels of phase 2 are no longer evident. Although there is some incised decoration, more deeply cut than the incisions on the phase 2 pottery, applied decoration including ladder, lattice, trellis and fish-scale motifs is dominant. Scalloped and notched rim forms appear for the first time. The phase 2 and phase 3 assemblages are of types previously termed 'Grooved Ware'(Hunter and MacSween, 1991), although the clear chronological difference coupled with a striking contrast in pottery technology with phase 3 indicates that they are distinct traditions.

Sherds were selected on the basis of context to establish TL chronologies (phases 1, 2.1, 2.2, 2.2, 2.3a, 2.3b, 3.1); decorated or diagnostic examples were excluded. Relationships between form, fabric and context are eagerly awaited (Hunter *et al.* forthcoming).

5.1.2 Sample selection / preparation

Equivalent dose estimates for the Pool sherds had been measured previously on alkali feldspar separates. Preparation followed similar procedures to Sanderson *et al.* (1985, 1988). Spare material from the laboratory archive was used in this study. Thirty samples were selected for the study. Fifteen from 'Early Neolithic' phases (phases 1, 2.1 and 2.2; TL dates bracketed between c. 3000-4000 BC), twelve from 'Late Neolithic' phases (phases 2.3a, 2.3b and 3.1; TL dates c. 2000 BC) and an additional three samples from phase 2.2 (SUTL samples 32, 33 and 29) with TL ages seemingly too young (c. 2000 BC). Details of the site phasing, context numbers, finds codes, tempering fabric, SURRC TL numbers and corresponding TL dates for all the samples analysed are shown in Table 5.1.

Discs were dispensed from either potassium, sodium or plagioclase density fractions (90-125 μm grain sizes) depending on material availability in the laboratory archive. TL was measured from 0-700°C at 5°Cs^{-1} using UV detection methods established earlier (Chapter 3; 3 mm 7-51 & 3 mm BG39 with spacer collar). The samples were then given an approximate 200 Gy ^{60}Co dose, and then annealed in a muffle furnace on a temperature sensed copper plate. The muffle furnace was set to 200°C and the plate was inserted for 30 minutes, and then allowed to cool in the laboratory. The TL was then re-measured.

5.1.3 TL results

The T_{max} and $T_{1/2}$ values for the archaeological, geological and laboratory induced TL are shown in Table 5.2. The errors on the overall means (listed in the final row of the table) of the T_{max} and $T_{1/2}$ data show a greater variation in the remnant geological results than the corresponding values from the archaeological and laboratory TL data, even when the estimated values for detection limits (ie. T_{max} >700°C; $T_{1/2}$ >650°C) for material from phase 1 are omitted; 555 ± 7°C and 507 ± 7°C respectively. The range of $T_{1/2}$ values over all the phases examined are as follows: archaeological 208-240°C; geological 477->650°C; laboratory 266-303°C. The mean $T_{1/2}$ results from each phase from the geological TL show a decreasing trend from phase 1 to 2.3a, increasing again in phases 2.3b and 3.1. The

Table 5.1 Pool samples used in thermometric analyses: site, fabric and TL age details

Phase	Context[a]	Finds code	Fabric[b]	SUTL no.	TL date[c] (BC)
1	2776	6585	Shell / rock	121a	3660 ± 750
	2886	6699	No details	122	4260 ± 920
	2886	6700	No details	123	2930 ± 580
	2886	6702	No details	125	3330 ± 770
	2886	6704	No details	126	3840 ± 860
	2776	6584	Shell / rock	127	3960 ± 1050
2.1	1244	5189	Untempered	75a	4020 ± 830
	1244	5355	Untempered	78a	3870 ± 1180
	1244	5360	Shell	79	4080 ± 570
	1330	5393	Shell	82	3370 ± 650
	1330	5394	Shell	83	4030 ± 550
2.2	1296	4972	Shell	26	3950 ± 650
	1296	4929	No details	27	3500 ± 500
	1299	4935	Untempered	30	3920 ± 650
	1302	5029	Shell	35	3310 ± 510
	1299	No details	No details	32	1710 ± 260
	1301	4973	Shell	33	1780 ± 390
	1299	4933	Shell	29	2070 ± 300
2.3a	1289	4989	Shell	11	2320 ± 370
	1289	4989	Shell	12	2300 ± 340
	1289	4986	Shell	13	2260 ± 400
	1289	4917	Shell	15	1840 ± 290
	1289	4917	Shell	16	2070 ± 350
	1294	4998	Shell & bone	17	2370 ± 380
	1294 / 1208	5004	Shell	20	2190 ± 370
2.3b	1228	4466	Shell	50	2110 ± 280
	1236	4559	Shell	52	2060 ± 300
	1236 / 1250	4550	Undiagnostic	54	2020 ± 350
3.1	0851	3402	70% rock	36	1870 ± 360
	0851	3541	10% rock	38	2170 ± 380

Notes:
[a] A forward slash denotes samples from a "contextual interface"
[b] Ceramic fabric analyses were carried out by Ann MacSween (MacSween, 1994, pers. comm.)
[c] TL dates measured by David Sanderson, Peter Clark and Andrew Dougans, SURRC East Kilbride,(Sanderson *et al.* forthcoming).

corresponding results for the archaeological TL show a gradual decrease from phases 1 to 2.3b but rising again in phase 3.1. Analysis of the archaeological $T_{1/2}$ data phase by phase using the t-test (assuming unequal variances; 5% significance level; two-tailed test) suggests none of the means are significantly different, and this outcome is not improved by dividing by the laboratory TL data. If this normalisation was successful it would raise the suggestion that variations in $T_{1/2}$ may to some extent be sample specific in terms of, for example, post thermal glow curve position, the success of mineral separation, disc/sample geometries or the type of mineral dispensed - all the samples are Na-feldspars except SUTL 126 and 78a which are K-feldspar, and SUTL 50 which is Plagioclase feldspar. However, further observations added to the data set may separate out the means statistically. The laboratory $T_{1/2}$ values are the result of a dynamic non-isothermal anneal; the temperature of the plate (measured with a type K thermocouple) rose in a smooth curve from 23.8 °C (at t = 0 s) to 195.6°C (at t = 1800 s), whereupon the plate was removed and by a further 900 s had cooled to 51.1°C. There was no discernible relationship between the position of discs on the copper plate and the $T_{1/2}$ values; the values were randomly distributed suggesting the temperature over the plate was uniform during the annealing cycle.

The dotted line splitting phase 2.2 is a demonstration of how the variation in $T_{1/2}$ may be decreased (both for geological and archaeological results) by removing those values corresponding to ages that are out of sequence with the rest of the data from the phase; samples SUTL 26, 27, 30 and 35 have TL ages of 3950 ± 650, 3500 ± 500, 3920 ± 650 and 3310 ± 510 BC respectively, whereas samples SUTL 32, 33 and 29 have TL ages of 1710 ± 260, 1780 ± 390 and 2070 ± 300 BC respectively. The laboratory TL results also confirm that the heating ramp has a high reproducibility with a value of less than 0.6% (std. error) for reference temperatures (ie. $T_{1/2}$) between 266-303°C.

Similarly high reproducibility was shown by records of the servo-lag measurements recorded at 700°C reference temperature on the first and second heating cycles for both the natural and the artificial TL measurements. Natural = 16.18 ± 0.06 (1 s.e., n = 51); Artificial = 16.49 ± 0.09 (1 s.e., n = 41). The high reproducibility of ramping conditions confirms the validity of comparing $T_{1/2}$ values.

Table 5.2 Pool ceramics TL results

Phase	SUTL no.	Archaeo TL temperatures (°C) [a]			Geo TL temperatures (°C) [b]			Laboratory TL temp. (°C) [c]	
		T_{max}	$T_{1/2}$	Mean $T_{1/2}$	T_{max}	$T_{1/2}$	Mean $T_{1/2}$	T_{max}	$T_{1/2}$
1	121a	262	222		> 700	> 650		332	286
	122	264	227		534	481		340	283
	123	285	236		> 700	> 650		348	292
	125	299	237		> 700	> 650		345	287
	126	262	232		> 700	> 650		354	297
	127	297	237	232 ± 3	> 700	> 650	> 622 ± 28	362	293
2.1	75a	262	223		568	492		356	298
	78a	281	229		559	511 [s]		349	298
	79	263	225		584 [p]	544 [p]		354	288
	82	284	239		566	530 [d]		339	282
	83	277	229	229 ± 3	659	616	539 ± 21	353	285
2.2	26	282	230		567 [s]	506 [s]		304	266
	27	282	225		527	483 [s]		324	279
	30	264	222		551	494		333	277
	35	271	225	226 ± 2	520	478	490 ± 6	315	276
	32	285	232		?	?		359	283
	33	273	240		571 [s]	522 [s]		324	279
	29	282	232	229 ± 2	?	?	497 ± 8	340	275

Reference temperatures measured from: [a] first peak of TL since thermal exposure in antiquity; [b] first peak of remnant geological TL after thermal exposure in antiquity confirmed by normalisation plateau; [c] first peak of annealed laboratory induced TL. Temperature parameters: [?] can not determine, although plateau confirms evidence of remnant geological TL; [s] determined by stripping scaled laboratory TL from natural TL; [p] determined from normalisation plateau; [d] determined by differentiating glow curve. Errors on all mean values are standard errors at 68% confidence level.

Table 5.2 continued...

Phase	SUTL no.	Archaeo TL temperatures (°C) [a]			Geo TL temperatures (°C) [b]			Laboratory TL temp. (°C) [c]	
		T_{max}	$T_{1/2}$	Mean $T_{1/2}$	T_{max}	$T_{1/2}$	Mean $T_{1/2}$	T_{max}	$T_{1/2}$
2.3a	11	295 [d]	233 [d]		?	?		356	291
	12	296	230		533	494 [s]		340	288
	13	285	211		517 [s]	477 [s]		334	291
	15	277	218		524	481 [s]		339	292
	16	265	221		537	499 [s]		332	285
	17	266	223		546	480		370	299
	20	284	229	224 ± 3	564	497	488 ± 4	344	292
2.3b	50	238	208		562	502		346	296
	52	276	223		?	?		371	297
	54	265	229	220 ± 6	571 [p]	541 [p]	522 ± 20	355	285
3.1	36	280	230		534 [s]	497 [s]		376	303
	38	281	239	235 ± 5	560 [s]	520 [s]	509 ± 12	325	276
Mean ± 1 s.e.		276 ± 2	228 ± 1		583 ± 13	534 ± 13		344 ± 3	287 ± 2

Reference temperatures measured from: [a] first peak of TL since thermal exposure in antiquity; [b] first peak of remnant geological TL after thermal exposure in antiquity confirmed by normalisation plateau; [c] first peak of annealed laboratory induced TL. Temperature parameters: [?] can not determine, although plateau confirms evidence of remnant geological TL; [s] determined by stripping scaled laboratory TL from natural TL; [p] determined from normalisation plateau; [d] determined by differentiating glow curve. Errors on all mean values are standard errors at 68% confidence level

5.1.4 Discussion

Implications of sampling strategy and preparation

Residual geological TL could feasibly indicate either (a) the highest thermal exposure in antiquity the ceramics have been subjected to, (b) the lowest (or perhaps an average) thermal exposure for each ceramic, or (c) randomly distributed thermal exposures.

For (a) to be true either each ceramic has had a uniform thermal exposure internally and externally and the wall thickness is small (thereby creating negligible thermal gradients), or sample selection and preparation has ensured a surface analysis in the region of highest thermal exposure for each ceramic. For (b) to be true the whole ceramic has been homogenised and portions that represent the ceramic as a whole prepared and analysed. For (c) to be true the thermal exposure over the surface of the ceramic, both externally and internally, is variable and selection of material from the ceramic for preparation is random.

Given (i) the limited recovery of whole buried ceramics, (ii) the restriction by the excavator of available material for analysis (due to the importance of diagnostic features, decoration, etc.), (iii) the preparation method carried out in this study which involved dissagregation of whole sherds (as opposed to surface sampling), (iv) the particular problems encountered at Pool with respect to lifting the pottery (Hunter and MacSween, 1991; Hunter *et al.*, forthcoming), and (v) the assumed variability of thermal exposure during pottery firing, the residual geological TL signals measured from the Pool pottery are most likely to indicate randomly distributed thermal exposures as in point (c) above.

However, from the mean $T_{1/2}$ results measured from the residual geological TL signals it is possible to observe both distinct variations between phases, and also low scatter within phases (particularly phases 2.2 and 2.3a; phase 2.1 if the highest value is discounted). Although it is not possible to say from the dating evidence (and for the majority of samples it may well be unlikely) whether the ceramics from a particular phase were fired in the same bonfire or simple kiln, the results suggest that a random distribution is not the case, and are more likely indicating either the lowest or perhaps an average thermal exposure. This

therefore implies that it is valid to compare the $T_{1/2}$ values from different phases in terms of a relative analysis. One may go further to tentatively suggest that the thermal exposure over the surface of the ceramics during firing may have been reasonably uniform, and the thermal gradients across ceramic structures relatively small.

Archaeological implications

(i) Firing technology

If one accepts that the sample set is representative of the site and mean $T_{1/2}$ values may be compared from different phases the $T_{1/2}$ results for residual geological TL may imply variation in firing technology. For the earliest phase (phase 1) 5 out of the 6 samples show no evidence of geological TL before 700°C which is confirmed by flat normalisation plateaux up to 700°C. In comparison geological signals were either detected unambiguously or confirmed by normalisation plateaux features in every other phase. This suggests ceramics from phase 1 were subjected to a far higher thermal exposure compared with the other phases. From phase 1 there is an observable trend to lower thermal exposures until phases 2.3b and 3.1. Here there is a rise in values once again, although the sample size for both phases is small and the scatter relatively large. Thus the results from the earliest Neolithic phase may suggest pottery firing was either conducted at a higher temperature, or for a much longer duration. This may indicate the technology of the firing process was more advanced in the earliest Neolithic remains of the site (weighted mean = 3508 ± 318 BC). In the next, and following phases, from the Late to the Early Neolithic (phases 2.1 to 2.3a; weighted means = 3889 ± 303 BC to 2162 ± 133 BC) the results indicate a progressive decline in technology, after which (phases 2.3b to 3.1; weighted means = 2070 ± 177 BC to 2012 ± 261 BC) there is a possible indication of slight enhancement in firing technology once again.

These results therefore may suggest that for the pottery assemblages at Pool the ceramic technology was more advanced for the earlier 'Unstan' tradition than the later 'Grooved Ware' traditions, and there is possible indications of a variation in firing technology within the 'Grooved Ware' assemblages themselves. There are various possible reasons for a

decline in pottery technology including pressure on fuel resources (discussed in point (ii) below), changing social structures or merely changes that evolve through adopting a new ceramic tradition. If, for example, the suggestion by Renfrew (1979) of a more centralised society of chiefdoms in the later Neolithic is accepted, one may suggest the decline in pottery technology at Pool is perhaps a reflection of a change in emphasis from small egalitarian communities, utilising the finer craft of the individual potter, to larger social structures with the culmination of major monuments (for example the striking mainland structures at Brodgar, Stenness and Maes Howe) at the expense of a poorer mass-produced ceramic product. The possibility of the 'Grooved Ware' assemblages being brought to Pool from elsewhere (or vice versa for the 'Unstan' material) may be dismissed because, although there is no physical evidence on site in terms of 'kilns' or wasters etc (Hunter pers. comm., 1997; Hunter *et al.* forthcoming), MacSween identified that local sources were used right the way through the Neolithic (MacSween, 1990).

The annealing of the TL of the feldspar minerals measured here is unlikely to be described accurately by the general expression formulated for isothermal annealing of F-1 (Chapter 4, section 4.1.3.2). However, assuming linear extrapolation of the expression for F-1 to higher temperatures or longer durations is valid, we may postulate combinations of temperatures and durations to achieve the measured geological $T_{1/2}$ values. For example, for a $T_{1/2}$ value of 500°C and assumed durations of between 1 and 12 hours, the isothermal burning temperatures the expression derives are about 391 and 368°C respectively. For the upper $T_{1/2}$ limit of about 650°C these values are 527 and 503°C for 1 and 12 hours respectively. It is fair to assume these values may be between 50 to 100°C in error of the values for the true relationship for the measured feldspars from the ceramics, but nevertheless give an indication of the variation in burning temperatures between phases and suggest an idea of the relatively modest temperatures the thermal exposures may represent. If one goes further to assume that the thermal gradients involved at the time of the ancient firing were relatively small, these ball park temperatures are suggestive of the fired temperatures at the ceramic surface.

(ii) Available resources and environmental factors

The $T_{1/2}$ results may merely be a reflection of the available fuel resource from the earlier Neolithic phases to the later phases. The same "firing recipe" may have been put into practice, with a consistent duration of firing, but the fuel resource may have changed or may have varied in abundance. However, the reasons for this change may include climatic factors, external aggression or a change of fuel due to exhaustion of nearby resources from over-foraging.

Palaeo-environmental evidence suggests a possible influence of climatic factors reducing the availability of fuel resources, and as a direct consequence limited resources would be rapidly exhausted. Davidson and Jones suggest prior to the formation of peat, brushwood, turf or seaweed was likely to be used as fuel (Davidson and Jones, 1993), although it would seem reasonable to suggest that animal dung could be added to this list. However, on Sanday modern surveys of surficial deposits show extensive wind blown sand cover but no indication of peat. Additionally it has been suggested that peat formation only commenced in Orkney c. 1800 BC and was only ready for combustion in the first millenium BC. From pollen assemblages (Glims Moss and Loch of Skaill on the mainland) Keatinge and Dickson (1979) show a presence until c. 3800 BC of birch-hazel woodland or scrub, with willow, ferns and tall herbs. Thereafter there is a decline and replacement by more sparse open vegetation, which they interpret as a climatic change with higher wind speeds, and colder wetter weather. Davidson and Jones (1993) discuss botanical evidence to suggest lower temperatures at this time, and a possible decline in temperature from c. 4400 to 3800 BC. Stronger winds would inhibit tree growth and cause physical damage and the effects of salt spray. Evidence from Maes Howe and Stenness (Caseldine and Whittington, 1976) suggests a treeless landscape about 2600 BC. The sand blow probably began about 3800 BC, and indeed the earlier sand layer at Pool is TL dated by the ceramic analyses between 3889 ± 303 BC (phase 2.1; weighted mean of SUTL samples 75a, 78a, 79, 82, 83) to 3606 ± 282 BC (phase 2.2a; weighted mean of SUTL samples 26, 27, 30, 35).

(iii) Wider implications of results

It is difficult to discern whether the variation in mean geological $T_{1/2}$ results is due to a change in technology linked to a change in ceramic tradition or to a change in the type or quantity of fuel used. However, the palaeo-environmental evidence would suggest the latter is more likely to be the reason, indicating a decline in availability of high temperature fuel derived from woodland or scrub, and a change to such fuel resources as turf, seaweed, animal dung or occasional driftwood.

From discussion of the sampling strategy and preparation above it is clear that more detailed analyses are necessary to test the archaeological assumptions. These include analysis of a more representative set of samples, using both ceramic surface and sliced core analyses at different sampling positions (eg. rim, base, body; external, internal), and comparing these results with those from homogenised portions. In addition Unstan and Grooved Ware material from other Neolithic Orkney settlements (eg. Knap of Howar, Skara Brae, Links of Noltland, Barnhouse) and burial sites (eg. Quanterness, Isbister, Pierowall) should be analysed to examine whether the same trends are shown elsewhere. Useful complementary information may be sought from analyses of hearthstone remains from settlement sites. If the same thermal exposure trend is shown from Early and Late Neolithic hearths this would reinforce an argument suggesting poorer fuel resources.

These analyses suggest that it may be possible to discern between different ceramic technologies or traditions where there are chronological or stratigraphical differences, but differences in decoration, fabric, etc are not clear. In the same way it may also be possible to establish differences between 2 or more contemporary kilns or potters. The above study has shown that geological $T_{1/2}$ values (but also archaeological $T_{1/2}$ - see discussion below) can, in certain instances, confirm the phasing of a site, and thus the stratigraphic relationships and the dating. This would have to be based on distinct $T_{1/2}$ means with low scatter.

TL dating implications

The position of the first rise of the TL glow curve is governed by a dynamic equilibrium between charge trapping in shallow traps and ambient temperature eviction. In the burial environment charge trapping is the end result of ionisation of parent atoms by α, β, and γ radiation in the surrounding soil matrix and cosmic radiation. Subsequent to firing, use, discarding and burial, a dynamic equilibrium will be set up that is dependent on the environmental dose rate and the burial temperature. Additionally, however, the equilibrium position will also be effected by the length of time of burial.

Thus if constant environmental dose rate and constant burial temperature (or uniform burial temperature periodicity) are assumed, the variable function is the burial time or age (assuming time between firing and burial is negligible), and the longer the burial time (or older the sample) the higher the temperature of the first rise of the glow curve.

Although the results from t-test analyses of the archaeological $T_{1/2}$ data suggest the means from each phase are not significantly different, the results (apart from the latest phase; 3.1) do suggest a decrease from the earliest to the latest phases, thereby fitting in with the above argument and confirming both the stratigraphic phasing of the site and the TL dating results.

It is important to bear in mind that there may be additional factors to assess when comparing archaeological $T_{1/2}$ values in this manner. These may include the following:

1) Variation of surface temperature (ie. climate)
2) Variation of burial temperature with depth from surface
3) Variation of thermal conductivity with burial medium (which is also related to point (1) above in terms of heat transfer considerations)

5.2 A study of 2 burnt stone mounds from Crawford, Clydesdale

5.2.1 Site/material description

Burnt mounds are composed of burnt stones and dark soil containing charcoal and ash. They are commonly found close to a source of water and are often crescentic in shape and irregular in outline. Other common features are purpose built hearths (or evidence of simple bonfires) and tank structures. The tanks may be in the form of a wooden trough or a pit lined with stone slabs and sealed with clay.

The simplest interpretation of the function of burnt stone mounds is of cooking places, where stones were heated in a fire place and then dropped into a tank of water. Once the water boiled joints of meat wrapped in straw or skin could be placed in it. When the stones became fractured after repeated heating/cooling they were discarded onto the mound. The size of such mounds and their proximity to settlement sites may indicate whether they were in common use for cooking for a small community, or were for occasional use as communal feasting areas after a hunt between a number of small communities, or perhaps had a more specialised ritualistic feasting function. However, as Hunter has suggested from field survey in Fair Isle (Hunter and Dockrill, 1990) burnt mounds are often the sole surviving element in the archaeological landscape due to their difficulty in removal, and, conversely, their relative small hazard to formal agriculture.

A slightly different interpretation on the same cooking theme is for roasting rather than boiling or broiling, where there is evidence of a pit with direct signs of heating. Where structural evidence has been excavated, for example the sites at Liddle and Beaquoy in Orkney (Hedges, 1975), the function of the site has been interpreted as both for settlement and cooking, whereas Barfield and Hodder (1987) suggest the sites they have excavated in Birmingham relate to washing or sauna activities. Additionally, Hunter and Dockrill (1990) suggest the large mound known as Shelly Knowe on the Tofts Ness peninsula on Sanday, Orkney has a specialised function as it appears to be contemporary with the nearby round-house complex (excavated by Dockrill, 1988; Hunter *et al*, forthcoming) which contains hearthstones in three different construction phases, and a stone tank from an earlier

structure, but no evidence of burnt stones, suggesting that the particular method of cooking interpreted from burnt mounds was not employed at the dwelling itself.

Burnt stone mounds occur over a long period in the British Isles from the early second millennium BC into the medieval period (date lists: Brindley and Lanting (1990); Barber (1990); Hodder (1990); Kelly (1990); Williams (1990)). In Orkney and Shetland, where there are in excess of 400 burnt mounds, they appear to begin around 1200 and not to extend much beyond the middle of the first millennium BC. Dated examples by TL include the Orkadian sites at Liddle, Barswick, Graemshall, Beaquoy, Fan Knowe and Knowe of Scorn (Huxtable *et al.*, 1976).

The two burnt stone mounds to the south of Crawford in Clydesdale were excavated by Banks (1996). The mounds were situated either side of three cairns excavated at Stoneyburn Farm by APG (Archaeology Projects Glasgow) in 1991.

The northern example (Figure 5.4) stood on a small knoll on the steep lower slopes of Ellershie Hill opposite the southern end of Crawford, beside a small burn. The mound itself had the classic crescentic shape of Barber's Class 1 mounds, which he characterises as *fulachta* (Barber, 1990). It was small feature, no more than two or three metres in length and a maximum width of two metres. It had a height of around 0.5 metres.

The southern example (Figure 5.5) was on flat ground and was partly cut by the Ellershie Burn on its eastern edge. The mound itself was very low, protruding above the soil by only a few centimetres. However, the section cut by the burn had a height of about 0.5 m. The mound was much lower than the northern example and was not crescentic in shape like the classic fulachta. However, due to high organic content in the surrounding soil, it was possible that the mound had suffered plough damage or topographical changes due to the alluvial action of the Ellershie Burn.

At the north mound samples were removed from the top, middle and base centre, and two peripheral locations. At the south mound samples were removed from the top and base centre, and northwest corner. Six samples were removed from each location. Additionally

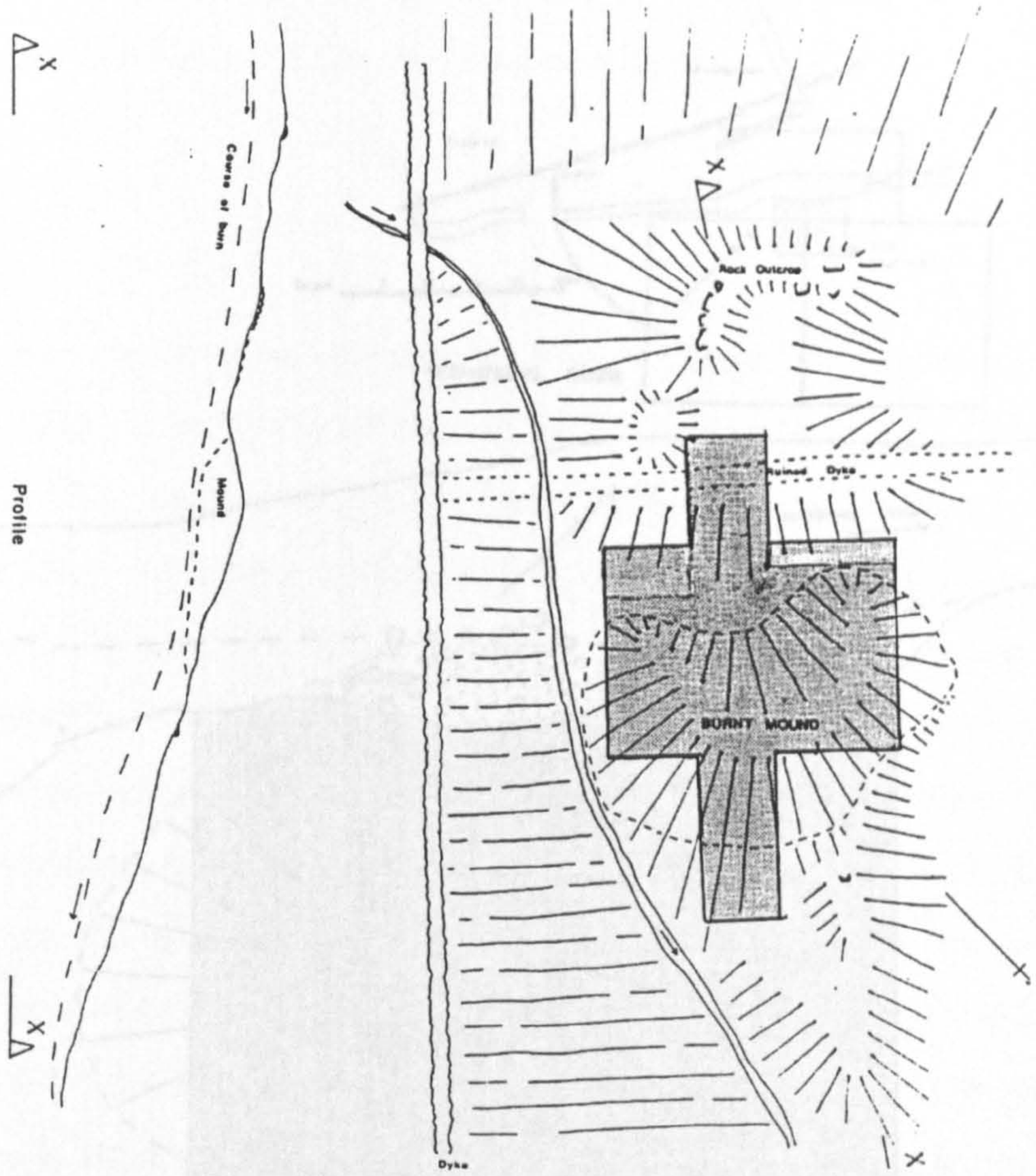

Figure 5.4 Northern burnt mound (reproduced with the kind permission of Iain Banks)

material assumed to be un-burnt was sampled from areas in close proximity to the mounds.

5.2.2 Sample preparation

In the laboratory those stones whose mass was greater than desirable for initial preparation (> 30-40 g), were cut with a water-cooled diamond rock saw in safe light conditions. Care was taken to cut samples from areas with visible scorch-marks, fire-cracked surfaces, etc., and to limit the depth of cut to reduce thermal gradient effects. Feldspar minerals were extracted from the samples using a similar technique to the method described by Mejdahl (1983; Mejdahl and Winther-Nielsen, 1982). The usual procedures of drying, crushing, sieving, heavy liquid (sodium polytungstate solution) separation with a centrifuge, and acid washes (10% HF, 10% HCl) were employed. The K-feldspar (2.51-2.58 gcm^{-3}) and Na-feldspar (2.58-2.62 gcm^{-3}) density fractions from a 90-125 μm grain size fraction were used

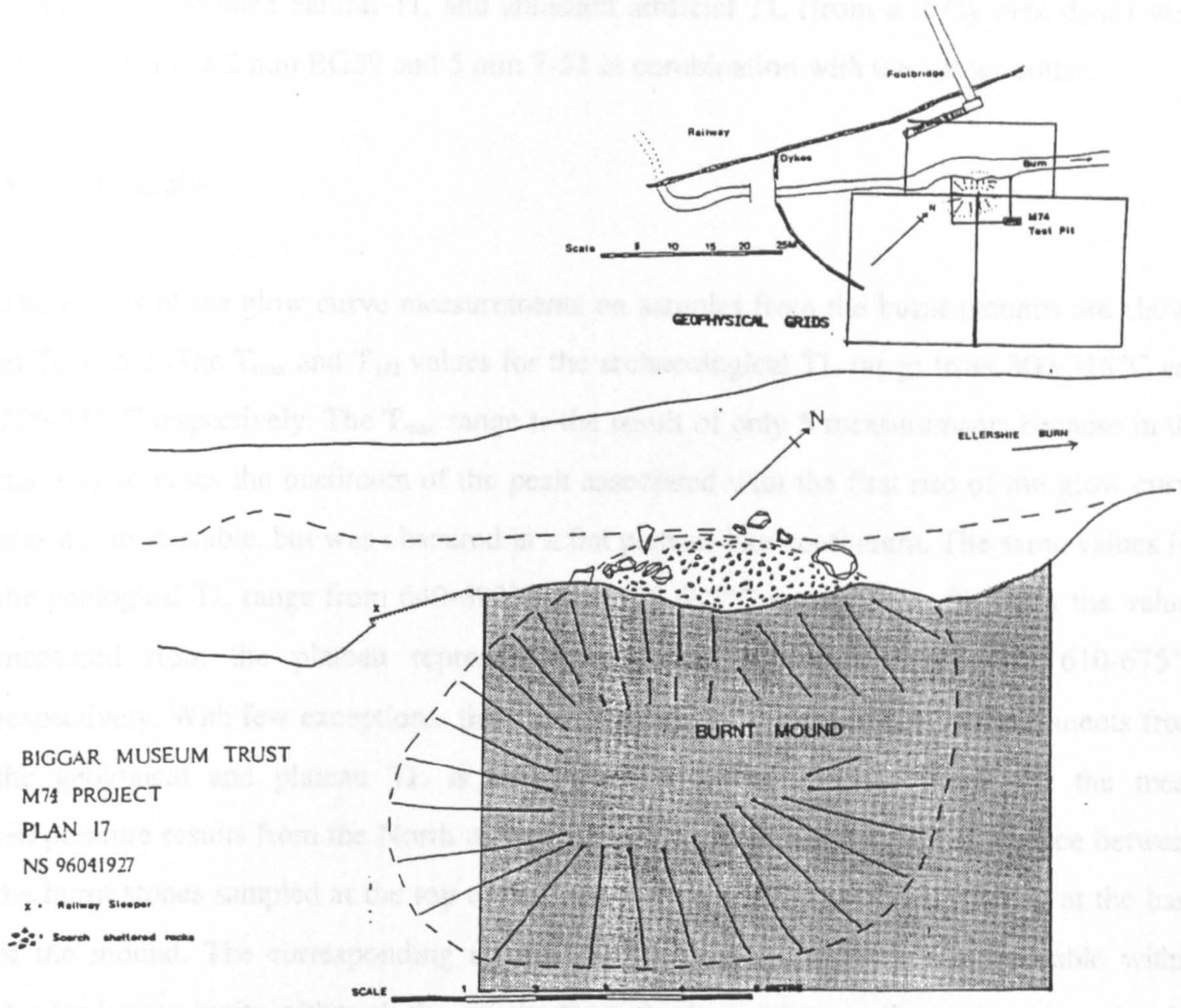

Figure 5.5 Southern burnt mound (reproduced with the kind permission of Iain Banks)

for experiments. If a sufficient yield was obtained the potassium fraction was used in preference due to the higher sensitivity observed in many luminescence studies (from observations by the author and as reported by Aitken, 1985). Three aliquots of each sample were dispensed onto disc (typically 5 mg of material) and the natural TL measured to 700°C. The discs were then given a 100 Gy ^{60}Co gamma dose and re-measured. As discussed in Chapter 3 (Section 3.2.3 and Figure 3.6) the use of 3 different filter arrangements was explored. $T_{1/2}$ values from archaeological, geological and plateaux (natural TL / artificial TL) TL were determined.

In parallel with the preparation of stones sampled from the two mounds, the material assumed to be un-burnt was prepared in a similar manner to above and glow curves of the

natural TL, annealed natural TL and annealed artificial TL (from a 2 Gy beta dose) were recorded using a 2 mm BG39 and 5 mm 7-51 in combination with the spacer collar.

5.2.3 TL results

The results of the glow curve measurements on samples from the burnt mounds are shown in Table 5.3. The T_{max} and $T_{1/2}$ values for the archaeological TL range from 300-318°C and 226-243°C respectively. The T_{max} range is the result of only 5 measurements because in the majority of cases the maximum of the peak associated with the first rise of the glow curve was not measurable, but was obscured in a flat plateau-like continuum. The same values for the geological TL range from 640-692°C and 598-682°C respectively. Similarly the values measured from the plateau representations range from 638-696°C and 610-675°C respectively. With few exceptions, the agreement between temperature measurements from the geological and plateau TL is extremely good. For the geological TL the mean temperature results from the North mound suggest there is a significant difference between the burnt stones sampled at the top to those at the base, the higher values being at the base of the mound. The corresponding results from the South mound are comparable within standard error limits, although the results from the base centre make a closer match with those from the top centre of the North mound. The higher standard errors in the geological (and plateau) TL data compared with the archaeological TL data shows there is greater variation in thermal exposure values.

Table 5.4 shows the results of TL measurements on potassium (K), sodium (N) and plagioclase (P) feldspar extracts from an un-burnt piece of stone (SUTL212). The first peak temperatures for the natural TL un-annealed, annealed for 100 s at 300°C and annealed for 100 s at 500°C show good reproducibility for all 3 density fractions; the un-annealed glow curves have a mean value for T_{max} of 266 ± 2°C and $T_{1/2}$ of 230 ± 2°C, and the corresponding mean values for the annealed glow curves are T_{max} of 376 ± 5°C and $T_{1/2}$ of 341 ± 3°C for 300°C annealing, and T_{max} of 594 ± 3°C and $T_{1/2}$ of 562 ± 11°C for 500°C annealing (the mean is taken as the average between the highest and lowest values and the errors as half their difference).

Table 5.3 Crawford Burnt Stone Mounds TL results

Sample	Location	ρ fraction (gcm^{-3})	Archaeo TL temp. (°C)[a]		Geo TL temperature (°C)[b]		Plateau TL temperature (°C)[c]	
			T_{max}	$T_{1/2}$	T_{max}	$T_{1/2}$	T_{max}	$T_{1/2}$
North								
SUTL183B	Base centre	2.58-2.62	?	240 ± 3[d]	683 ± 10	655 ± 18	685 ± 12	660 ± 10
SUTL186	Base centre	2.58-2.62	?	*239 ± 3*	*679 ± 12*	669 ± 14	*678 ± 11*	*666 ± 9*
				239 ± 1	**680 ± 5**	**661 ± 7**	**680 ± 5**	**664 ± 4**
SUTL188	Top centre	2.58-2.62	?	239 ± 1[d]	*649 ± 0*	632 ± 13	*650 ± 1*	*634 ± 13*
SUTL189A	Top centre	2.58-2.62	312 ± 7	238 ± 5[d]	657 ± 13	636 ± 11	*653 ± 9*	*631 ± 15*
				238 ± 1	**653 ± 4**	**631 ±5**	**651 ± 4**	**636 ± 6**
South								
SUTL219	Base centre	2.58-2.62	?	231 ± 5[d]	664 ± 11	634 ± 11	666 ± 6	636 ± 9
SUTL222	Base centre	2.51-2.58	*301 ± 1*	*237 ± 3*[d]	*647 ± 7*	*619 ± 6*	*646 ± 8*	*618 ± 6*
				233 ± 3	**658 ± 6**	**629 ± 6**	**658 ± 6**	**630 ± 6**
SUTL225A	Top centre	2.51-2.58	?	236 ± 5[d]	658 ± 10	606 ± 8	669 ± 1	613 ± 3
SUTL226	Top centre	2.58-2.62	?	*237 ± 2*[d]	*673 ± 6*	*634 ± 6*	668 ± 15[1]	632 ± 15[1]
				236 ± 2	**663 ± 6**	**616 ± 8**	**669 ± 1**	**618 ± 5**

Reference temperatures measured from: [a] first peak of TL since thermal exposure in antiquity; [b] first peak of remnant geological TL after thermal exposure in antiquity confirmed by normalisation plateau; [c] first rise of normalisation plateau (natural TL / artificial TL) corresponding to natural geological peak. Temperatures listed are the average of the largest and smallest values from three repeats of each sample and the associated error is estimated as half the difference between these two temperature values. Figures in **bold** are the mean and standard error (68% confidence limit) of all the measurements from a particular location. Temperature parameters: figures in *italics* are where only two temperatures could be measured; [?] uncertain T_{max} due to multiple components; [1] only one measurable plateau - errors are estimated as ± 15°C; [d] all values determined by differentiation.

Table 5.4 Un-burnt stone from Crawford: natural TL and laboratory annealing TL results

Sample[a]	Run number	Annealing regime[b]	First peak temperature (°C)[c]	
			T_{max}	$T_{1/2}$
Natural				
212KA	1	no anneal	264[d]	228[d]
212KB	1	300°C for 100 s	378	343
212KC	1	300°C for 100 s	379	338
212KD	1	500°C for 100 s	~591[d]	~555[d]
212KE	1	500°C for 100 s	?	~573[d]
212NA	1	no anneal	268	232
212NC	1	300°C for 100 s	370	339
212ND	1	500°C for 100 s	~595[d]	~556[d]
212PA	1	no anneal	268	230
212PB	1	300°C for 100 s	377	342.5
212PC	1	300°C for 100 s	376	341.5
212PD	1	500°C for 100 s	596	560
212PE	1	500°C for 100 s	592	551
Artificial				
212KA	2	200°C for 12100 s	365	319.5
212KB	2	200°C for 12100 s	346	320.5
212NA	2	200°C for 12100 s	356	327.5
212NB	2	200°C for 12100 s	365	325.5
212PA	2	200°C for 12100 s	368	325.5
212PC	2	200°C for 12100 s	387	338
212KC	2	200°C for 3203 s	334	310.5
212KD	2	200°C for 3161 s	352	308.5
212NC	2	200°C for 76057 s	387	342
212ND	2	200°C for 76210 s	393	347
212KA	3	200°C for 61620 s	380	340.5
212KB	3	200°C for 61620 s	385	342.5
212NA	3	200°C for 61620 s	380	344
212PA	3	200°C for 61620 s	397	351.5
212PC	3	200°C for 61620 s	392	356.5

[a] feldspar fraction: K = potassium, N = sodium, P = plagioclase; [b] natural signals were annealed using the heater plate of the TL oven. Artificial signals were annealed in the TL preparation oven; [c] reference temperatures measured from the first peak of the TL glow curve; [d] values determined by differentiation.

The mean un-annealed $T_{1/2}$ value is lower than all the mean archaeological values for the burnt material which is contrary to the general pattern with decreasing sample age shown by the Pool results.

5.2.4 Discussion

Geological TL

The first observation to note is that all of the thermal exposures of the samples are relatively high, but all the residual geological signals are detectable with 700°C TL measurement, and all are confirmed with fairly high precision by the plateau results. Assuming that sampling strategy and preparation procedures allow the results of the residual geological TL measurements to be compared (cf. limitations of sampling strategy and preparation discussed for the Pool material), the mean $T_{1/2}$ results suggest the thermal exposures of the samples from the base centre position of the North mound are significantly higher than the top centre position. Additionally, the values from the top centre position are equivalent to both the top and base centre from the South mound.

A possible interpretation of the difference shown in the North mound results may be the use of a fuel which burns with a higher temperature resulting in higher thermal exposures for material deposited in the earlier use of the mound. This may imply simply a change in fuel resources or possibly a variation in the function from the earlier to the later use of the mound. Additionally the results may suggest a variation in the simple technological process involved (eg. stones heated significantly longer in the earlier use of the mound).

Environmental analyses (Banks, forthcoming) suggest no distinct difference in the types of woods used as fuels in the two mounds but do indicate frequent fragments of peat from the 'centre' of the northern mound. Spencer (1989) in firing experiments has observed higher burning temperatures for blocks of peat than small logs of elm and spruce. Although neither of these wood types were present in the environmental samples from the mounds, the higher thermal exposure estimates are possibly due to the use of peat in the northern mound. This may in turn indicate, as Banks suggests, that supplies of wood were running low and peat

was used as an alternative fuel, although the higher thermal exposure estimates relate to the earlier use of the north mound rather than later where an interpretation of substitution of peat for wood with declining local woodland is more feasible. So why the use of peat? Does this indicate a change in function for the north mound or perhaps a different cooking process?

Banks favours the common *fulacht fiadh* explanation for the Crawford mounds and indeed the small amount of artefactual evidence and the lack of evidence for an alternative function supports the interpretation of the mounds as cooking sites. However, although Banks reports that the base of the troughs on both sites had no visual indication of burning, in hindsight it would have been useful to test samples of the troughs using TL to determine whether a *mu-mu* explanation was likely (ie. the samples would have relatively high thermal exposures). On the other hand, if TL from trough samples reinforced a *fulacht fiadh* interpretation the thermal exposure data would be extremely interesting since the temperature involved would not exceed 100°C (boiling water) and thus would allow estimation of cooking times or duration of use, etc.

Utilising the expression formulated from the isothermal annealing of F-1 (ie. $T_{1/2}$ = 23.922*log(t_{anneal})+1.071*T_{anneal}; Chapter 4, section 4.1.3.2) gives $T_{1/2}$ estimates of 369°C for 100 s at 300°C and 583°C for 100 s at 500°C. Additionally the expression predicts the following $T_{1/2}$ values for 200°C annealing: 298°C for 3200 s; 312°C for 12100s; 329°C for 61620 s; 331 for 76210 s. Those predicted values involving temperatures above 350°C and durations in excess of 22100 s are calculated assuming that linear extrapolation of the F-1 expression to higher temperatures and longer times than the empirical data set is valid. Interesting parallels may be observed between these predicted values, and the values derived from the annealed natural and artificial TL from the un-burnt sample (100 s at 300°C = 341 ± 3°C; 100 s at 500°C = 562 ± 11°C; for 200°C annealing 3203 s = 309.5 ± 1°C, 12100 s = 326 ± 3°C, 61620 s = 347 ± 3°C, and 76210 s = 345 ± 3°C). Although the estimated values from the F-1 expression and the empirical values from the un-burnt material do not give the same results, there is a suggestion that the annealing experiments on the separated minerals from the un-burnt material are showing similar behaviour to F-1. Conversely, the results from the un-burnt material suggest linear extrapolation of the F-1 expression may be valid.

From these observations it is possible to tentatively suggest temperature figures from the thermal exposure measurements on the burnt stones. Firstly, it is necessary to make the following assumptions: (a) a number of heatings and dowsings may have taken place (cf. Buckley, 1990) but only the highest thermal exposure is of relevance, (b) the measured TL indicates the minimum value (ie. due to possible sampling within a thermal gradient) for the highest thermal exposure, and (c) the duration of heating was from 15 minutes (cf. Buckley, 1990) to a maximum of, say, 12 hours (cf. Hurl, 1990). The F-1 expression would thus predict temperatures for the base of the North mound of 551°C (15 min) and 514°C (12 h), and for the top of the North mound of 523°C (15 min) and 486°C (12 h). Similarly, for the South mound base 521°C (15 min) and 484°C (12 h), and the South mound top 509°C (15 min) and 472°C (12 h). An estimate of the error associated with these values is at maximum about ± 46°C which is the maximum absolute difference between the estimates derived from the F-1 expression compared with the empirical values of $T_{1/2}$ measured from the annealing experiments on un-burnt material.

Considering that sampled stones may well have been fragments of the original stones used in the heating/dowsing process but the precision for mean $T_{1/2}$ values taken from different stones in the same location is reasonably high, suggests the thermal gradients between the surface and interior may have been fairly modest. With this in mind the estimates above may represent the temperatures of the fires involved. However, analyses of the cell structure of charcoal removed from the mounds indicate the temperature of the fires were about 700°C (Banks, pers. comm.). If this value is correct it would suggest the temperatures quoted above are over 200°C lower than the true temperature of the fires. A more detailed analysis involving careful examination of burnt stones to determine surfaces in direct contact with the fires (as opposed to sampling within fractured cores) coupled with a sampling method to enable TL measurements of thin slices along a core of material taken from the surface (as discussed for ceramics in the above study) would be sufficient to determine a more accurate surface temperature. Having said this the temperatures within a fire can vary quite considerably (Spencer, 1989) and the contrast shown here may be a result of the difference of the burning temperature of the wood in question compared to the thermal exposure of the stones.

The function of burnt stone mounds is an interesting and challenging topic. These results suggest there is further scope for TL measurements of burnt stone material utilising a careful sampling technique with additional analyses of trough contents and structure. A promising area which may shed more light on the function of burnt stone mounds is the marriage of environmental, artefactual, and structural evidence with luminescence analyses.

Archaeological TL

Based on the argument and assumptions (including constant environmental dose rate and burial temperature) presented in the Pool ceramics discussion the mean archaeological $T_{1/2}$ results suggest the following: (a) the base and top of the North mound are contemporary; (b) the top of the South mound is likely to be contemporary with the North mound, but there is perhaps an indication it may be a later feature; (c) the base of the South mound is a later feature than the North mound; (d) the base of the South mound may not be contemporary with the top of the South mound.

The initial TL dating program at SURRC using standard microdosimetric models has shown variable preliminary results (North mound base 1.80-5.62 ka BP; North mound top 1.99-2.29 ka BP; South mound base 3.30-4.59 ka BP; South mound top 1.91-4.14 ka BP), although subsequent NAA analyses on the feldspar grains imply variable internal activity and alternative microdosimetric models are being investigated. The archaeological $T_{1/2}$ results may shed light on the TL dating results, and the suggestion of contemporary association is confirmed by ^{14}C AMS dates (North, cal BP 3564-3387; 4073-3842. South, cal BP 4223-3985 - all 1 sigma).

The mean $T_{1/2}$ result from the un-burnt material (230 ± 2°C) is lower than all the corresponding values for the burnt material (233-239°C). This conflicts with the argument put forward and the general trend shown by the results for the Pool material. However, this anomalous equilibrium position is perhaps an indication of a much colder previous "geological" climate coupled with a different burial environment.

5.3 Domestic hearthstones from Dunion Hill, near Jedburgh

5.3.1 Site/material description

Hearthstones from the Iron Age hillfort at Dunion Hill near Jedburgh (Rideout, 1992) had previously been sampled for TL dating, and material remaining in the laboratory archive was used for this study. Feldspar inclusions (90-125 μm) from eight samples of burnt stone from the hearths of houses 2 (Area 1), 6 (Area 3) and 7 (Area 4) (contexts F1031, F9014 and F12003 respectively) were examined from the Dunion Hill material.

The part of the fort excavated between 1984-1986 (Figure 5.6) was shown to be an annexe to the main fort (much of which had been destroyed by extensive quarrying). The eight houses excavated in this area were constructed on unlevel ground compared with the relative level surface of the summit within the main defences. This necessitated the construction of platforms to provide level sites for the houses. The houses were elliptical in shape, and for the most part with the long axis of the ellipse set along the face of the hill.

House 2 (Figure 5.7) This house was about 6 m wide and of unknown length. The house was in poor preservation although the surviving evidence suggested that the structures of 2 phases had occupied the scoop. The second phase contained the hearth. Other features of phase 2 included a paved area, evidence of a possible doorway and walls of about 1 m thickness. The hearth, overlying the floor of phase 1, consisted of a thin sandstone slab (now broken) with dimensions of about 1 m by 0.6 m, abutting the south side of a large (1.5 x 1.5 m) basalt boulder. The boulder was naturally bedded in the till protruding 0.25 m above the floor. Three samples from the hearth gave a TL date of 70 ± 190 BC (random error, RE), 210 (systematic error, SE). Radiocarbon dating was carried out on charcoal (hazel and willow roundwood) from a pit (which also contained a beehive quern and seeds) associated with phase 1 activity giving a date of 2000 ± 55 bp (50 ± 55 bc, cal BC 94-AD 62 @ 1σ; GU-2178), and also on charcoal lying on the phase 1 floor beneath the hearth of phase 2 which gave a date of 1970 ± 80 bp (20 ± 80 bc, cal BC 92-AD 113 @ 1σ; GU-2171). This dates phase 1 and provides a *terminus post quem* for the phase 2 hearth.

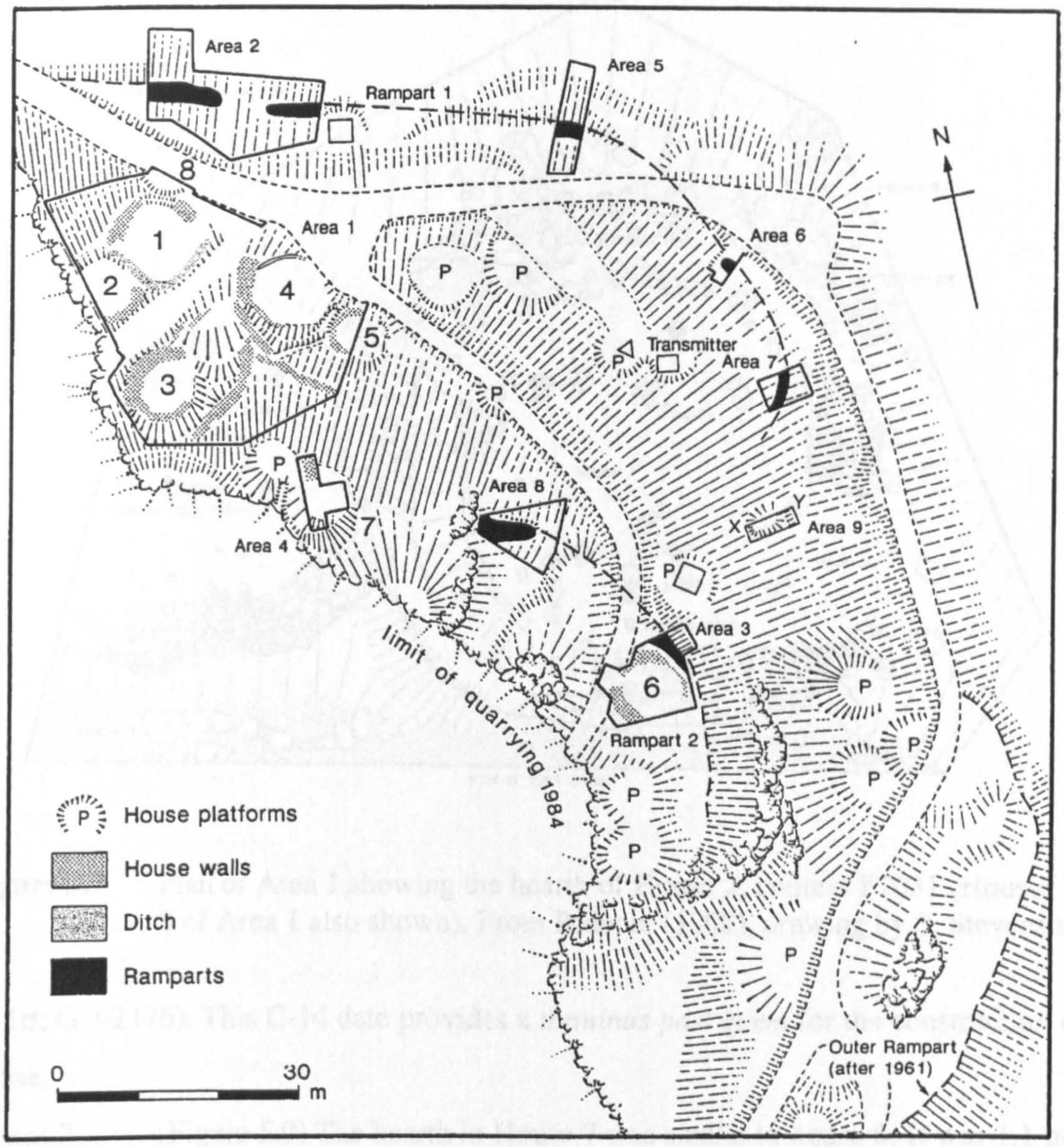

Figure 5.6 Plan of areas excavated during 1984-1986. From Rideout (1992), drawing by S. Stevenson.

House 6 (Figure 5.8) The house wall was poorly preserved. A doorway was identified from its paved floor, which continued outside the house for a short distance to merge with a pebbled road surface; inside the paving formed an elliptical platform edged with upright stones. The rest of the house floor was lower and apparently earthen. The hearth was located about 1 m from the widest part of the paving, near the centre of the house. It consisted of a subrectangular stone base about 1.2 m by 0.6 m, formed of small sandstone slabs. Two of the slabs produced a mean TL date of AD 60 ± 220 (RE), 220 (SE). Charcoal from a shallow negative feature beneath the wall, identified as alder, birch, and hazel roundwood produced a date of 2120 ± 110 bp (170 bc ± 110 bc, cal BC 366-10

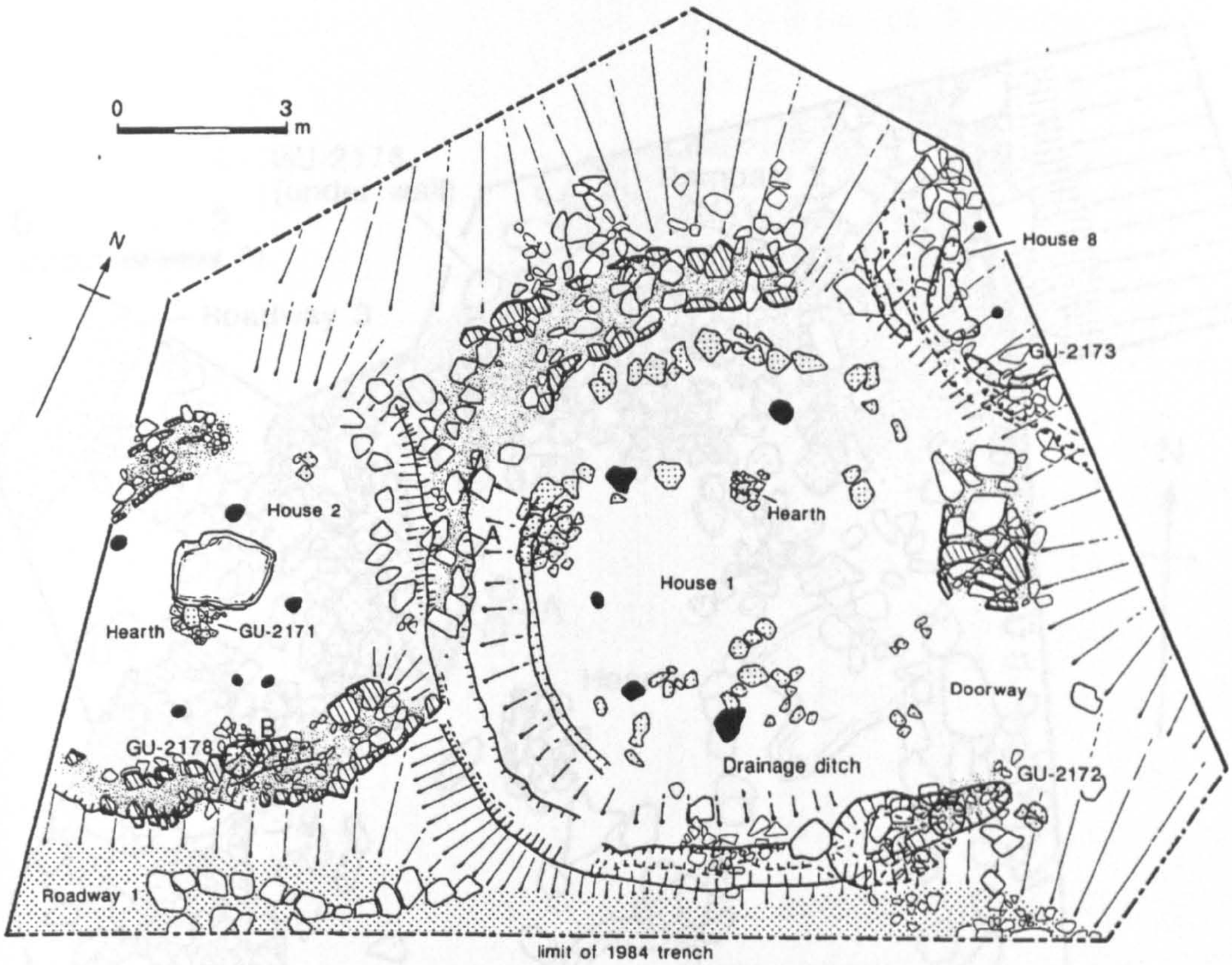

Figure 5.7 Plan of Area 1 showing the hearth of House 2, context F1031 (Houses 1 and 8 of Area 1 also shown). From Rideout (1992), drawing by S. Stevenson.

@ 1σ; GU-2176). This C-14 date provides a *terminus post quem* for the construction of the house.

House 7 (Figure 5.9) The hearth in House 7 was similar to house 6. It was 1.1 m long and 0.8 m wide constructed of flat sandstone slabs edged by upright stones. The house had a north facing door with evidence of paving at the threshold and internally. Samples from the hearthstone gave a TL date of AD 180 ± 170 (RE), 180 (SE). Charcoal (oak) from a single stone-packed post-hole produced a radiocarbon date of 5550 ± 100 bp (3600 ± 100 bc, cal BC 4500-4340; GU-2177). Rideout (1992) suggests that the early date may be the result of charcoal from a Mesolithic / Neolithic fire (natural or anthropogenic) on the hill that was accidentally incorporated into the post-hole backfill. Alternatively, the timber could have been bog oak re-used in the Iron Age house.

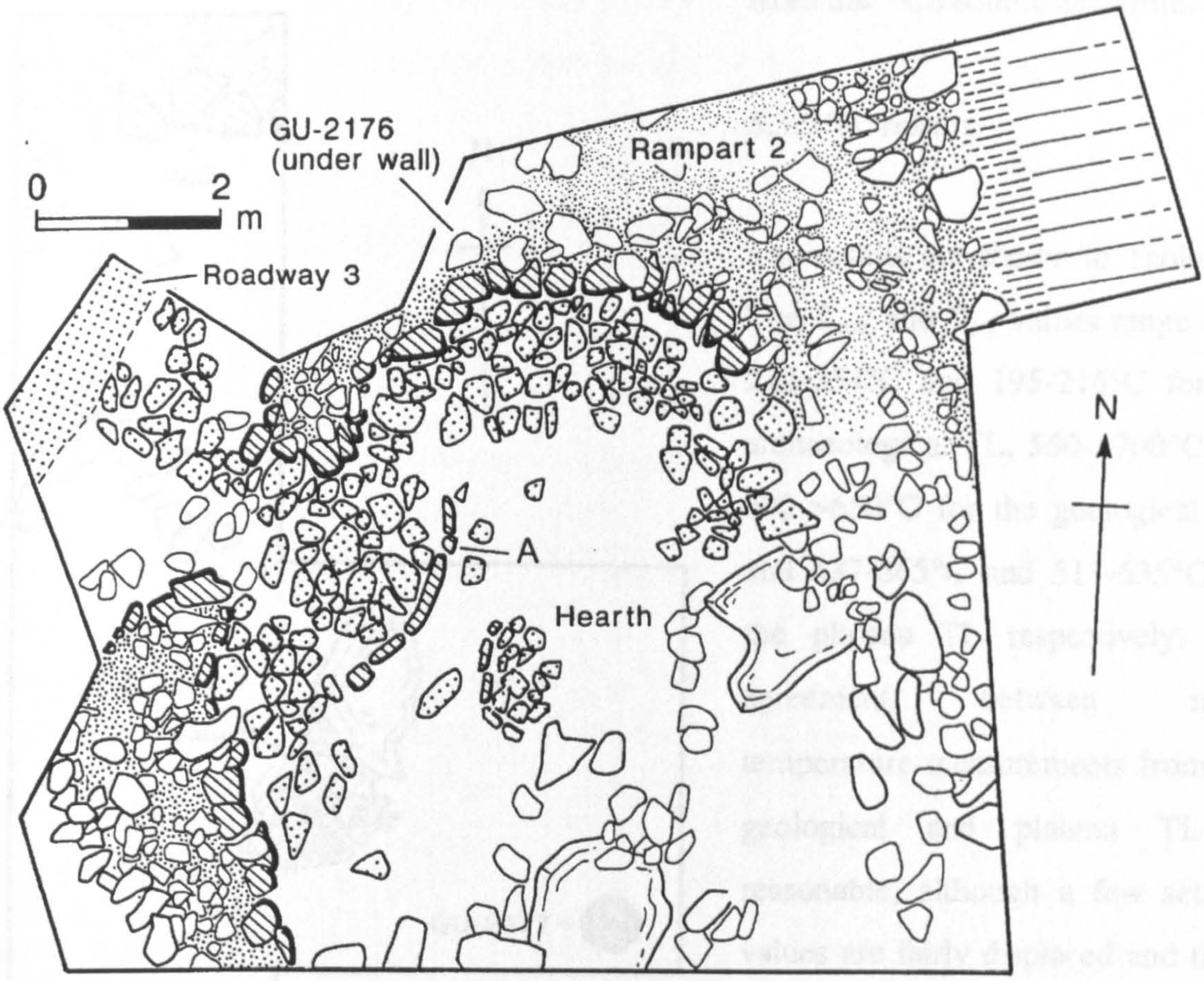

Figure 5.8 Plan of Area 3 with House 6 and associated hearth (context F9014). From Rideout (1992), drawing by S. Stevenson.

5.3.2 Sample preparation

Samples were prepared in a similar manner to the burnt stones from Crawford. 30 g portions of each sample were carefully cut from the bulk using a water-cooled rock saw and then feldspar fractions prepared as described above. The preparation used was a standard feldspar inclusion method, similar to that developed for vitrified forts (Sanderson *et al*, 1985, 1988). The preparation was reported in the Dunion Hill monograph (Sanderson, 1992; appendix 20).

Duplicate discs of available fractions were dispensed onto disc. A 3 mm BG39, 5 mm 7-51 and 3 mm BG3 filter combination was used for experiments. T_{max} and $T_{1/2}$ values were measured from natural (archaeological and geological positions) and plateau (artificial / natural TL). The laboratory dose administered after natural TL measurement was 100 Gy

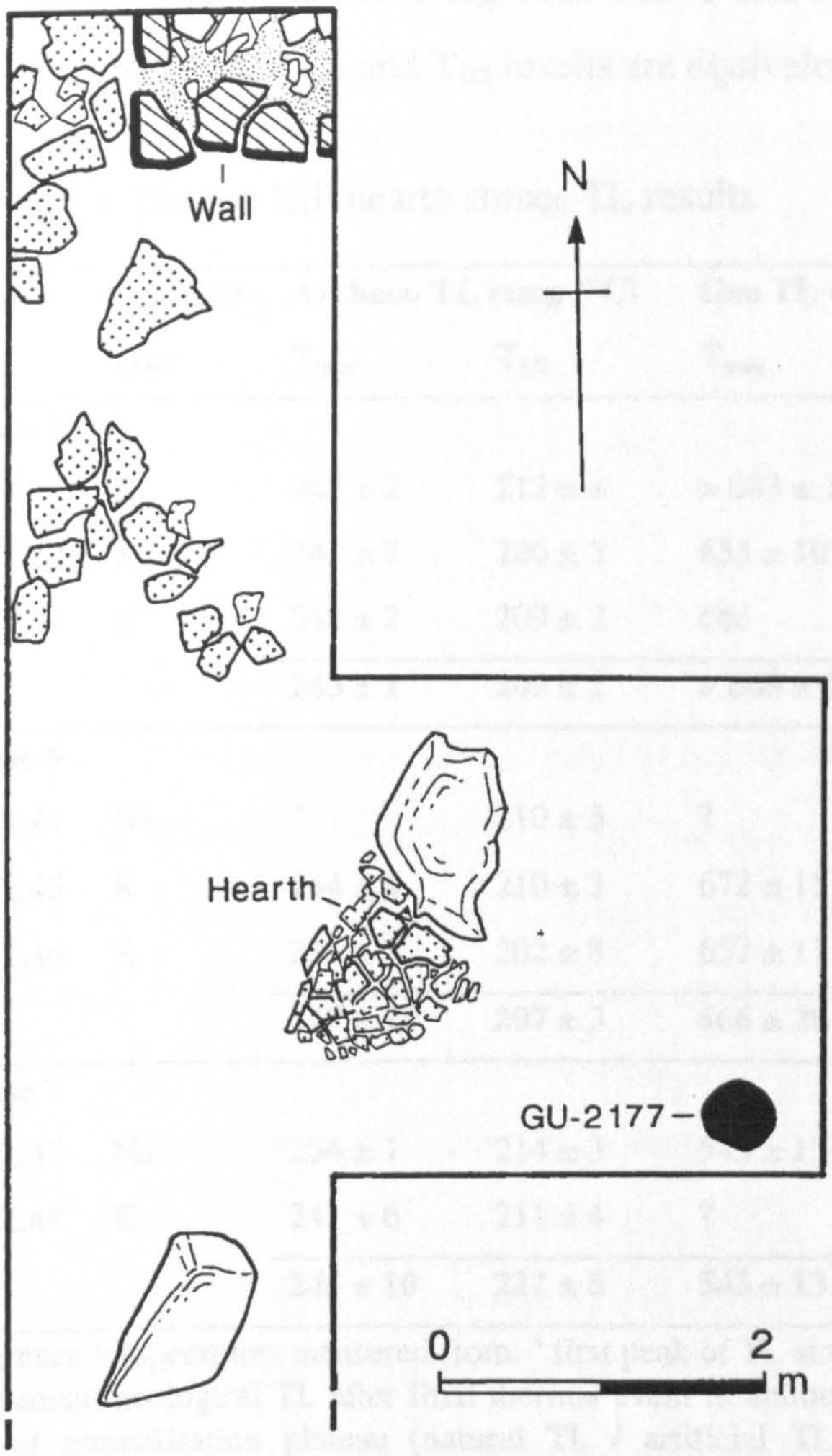

Figure 5.9 Plan of Area 4 showing House 7 and associated hearth (context F12003). From Rideout (1992), drawing by S. Stevenson.

from the ^{60}Co source as before.

5.3.3 TL results

The results are shown in Table 5.5. The T_{max} and $T_{1/2}$ values range from 222-254°C and 195-216°C for the archaeological TL, 550->700°C and 492->650°C for the geological TL, and 537-665°C and 511-635°C for the plateau TL respectively. The agreement between mean temperature measurements from the geological and plateau TL is reasonable, although a few sets of values are fairly displaced and there is quite high scatter on some individual measurements. Additionally there is a large variation in values for a particular house. However, the overall means (in bold) suggest that the hearth in house 7 has had a lower thermal exposure than the hearths in houses 2 and 6 which are roughly equivalent. If the measurement from SUTL41 which is above the detection limits of the method is removed the geological T_{max} and $T_{1/2}$ mean values for house 2 are 661 ± 5°C and 621 ± 6°C respectively. These values still fit in well with the result from house 6.

A large variation in measurements in the high temperature region for individual samples is interpreted principally to be a result of measurement errors due to low signal to background ratios (especially for samples with poor sensitivity), but additional factors may be the effect

of small fluctuations in servo lag from disc to disc and variations in disc-sample geometries. The archaeological T_{max} and $T_{1/2}$ results are equivalent within the error assessment.

Table 5.5 Dunion Hill hearth stones TL results

Sample	Feldspar type	Archaeo TL temp (°C)		Geo TL temp (°C)		Plateau TL temp (°C)	
		T_{max}	$T_{1/2}$	T_{max}	$T_{1/2}$	T_{max}	$T_{1/2}$
House 2							
SUTL41	K	245 ± 2	212 ± 4	> 683 ± 17	> 643 ± 7	?	?
SUTL42	K	241 ± 3	206 ± 2	655 ± 10	615 ± 6	656 ± 10	622 ± 13
SUTL43	K	242 ± 2	209 ± 2	*666*	*617*	*631*	*584*
		243 ± 1	**209 ± 1**	**> 668 ± 9**	**> 626 ± 7**	**648 ± 17**	**610 ± 26**
House 6							
SUTL44	Na	?	210 ± 3	?	?	?	?
SUTL45	K	244 ± 4	210 ± 3	672 ± 15	598 ± 9	*661*	*603*
SUTL46	K	231 ± 9	202 ± 8	657 ± 11	619 ± 29	*623*	*592*
		247 ± 13	**207 ± 3**	**666 ± 20**	**618 ± 29**	**642 ± 19**	**598 ± 6**
House 7							
SUTL47	Na	254 ± 1	214 ± 3	543 ± 13	501 ± 9	547 ± 10	521 ± 10
SUTL48	K	241 ± 6	211 ± 4	?	510 ± 2	569 ± 13	539 ± 9
		245 ± 10	**212 ± 5**	**543 ± 13**	**502 ± 10**	**560 ± 23**	**530 ± 17**

Reference temperatures measured from: [a] first peak of TL since final thermal event in antiquity; [b] first peak of remnant geological TL after final thermal event in antiquity confirmed by normalisation plateau; [c] first rise of normalisation plateau (natural TL / artificial TL) corresponding to natural geological peak. Temperatures listed are the average of the two values and the associated errors are half the difference between them. Figures in **bold** are the mean and standard error of all the measurements from a particular house. Temperature parameters: figures in *italics* are where only one temperature could be measured; [?] unable to measure.

5.3.4 Discussion

Geological TL

The mean geological $T_{1/2}$ results suggest the hearths have all had different thermal exposures. The hearth from house 2 is the highest, then house 6, and the lowest is house 7. Each house exhibits a certain degree of variability in results between samples, in particular house 2 where one of the hearth samples (SUTL41) is above the detection limit of the system. The variability may either be due to sampling inconsistencies or spatial distribution

of the slabs in each hearth relative to the highest thermal exposure. Other than the possibility of sampling inconsistencies and sample preparation between houses, the variation in thermal exposure between each hearth may possibly suggest either a variation in function or status between houses. For example, a hotter hearth burning for a longer time may suggest a house for a more important member of the community, or a house for which more communal cooking and other daily activities took place. In addition the variation in thermal exposure may merely indicate a slightly different type of fuel with a higher burning temperature.

The eight houses investigated in the 1984-1986 excavations (Rideout, 1992) were all platform constructions built on the sloping northwest flanks of Dunion Hill, probably within a defensive annexe to the main fort which stood on the relative level surface of the summit. All the excavated houses were similar in construction, size and shape, and contained common features such as hearths, paving and post rings. The similarity of the excavated houses implies that the variation in thermal exposure data is more likely due to differences in sampling position or fuel, rather than status or function.

Although the latter two reasons can not be totally dismissed, the position of these structures on poorer ground in an annexe to the main fort coupled with the restrictions on space discussed by Rideout (1992) suggests they may have been simple domestic structures with occupants of a lower status compared to those in the central body of the fort on the better ground of the summit plateau. The two house structures examined by Proudfoot between 1961-1962 (in Rideout, 1992), within the main defences of the fort, suggests they were similar in many respects to those examined in the annexe. However, this is the only other excavated evidence from Dunion Hill of an estimated total from revised plans of 66 structures (Rideout, 1992), almost all now lost to the quarry site.

TL analyses have potential in an exercise such as this to determine through variations in thermal exposure of hearth remains differences in function, fuel or status. As discussed for the analyses of ceramics and burnt stones above, careful sampling methods (particularly as regards the spatial context in this example) should be employed to ensure the accuracy of results. These analyses show a significant variation in thermal exposure between the hearths

of houses 2, 6 and 7, but the addition of the structural, artefactual and environmental evidence suggests a difference in fuel burning temperatures, rather than variations in house function or status.

Archaeological TL

The archaeological $T_{1/2}$ mean results are equivalent within error which suggests the houses are contemporary and supports the TL dating evidence.

5.4 Domestic hearthstones from Tofts Ness, Sanday

5.4.1 Site/material description

The northern peninsula of Tofts Ness, Sanday, is a rich prehistoric landscape covering an area of about 150 hectares preserved largely by burial in wind blown sand. The area was described at length by Wood, a local antiquarian, in the mid nineteenth century (NSA, 1845) whose investigations suggested evidence of funerary monuments. An RCAHMS survey of the area carried out in 1980 drew attention to the varied range of monuments present (Stevenson, 1980) and prompted archaeological assessment ahead of a scheduling program. In addition to the major burnt mound complex of Shelly Knowe, fluxgate gradiometer survey (conducted by J. Gater) showed the presence of a round-house structure situated about 250 m to the west (Hunter and Dockrill, 1990).

The roundhouse structure was excavated by Steve Dockrill in four field seasons from 1985-1988 (Dockrill, 1988; Hunter *et al.*, forthcoming). A multiphase settlement mound was unearthed with evidence of occupation from the Neolithic through to the Early Iron Age. TL analyses on ceramics and burnt stones from hearths from the earlier occupation gave dates for phases A and B of 2600 and 2400 BC respectively which were confirmed by ^{14}C analyses of animal bones. The main round-house structure (Area C) comprised multi-phase occupation and reconstruction and contained a sequence of hearthstones. Dates from the hearthstones suggested occupation from the Late Bronze Age to the Early Iron Age.

Samples from each of three distinct hearths (features 0741, 0889 and 1614) were examined from the main round house structure (Area C). The primary hearth of the round house (1614), set against the west wall, was in use in the first phase of occupation (SUTL104; SUTL105) and is shown in the plan of Area C in Figure 5.10. The two other hearths are later (0741 sealing 0889) and are positioned in the centre of the round house. The 0741 and 0889 contexts are beneath the hearth structure which is shown in a later plan of Area C (Figure 5.11). SURRC TL dates for context 0889: SUTL94 = 590 ± 260 AD; 97b; 98b = 2360 ± 640 BC; 99c = 3040 ± 870 BC; 101b = 1470 ± 430 BC. SURRC TL dates for context 0741: SUTL91b = 860 ± 210 BC; SUTL92.

5.4.2 Sample preparation

As with the Pool and Dunion Hill sites, material had previously been sampled for TL dating at SURRC and alkali feldspar separates remaining in the laboratory archive were used for this study. The sample preparation was carried out in the same manner as the Crawford and Dunion Hill burnt stones. TL measurements were performed from 0-700°C at 5°Cs^{-1} using 3 mm BG39, 5 mm 7-51 and 3 mm BG3 filters.

5.4.3 TL results

The results of the glow curve measurements on the Tofts Ness hearthstone samples are shown in Table 5.6. The T_{max} and $T_{1/2}$ values for the archaeological peak range from 229-285°C and 199-229°C respectively. The average results show a general trend of decreasing $T_{1/2}$ from the latest (0741) to the earliest (1614) contexts, although the results from SUTL94 and SUTL97b are anomalously low and high respectively, and the relatively large decrease in values for samples from context 1614 is quite notable particularly SUTL105. Additionally, the decreasing trend conflicts with the results shown by the Pool archaeological $T_{1/2}$ data. The remnant geological signals are yet more intriguing. From the latest context (0741) the average results from the two samples are very different. The

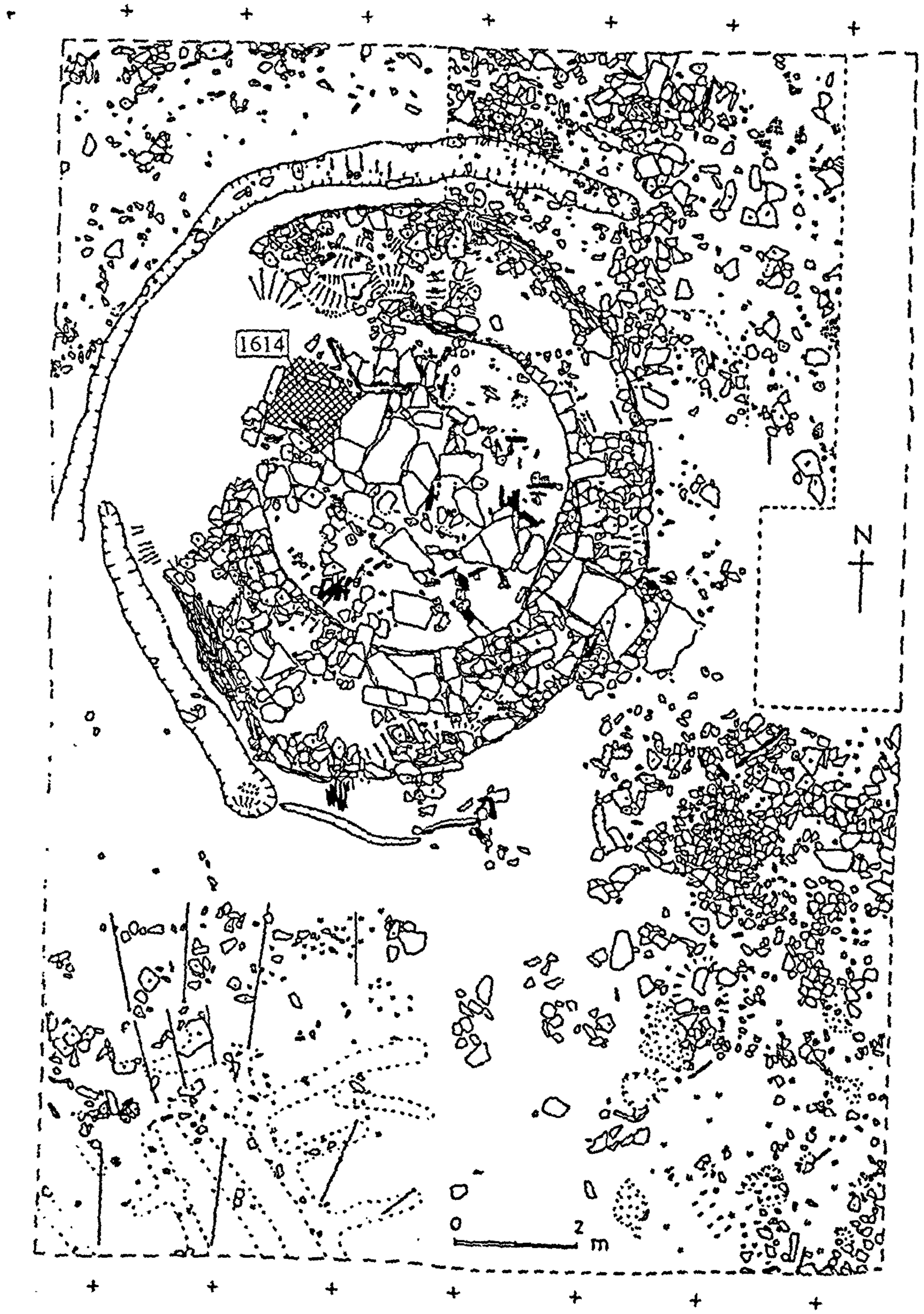

Figure 5.10 Plan of the Late Bronze Age structure (primary phase) showing hearth 1614 set against the west wall (from Dockrill, 1988).

results from the earliest context (1614) are more consistent (the plateau $T_{1/2}$ result for

Figure 5.11 Plan of the Late Bronze Age structure (later phase). Contexts 0741 and 0889 are below the central hearth shown (from Dockrill, 1987).

SUTL104 is perhaps a more reliable figure) although the values still indicate some variability. However, the picture becomes even more complicated when the results for the intermediate context (0889; sealed by 0741) are examined. The plateau results for nearly all

Table 5.6 Tofts Ness hearthstones TL results

Context	SUTL no.	ρ fraction (gcm^{-3})	Archaeo TL temp. (°C)[a]		Geo TL temperatures (°C)[b]				Plateau comments
			T_{max}	$T_{1/2}$	T_{max} (1)	$T_{1/2}$ (1)	T_{max} (2)	$T_{1/2}$ (2)	
0741	91b	2.58-2.62	264 ± 4[d]	218 ± 1[d]	432 ± 3	378 ± 1			rises continuously from ~350°C
	92	2.51-2.58	255 ± 1	219 ± 1[d]	653 ± 7	621 ± 2			v. noisy but confirms geological result
0889	94	2.51-2.58	246 ± 10	209 ± 5	476 ± 11	420 ± 8[s]	619 ± 18	572 ± 19	rises continuously from ~400°C
	97b	2.58-2.62	277 ± 8	225 ± 5	?	?			? - poor sensitivity
	98b	2.51-2.58	242 ± 3	215 ± 1	394 ± 10	349 ± 3	664 ± 7	624 ± 9	2 plateau beginning ~300 and 500°C
	99c	2.51-2.58	247 ± 1	216 ± 0	433 ± 2	380 ± 2	646 ± 6	604 ± 4	2 plateau beginning ~350 and 580°C
	101b	2.51-2.58	247 ± 6	215 ± 2	434 ± 10	381 ± 4	643 ± 2	584 ± 3	2 plateau beginning ~350 and 520°C
1614	104	2.51-2.58	243 ± 0	210 ± 1	*~666*	*~645*			confirms result: T_{max} = *671*, $T_{1/2}$ = *626*
	105	2.51-2.58	233 ± 4	202 ± 3	~635 ± 2	~592 ± 3			plateau rises ~500°C

Reference temperatures measured from: [a] first peak of TL since thermal exposure in antiquity; [b] first peak of remnant geological TL after thermal exposure in antiquity confirmed by normalisation plateau. Temperatures listed are the average of two repeats and the associated error is estimated as half the difference between the two values. Temperature parameters: [?] can not determine; [s] determined by stripping scaled laboratory TL from natural TL; [d] determined by differentiating glow curve.

the samples from this context (apart from SUTL97b for which the signal intensity was too poor) suggest that there is not only a high temperature peak, but also a lower temperature peak at a much lower plateau level.

5.4.4 Discussion

Geological TL

The $T_{1/2}$ values from the earliest context (1614) imply a variation in thermal exposure, although this may be due to the relationship between sampling position and spatial variability of temperature within the hearth. Spatial variability is the likely explanation for the large difference in $T_{1/2}$ values between the 2 samples from the latest context (0741), implying that sample SUTL92 was from the central region of the hearth and sample SUTL91b remote from the most intense source of heat. However, the possibility of the result for SUTL91b being anomalous due to sub-sampling of the hearth fragment in a lower than maximum thermal exposure region can not be ruled out.

Earlier analyses of natural TL to 500°C showed double or triple peak formations. These glow curves were measured and noted prior to this study during the TL dating program. Secondary peaks appearing at relatively low glow temperatures (from about 300°C upwards; examples included SUTL 91b, 94, 98b, 99c, 101b,) were interpreted as geological TL features, many of which were confirmed subsequent to re-dosing and read-out in the laboratory. The explanation for these features was that these hearthstones were not as well zeroed as earlier examples. The archaeological interpretation was the use of the peat-like soils present at Tofts Ness that had formed in the poorer climate of the Bronze Age, which were a much poorer source of fuel.

However, analysis to 700°C has shown further higher temperature peaks and, apart from SUTL91b which appears to have been only modestly heated, all the other samples from the intermediate context show evidence of double plateaux (although the data for SUTL94 is perhaps not as clear). The first plateau (at a lower temperature) is much lower compared with the second high temperature plateau. This suggests the samples have been heated twice

in antiquity. Dockrill (pers. comm.) made the suggestion that the samples from the hearth from context 0889 may be heated by the hearth in context 0741, which seals 0889. The results suggest this is exactly what has happened. The high temperature geological TL results indicate the original highest thermal exposure when the hearth in context 0889 was in use, whereas the lower temperature TL results indicate the thermal exposure that the same hearth has had as a result of being beneath the latest hearth structure in context 0741.

Therefore the following observations may be made for the samples from context 0889:

1) The higher temperature geological TL shows some variation which may perhaps indicate spatial variability of hearth samples.
2) The results suggest fairly similar thermal exposures to the hearths in 0741 and 1614, and this may imply that there was little variation in hearth temperatures or fuel
3) Equivalent dose estimates calculated from the temperature region before the lower temperature plateau will date the thermal exposure from the hearth of context 0741
4) Equivalent dose estimates calculated in the temperature region after the rise of the lower temperature plateau and before the rise of the high temperature plateau will date the thermal exposure of the hearth in context 0889.

The principal archaeological interpretation from the high temperature TL data is that it is likely that the same fuel (or fuels with similar burning temperatures) were used throughout the occupation of the roundhouse. Similar to investigations of Orkney ceramics discussed above, thermal exposure data from a suite of hearthstone samples from different Orkney settlement sites may reveal information about fuel availability which may support archaeological evidence of changes in climate, function of structures or changes in society. This study has been particularly useful in highlighting potential problems for TL dating.

Archaeological TL

Following on from the discussion above, since the low temperature TL from the hearth samples from context 0889 is likely to be dating thermal exposure from hearth 0741, then the archaeological $T_{1/2}$ values for these samples should be equivalent to the same values from 0741. The results suggest this may be the case, although SUTL94 and 97b appear to

be anomalous and the other values are all slightly lower. In context 1614 the results are much lower but with poor agreement. In general there is a trend of increasing $T_{1/2}$ from the earliest to the latest contexts which is contrary to the pattern shown by the Pool results.

5.5 Investigation of the fire damaged concrete lining of Store Bælt bored tunnel, Denmark

5.5.1 Introduction

The aim of this work was to provide an objective means of defining the extent of fire damage to a concrete tunnel lining. The use of TL to assess the fire damage of concrete structures was first suggested by Placido (Placido, 1980; Placido, 1981; Smith and Placido, 1980). Calibration experiments were performed to ensure accurate temperature determinations from the TL measurements. This was done using a set of reference samples taken from an unfired area of the structure, and exposed to known thermal treatments in the laboratory furnace. In addition to the observations that both temperature and duration of thermal exposure contribute to the extent of the erasure of the geological TL signal (Placido, 1980, 1981), it was also recognised that there may be a direct correlation between bulk compressive strength of heavily damaged concrete and the TL results (Smith and Placido, 1980).

To evaluate and apply the TL method to samples from the Store Bælt tunnel it was first necessary to obtain samples of unfired material which were subject to isothermal annealing and TL analysis. A small set of blind test samples was then analysed, and thereafter a set of unknown test samples taken from the tunnel were examined and compared with reference data. The temperature range of greatest interest was defined previously to be around 200°C, at which temperatures there are few petrographic indicators of fire damage, but concern that there may be potential damage to the epoxy coatings surrounding reinforcement bars.

5.5.2 Sample description

The samples were submitted by L. Fear (Mott MacDonald), and given SURRC record numbers before commencing preparation.

The concrete contains fragments of Bornholm granite, typically between about 0.1 - 1 cm^3, which contain quartz and feldspar minerals suitable for TL analysis. The reference material (Mott MacDonald Reference 14; SURRC TL 241A-241L) and blind test samples

(Reference 9,10,11; SURRC TL 242-244) were cores (Ø 6 cm, varying between 3 and 5 cm in length) removed from a region of the tunnel unaffected by the fire. The reference material was submitted with no further treatment, whereas the blind test samples were submitted after unknown annealing treatment in a furnace in Denmark.

A series of 15 unknown test samples were examined, from a larger set of samples collected in the tunnel. Samples were presented as small chips, removed by cold chisel in the tunnel, and two cores (Ø 25 mm) taken from selected positions. TL measurements were made on the core samples at several depths. Samples were numbered according to their sequence in the concrete ring sections making up the tunnel, and the SURRC reference to the individual sample from which subsampling took place in the case of cores (R11-R30; SURRC TL 245-257).

5.5.3 Preparation and analysis

5.5.3.1 Reference samples

Granite aggregates were obtained by gently breaking up the reference material using a cold chisel. Any concrete matrix adhering to the granite inclusions was removed with a scalpel to prevent possible contamination. Approximate 15 g portions of the aggregate were annealed on a temperature sensed copper plate (5 type K Cr-Al thermocouples) inside a muffle furnace for 8 hours at the following temperatures: 100, 125, 150, 175, 200, 225, 250, 300, 350, 400 and 500°C. The annealing temperature was controlled to better than ± 5°C and logged carefully. Samples were removed from the furnace and allowed to cool in air. Small pieces of aggregate (typically 0.5-2 g; the remainder placed in light tight storage in the TL laboratory) were crushed, and sieved to extract a silicate fraction from 90-125 μm. After a 30 min HCl treatment, the material was given de-ionised water and acetone washes, and allowed to dry at 50°C in the preparation laboratory oven for 10-20 mins. The material was then dispensed onto discs in duplicate samples and TL recorded to 500°C at 5°Cs^{-1}, using a 3 mm BG1 and 3 mm KG3 filtered PMT.

After measurement of the first glow curve (G1), the samples were given a 5 Gy beta dose, pre-annealed at 50°C for 30 minutes, and re-measured in a second glow (G2) to examine the shape of the complete TL curve from 100°C upwards. The ratios of the first to second glow (G1/G2) curves were plotted as a function of glow temperature. Both G1 curves and G1/G2 ratios were used to evaluate $T_{1/2}$ values for each observation. These data were used to identify the residual geological TL signals, where detectable. For samples which showed no remaining geological TL below 500°C TL analyses were repeated up to 700°C, under the same conditions, but using the UV detection window (3 mm 7-51 and a 3 mm BG39) established in Chapter 3.

5.5.3.2 Blind test samples

Aggregate chips were removed from these samples with a cold chisel in the same manner as above. They were prepared (crushing, sieving, HCl wash, dispensed onto disc) and measured in the same manner.

5.5.3.3 Unknown test samples

Once again the same preparation and analysis was performed. In some of the concrete chips submitted there were no large granite inclusions, but small ~1 mm grains were visible. In these cases the whole sample was prepared using the set procedure for granite inclusions. Additionally some of the core material was sampled into relatively thin (between 1.6 and 2.3 mm) sections using a water-cooled rock saw. Again in these instances the whole sample was prepared.

5.5.4 Results

5.5.4.1 Reference samples

Tables 5.7 and 5.8 summarise the results from reference samples measured to 500°C and 700°C respectively. All glow curves show a continuous TL response up to 500°C, with low sensitivity between 500 and 700°C. The curve shapes are consistent with those expected

Table 5.7 Results from reference material: 500°C TL runs.

SUTL number	Sample	File reference	$T_{1/2}$ (°C)	Annealing temperature (°C)
241U	14	241U0001/1	232 ± 6	0
241U	14	241U0002/2	228 ± 6	0
241U	14	241U0003/3	223 ± 6	0
241I	14	241I0001/1	232 ± 2	100 ± 4
241I	14	241I0002/2	232 ± 2	100 ± 4
241L	14	241L0001/1	239 ± 3	125 ± 4
241L	14	241L0002/2	242 ± 3	125 ± 4
241H	14	241H0001/1	269 ± 2	150 ± 4
241H	14	241H0002/2	270 ± 2	150 ± 4
241J	14	241J0001/1	283 ± 2	175 ± 4
241J	14	241J0002/2	282 ± 2	175 ± 4
241A	14	241A0001/1	310 ± 2	200 ± 4
241A	14	241A0002/2	314 ± 2	200 ± 4
241K	14	241K0001/1	343 ± 3	225 ± 4
241K	14	241K0002/2	340 ± 3	225 ± 4
241E	14	241E0001/1	363 ± 2	250 ± 4
241E	14	241E0002/2	363 ± 2	250 ± 4
241B	14	241B0001/1	423 ± 2	300 ± 4
241B	14	241B0002/2	420 ± 2	300 ± 4
241F	14	241F0001/1	482 ± 2	350 ± 4
241F	14	241F0002/2	479 ± 2	350 ± 4
241C	14	241C0001/1	> 500	400 ± 4
241C	14	241C0002/2	> 500	400 ± 4
241G	14	241G0001/1	> 500	450 ± 4
241G	14	241G0002/2	> 500	450 ± 4
241D	14	241D0001/1	> 500	500 ± 4
241D	14	241D0002/2	> 500	500 ± 4

from unseparated silicate materials, and exhibit a variation from sample to sample which is most likely due to the variations in proportions of quartz and feldspars in each test disc. Paired reproducibility is good.

It is notable that samples annealed above 350-400°C had no detectable TL in the 500°C runs. The 700°C data showed weak residual signals, from which approximate limits to $T_{1/2}$

Table 5.8 Results from calibration material: 700°C runs

SUTL number	Sample	File reference	$T_{1/2}$ (°C)	Annealing temperature (°C)
241F	14	241F0003/3	530 ± 20	350 ± 4
241F	14	241F0004/4	522 ± 5	350 ± 4
241C	14	241C0003/3	> 600	400 ± 4
241C	14	241C0004/4	> 600	400 ± 4
241G	14	241G0003/3	> 600	450 ± 4
241G	14	241G0004/4	> 600	450 ± 4
241D	14	241D0003/3	> 600	500 ± 4
241D	14	241D0003/3	> 600	500 ± 4

could be inferred. However accurate definition of $T_{1/2}$ would require either greater sensitivity than available from unseparated samples or alternatively instrumental developments to improve signal detection above background.

Despite glow shape variations the reference samples show an excellent relationship between $T_{1/2}$ values and the annealing temperature. A preliminary analysis based on observations from samples annealed at 150, 200, 250 and 300°C for 8 hours was approximated by a linear function with a correlation coefficient of 0.997. Annealing temperature, within the 150-300°C range was predicted with a precision better than ±10°C by the relation $T = 0.98 * T_{1/2} - 110$°C, where T is the annealing temperature. This relationship was used as the basis for preliminary estimates of the effective temperatures reached by the first set of test samples submitted. However, the lower temperature range showed a trend to non-linear behaviour, and preliminary estimates of effective temperature would err on the side of slightly overestimating thermal exposure for samples heated to less than 150°C.

With the full set of reference data it was possible to compensate for the non-linear behaviour. A quadratic fit to the full data set gave an improved correlation coefficient of 0.998, and annealing temperature was predicted with a precision better than ±10°C by the relation: $T = 0.0016T_{1/2}^2 + 2.02T_{1/2} - 278.6$ °C.

5.5.4.2 Blind test samples

Tables 5.9 and 5.10 summarise the results from the blind test samples measured to 500°C and 700°C respectively. Samples 10 and 11 had been heated to temperatures greater than 350°C, and showed no remaining TL below 500°C. The two repeats from sample 9 gave $T_{1/2}$ values of 406 ± 3°C and 409 ± 3°C, which correspond to *effective temperatures* (utilising the quadratic expression derived from the reference calibration) of 278 ± 10°C and 280 ± 10°C respectively for 8 hours duration. The annealing regime for sample 9 undertaken by Mott-MacDonald was in fact 6 hours exposure to approximately 300°C. Given the shorter duration of heating, and the possibility of thermal gradients in the furnace used to heat the blind samples, this was in reasonable agreement.

Table 5.9 Results from blind test material: TL runs to 500°C.

SUTL number	Sample	File reference	$T_{1/2}$ (°C)	Effective temperature (°C)
242	9	24200001/1	406 ± 3	278 ± 10
242	9	24200002/2	409 ± 3	280 ± 10
243	10	24300001/1	> 480	> 350-400
243	10	24300002/2	> 500	> 350-400
244	11	24400001/1	> 500	> 350-400
244	11	24400002/2	> 500	> 350-400

Table 5.10 Results from blind test material: TL runs to 700°C

SUTL number	Sample	File reference	$T_{1/2}$ (°C)	Effective temperature (°C)
243	10	24300003/3	> 550-600	> 350-400
243	10	24300004/4	> 550-600	> 350-400
244	11	24400003/3	> 550-600	> 350-400
244	11	24400004/4	> 550-600	> 350-400

5.5.4.3 Unknown test samples

Results from unknown test samples are shown in Table 5.11. As with the estimate for the annealing temperature of the blind test sample above, the *effective temperatures* are calculated from the quadratic expression derived from the reference material calibration. This expression is based on an 8 hour isothermal anneal. Since the real fire was likely to be

non-isothermal in character it is feasible, within limits, that the samples have been briefly heated to higher temperatures than the effective temperatures; however if this is so for the

Table 5.11 Results from unknown test samples

SUTL number	Sample	File reference	$T_{1/2}$ (°C)	Effective temperature (°C)
255	R11	25500001/1	213 ± 4	79 ± 10
255	R11	25500002/2	220 ± 4	88 ± 10
256	R12	25600001/1	216 ± 3	83 ± 10
256	R12	25600002/2	221 ± 3	89 ± 10
245A	R15 core 2.1 ± 0.2 mm	245A0001/1	309 ± 2	193 ± 10
245A	R15 core 2.1 ± 0.2 mm	245A0002/2	309 ± 2	193 ± 10
245	R15 core 0-1 cm	24500001/1	304 ± 2	188 ± 10
245	R15 core 0-1 cm	24500002/2	302 ± 2	186 ± 10
246	R15 core 4 cm	24600001/1	282 ± 2	164 ± 10
246	R15 core 4 cm	24600002/2	280 ± 2	162 ± 10
247	R15 core 19 cm	24700001/1	219 ± 2	87 ± 10
247	R15 core 19 cm	24700002/2	219 ± 2	87 ± 10
257	R16 chip	25700001/1	231 ± 2	103 ± 10
257	R16 chip	25700002/2	232 ± 2	104 ± 10
248A	R16 core 1.6 ± 0.2 mm	248A0001/1	327 ± 2	211 ± 10
248A	R16 core 1.6 ± 0.2 mm	248A0002/2	319 ± 2	203 ± 10
248	R16 core 0-1 cm	24800001/1	307 ± 4	191 ± 10
248	R16 core 0-1 cm	24800002/2	305 ± 4	189 ± 10
249	R16 core 5 cm (re-bar)	24900001/2	268 ± 2	148 ± 10
249	R16 core 5 cm (re-bar)	24900003/3	268 ± 2	148 ± 10
250	R16 core 20 cm	25000001/1	231 ± 2	103 ± 10
250	R16 core 20 cm	25000002/2	229 ± 2	100 ± 10
251	R17	25100001/2	227 ± 2	97 ± 10
251	R17	25100003/3	227 ± 2	98 ± 10
252	R20	25200001/2	238 ± 2	112 ± 10
252	R20	25200003/3	226 ± 2	96 ± 10
253	R25	25300001/2	232 ± 2	104 ± 10
253	R25	25300003/3	232 ± 2	104 ± 10
254	R30	25400001/2	212 ± 3	78 ± 10
254	R30	25400003/3	207 ± 3	71 ± 10

majority of the duration of the fire the tunnel would have been subjected to lower temperatures than those indicated in Table 5.11. In principle the calibration data set could be extended to cover other times than 8 hours, and investigate the magnitude of variation in *effective temperatures* from real samples.

The effective temperatures from rings 11, 12 and 30 are below 100°C, and are only slightly different than those corresponding to unheated materials.

Preliminary analysis of the core samples from rings 15 and 16 gave results which were lower than had been originally expected. To investigate the possibility of a strong thermal gradient additional analysis of samples from the surface 1-2 mm were undertaken. Ring 15 reached surface temperatures equivalent to 193 ± 10°C for 8 hours, the effective temperature decreasing to 187 ± 10°C between 0-1 cm, to 164°C 4 cm into the material and to 87°C at a depth of 19 cm. Ring 16 has the highest effective temperature; surface temperatures being equivalent to exposure to 205 ± 10°C for 8 hours. Averaged over the first 0-1 cm this reduced to 190°C. The re-inforcing bar at 5 cm depth reached approximately 148°C, and samples at 20 cm depth were heated to 103°C. The ring 16 chip sample, which came from a different radial section shows much lower thermal exposure; equivalent to only 104°C over 8 hours. Ring 17 appears to have been only modestly heated, as do rings between 17 and 30.

5.5.5 Discussion

This study has shown that there is a systematic relationship between the extent of thermal exposure of both reference samples and unknown test samples taken from the Store Bælt tunnel, and residual geological TL. Although the unseparated polymineral samples show a range of different TL glow shapes, which relate to mineralogical variations, there is a consistent relationship between annealing temperature and the $T_{1/2}$ values measured from the residual geological TL. This, therefore, provides a basis for assessing the extent of fire damage, which is expressed in this study in terms of the effective temperature equivalent to an 8 hour isothermal anneal. There is potential to calibrate the system to other times, therefore providing a basis for interpretation of shorter and longer thermal events.

TL analysis to 500°C provides a means of assessing 8 hour thermal exposures to temperatures of 350-400°C. The unfired material produces $T_{1/2}$ values equivalent to thermal exposures below 100°C. Within this range the effective temperature can be estimated with a precision of approximately ±10°C. TL measurements up to 700°C are possible, but give lower sensitivities and provide a qualitative indication of heat treatment up to 450°C. It may be possible to enhance performance in this region by separation of individual feldspar fractions or by further instrumental developments.

The results from the unknown test samples imply that the spatial extent and effective temperatures of fire damage to the Store Bælt tunnel are considerably less than originally expected. The samples do not appear to have been heated to an extent which is normally associated with structural damage to the concrete; the reinforcing bars have not apparently been heated to sustained temperatures to damage their coatings, and in many places the surfaces have not been heated above 100°C for extended periods. These conclusions imply that considerable savings could be made on remediation work, in comparison with original expectations.

Chapter 6: Photostimulated luminescence experiments

This chapter describes experiments performed on a PSL excitation spectrometer and an IR pulsed diode array, both described previously in Chapter 3 (Sections 3.4 and 3.5). Investigations were made of the effect of annealing on the excitation spectrum of F-1 feldspar, and pulsed annealing experiments using the same material but with stimulation from the IR diode array. Both these experiments were conducted to investigate whether PSL has potential as an indicator of thermal exposure. In addition, experiments were conducted to investigate whether PSL has a response to temperature and time of thermal exposure which is different to the temperature and time response observed from TL experiments in Chapter 4, thereby enabling resolution of temperature and time variables. As before samples of F-1 feldspar were utilised, which were given the same thermal exposure but heated with two different temperature and time schemes, and combined IR PSL and TL measurements recorded. Finally measurements were made on material from the experimental hearth (introduced in Chapter 4) to investigate PSL signals from separated feldspars and polymineral whole samples.

6.1 Annealing experiments on F-1 feldspar

6.1.1 Excitation spectroscopy: measurement protocol and sample preparation

The spectrometer was set up to scan from 450 to 950 nm with a scan speed of 120 nm min^{-1} and dwelling in each channel for 0.5 s. The monochromator was used with the 600 lines mm^{-1} (1000 nm blaze) diffraction grating. The entrance and exit slits to the monochromator were set at 4 mm, and GG-395 and GG-475 short cut filters were positioned at the entrance and exit of the monochromator respectively. Detection in the UV part of the spectrum was achieved with a 3 mm UG11 and 2 mm BG39.

The experiment proceeded in three stages:

a) 30 mg aliquots of a 90-125 μm sieve fraction of F-1 (no laboratory irradiation) were annealed for 600 s at temperatures of 100, 300, 400 and 500°C, and duplicate discs prepared. Un-annealed and blank discs were also incorporated into the experiment. The

blank discs were measured routinely through the experiment to ensure feldspar from previous runs had not contaminated the measurement chamber.

b) 2 g of F-1 was annealed in the muffle furnace for 5 mins at 600°C to remove the natural (geological) signal. The sample was given an approximate 1 kGy dose in the ^{60}Co source and then 30 mg aliquots were annealed in the muffle furnace for 600 s at 100, 200, 300, 400 and 500°C. Annealed feldspar, un-annealed feldspar and blank discs were prepared and measured as before.

c) Additional 30 mg aliquots from the 1 kGy dosed F-1 in (b) were annealed in the muffle furnace for 600 s at 320, 340, 360 and 380°C. Duplicate discs were dispensed from these aliquots and from the annealed aliquots in (b), and as before these were measured including discs of un-annealed 1 kGy F-1 and blanks. The temperature of the heater plate in the measurement chamber was carefully monitored throughout the scanning sequence. The same discs were then annealed in the muffle furnace at 500°C for 20 min, dosed to 1 kGy in the ^{60}Co source, and measured on the spectrometer. As before blank discs were run in parallel, and once again the temperature of the heater plate was carefully monitored.

6.1.2 Excitation spectroscopy: results

Figure 6.1 shows all the excitation spectra from experiment (a). The un-annealed and 100°C results show the same features as those observed by Clark (Clark, 1992; Clark and Sanderson, 1994) for spectra that have not been normalised to the xenon lamp power spectrum; namely a continuum in the *visible* region (450-650 nm) comprising a number of excitation bands and a further excitation band (or bands) in the *infra-red* region (850-900 nm) with two prominent peaks occurring as a result of superimposition of the lamp spectral lines. The low intensity features in the background signal between about 700-750 nm and 450-650 nm shown in Figure 6.1a, are an anomalous feature due to slight white light leak through the monochromator and slight sample chamber contamination respectively. The slight shifts in relative position of spectra is due to occasional software synchronisation problems between triggering the start of pass on the MCS with the start of the stepper motor.

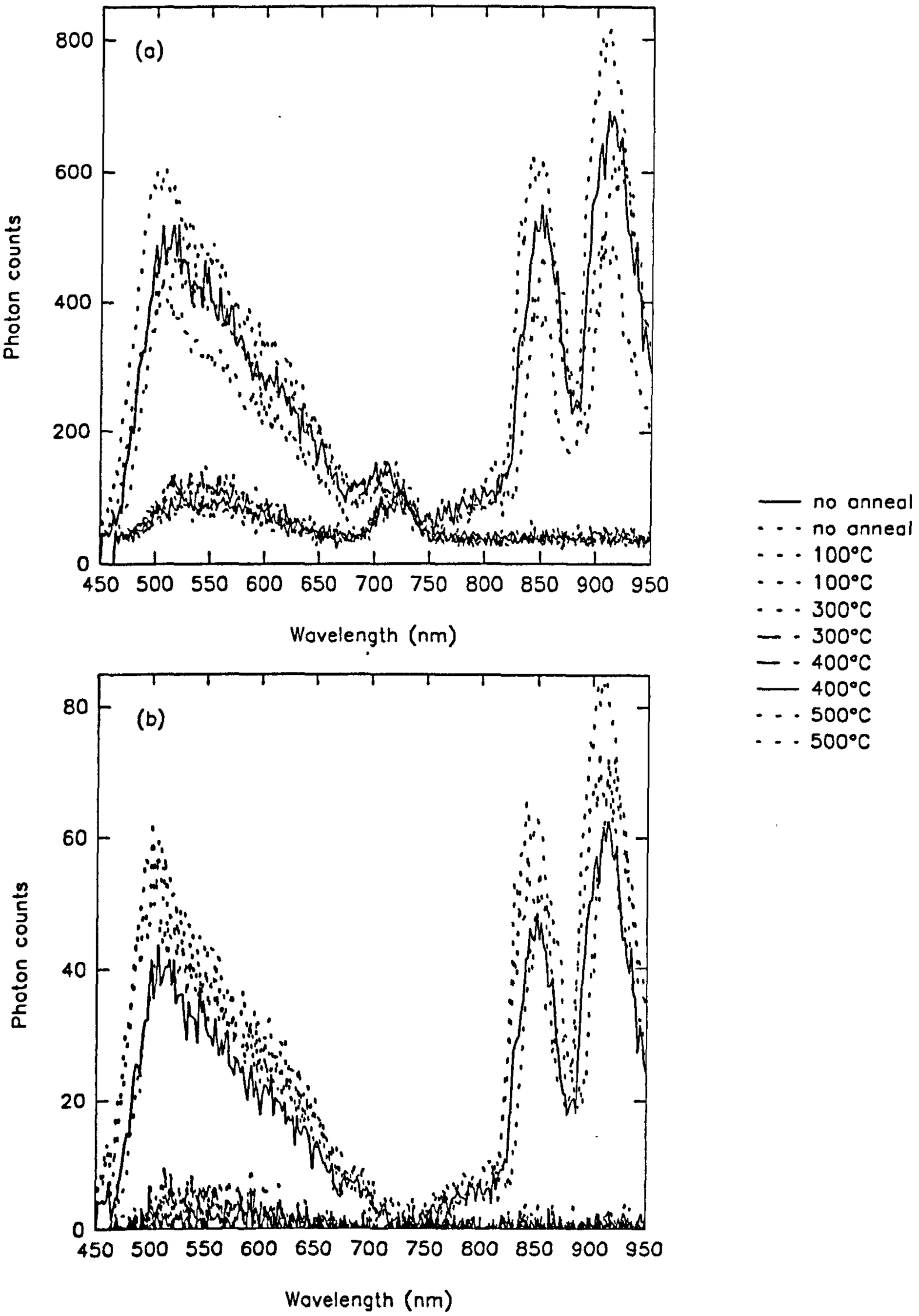

Figure 6.1 PSL excitation spectra (not power normalised) from natural (geological) F-1 feldspar subsequent to annealing for 600 s at the temperatures shown. (a) gross counts for all individual spectra including background spectrum; (b) net counts (background subtracted) mass normalised.

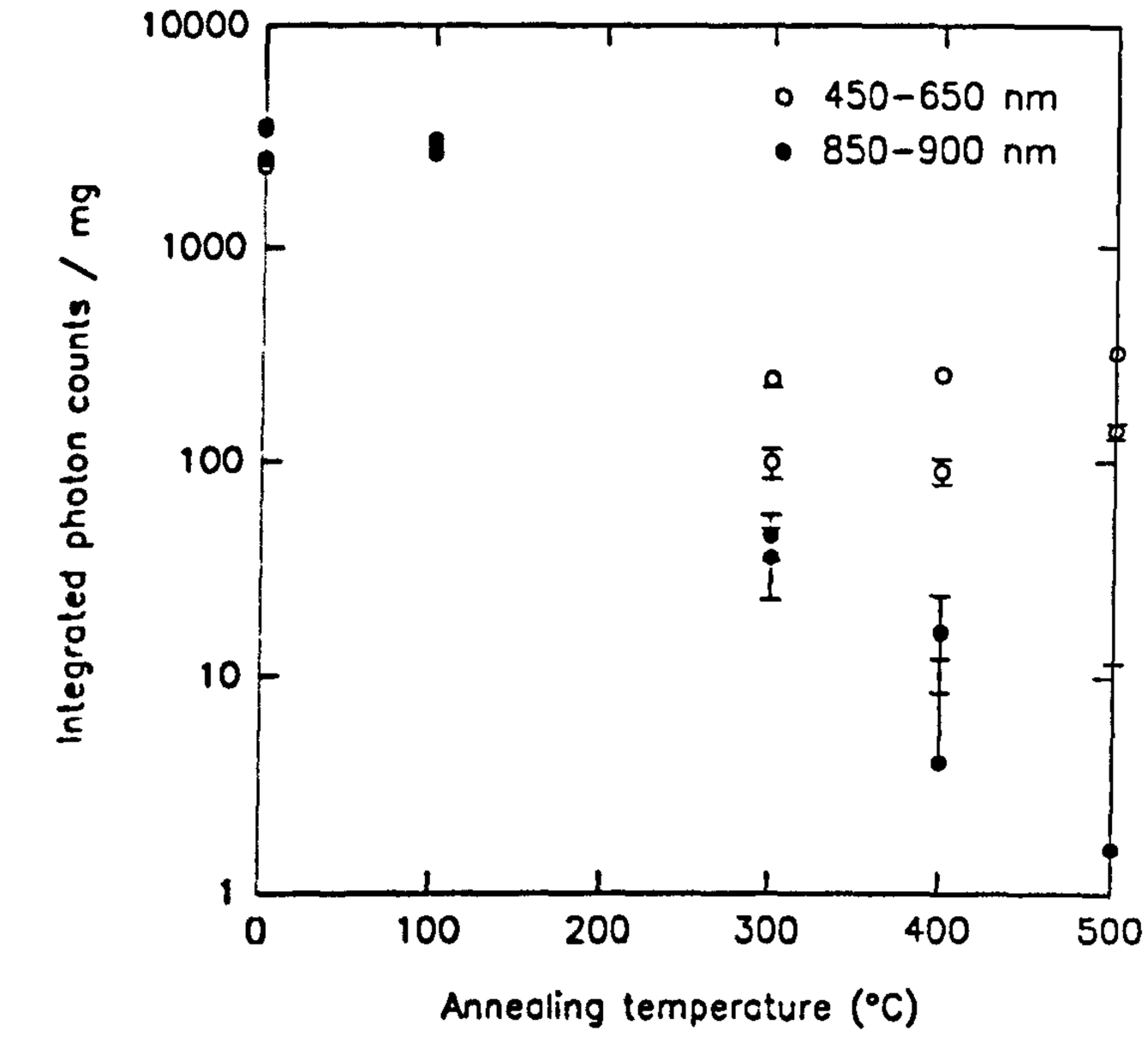

Figure 6.2 Effect of annealing for 600 s at the temperatures shown on the excitation spectrum of natural (geological) F-1 feldspar.

The results show that the signal is maintained for 100°C annealing but at 300°C and higher there is a dramatic reduction of signal strength, although there is a suggestion that the visible region is more stable with evidence of a signal surviving. This is emphasised in Figure 6.2 where a log intensity scale has been used to show the continued reduction of the infra-red signal into the background levels, whereas the visible signal appears to plateau off.

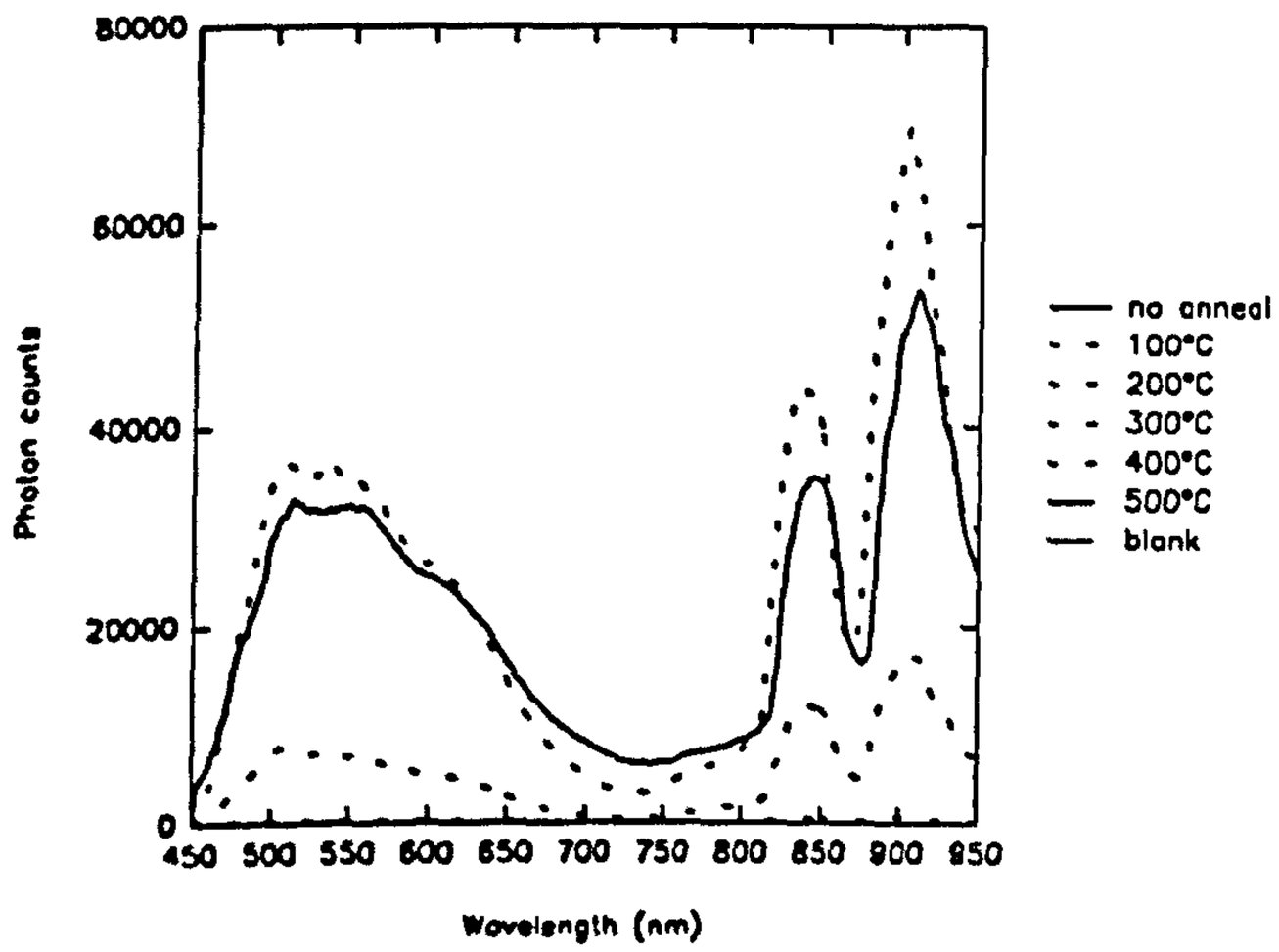

Figure 6.3 PSL excitation spectra (not power normalised) from 1 kGy dosed F-1 feldspar annealed for 600 s at the temperatures shown.

The results of experiment (b) are shown in Figure 6.3. The higher signal intensity from the laboratory dose reveals further details of the excitation spectrum in the visible region including possible excitation bands at about 500, 550 and 600 nm (as noted by Clark, 1992; Clark and Sanderson, 1994). The results of annealing show the same general pattern as in experiment (a) with two notable exceptions. Firstly, the additional data for 200°C shows an

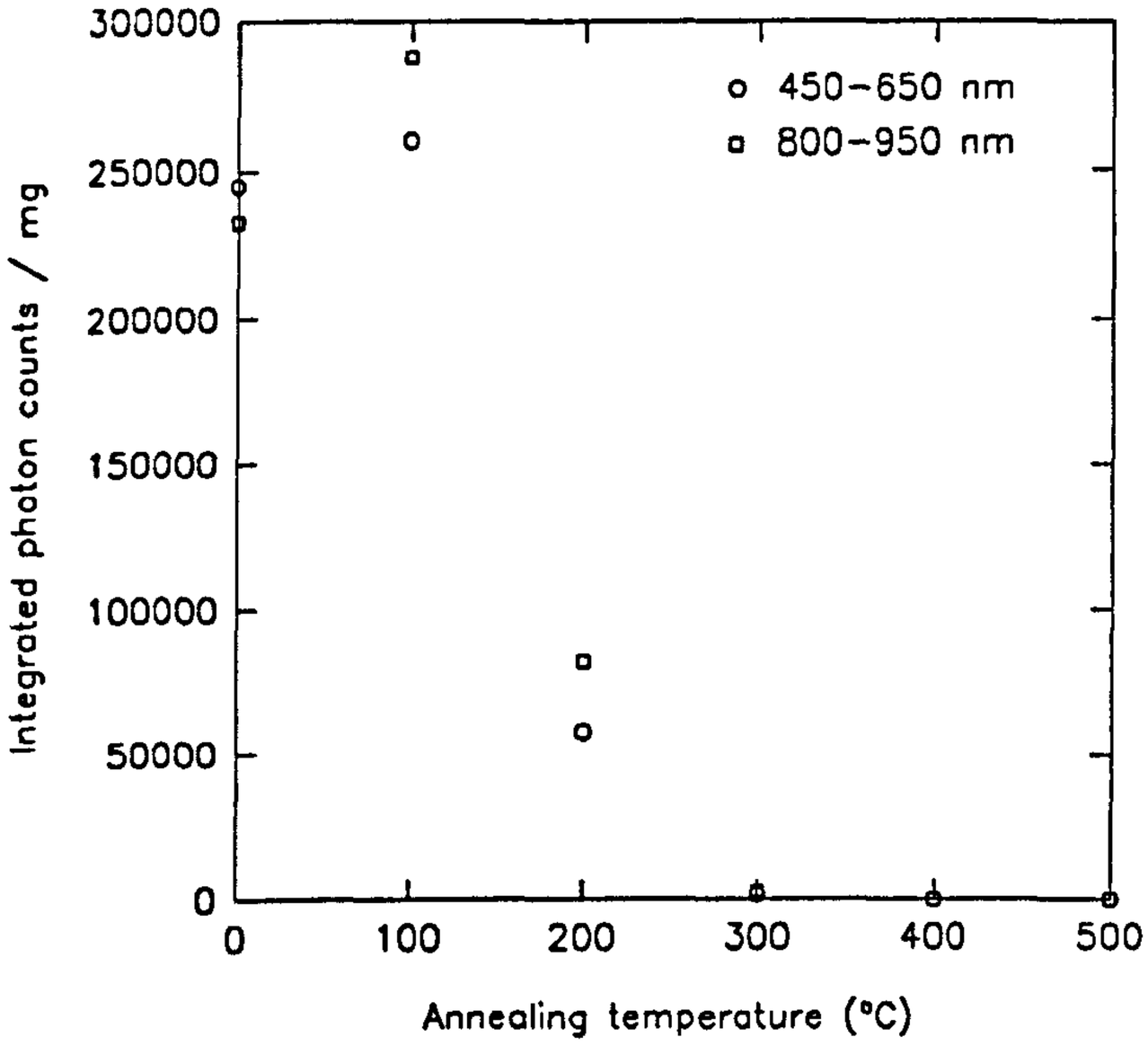

Figure 6.4 Effect of annealing for 600 s at the temperatures shown on the excitation spectrum of 1 kGy dosed F-1 feldspar.

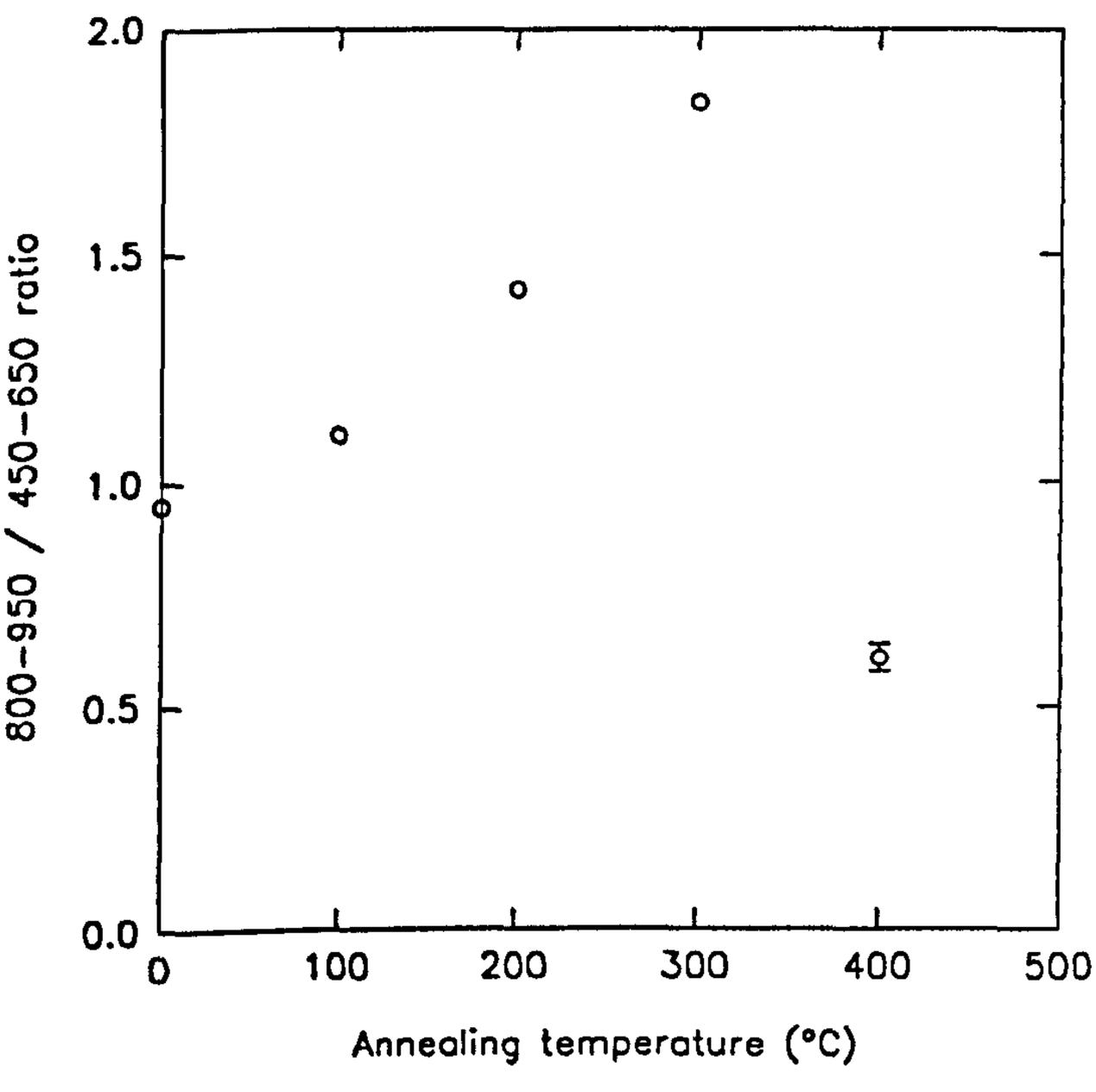

Figure 6.5 Variation in infra-red/visible ratio with annealing temperature.

intermediate reduction of signal between high intensity signals (un-annealed and 100°C data) and the low intensity signals near the background level (300, 400 and 500°C data). Secondly, there is a clear suggestion that the 100°C annealing has the effect of increasing the signal level above the un-annealed spectrum in the infra-red and visible regions, whereas between 650 to 800 nm the signal is relatively diminished.

Figure 6.4 shows the effect of increased signal after 100°C annealing more clearly with a further suggestion that the relative increase in the infra-red region is higher than in the visible. The variation of the ratio of infra-red/visible regions is shown in Figure 6.5. This shows a relative increase not only at 100°C but also increasing further due to 200 and 300°C annealing, before decreasing at 400°C.

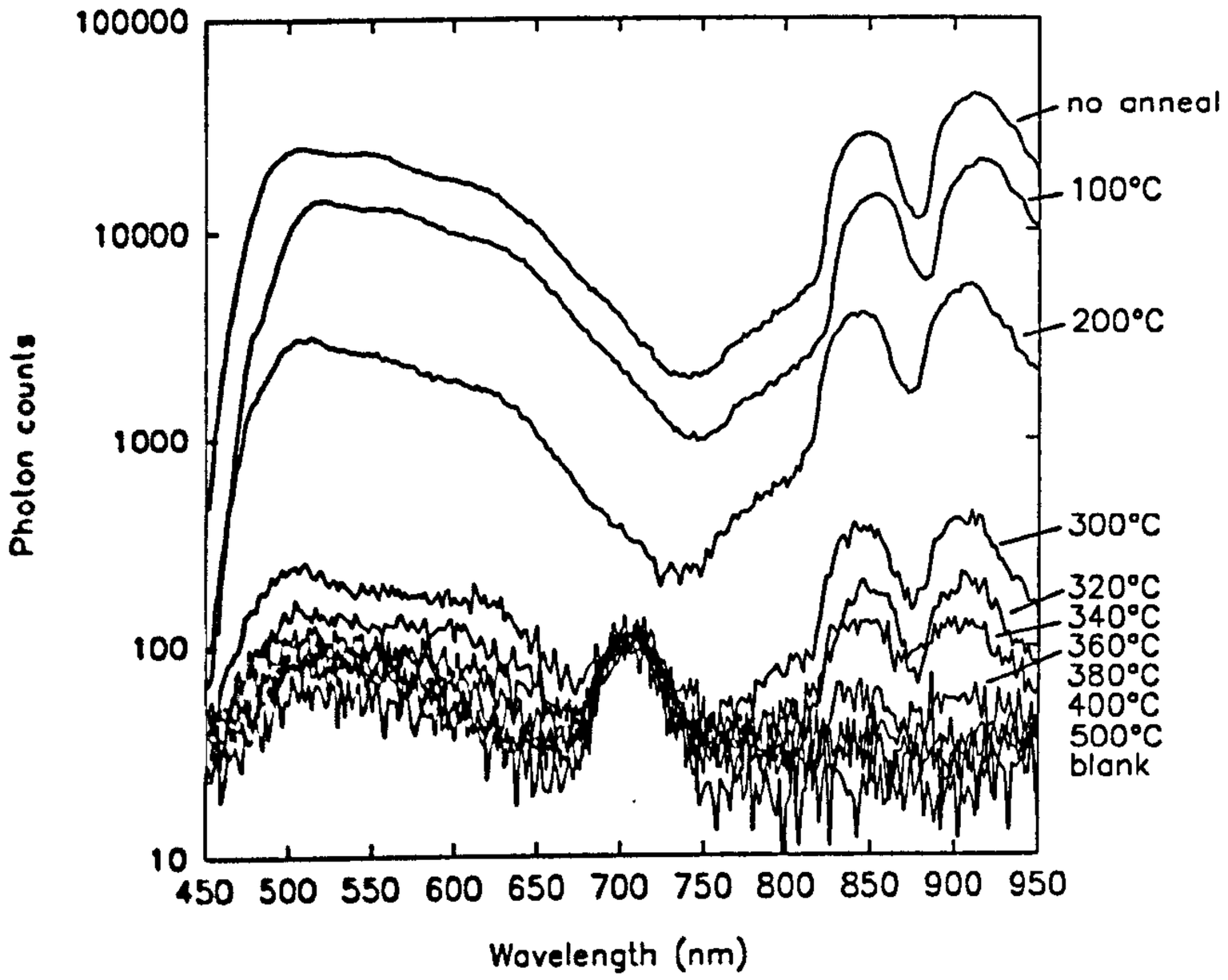

Figure 6.6 PSL excitation spectra (not power normalised) from 1 kGy dosed F-1 feldspar annealed for 600 s at the temperatures shown.

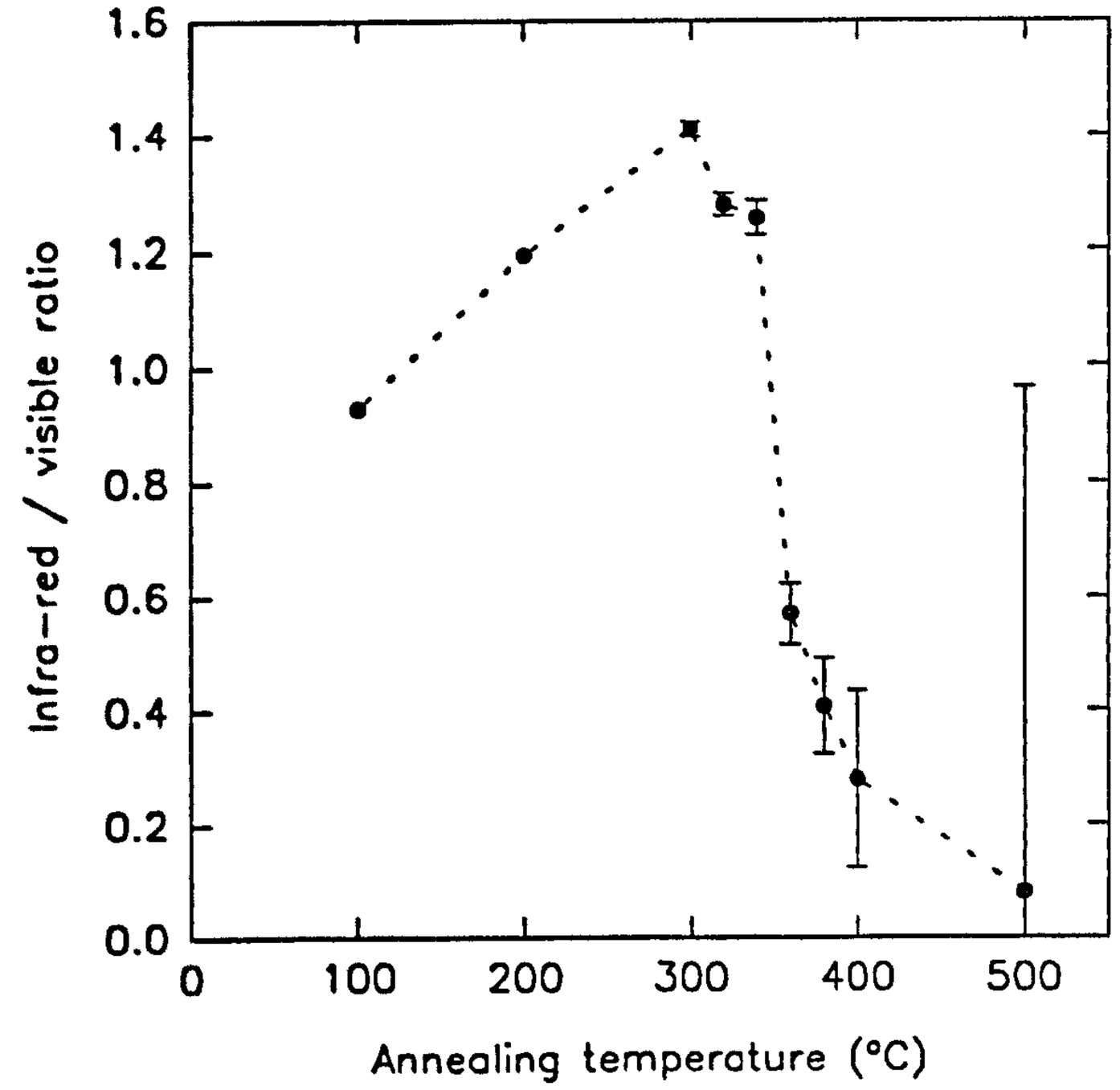

Figure 6.7 Variation in infra-red/visible ratio with annealing temperature - experiment (c).

Figure 6.6 shows excitation spectra measured in experiment (c). Aliquots annealed at 320, 340 and 360°C have observable spectra, particularly the surviving peaks in the infra-red. Thereafter the intensity of individual spectra are close to or at the background level of the system. The additional samples annealed at 320, 340, 360 and 380°C in experiment (c) show more detail of the switch from high to low infra-red/visible ratio values (Figure 6.7). Once again there is clear evidence of an increase in signal in the 100, 200 and 300°C data before the switch to low values occurs.

6.1.3 Pulsed annealing of IR PSL: software developments and experiments

The software which controls measurement and data recording for the pulsed IR diode instrumentation was altered to pursue pulsed annealing studies. The pulsed annealing code was written to proceed as follows:

1) Set annealing temperature (T_{anneal}°C) whilst holding for t_{delay} s
2) Anneal for t_{anneal} s at T_{anneal}°C
3) Cool to 0°C for t_{cool} s
4) Set $T_{measure}$°C whilst holding for 10 s
5) Measure shine curve for t_{shine} s and file it
6) T_{step} to next annealing temperature (where $T_{step} = (T_{anneal,max} - T_{anneal,min}) / n_{steps}$) and repeat.

Control samples were run in parallel but $T_{anneal,max} = T_{anneal,min} = T_{measure}$.

The instrumentation for annealing experiments was set up with a IR diode collar that slots between the oven and PMT on the TL systems. The software therefore controls not only the measurement and recording from the diode collar but also the temperature of the heater plate in the TL oven. Additional lines of code were included to read the thermocouple voltage from the heater plate so that the temperature could be automatically monitored during annealing and IR measurement cycles. Further software developments were included to enable a temperature-stepping isothermal routine to be implemented (an additional step was added in the code described above between steps (5) and (6) which repeats steps (1) to (5) for n cycles), to solve the problem of data misreads by holding the counters while

reading, and to improve heater plate temperature monitoring by averaging a number of readings from the ADC.

For pulsed annealing experiments the instrumentation was set up with a KG3 filter in the PMT and a BG39 in the diode collar. The material used for experiments was a 90-125 μm sieve fraction of geological material (ie. no pretreatments) of F-1 feldspar. Two discs were dispensed, one for pulsed annealing and the other a control. The experimental parameters were as follows:

$T_{anneal,min}$	:	100°C
$T_{anneal,max}$	:	400°C
n_{steps}	:	30 (ie. T_{step} = 10°C)
t_{delay}	:	5 s
t_{anneal}	:	30 s
t_{cool}	:	60 s
$T_{measure}$	:	40°C
t_{shine}	:	3 s (3 cycles of 1 s)

For the control run on each annealing cycle the temperature was set to $T_{measure}$ (ie. 40°C). The data for the control run was used to calculate bleach correction factors at each step.

6.1.4 Pulsed annealing of IR PSL: results

The results (Figure 6.8) show scatter but no reduction in signal before 160°C. Thereafter there is an increased response until about 230°C whereupon the curve drops rapidly until about 400°C. The results show the same increase in signal before reduction as shown by excitation spectroscopy.

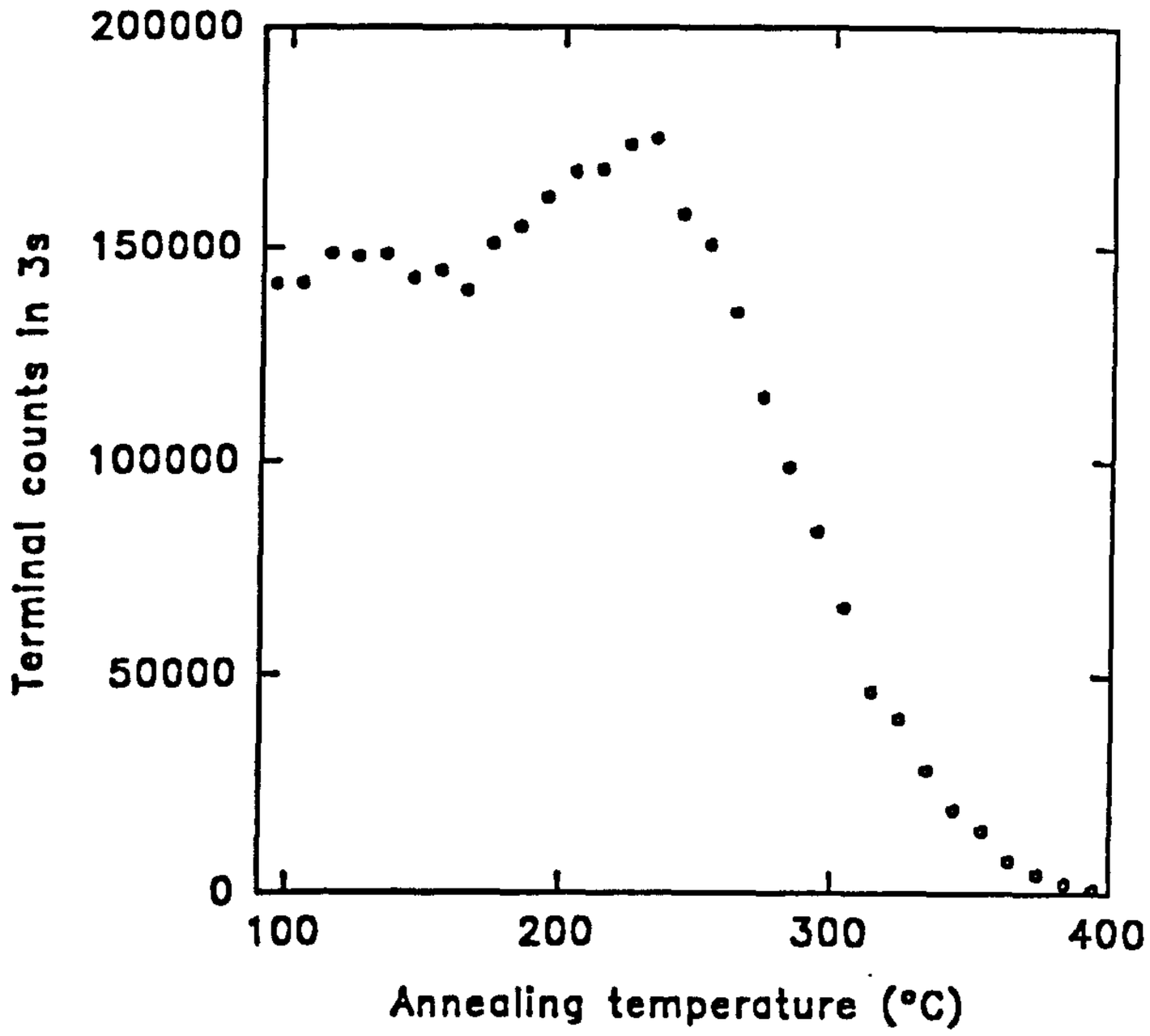

Figure 6.8 Pulsed annealing of IR PSL (bleach corrected) for a geological F-1 disc.

6.1.5 Summary and discussion

PSL excitation spectra have been measured on F-1 feldspar samples from 450-950 nm with a spectral bandpass of 37.5 nm. Measurements on geological and laboratory irradiated samples show broadly similar spectra, although the signal intensity for the 1 kGy samples is greatly enhanced and the same features as noted by Clark (Clark, 1992; Clark and Sanderson, 1994) are discernible. Ten minute annealing at 100°C suggests enhancement (particularly in the infra-red (800-590 nm) but also in the visible (450-650 nm)) in signal intensity from experiments (a) and (b), but this result is not shown in (c), where a reduction in intensity is observed as a result of 100°C annealing. Signal strength is greatly reduced by 200°C, and 300, 400 and 500°C produce signal levels close to background. Evidence from the excitation spectra and more clearly from plots of the infra-red and visible integral counts show there is a surviving component in the visible that has a higher stability than the infra-red region (again reported by Clark, 1992; Clark and Sanderson, 1994). The ratio of infra-red to visible regions shows a relative increase in the infra-red until 300°C annealing.

Further data from experiment (c) provides more detail in the drop off from high to low ratios. These results are new data demonstrating a hitherto un-observed shift in PSL excitation spectra due to thermal annealing.

The pulsed annealing results of the pulsed IR PSL of F-1 show similar behaviour to the excitation spectroscopy. In terms of $T_{1/2}$ the switch from the highest to the lowest signal level is defined by temperatures of about 282 to 464°C (using F-1 expression for TL from Chapter 4 and 30 s pulsed anneal). If one assumes that T_{max} is about 50°C higher than $T_{1/2}$, and the IR stimulated signal derives from the same luminescence trap as the TL signal, then the TL peak (or limited continua of peaks; cf. Bøtter-Jensen *et al.*, 1991; Duller, 1994; Barnett and Bailiff, 1997) responsible resides at a T_{max} of about 330°C.

A feasible explanation for the increased signal in the infra-red is the thermal transfer of charge to a trapping region which may then be stimulated by the IR wavelengths. Similar enhanced signals have been shown in pulsed annealing studies on cleaved chips (c. 1 x 1 x c.0.5 mm) from microcline samples by Bailiff and Poolton (1991) who show a rise at about 130°C (samples were subjected to rapid heating at $10°Cs^{-1}$ to the selected temperature and then cooled to RT and measured) before a reduction in signal to about 450°C. Similar experiments were performed on chips from albite, sanadine and labradorite samples. Albite showed further enhancement than microcline (from RT to about 250°C), and the sanadine and labradorite samples showed no noticeable enhancement (indeed for labradorite the signal is significantly reduced). In contrast pulsed annealing experiments conducted by Duller (1994) have shown a flat IR response (180-211 μm K-feldspar separates from a dune sand; $10°Cs^{-1}$ heating to selected temperature and 0.1 s anneal, cooled for 2 mins and IR measured for 0.1 s at 50°C) until the annealing temperature at which the loss of charge becomes very much greater, and thereafter a smooth reduction. Bøtter-Jensen *et al.* (1991) have shown a similar result to Duller from pulsed annealing experiments (100-200 μm K-feldspar separates from a Quaternary sediment; 10 s annealing, 3 s IR measurement). Recent observations by Clarke and Rendell (1997) from emission spectra from $NaAlSi_3O_8$ phases in alkali feldspars (albite CLBR, sodium feldspar standard NIST99A, perthitic orthoclase) suggest a thermally unstable peak at 290 nm which with increased temperature causes charge transfer to peaks at 380 and 550 nm giving rise to similar enhanced IR stimulated

signals. They suggest that the 290 nm emission would not be present in natural samples. However, this does not explain the rise in remnant IR signal present in the geological F-1 samples analysed here.

The switch from high to low signal level or high to low ratio is showing a feasible thermometry mechanism. The dynamics of changes in IR PSL response due to varied thermal exposure need to be explored further, particularly in the light of the rapid switch which is the result of stimulation of either a single trap or a limited trap distribution. Following on from this, the length of the transition, in terms of variation in thermal exposure, between high and low remnant IR signals is a possible indicator of the extent of trapped charge distributions.

6.2 PSL / TL complimentary behaviour

For a single first order trap kinetic theory predicts a different ratio of luminescence intensity at time t and t = 0 (ie. from Equations 2.13 and 2.18) for the same thermal exposure but differing temperature (T) and duration (t). Thus an experiment was devised to test whether 2 aliquots of F-1 given the same thermal exposure but different heating temperature and duration combinations would give the same $T_{1/2}$ results from TL but different ratios from pulsed IR results.

6.2.1 Experiment protocol

A portion of the 100 Gy F-1 stock was sieved to produce <150 μm grains and 8 discs dispensed. The first 4 discs were measured for 3 cycles of 1 s on the pulsed IR instrument (diode collar on TL system; 4 mm BG39 in PMT). Two of the discs were then placed in the TL preparation oven and annealed for 581502 s (6 d 17 h 31 min 42 s) at 100°C. From the thermal exposure expression for F-1 derived in Chapter 4 (Section 4.1.3.2, Figure 4.11) this equates to a T_{in} value of 245°C from TL. The other 2 discs were used as controls and during this period were kept at laboratory temperature in the dark. Repeat measurements were then made of the pulsed IR signals for all 4 discs (3 cycles for 1 s) and finally TL

signals were measured on the 2 annealed discs from 0-500°C at 5°Cs^{-1} (7-59 and KG1 filters) and $T_{1/2}$ values recorded.

The remaining 4 discs were treated in the same manner except the 2 discs to be annealed were heated for 19 s at 200°C in the TL measurement oven. Again, from the F-1 expression this thermal exposure equates to a $T_{1/2}$ value of 245°C.

6.2.2 Results

The results are shown in Table 6.1. Bleach corrected ratios for 100°C annealing give values of 0.787 ± 0.002 for the 1st cycle, and 0.7955 ± 0.0025 for the sum of all 3 cycles for a $T_{1/2}$ of 241 ± 0°C. The corresponding data for the 200°C anneal is 0.959 ± 0.005, 0.9555 ± 0.0105 and 238 ± 2°C. The $T_{1/2}$ values are reasonably close to the predicted value from the thermal exposure expression. The lower value from the 200°C annealing results may be due to a slight thermal lag between the heater plate in the TL oven and the sample surface, or because of the relatively short exposure necessary possible timing errors and temperature stability errors. Additionally, a more accurate value for the duration at 200°C is 19.39 s, and therefore the extra 39 hundredths of a second may be a contributing factor.

Table 6.1 Results of pulsed IR and TL measurements on F-1 samples

Disc	I_0	ΣI_0	Anneal (A/B)	I_1	ΣI_1	I_1 / I_0	$\Sigma I_0/\Sigma I_1$	Bleach corrected I_1 / I_0	Bleach corrected $\Sigma I_0/\Sigma I_1$	$T_{1/2}$ (°C)
1	297118	862378	A	208454	635758	0.702	0.737	0.789	0.798	241
2	310637	907109	A	216823	663573	0.698	0.732	0.785	0.793	241
3	343659	1010989		302160	926958	0.879	0.917			
4	349275	1041433		314511	967565	0.900	0.929			
5	305363	901619	B	264976	809087	0.868	0.897	0.954	0.945	240
6	328311	955805	B	287911	876180	0.877	0.917	0.964	0.966	236
7	304269	888115		276979	852068	0.910	0.959			
8	340612	997894		309965	938655	0.910	0.940			

Notes: I_0 is the pulsed IR intensity recorded from the first cycle. ΣI_0 is the sum of all 3 cycles. Anneal A is 581502 s at 100°C. Anneal B is 19 s at 200°C. I_1 is the pulsed IR intensity recorded from the first measurement cycle subsequent to annealing. ΣI_1 is the sum of all 3 cycles subsequent to annealing. The bleach correction was calculated by dividing the remnant intensity of the annealed samples by the average remnant intensity of the control samples.

However from the pulsed IR ratios there is a clear difference between the two thermal exposure schemes, suggesting that the two luminescence measurements are complimentary.

6.2.3 Discussion

These results demonstrate that the same thermal exposure produced by different temperature and duration of annealing produces comparable $T_{1/2}$ values from TL but different remnant intensity ratios from IR PSL. The measurable variables from fired archaeological or modern materials (assuming the thermal exposure does not remove the luminescence signals) are $T_{1/2}$ from TL and I_1 from pulsed IR PSL (I_0 is unknown). Luminescence measurements made along a core of material subject to a thermal gradient would reveal variation in $T_{1/2}$ from TL, but the same I_1 values from IR PSL may possibly be measured from samples taken from different regions. It may therefore be possible to retrieve two samples with different $T_{1/2}$ values but the same I_1.

It may be feasible to reconstruct I_0 values either by measuring only modestly heated or unburnt samples from a core, by re-irradiation, or by a pulsed annealing calibration. Using appropriate annealing calibrations it may be possible to construct a sequence of I_1/I_0 and $T_{1/2}$ relationships along a thermal gradient and discern independent temperature and time variables that equate to an average temperature (that relates to an isothermal anneal) and duration at that temperature. Where necessary heat transfer models (as discussed in Chapter 2, Sections 2.4.3 and 2.4.5) could be incorporated to translate estimated temperatures from the body of a specimen to the surface.

6.3 PSL measurements on samples from the model hearth

6.3.1 Excitation spectroscopy

Using the same spectrometer set up described in Section 6.1.1 above alkali feldspar fractions from core 2x,3y from the model hearthstone (Chapter 4; Section 4.2.3) were measured to investigate the variation in the excitation spectrum along a thermal gradient. Unfortunately all of the signals from the potassium, sodium and plagioclase fractions were

equivalent to background scans which was interpreted as a combination of insufficient power to the sample, poor sample yields or poor sample sensitivity. The same experiment was carried out with duplicated whole sample (un-sieved) polymineral discs but once again none of the samples gave results above background scans of the spectrometer.

6.3.2 Measurement of pulsed IR PSL from whole samples from the model hearth

The whole sample (un-sieved) polymineral discs prepared from core 2x,3y of the model hearth (as described above) were measured in the prototype pulsed infra-red device. The measurement procedure comprised twenty 1 s cycles. Sample discs were interleaved with measurements of the device with an empty chamber and blank discs.

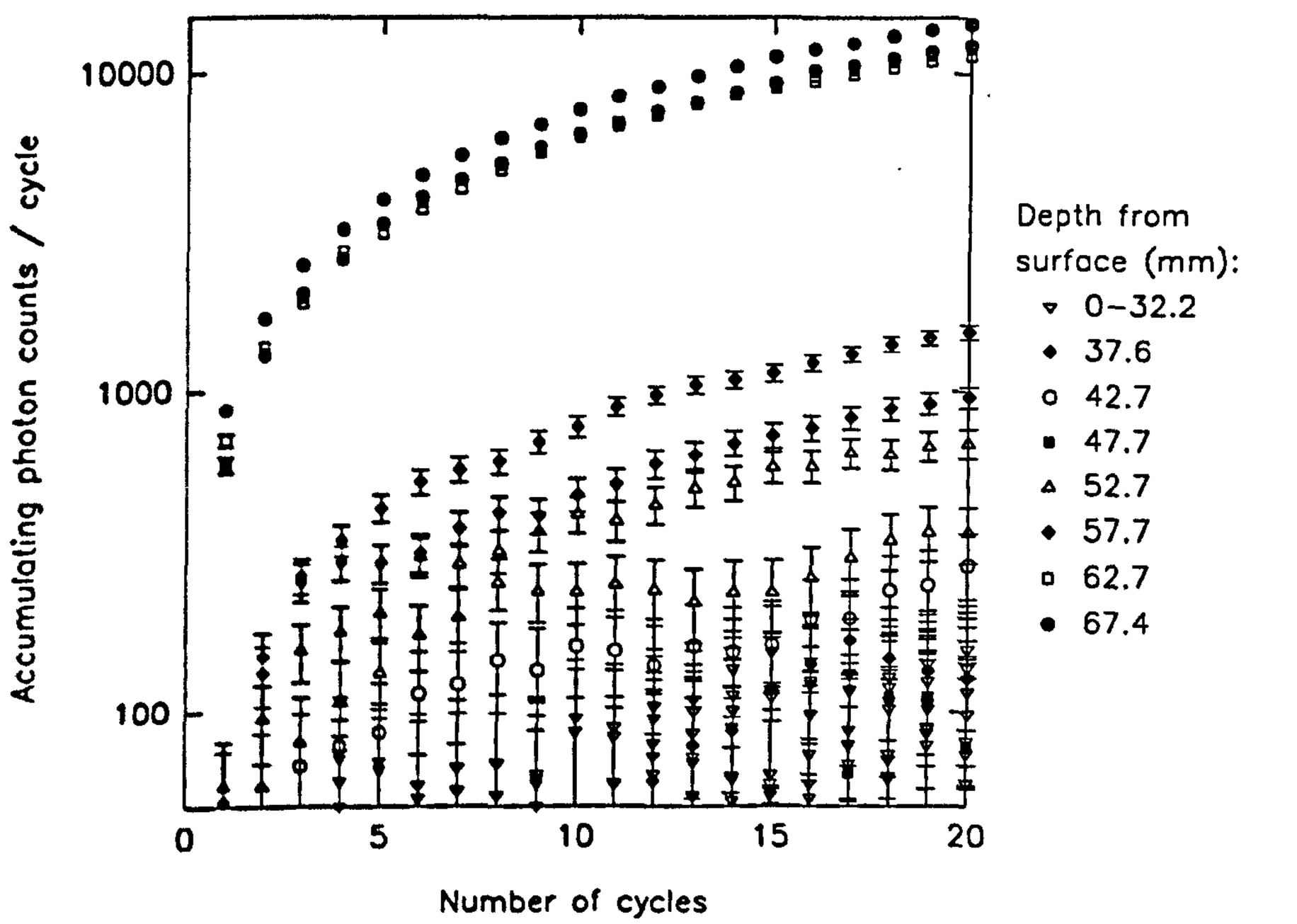

Figure 6.9 Pulsed IR PSL results of un-sieved polymineral samples from core 2x,3y with variation in core depth.

Figure 6.9 shows the cumulative counts over the measurement time. The data represent the duplicate samples run from each section of the core. From a mean depth of about 52.7 mm the signal rapidly grows. A plot of total counts over the measurement time against sample

depth (Figure 6.10) shows this signal more clearly, which is analogous to the switch seen in the excitation spectroscopy and pulsed annealing work.

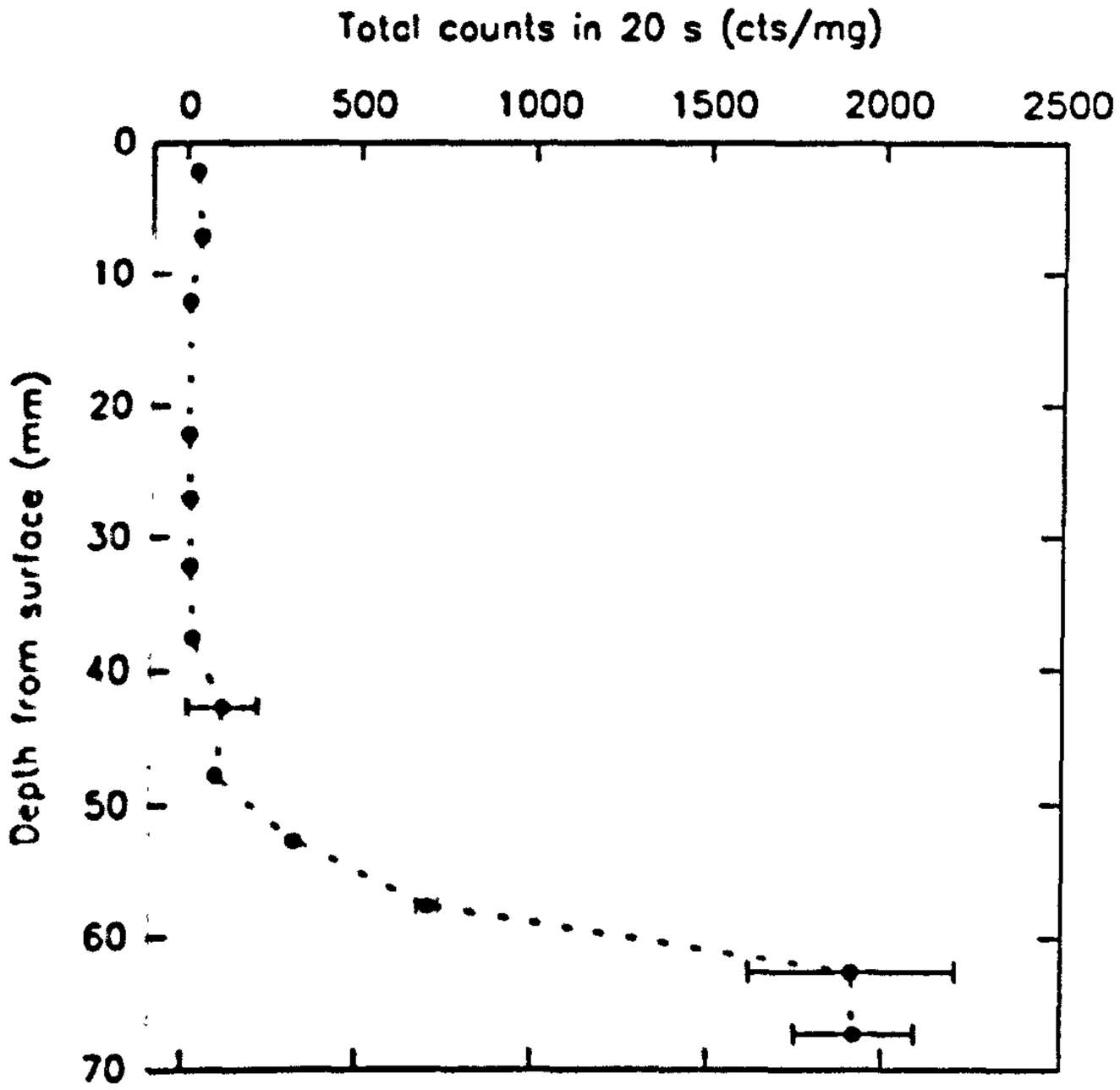

Figure 6.10 Variation in total counts of IR pulsed PSL (mass normalised) with section depth for core 2x,3y.

6.3.3 Discussion

This result shows that it is possible to recover pulsed IR stimulated signals from whole sample aliquots. PSL Excitation spectroscopy is also potentially a useful thermometry tool, although problems with low sensitivity need to be addressed. As shown by the annealing experiments above the switch from background to high signal levels occurs rapidly over a shorter range of thermal exposures than has been shown by continuous trap distributions associated with TL measurements. The results present the possibility of a thermal exposure profiling tool, and with complimentary measurements from TL (as discussed in Section 6.2) may be able to deconvolute temperature and time parameters.

Chapter 7: Discussion

7.1 Summary and discussion

The information thermometry studies may glean from archaeological or modern heated materials may be broadly characterised into the following three levels:

I A simple qualitative investigative tool to determine whether materials have been exposed to heat

II A quantitative indicator of the thermal exposure which relates to a combination of temperature and duration variables of a thermal event

III Absolute temperature and duration determination

The following discussion will consider the results from luminescence studies in this thesis in terms of the above 3 levels. Firstly level I is considered, then the approaches to investigate level III are discussed, and finally level II is considered.

Level I

Analysis of the effect of heating both separated feldspar minerals and polymineral samples (with minimum pretreatments) has demonstrated that TL signals show a progressive move to higher analysis temperature positions with increased annealing (Section 4.1). It has been shown from a consideration of first order kinetics (Section 2.2.4) and from controlled experiments on IAEA F-1 potassium feldspar (Section 4.1) that the position of the first rise of the TL of an annealed specimen is determined by both temperature and time parameters. However, the time dependence of TL is much less than the temperature dependence (Section 4.1.3.2). The combination of the progressive nature of TL removal and the results of initial rise measurements demonstrate a continuous trap distribution in feldspar systems (Sections 4.1.4 and 4.1.5). Thus, for heated lithic and ceramic specimens, which contain feldspar mineral assemblages, the removal of TL will be related to the temperature of the thermal event.

The position to which TL is removed by thermal treatment has been measured using a hitherto unused glow curve parameter (Section 4.1.2), which records the position of the annealed peak by measurement of the first rise (in terms of analysis temperature) at half the glow curve peak maximum ($T_{1/2}$). For modern specimens which have had an unknown thermal history the $T_{1/2}$ position is measured from the first rise in luminescence in the TL glow curve (eg. concrete samples in Section 5.5). For archaeological specimens of unknown thermal history the interpretation of the glow curve is slightly more complicated because the luminescence signal may be a composite curve of archaeological and geological TL (eg. Section 3.2.3). This situation occurs when thermal exposure in antiquity has removed part of the geological TL, and over the relatively short period to modern day analysis archaeological radiation history has produced an additional TL signal. In this case the correct $T_{1/2}$ position is measured from the rise of the geological TL signal. For both modern and archaeological specimens a comparison of the natural TL to an artificial TL signal induced in the laboratory is made by dividing the natural by the artificial to produce a so-called plateau. This test confirms the measured position of $T_{1/2}$ in modern and archaeological examples (archaeological examples: Sections 5.1, 5.2, 5.3 and 5.4; modern examples: Section 5.5).

The application of this method in modern materials is the comparison of $T_{1/2}$ values from the unknown specimen with a sample of the same material which is known to be un-burnt. If the unknown sample has a greater $T_{1/2}$ value than the un-burnt sample then the unknown is assumed to have been heated. Alternatively, if an un-burnt specimen is unavailable, a comparative analysis of specimens either sectioned from a core of material, or sampled across the surface under examination, could be carried out.

To determine whether archaeological specimens have been heated the analysis may be carried out on a single sample. If the $T_{1/2}$ value for the remnant geological signal is greater than the corresponding value for the archaeological signal then the sample may be assumed to be heated. For this analysis the plateau test plays an important role in identifying the presence of the remnant geological signal. The explanation for why the geological $T_{1/2}$ may be compared with the archaeological $T_{1/2}$ is because the position of the first rise of the archaeological signal is dependent upon an equilibrium between trap filling and eviction at

the storage temperature over the storage time. Thus if the specimen had not been heated the geological $T_{1/2}$ position would be at the same equilibrium position. As with a modern material analysis a more involved study could include sampling a core of material or removing specimens over a surface.

In both archaeological and modern studies analyses should be replicated to calculate statistical means and associated errors, and appropriate statistical analyses (eg. t-test) carried out. Additionally, the reproducibility of TL temperature ramp should be regularly monitored (as discussed in Chapter 3), and TL measurements made of stocks of material which give known $T_{1/2}$ values for both the minimum and maximum detection limits of the system.

The minimum detectable $T_{1/2}$ varies slightly according to the environmental temperature equilibrium position discussed above, but has an approximate value of 240°C for the archaeological and modern materials examined in this thesis (Chapter 5). The maximum detectable $T_{1/2}$ value has been shown to be about 650°C (maximum TL ramp to a reference temperature of 700°C at 5°Cs^{-1}; examples in Section 3.2.3), although later developments in electronics have extended this to about 750°C (Section 3.2.2; reference temperature of 800°C).

There is also scope for using a simple IR PSL test to determine whether material has been heated or not. According to pulsed annealing results from F-1 feldspar the minimum thermal exposure before a significant decrease in signal is observed equates to a $T_{1/2}$ value from TL of about 282°C (30 s annealing at 230°C; Section 6.1.5). A sample which displays the same annealing characteristics as F-1, and has been heated above this thermal exposure would show a decrease in the IR PSL signal compared to an un-burnt sample. However, the relationship of remnant PSL with annealing temperature is complicated due to observed charge transfer effects (Sections 6.1.4 and 6.1.5), which have also been shown to vary for different mineral types (eg. Bailiff and Poolton, 1991). Thus calibration measurements would need to be carried out (eg. sample profiling, re-irradiation or pulsed annealing, or a combination of these).

Level III

Three approaches have been examined to determine independent temperature and time values from thermally exposed materials:

i) A new multi-trap model for thermal exposure using first order kinetics has been formulated based on the relative retention of a system containing 2 metastable and 1 stable TL traps (Section 2.2.5). The minimum requirement is 3 independent TL peaks from which estimates may be made of natural and artificial (subsequent to re-irradiation) peak intensities, and E and s parameters.

ii) The results of TL and IR PSL measurements on two samples of F-1 feldspar which have had the same thermal exposure but for different temperature and duration combinations show the same $T_{1/2}$ values from TL but different remnant IR PSL values (Section 6.2).

iii) From heat transfer theory the one dimensional transient solution for a semi-infinite slab (Section 2.4.3) may possibly be utilised to determine independent temperature and time parameters by a thermal gradient analysis using TL results.

The model described in (i) is an idealised system, although potentially it may be applied to synthetic phosphors such as LiF or CaF_2. Additionally, in materials where the glow curve comprises broad features or a continuum (for eg. K-feldspars), as opposed to a number of distinct peaks, individual broad features or integrated regions may possibly be treated in the same way as individual peaks (cf. Durrani et al., 1977). It is feasible that interactive kinetic solutions (eg. Levy, 1985) may be used where simple first order conditions (and series of disconnected traps) do not apply. This model assumes that there is negligible fading (although a fading correction could be implemented), and dose accumulation after the thermal event does not affect the relative intensity of measured peaks. The temperature range of the method is limited due to less chance of a 3 peak system remaining with increased thermal exposure.

The results described in (ii) indicate that a method involving combined TL and IR PSL measurements on the same samples could de-convolute temperature and duration

parameters. However, in real samples the initial intensity I_0 of IR PSL is unknown. It may be possible to reconstruct I_0 by sample profiling down a thermal gradient, re-irradiation or a pulsed annealing calibration, or a combination of these. Pulsed annealing results (Sections 6.1.3-6.1.5) show that the temperature range of a potential IR PSL thermometer is small, although there may be a limited trap distribution (cf. Duller, 1994; Bøtter-Jensen *et al.*, 1991; Barnett and Bailiff, 1997) over which a small range of thermal exposures will operate.

Based on the assumption that the duration of the thermal exposure is the same for all sampling positions along a core of material which has been subject to a thermal gradient, it is feasible from point (iii) that $T_{1/2}$ parameters from TL may be utilised to produce simultaneous equations to solve independent temperature and time variables. To enable this study calibration measurements will need to be carried out to establish how $T_{1/2}$ relates to temperature and time for the particular mineral/material being analysed (cf. empirical relationship formulated for F-1 in Section 4.1.3.2). However, if this method works it will only provide approximate solutions to real situations.

In all the level III approaches discussed above the temperature is assumed to be isothermal. In real fires temperature is a dynamic variable (as demonstrated in Section 4.2.2) and therefore the above approaches would estimate a mean temperature figure that is less than the maximum temperature. Since temperature and time are complimentary variables, duration values would, in contrast, be over estimated.

Level II

The results relevant to level II may be summarised as follows:

i) Separated feldspar minerals and polymineral samples (with minimum pretreatments) demonstrate TL signals show a progressive move to higher analysis temperatures with increased annealing (Sections 4.1 and 4.2).

ii) A new glow curve parameter, $T_{1/2}$, may be measured to high precision (Section 4.1.2). If the T_{max} value for a glow curve peak is either obscured or not measurable, $T_{1/2}$ may still be determined by differentiation of the glow curve. Although the position of $T_{1/2}$

is not a mathematical inflection many examples of differentiated glow curves from Chapter 5 show very high reproducibility between values measured from un-differentiated and differentiated glow curves.

iii) For IAEA F-1 potassium feldspar the annealed glow curve position is characterised by a linear increase in temperature and a logarithmic increase in time (Section 4.1.3.2). A constrained linear regression analysis confirms the hypothesis that a linear-log temperature-time dependence provides a reasonable description of the behaviour. The general expression from the regression results is $T_{1/2} = 23.922 \log_{10}(t_{anneal}) + 1.071 T_{anneal}$.

iv) Kinetic simulations have shown that a continuous linear distribution of first order traps give a reasonable fit to the general expression derived from the regression analysis on the empirical results from F-1 (Section 4.1.4).

v) Values for the activation energies estimated from the glow curves from the F-1 results confirm the trap distribution (Section 4.1.5).

vi) The progressive exposure monitor demonstrated by the F-1 experiments has been shown to work for separated feldspars and polymineral samples subjected to non-isothermal exposure within an experimental hearthstone (Section 4.2).

vii) Oven and detection developments have enabled TL to be recorded to 700°C with high precision in measured $T_{1/2}$ values and temperature ramp. Latter developments in electronics have extended the temperature to 800°C (Sections 3.2.2 and 3.2.3).

viii) Empirical results from the TL system (Section 3.3.3) suggests Betts and Townsend (1993) and Piters (1993) heat transfer models (Section 2.5) are not applicable to composite sample geometries (ie. disc and mineral grains), which are the most common geometries in use in TL analyses.

Points (i), (ii), (vi) and (vii) have already been touched on in discussion of level I information. The majority of work in this thesis has concentrated on TL analyses and has demonstrated the ability to record $T_{1/2}$ values from a variety of materials from archaeological and modern contexts (Chapter 5). It has been demonstrated in Chapter 4 that $T_{1/2}$ is a quantitative indicator of thermal exposure which relates to a combination of temperature and duration variables of a thermal event.

There are two possible analysis methods; (a) absolute sample temperature analysis and (b) relative sample temperature analysis. Both these methods have been previously discussed in Section 3.3.4. In method (a) the thermal lag between the temperature of the heater plate and sample must be estimated to correct measured $T_{1/2}$ values. This is a complicated process involving heat transfer solutions, and as mentioned in point (viii) above current models for the distribution of temperature in TL analysis do not consider a composite sample geometry. The TL analyses in this thesis were conducted using method (b) which relies upon high reproducibility of TL ramp and sample geometry, and precise annealing in laboratory ovens and furnaces. An international interlaboratory comparison of temperature calibration and characterisation of TL instrumentation was recently carried out utilising the methods discussed in Chapter 4 with isothermally annealed F-1 samples (Sanderson *et al.*, 1996a).

Some of the main conclusions from analysis of material discussed in Chapter 5 from archaeological and modern contexts are summarised below:

i) Analysis of ceramics from Early and Late Neolithic contexts at Pool on Sanday, Orkney, possibly imply a change in firing technology in the Late Neolithic from the use of higher to lower thermal exposures, although the results may be a reflection of the change in climate and fuel availability at that time. Archaeological $T_{1/2}$ results confirm the stratigraphic phasing of the site and the TL dating results.

ii) Results from the study of 2 burnt stone mounds at Crawford suggest possible variation in fuel between mounds and estimates of the temperatures involved in heating the stones range from 472-551°C. Archaeological $T_{1/2}$ results suggest the 2 sites are contemporary.

iii) Geological $T_{1/2}$ results from Dunion Hill suggest the hearths have all had different thermal exposures. Variability between samples from the same hearth may either be due to sampling inconsistencies or spatial distribution of the slabs in each hearth relative to the highest thermal exposure. The variation in thermal exposure between each hearth may suggest either a variation in function or status between houses. Archaeological $T_{1/2}$ results are equivalent within error which suggests the houses are contemporary and supports the TL dating evidence.

iv) Hearthstone samples from Tofts Ness on Sanday, Orkney, also show a variation in $T_{1/2}$ values attributed to the relationship between sampling position and spatial variability of temperature over the hearth. The evidence of double plateaux suggests one of the hearths has been heated twice in antiquity which has implications for TL dating.

v) The study of fire damaged concrete from the Store Bælt bored tunnel has shown that the spatial extent and effective temperatures of fire damage are considerably less than originally expected. The samples do not appear to have been heated to an extent which is normally associated with structural damage to the concrete; the reinforcing bars have not apparently been heated to sustained temperatures to damage their coatings, and in many places the surfaces have not been heated above 100°C for extended periods. These conclusions imply that considerable savings could be made on remediation work, in comparison with original expectations.

7.2 Future work

i) High temperature TL. There is potential for TL system development to enable higher temperature analysis. The Hoya U-340 filter may be particularly efficient at blocking black body emission at high temperature. Additionally further developments such as thermal radiation masks, low emissivity materials or coatings (eg. Au, Rh, Ag) for heater plates and sample discs, reflecting cones, lenses, fibre optics and light guides may considerably improve signal to noise ratios.

ii) Kinetic models. There is scope to develop the 3 trap model in terms of trap filling and interactive kinetics. The application of this model to synthetic phosphors (or perhaps natural minerals such as quartz or feldspar) is a very interesting area to explore.

iii) Archaeological studies.

a) Possible further thermometry studies include the temperatures associated with pottery kilns, identification of the use of fire on early hominid sites and in early mines, and the identification and technical analysis of burnt flints.

b) The comparison of the Pool ceramic results with results from analyses of ceramics from other Orkadian (for example Barnhouse, Stonehall, Knap of Howar, etc.) and mainland Scotland Neolithic assemblages.

c) Higher temperature analyses. Interesting archaeological materials to analyse with a higher temperature system include crucibles, tuyeres and kilns from early metal working, and the temperatures associated with vitrified forts.

iv) Other applications:

a) Studies of meteorites

b) Temperature of formation of minerals

c) Blocking temperatures

d) It is sometimes difficult to discern whether the formation of striae on rock surfaces is due to pyroclastic flow or glacial action (Sparks, 1995, pers. comm.). A simple luminescence test could be utilised to resolve this problem.

e) Temperature of pyroclastic flows.

v) PSL. This is a very interesting area that needs more exploration particularly regarding excitation spectroscopy of annealed mineral systems with the use of a higher sensitivity set up. Another interesting area that may be explored is phototransferred thermoluminescence (PTTL).

7.3 Conclusion

The measurement of T_{ln}, defined in this thesis as thermal exposure, by TL analysis is an extremely powerful technique, enabling very precise (± 1 or 2°C) results which are intrinsically related to the dynamic temperature and time evolution of real non-isothermal fires. The range of T_{ln} measurement is about 240-750°C which is higher than any previous luminescence thermometry method and the majority of non-luminescence methods. The analysis range may possibly be increased by further instrumental development. The results of the F-1 annealing experiment demonstrate a very acceptable error on estimated absolute temperature (assuming a range of exposure times) compared to other methods. Results from F-1 feldspar, the experimental hearth, archaeological material and concrete samples show the method is applicable to a range of materials and separated feldspar minerals and polymineral samples. The technique is relatively inexpensive to carry out in established luminescence laboratories, and is rapid to perform particularly with the use of automated systems.

Bibliography

Adirovitch, E. I. (1956) La formule de Becquerel et la loi élémentaire du déclin de la luminescence des phosphores cristallins. *Le Journal de Physique et le Radium*, 17, 705-707.

Aitken, M. J. (1974) *Physics and Archaeology*, 2nd edition. Oxford University Press.

Aitken, M. J. (1985) *Thermoluminescence dating*. Academic Press, London.

Aitken, M. J. (1992) Optical dating. *Quat. Sci. Rev.* 11, 127-131.

Aitken, M. J. (1994) Optical dating: A non-specialist review. *Quat. Geochron. (Quat. Sci. Rev.)* 13, 503-508.

Aitken, M. J., Fleming, S. J., Reid, J. and Tite, M. S. (1968a) Elimination of spurious thermoluminescence. *Thermoluminescence of geological materials* (ed. D. J. McDougall), Academic Press, London, 133-142.

Aitken, M. J. and Thompson, J. (1968) Determination of heat penetration in archaeological remains. *Thermoluminescence of geological materials* (ed. D. J. McDougall), Academic Press, London, 413-417.

Aitken, M. J., Tite, M. S. and Reid, J. (1964) Thermoluminescent dating of ancient ceramics. *Nature* 202, 1032-1033.

Aitken, M. J., Zimmerman, D. W. and Fleming, S. J. (1968b) Thermoluminescent dating of ancient pottery. *Nature* 219, 442-444.

Bailiff, I. K. (1976) Use of phototransfer for the anomalous fading of thermoluminescence. *Nature* 264, 531-533.

Bailiff, I. K. and Poolton, N. R. J. (1991) Studies of charge transfer mechanisms in feldspars. *Nucl. Tracks Radiat Meas.* 18, No. 1/2, pp. 111-118.

Bailiff, I. K. and Younger, E. J. (1988) Computer-controlled TL apparatus. *Nucl. Tracks Radiat. Meas.* 14, 171-176.

Banks, I. (1996) The excavation of two burnt stone mounds at Crawford, Strathclyde. *Glasgow Archaeological Journal*, in press.

Barber, J. (1990) Scottish burnt mounts: variations on a theme. *Burnt Offerings: International Contributions to Burnt Mound Archaeology* (ed. V. M. Buckley). Wordwell Ltd., Dublin, 98-104.

Barfield, L. and Hodder, M. (1987) Burnt mounds as saunas, and the prehistory of bathing. *Antiquity* 61, 370-379.

Barnett, S. M. and Bailiff, I. K. (1997) Infrared stimulation spectra of sediments containing feldspars. *Radiat. Meas.* (in press).

Becker, K. (1974) On the discovery of TL. *Health Physics* 27, 321-322.

Betts, D. S., Couturier, L., Khayrat, A. H., Luff, B. J. and Townsend, P. D. (1993) Temperature distribution in thermoluminescence experiments. I: experimental results. *J. Phys. D: Appl. Phys.* 26, 843-848.

Betts, D. S. and Townsend, P. D. (1993) Temperature distribution in thermoluminescence experiments. II: some calculational models. *J. Phys. D: Appl. Phys.* 26, 849-857.

Bonfiglioli, G., Brovetto, P. and Cortese, C. (1959) Thermoluminescence and F-centers. II. Experimental. *Phys. Rev.* 114 (4), 956-960.

Bonfiglioli, G. (1968) Criteria for the design of thermoluminescence apparatus. *Thermoluminescence of geological materials* (ed. D. J. McDougall), Academic Press, London, 169-174.

Bøtter-Jensen, L. (1988) The automated Risø TL dating reader system. *Nucl. Tracks Radiat. Meas.* 14, 177-180.

Bøtter-Jensen, L. and Bungaard, J. (1978) An automated reader for TL dating. *PACT J.* 2, 48-56.

Bøtter-Jensen, L. Ditlefsen, C. and Mejdahl, V. (1991) Combined OSL (infrared) and TL studies of feldspars. Nucl. Tracks Radiat. Meas. 18, No. 1/2, 257-263.

Bowman, S. G. E. (1979) Phototransferred thermoluminescence in quartz and its potential use in dating. *PACT J.* 3, 381-400.

Boyle, R. (1664) Experiments and considerations upon colours with observations on a diamond that shines in the dark. Henry Herringham, London.

Braünlich, P., Kelly, P. and Fillard, J. P. (1979) Thermally stimulated luminescence and conductivity. *Thermally Stimulated Relaxation in Solids* (ed. P. Braünlich). Springer-Verlag.

Brindley, A. L. and Lanting J. N. (1990) The dating of fulachta fiadh. *Burnt Offerings: International Contributions to Burnt Mound Archaeology* (ed. V. M. Buckley). Wordwell Ltd., Dublin, 55-56.

Brou, R. and Valladas, G. (1975) Appareil pour la mesure de la thermoluminescence de petits échantillons. *Nucl. Instrum. Methods* 127, 109-113.

Buckley, V. M. (1990) Experiments using a reconstructed fulacht with a variety of rock types: implications for the petromorphology of fulachta fiadh. *Burnt Offerings: International Contributions to Burnt Mound Archaeology* (ed. V. M. Buckley). Wordwell Ltd., Dublin, 170-172.

Burch, W. M. (1967) Thermoluminescence, low radiation dosage and black-body radiation. *Phys. Med. Biol.*, 12, 523-530.

Carslaw, H. S. and Jaeger, J. C. (1959) *Conduction of heat in solids*, 2nd edition, Clarendon, Oxford.

Caseldine, C. J. and Whittingdon, G. (1976) Pollen analysis of material from the Stones of Stenness, Orkney. In: The Stones of Stenness, Orkney (J. N. G. Ritchie), *Proc. Soc. Antiq. Scot.*, 107, 37-40.

Chen, R. and Kirsh, Y. (1981) *Analysis of thermally stimulated processes*. Pergamon, London.

Clark, R. J. (1992) Photostimulated luminescence as an archaeological dating tool. Unpubl. Ph. D. thesis, University of Glasgow, Glasgow, U.K.

Clark, R. J. and Sanderson, D. C. W. (1994) Photostimulated luminescence excitation spectroscopy of feldspars and micas. *Radiat. Meas.* 23, Nos 2/3, 641-646.

Clarke, M. L. and Rendell, H. M. (1997) Infra-red stimulated luminescence spectra of alkali feldspars. *Radiat. Meas.* (in press).

Christodoulides, C., Ettinger, K. V. and Fremlin, J. H.(1971) The use of TL glow peaks at equilibrium in the examination of the thermal and radiation history of materials. *Modern Geology* 2, 275-280.

Daniels, F., Boyd, C. A. and Saunders, D. F. (1953) Thermoluminescence as a research tool. *Science* 117, 343-349.

Davidson, D. A. and Jones, R. L. (1993) The environment of Orkney. *The Prehistory of Orkney* (ed. A. C. Renfrew), 3rd Edition, Edinburgh University Press, 10-35.

Dockrill, S. J. (1988) *Excavations at Tofts Ness, Sanday - Interim 1987*. Department of Archaeological Sciences, University of Bradford.

Dort, W. Jnr., Zeller, E. J., Turner, M. D. and Vaz, J. E. (1965) Paleotemperatures and chronology at archaeological cave site revealed by thermoluminescence. *Science*, 150, 480-481.

Duller, G. A. T. (1994) A new method for the analysis of infrared stimulated luminescence data from potassium feldspars. *Radiat. Meas.* 23, Nos 2/3, 281-285.

Durrani, S. A., Khazal, K. A. R. and Ali, A. (1977) Temperature and duration of the shadow of a recently-arrived lunar boulder. *Nature* 266, 411-415.

El-Kolaly, M. A., Rao, S. M. D., Nambi, K. S. V. and Ganguly, A. K. (1980) Observations on a high temperature peak in the thermoluminescence of fluorites. *Pramana*, 14, 2, 165-173.

Fleming, S. J. (1979) *Thermoluminescence Techniques in Archaeology*. Oxford University Press, New York.

Galloway, R. B. (1990) Notes on a recently constructed TL system. *Ancient TL* 8, 10-11.

Galloway, R. B. (1991) A versatile 40-sample system for TL and OSL investigations. *Nucl. Tracks Radiat. Meas.* 18, 265-271.

Ganguly, S. and Kaul, I. K. (1984) Analysis of thermoluminescence glow peaks from natural calcium fluoride. *Modern Geology* 8, 155-161.

Garlick, G. F. J. and Gibson, A. F. (1948) The electron trap mechanism of luminescence in sulphide and silicate phosphors. *Proc. Phys. Soc.* 60, 574-590.

Garlick, G. F. J. and Robinson, I. (1972) The thermoluminescence of lunar samples. *The Moon* (ed.s S. K. Runcorn and H. Urey). International Astronomers Union, Dordrecht. 324-329.

Göksu, H. Y., Fremlin, J. H., Irwin, H. T. and Fryxell, R. (1974) Age determination of burned flint by a thermoluminescent method. *Science* 183, 651-654.

Göksu, H. Y., Weiser, A. and Regulla, D. F. (1989) 110°C TL peak records the ancient heat treatment of flint. *Ancient TL*, 7, No. 1, 15-17.

Gotlib, V. I., Kantorovich, L. N., Grebenshicov, V. L., Bichev, V. R. and Nemiro, E. A. (1984) The study of thermoluminescence using the contact method of sample heating. *J. Phys. D: Appl. Phys.*, 17, 2097-2114.

Grenet, J., Vautier, C., Carles, D. and Chabrier, J. J. (1973) *Phil. Mag.* 28, 1265-

Grigull, U. and Sandner H. (1984) *Heat Conduction.* International Series in Heat and Mass Transfer. Springer, Berlin.

Grögler, N., Houtermans, F. G. and Stauffer, H. (1960) Ueber die daiterung von keramik und ziegel durch thermolumineszenz. *Helv. Phys. Acta.* 33, 595-596.

Guérin, G. and Valladas, G. (1980) Thermoluminescence dating of volcanic plagioclases. *Nature* 286, 697-699.

Halperin, A. and Braner, A. A. (1960) Evaluation of thermal activation energies from glow curves. *Phys. Rev.* 117, 408.

Hedges, J. W. (1975) Excavation of two Orkadian burnt mounds at Liddle and Beaquoy. *Proc. Soc. Antiq. Scot.* 106, 39-98.

Helfrich, W., Riehl, N. and Thoma, P. (1964) *Phys. Letts.* 10, 31-

Henzinger, R. C., Vana, N. and Kubelik, M. (1993) Development of the fully automated thermoluminescence read out system HVK and its application in dosimetry and archaeometry. Abstract for a poster presented at the 7th International Specialist Seminar on TL and ESR dating, Krems, Austria, 5-9 July 1993.

Hodder, M. A. (1990) Burnt mounds in the English West Midlands. *Burnt Offerings: International Contributions to Burnt Mound Archaeology* (ed. V. M. Buckley). Wordwell Ltd., Dublin, 106-111.

Horowitz, P. and Hill, W. (1990) *The Art of Electronics*, 2nd edition, Cambridge University Press.

Horowitz, Y. S. (1984) *Thermoluminescence and Thermoluminescent Dosimetry Volumes I, II & III*, CRC Press, Florida.

Horowitz, Y. S. and Yossain, D. (1995) *Computerised glow curve deconvolution: application to thermoluminescence dosimetry* (Radiation Protection Dosimetry, 60, No.1). Nuclear Technology Publishing.

Hunter, J. R., Bond, J. M., Dockrill, S. J. and Smith, A. N. (forthcoming) *Archaeological investigations in Sanday, Orkney.* Edinburgh: Society of Antiquaries of Scotland. Monograph series.

Hunter, J. R. and Dockrill, S. J. (1990) Recent research into burnt mounds on Fair Isle, Shetland, and Sanday, Orkney. *Burnt Offerings: International Contributions to Burnt Mound Archaeology* (ed. V. M. Buckley). Wordwell Ltd., Dublin, 62-68.

Hunter, J. R. and MacSween, A. (1991) A sequence for the Orcadian Neolithic? *Antiquity* 65, 911-914.

Huntley, D. J., Godfrey-Smith, D. I. and Thewalt, M. L. W. (1985) Optical dating of sediments. *Nature* 313, 105-107.

Hurl, D. (1990) An anthropologist's tale. *Burnt Offerings: International Contributions to Burnt Mound Archaeology* (ed. V. M. Buckley). Wordwell Ltd., Dublin, 154-155.

Huxtable, J., Aitken, M. J., Hedges, J. W. and Renfrew, A. C. (1976) Dating a settlement pattern by thermoluminescence: the burnt mounds of Orkney. *Archaeometry* 18, 1, 5-17.

Ichikawa, Y. (1965) Dating of ancient ceramics by thermoluminescence. *Bulletin of the Institute of Chemical Research, Kyoto University* 43, 1-6.

Incropera, F. and De Witt, D. (1990) *Fundamentals of Heat and Mass Transfer.* 3rd edition. John Wiley, Canada.

Ingersoll, L. R., Zobel, O. J. and Ingersoll, A. C. (1954) *Heat Conduction with Engineering, Geological and Other Applications.* University of Wisconsin Press.

Johnson, N. M., (1966) Geothermometry from the thermoluminescence of contact-metamorphosed limestone. *Journal of Geology*, 74, 607-619.

Kaye, G. W. C. and Laby, T. H. (1986) *Tables of Physical and Chemical Constants.* Longman, UK.

Keatinge, T. H. and Dickson, J. H. (1979) Mid-Flandrian changes in vegetation on Mainland Orkney, *New Phytol.* 82, 585-612

Kelly, R. S. (1990) Recent work in north-west Wales: the excavation of a burnt mound at Graeanog, Clynnog, Gwynedd, in 1983. *Burnt Offerings: International Contributions to Burnt Mound Archaeology* (ed. V. M. Buckley). Wordwell Ltd., Dublin, 117-128.

Kennedy, G. C. and Knopff, L. (1960) Dating by thermoluminescence. *Archaeology* 13, 147-148.

Kingery, W. D. and Gourdin, W. H. (1976) Examination of furnace linings from Rothenburg site #590 in Wadi Zaghra. *Journal of Field Archaeology*, 3, 351-353.

Kitis, G., Tsakiri, M. and Charalambous, St. (1989) Thermoluminescence dating activities by the TL-group of Thessaloniki University. *PACT* 15, 117-124.

Kreith, F. (1965) *Principles of heat transfer*, 2nd edition, International Textbook Company.

Levy, P. W. (1979) Thermoluminescence studies having applications to geology and archaeometry. *PACT* 3, 466-480.

Levy, P. W. (1985) Thermoluminescence kinetics in materials exposed to the low doses applicable to dating and dosimetry. *Nucl. Tracks Radiat. Meas.*, 10, Nos 4-6, 547-556.

Lovering, T. G. (1958) Temperatures and depth of formation of sulfide ore deposits at Gilman, Colorado. *Economic Geology*, 53, 689-707.

MacSween, A. (1990) The Neolithic and Late Iron Age pottery from Pool, Sanday, Orkney. Unpublished Ph. D. thesis, University of Bradford.

MacSween, A. (1992) Orcadian grooved ware. In: *Vessels for the Ancestors. Essays on the Neolithic of Britain and Ireland in honour of Audrey Henshall* (Sharples, N. and Sheridan, A. (eds)), 261-271.

McKeever, S. W. S. (1984) *Thermoluminescence materials* (Radiation Protection Dosimetry, 8, No.s 1-2). Nuclear technology publishing.

McKeever, S. W. S. (1985) *Thermoluminescence of solids.* Cambridge University Press.

McKeever, S. W. S., Moscovitch, M. and Townsend, P. D. (1995) *Thermoluminescence dosimetry materials: properties and uses.* Nuclear Technology Publishing.

Mahesh, K., Weng, P. S. and Furetta, C. (1989) *Thermoluminescence in solids and its applications.* Nuclear Technology Publishing

May, C. E. and Partridge, J. A. (1964) *J. Chem. Phys.*, 40, 1401-

Mazess, R. B. and Zimmerman, D. W. (1966) Pottery dating from thermoluminescence. *Science* 152, 347-348.

Mejdahl, V. (1969) Thermoluminescence dating of ancient Danish ceramics. *Archaeometry* 11, 99-104.

Mejdahl, V. (1983) Feldspar inclusion dating of ceramics and burnt stones. *PACT* 9, 351-364.

Mejdahl, V. and Winther-Nielsen, M. (1982) TL dating based on feldspar inclusions. *PACT* 6, 426-437.

Morozov, G. V. (1968) The relative dating of Quaternary Ukrainian sediments by the thermoluminescence method. *8th International Quaternary Association Congress*, Paris, p.167. U. S. Geological Survey Library, Washington, D. C., Cat. No. 208M8280.

Nash, A. E., Attix, F. H. and Schulman, J. H. (1965) Spurious thermoluminescence of CaF_2:Mn and LiF(TLD-100). *Proc. Int. Conf. Lumin. Dosim.* (Stanford), 244-256.

NSA (1845) *New statistical account of Scotland, vol. XV, Sutherland, Caithness, Orkney, Shetland-general index.* Edinburgh and London.

Owen, G. P. and Charlesby, A. (1974) *J. Phys. C: Sol. St. Phys.*, 7, L400.

Piters, T. M. (1993) A study into the mechanism of thermoluminescence in a LiF:Mg,Ti dosimetry material. PhD Thesis, Delft University of Technology.

Placido, F. (1980) Thermoluminescence test for fire-damaged concrete. *Mag. Concrete Res.* 32, No. 111, 112-116.

Placido, F. (1981) Thermoluminescence: a way of testing fire-damaged concrete. *FIRE*, 464-465.

Ralph, E. K. and Han, M. C. (1966) Dating of pottery by thermoluminescence. *Nature* 210, 245-247.

Randall, J. T. and Wilkins, M. H. F. (1945a) Phosphorescence and electron traps I. The study of trap distributions. *Proc. Roy. Soc. Lond.*, A 184, 367-389.

Randall, J. T. and Wilkins, M. H. F. (1945b) Phosphorescence and electron traps II. The interpretation of long-period phosphorescence. *Proc. Roy. Soc. Lond.*, A 184, 390-407.

Rice, P. M. (1987) *Pottery Analysis: A source book.* University of Chicago Press.

Rideout, J. S. (1992) The Dunion, Roxburgh, Borders. *Hillforts of Southern Scotland* (eds J. S. Rideout, O. A. Owen, E. Halpin). AOC (Scotland) Ltd., Edinburgh, 73-119.

Romberg, G. P. and Prepejchal, W. (1977) Thermoluminescent dosimeters (TLD's) used to monitor temperature exposure. *5th International Conference on Luminescence Dosimetry, Sao Paulo, Brazil 14-17 February 1977*, 387-392.

Ronca, L. B. (1964) Minimum length of time of frigid conditions in Antarctica as determined by thermoluminescence. *American Journal of Science*, 262, 767-781.

Sanderson, D. C. W. (1982) The thermoluminescence of archaeological glass. Unpubl. M. Phil. thesis, University of Bradford, Bradford, U.K.

Sanderson, D. C. W. (1983) A microcomputer for control and processing in a TL dating system. *Proceedings of the 22nd Symposium on Archaeometry*, University of Bradford, Bradford, U.K., 150-157.

Sanderson, D. C. W. (1990) Luminescence detection of irradiated foods, in *Food Irradiation and the Chemist* (ed. D. E. Johnston and M. H. Stevenson), Royal Society of Chemistry, 25-56.

Sanderson, D. C. W. (1991) Photostimulated luminescence (PSL): a new approach to identifying irradiated food. *Potential new methods of detection of irradiated food* (ed. J. Raffi), European Commission, Report EUR 13331 EN.

Sanderson, D. C. W. (1992) Thermoluminescence dates (specialist report for The Dunion, Roxburgh, Borders - J. S. Rideout) *Hillforts of Southern Scotland* (eds J. S. Rideout, O. A. Owen, E. Halpin). AOC (Scotland) Ltd., Edinburgh, 106-108 and Appendix 20 (pp. 156-157).

Sanderson, D. C. W., Placido, F. and Tate, J. O. (1985) Scottish vitrified forts: background and potential for TL dating. *Nucl. Tracks Radiat. Meas.* 10, Nos 4-6, 799-809.

Sanderson, D. C. W., Placido, F. and Tate, J.O. (1988) Scottish vitrified forts: TL results from six study sites. *Nucl. Tracks Radiat. Meas.* 14, 307-316.

Sanderson, D. C. W., Slater, C. and Cairns, K. J. (1989) Detection of irradiated food, *Nature* 340, 23-24.

Sanderson, D. C. W., Carmichael, L. A., Clark, P. A. and Clark, R. J. (1990) Development of luminescence tests to identify irradiated food. Final Report: Maff project N1701. Scottish Universities Research and Reactor Centre.

Sanderson, D. C. W., Carmichael, L. A., Ni Riain, S., Naylor, J. and Spencer, J. Q. (1994) Luminescence studies to identify irradiated food, *Food Science and Technology Today*, 8 (2), 93-96.

Sanderson, D. C. W., Carmichael, L. A. and Naylor, J. D. (1996a) Establishing luminescence detection methods for irradiated fruits, vegetables and shellfish. *Scottish Universities Research and Reactor Centre, Third Report 1B073.*

Sanderson, D. C. W., Carmichael, L. A. and Naylor, J. D. (1996b) Recent advances in thermoluminescence and photostimulated luminescence detection methods for irradiated foods. *Royal Society of Chemistry*, in press.

Schulman, J. H., Attix, F. H., West, E. J. and Ginther, R. J. (1960) *Rev. Sci. Instrum.*, 31, 1263-

Sheppard, P. J., Pavlish, L. A. and Hancock, R. G. V. (1983) The use of thermoluminescence (TL) in an investigation of heat treatment in the Epipalaeolithic of North Africa. *Proceedings of the 22nd Symposium on Archaeometry*, University of Bradford, Bradford, U.K., 145-149.

Smith, L. and Placido, F. (1980) Thermoluminescence: a comparison with the residual strength of various concretes. *Proceedings of the American Concrete Institution Convention, San Juan, Puerto Rico.*

Spanne, P. (1984) TL readout instrumentation. In *Thermoluminescence and Thermoluminescent Dosimetry Volume III* (ed. Y. S. Horowitz), 2-47, CRC Press Florida.

Spencer, J. Q. (1989) Heat transfer within hearthstones: implications for TL dating. Scottish Universities Research and Reactor Centre, East Kilbride. Internal Report.

Stevenson, J. B. (1980) Tofts Ness: Fieldwork July 1980. *RCAHMS 1980*, 33.

Strickertsson, K. (1985) The thermoluminescence of potassium feldspars. *Nucl. Tracks Radiat. Meas.* 10, Nos 4-6, 613-617.

Sunta, C. M. (1979) Mechanism of phototransfer of thermoluminescence peaks in natural CaF_2. *Phys. Stat. Sol.* (a)53, 127-135.

Sunta, C. M. and David, M. (1982) Firing temperature of pottery from pre-dose sensitization of TL. *PACT* 6, 460-467.

Sutton, S. R. and Zimmerman, D. W. (1976) Thermoluminescence dating using zircon grains from archaeological ceramics. *Archaeometry* 18, 2, 125-134.

Sutton, S. R. and Zimmerman, D. W. (1977) Hints on spurious reduction. *Ancient TL* 1, 7.

Templer, R. H. (1986) A high performance TL disc. *Ancient TL*, 4, 9.

Templer, R. H. and Smith, B. W. (1988) Auto-regenerative TL dating with zircon inclusions from fired materials. *Nucl. Tracks Radiat. Meas.* 14, 329-332.

THORN EMI (1986) *Photomultipliers.* A general catalogue published by THORN EMI Electron Tubes Ltd.

Tite, M. S. (1966) Thermoluminescent dating of ancient ceramics: A reassessment. *Archaeometry* 9, 155-169.

Tite, M. S., Hughes, M. J., Freestone, I. C., Meeks, N. D., and Bimson, M., (1990) Technological characterisation of refractory ceramics from Timna. *The Ancient Metallurgy of Copper (Researches in Arabah 1959-1984 Vol. 2)* (Rothenburg, B. ed.), 158-175, Institute for Archaeo-Metallurgical Studies, London.

Tite, M. S. and Maniatis, Y. (1975) Examination of ancient pottery using the scanning electron microscope. *Nature* 257, 122-3.

Tite, M. S., Maniatis, Y., Meeks, N. D., Bimson, M., Hughes, M. J. and Leppard, S. C. (1982) Technological studies of ancient ceramics. *Early Pyrotechnology* (Wertime, T. A. and Wertime, S. F., eds.), 61-71, Smithsonian Institution Press, Washington.

Tite, M. S. and Waine, J. (1962) Thermoluminescent dating: a re-appraisal. *Archaeometry* 5, 53-79.

Touloukian, Y. S. and De Witt, D. P. (1970) Thermal radiative properties; metallic elements and alloys. *Thermophysical Properties of Matter*, vol 7. Plenum Press, New York.

Touloukian, Y. S., Judd, W. R. and Roy, R. F. (1981) *Physical Properties of Rocks and Minerals*, McGraw-Hill, New York.

Trowbridge, J. and Burbank, J.E. (1898) Phosphorescence produced by electrification. *Am. J. Sci.*, Ser. 4, 5, 55-56.

Urbach, F. (1930). *Wiener Ber.*, 139, 363.

Valladas, G., Gillot P. Y., and Guérin, G. (1979) Dating Plagioclase ? *PACT J.* 3, 251-257.

Valladas, G. and Valladas, H. (1978) High temperature thermoluminescence. In *18th Inter. Symp. Archaeometry Archaeol. Prospecti.*, 506-510.

Valladas, H. (1980) Investigation of thermoluminescence of burnt sandstones from prehistoric sites. *Nucl. Instrum. Methods* 175, 230-232.

Vana, N., Erlach, R., Fugger, M., Gratzl, W., and Reichhalter, I. (1988) A computerised TL read out system for dating and phototransfer measurements. *Nucl. Tracks Radiat. Meas.* 14, 181-184.

Vaz, J. E. (1983) The effect of insolation on the thermoluminescence response of an archaeological stone sculpture. *PACT* 9, II, 335-342.

Visocekas, R. (1978) La luminescence de la cacite après iradiation cathodique: TL et luminescence par effect tunnel. Thèse, Université Pierre et Marie Curie, Paris 6.

Visocekas, R. (1979) Miscellaneous aspects of artificial TL of calcite: emission spectra, athermal detrapping and anomalous fading. *PACT J.* 3, 258-265.

Visocekas, R., Ceva, T., Marti, C., Lefaucheux, F., and Robert M. C. (1976) Tunnelling processes in afterglow of calcite. *Physica Status Solidi* A 35, 315-327.

White, F. M. (1984) *Heat transfer.* Addison-Wesley

Wiedemann, E. and Schmidt, G.C. (1895) *Ann. Phys. Chem. Neue Folge*, 54, 604.

Williams, G. H. (1990) Burnt mounds in South-West Wales. *Burnt Offerings: International Contributions to Burnt Mound Archaeology* (ed. V. M. Buckley). Wordwell Ltd., Dublin, 129-140.

Wintle, A. G. (1973) Anomalous fading of thermoluminescence in mineral samples. *Nature* 245, 143-144.

Wintle, A. G. (1975) Thermal quenching of thermoluminescence in quartz. *Geophysical Journal of the Royal Astronomical Society* 41, 107-113.

Wintle, A. G. (1993) Recent developments in the optical dating of sediments. *Radiation Protection and Dosimetry*, 47, 627-635.

Wintle, A. G. (1977) Detailed study of a thermoluminescent mineral exhibiting anomalous fading. *Journal of Luminescence* 15, 385-393.

Wintle, A. G. and Huntley, D. J. (1979) Thermoluminescence dating of a deep sea core. *Nature* 279, 710-712.

Wintle, A. G. and Huntley, D. J. (1980) Thermoluminescence dating of ocean sediments. *Can. J. Earth Sci.* 17, 348-360.

Wintle, A. G. and Huntley, D. J. (1982) Thermoluminescence dating of sediments. *Quat. Sci. Rev.* 1, 31-53.

Zeller, A. N. (1968) The influence of microclimate upon the thermoluminescence of rock. *Thermoluminescence of geological materials* (ed. D. J. McDougall), Academic Press, London, 507-518.

Appendix A: Published Articles

Pergamon

Radiation Measurements, Vol. 23, Nos 2/3, pp. 465–468, 1994

1350-4487/94 $7.00 + .00

1350-4487(94)E0025-U

MAPPING THERMAL EXPOSURE BY LUMINESCENCE THERMOMETRY

JOEL Q. SPENCER and DAVID C. W. SANDERSON
Scottish Universities Research and Reactor Centre, East Kilbride, Glasgow G75 0QU, U.K.

Abstract—It has been shown in previous studies that residual geological thermoluminescence (TL) signals can be used to assess fire damage and thermal exposure, both of which are of some interest in archaeological contexts. Detailed studies of the removal of TL from pure alkali feldspars have shown systematic relations between measured glow curve parameters and the temperatures and durations of isothermal annealing. However, in most archaeological cases, the temperature–time profile is variable and unknown. To examine the relationship between TL characteristics and thermal history under more realistic conditions, a model hearthstone was constructed containing a three-dimensional matrix of 64 thermocouples and the spatial variations in temperature monitored during the course of two experimental fires. Cores were removed from the stone at 18 locations where direct thermocouple correlations could be made, and at a further two locations, to interpolate the radial temperature distribution. Each core was sectioned and samples extracted for TL and PSL analysis, thus providing a representative set of samples which had been exposed to different maximum temperatures and a dynamic thermal exposure. TL measurements were made from room temperature to 700°C using a UV-filtered reader, and PSL measurements were made using a high sensitivity infrared pulsed diode array. The TL results, parametrized in terms of the position of the residual geological signal, are compared with thermocouple data integrated with respect to time over the course of the known thermal exposure, taking account of the empirical form of the complementary temperature–time relationships deduced from studies of pure minerals. This provides a means of quantifying thermal exposure for a generalized thermal event, which can be directly related to measured luminescence indicators.

1. INTRODUCTION

TRACING the path of exploitation of fire in the past, its use, control and the ability to achieve increasingly higher temperatures is extremely useful to archaeologists, particularly for revealing information on the development and technological advancement of prehistoric societies. The prevalence of fired ceramics on archaeological sites stresses the importance of fire in the past, which is made evident by the number of methods established to estimate firing temperatures (Rice, 1987). However, doubts have been raised by Gosselain (1992) concerning the use of estimates of maximum or initial firing temperature for studies of ceramic technology. His observations of ethnographic and ceramic experimental firings have shown both a large overlap of thermometric data for different types of firing structures, and considerable variations in temperature in the same firing and on the same pot. He concludes by suggesting that only information concerning heating rate and time of exposure may permit technological inferences.

As previous studies have shown, residual geological thermoluminescence (TL) signals can be used to assess fire damage and thermal exposure (e.g. Placido, 1980; Aitken and Thompson, 1968; Spencer and Sanderson, 1991, 1992; Valladas, 1980). A luminescence approach is perhaps more relevant for thermometric analysis as it can reveal information concerning the overall thermal exposure in terms of the temperature and duration. This information coupled with estimates of maximum temperature is a very powerful technique in studies of ancient fire-technology. Lithic materials may also be studied using this technique to investigate, for example, the use of fire concerned with extraction and processing in early mines, fires in domestic environments (e.g. hearthstones, pot boilers, burnt flint), and smelting and smithing technologies.

This paper describes an investigation into the relationship between TL characteristics and thermal history by analysing material with a known thermal exposure from a model hearthstone.

2. HEARTHSTONE SIMULATION AND SAMPLING

A simulated archaeological hearth was constructed to accurately map the progression of heat in three dimensions from experimental fires. A large sandstone slab from Stromness on mainland Orkney was cut into a uniform cuboid shape (approximately

40 × 40 × 7 cm) with the use of industrial water-cooled rock saws. Sixteen sets of four holes were drilled into the stone in a 4 × 4 grid (Fig. 1) with a milling machine. The depths of the four holes were 15, 30, 45 and 60 mm for each set producing four distinct layers within the stone. Sixty-four type K (chromel–alumel) thermocouples were cemented into the holes and the stone inverted for firing experiments. Thus, from the upper surface, the four temperature sensing layers were at depths of 10, 25, 40 and 55 mm. A 64-way thermocouple amplifier–multiplexer interface was constructed to log the temperature–time characteristics of two experimental fires and associated cooling curves by computer. For a detailed account of the hearth construction, interface design, experimental fires and thermocouple data, consult Spencer (1989).

Cores were removed from the stone using an 11 mm internal diameter water-cooled diamond tipped coring drill. Eighteen cores were removed in total; 16 from the 4 × 4 grid positions, between the four thermocouples at each position, and at a further two locations to interpolate the radial temperature distribution. Each core was cut into 14 5 mm long sections using a water-cooled diamond impregnated rock saw. Sections corresponding to the thermocouple positions were selected, providing a representative set of samples which had been exposed to different maximum temperatures and a dynamic thermal exposure.

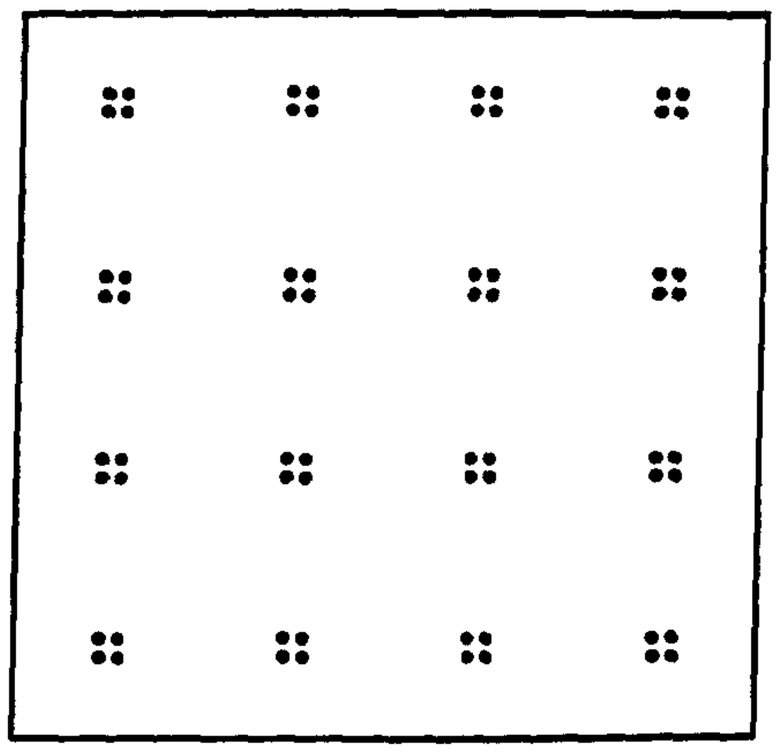

FIG. 1. Position of holes in the stone for thermocouples.

3. SAMPLE PREPARATION AND LUMINESCENCE MEASUREMENTS

Comparison of TL results from initial experiments showed little variation between whole sample and alkali feldspar mineral separates, and therefore a polymineral or whole sample analysis was adopted. Each section was crushed with a pestle and mortar, and sieved through a coarse 150 μm mesh. The sieved fractions (<150 μm) were treated with 10% HCl for 30 min, washed in acetone and dried at 50°C for 30 min before dispensing onto stainless steel discs.

TL measurements were made from room temperature to 700°C at 5°C s^{-1} using a UV-filtered photomultiplier tube (Corning 7-51 and Schott BG39) in a similar manner to Valladas and co-workers (Valladas and Valladas, 1978; Valladas *et al.*, 1979). The samples were then irradiated with a 200 Gy ^{60}Co dose, and annealed in a muffle furnace (set to 200°C) on a copper plate before performing normalization TL measurements. The annealing temperature was monitored by five Cr–Al thermocouples bolted to the plate. The plate reached a maximum temperature of 195°C in 29 min and was then removed from the furnace.

Infrared stimulated luminescence (IRSL) measurements, made using a high sensitivity pulsed diode array (9 880Δ80 nm 20 mW LEDs, filtered with a 780 nm long-pass filter and Schott BG39 detection window), have been recorded on the same material incorporating optical and thermal normalization routines, the results of which will be discussed elsewhere.

4. THERMOCOUPLE DATA AND TL RESULTS

Figure 2 shows thermocouple data for the experimental fires ((a): peat; (b): wood) from two distinct

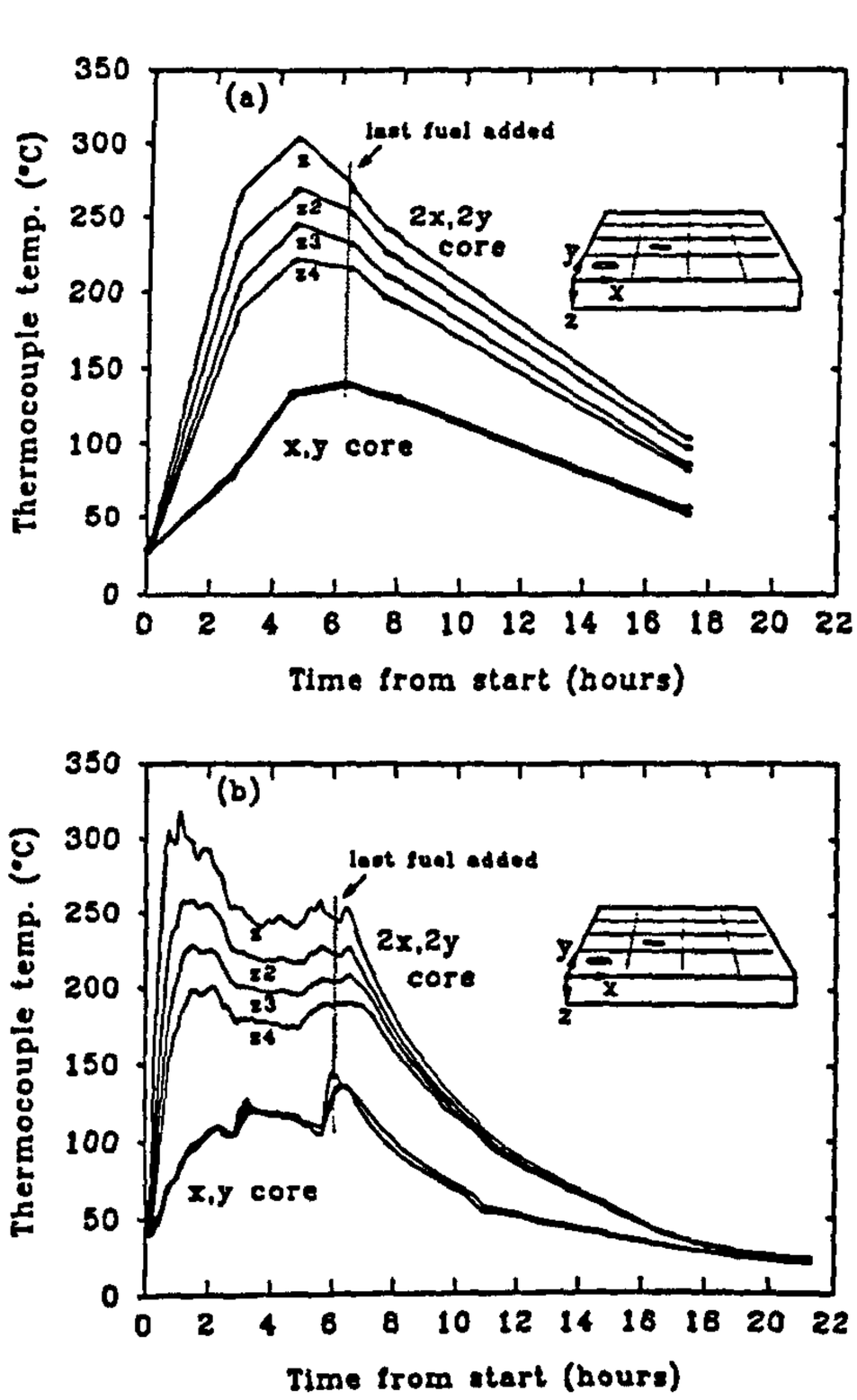

FIG. 2. Examples of thermocouple data for the experimental fires: (a) peat and (b) wood; z = 10 mm, $z2$ = 25 mm, $z3$ = 40 mm, $z4$ = 55 mm.

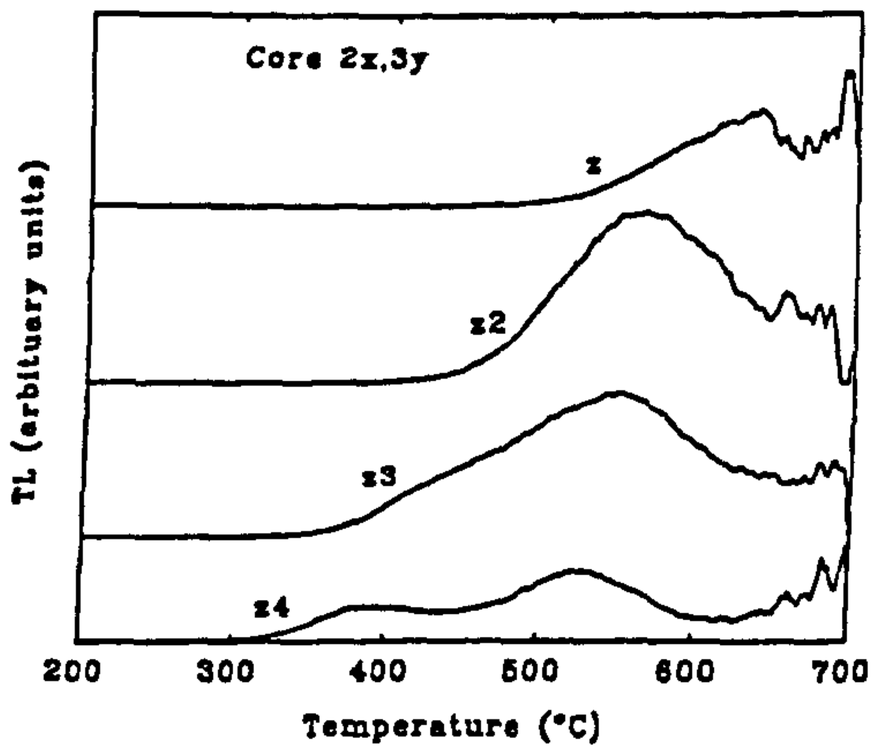

FIG. 3. *Examples of residual geological TL signals observed down a core removed from the central region of the stone.*

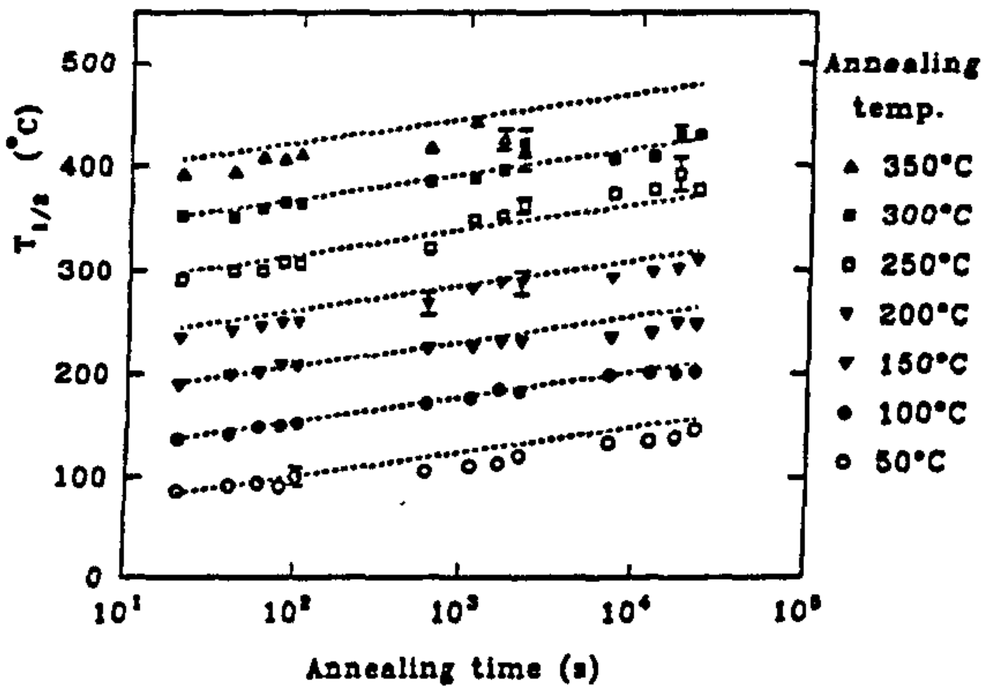

FIG. 4. Relationship between $T_{1/2}$ and the temperatures and durations of isothermal annealing for samples of IAEA F-1 potassium feldspar (– – – = constrained linear regression analysis).

areas of the stone; one centrally located ($2x$, $2y$) and beneath the main heat of the fires, the other at a corner (x, y). The data from both fires clearly demonstrate a temperature gradient in the centre compared with equilibrium conditions at the edge, and a large temperature gradient in the x–y plane. The thermal gradients observed in the stone are higher than a simulation closer to a real archaeological hearth due to a higher heat flow from beneath and at the sides of the stone. A linear interpolation has been used to approximate the temperature distribution between points in Fig. 2(a), where data were lost.

The TL results were parametrized in terms of the position of the residual geological signal $T_{1/2}$. $T_{1/2}$ may be defined as the temperature on the first rise at half the peak maximum (Spencer and Sanderson, 1991). The $T_{1/2}$ values for the 72 samples measured range from 247 to 577°C. For the normalization runs, the mean $T_{1/2}$ value was 304.06 ± 9.67°C (1σ). Examples of the natural residual geological signals observed down a core from the central region of the stone are shown in Fig. 3. As sampling depth is increased (from z to $z4$) away from the surface of the stone (and the source of heat), there is clearly a dramatic increase in the signal remaining due to the thermal gradient. Problems encountered in the determination of $T_{1/2}$, for example the unclear peak maximum in curve z and the two components in curve $z3$, may be resolved by calculating the maximum of the first derivative. The results have not so far been corrected for thermal lag and thermocouple non-linearity, although this is in progress.

5. ISOTHERMAL ANNEALING EXPERIMENTS

Detailed studies of the removal of TL from a pure potassium feldspar standard reference material (IAEA F-1) have shown systematic relations between $T_{1/2}$ values and the temperature and durations of isothermal annealing up to 350°C (Spencer and Sanderson, 1991). The complementary relationships between glow curve modification, annealing temperature and duration imply a linear dependence of $T_{1/2}$ on annealing temperature and log(time) (Fig. 4). A constrained linear regression analysis was performed on these data to test whether an equally spaced parallel line model would fit the results adequately over the temperature range up to 450°C.

This supports the concept of a simple complementary relationship, whereby the thermal exposure for any combination of isothermal events may be evaluated by integrating the product of temperature and log(time), thus:

$$\text{Thermal exposure} \propto \int_0^t T(t) \cdot \log(t)\, dt, \quad (1)$$

where T is the annealing temperature and t is the annealing time or duration. In this way, non-isothermal heating cycles may also potentially be represented by a similar thermal exposure index, which in principle will correlate with the measured $T_{1/2}$ parameters from subsequent TL measurement.

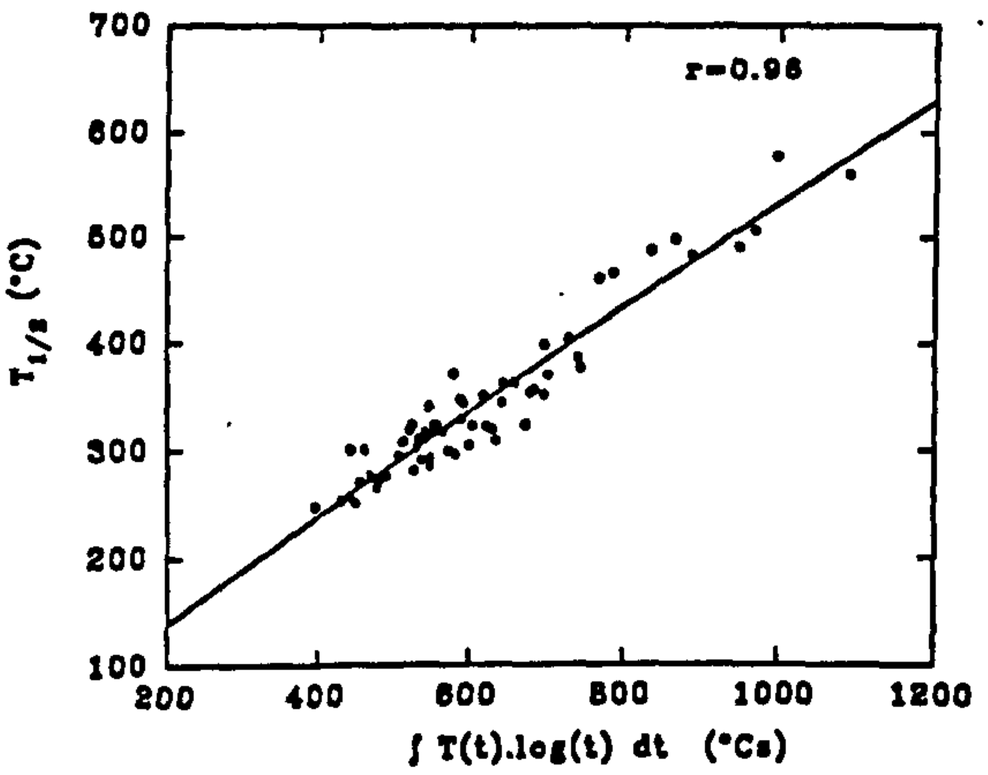

FIG. 5. Correlation between $T_{1/2}$ results and thermal exposure index values ($\int T(t) \cdot \log(t)\, dt$) for samples from a simulated hearth.

RM 23 2-3—O

6. EXTENSION OF MODEL TO HEARTHSTONE SIMULATION RESULTS

The demonstration of a linear correlation between TL parameters and the thermocouple integrated $T(t)\log(t)$ function for the sum of the two fires is shown in Fig. 5. The integration was calculated from a start time of 10 s for both fires. Additive and multiplicative corrections were made to $T_{1/2}$ values using the normalization results. In both instances, the correlation coefficient (r) gave lower values of 0.95 and 0.94, respectively.

7. DISCUSSION AND CONCLUSION

As described above, cores were removed in the central square centimetre region between each set of four thermocouple holes. Therefore, the temperatures sensed at the thermocouples and the temperatures responsible for the position of measured residual geological TL may be to some extent spatially separated, and due to observed thermal gradients, varying to some degree, either higher or lower, dependent on relative position. This is perhaps the most likely reason for any scatter in the correlation in Fig. 5, although stone inhomogeneities and the conductive influence of alumina–porcelain ceramic sheathes (used for thermocouples) may be contributing factors. Additional scatter in $T_{1/2}$ values may be due to variations in mineral composition, although this is not implied from the general trend in the normalization results.

The resultant linear correlation between the TL results, parametrized in terms of the residual geological signal, and thermocouple data expressed as an integrated $T(t)\log(t)$ function, allows acceptance of the complementary behaviour of temperature and duration variables and provides a means of quantifying thermal exposure unambiguously for specimens of unknown temperature and time profile. It also confirms that this relationship can be extended to the non-isothermal behaviour in a real hearthstone and that the form of the relationship can be cautiously extended to other silicate matrices.

This research has provided a direct experimental demonstration of the effect of well-documented fires on geological TL signals, and shows how TL can indicate the extent of spatial variation in thermal exposure under controlled conditions.

Acknowledgements—We would like to thank Beverley Smith for selecting the sandstone flag and arranging freight from Orkney to East Kilbride, and Dr Marian Scott for assistance with statistics. Thanks also to "Experimental Archaeologists" Peter Clark and Andrew Hursthouse, and to Peter Mellon. JQS is grateful to the Science-based Archaeology Committee of the Science and Engineering Research Council for the receipt of a studentship.

REFERENCES

Aitken M. J. and Thompson J. (1968) Determination of heat penetration in archaeological remains. In *Thermoluminescence of Geological Materials* (Edited by McDougall D. J.), pp. 413–417. Academic Press, London.

Gosselain O. P. (1992) Bonfire of the enquiries. Pottery firing temperatures in archaeology: What for? *J. Arch. Sci.* 19, 243–259.

Placido F. (1980) Thermoluminescence test for fire-damaged concrete. *Mag. Concrete Res.* 32, 112–116.

Rice P. M. (1987) *Pottery Analysis: A Sourcebook.* University of Chicago Press, Chicago.

Spencer J. Q. (1989) Heat transfer within hearthstones: implications for TL dating. Scottish Universities Research and Reactor Centre internal report, East Kilbride, Glasgow, Scotland, pp. 1–13.

Spencer J. Q. and Sanderson D. C. W. (1991) An introduction to luminescence archaeothermometry. In *Proc. 3rd Conf. Archaeological Sciences*, University of York (Edited by Szymanski J. E.), in press.

Spencer J. Q. and Sanderson D. C. W. (1992) Luminescence archaeothermometry of burned stones (presented to Archaeometry 92 Symp., Los Angeles, California, March 1992), in preparation.

Valladas H. (1980) Investigation of thermoluminescence of burnt sandstones from prehistoric sites. *Nucl. Instrum. Methods* 175, 230–232.

Valladas G., Gillot P. V. and Guérin G. (1979) Dating plagioclase? *PACT* 3, 251–257.

Valladas G. and Valladas H. (1978) High temperature thermoluminescence. In *Proc. 18th Inter. Symp. Archaeometry and Archaeol. Prospecti.* 14–17 March, Bonn, pp. 506–510.